VOLUME 22 (1961) No. 3

NUCLEAR PHYSICS

JOURNAL DEVOTED TO THE EXPERIMENTAL AND THEORETICAL STUDY OF THE FUNDAMENTAL CONSTITUENTS OF MATTER AND THEIR INTERACTIONS

EDITOR: L. ROSENFELD · COPENHAGEN

E. ARBMAN and I. B. HÄLLER, On the decay of barium 129 341

A. G. EKSPONG, A. FRISK, S. NILSSON and B. E. RONNE, Antiproton annihilations in complex nuclei 353

D. I. BLOKHINTSEV and WANG YUNG, $\pi\pi$ Interactions in πN-collisions at high pion energies 410

W. W. TRUE and E. K. WARBURTON, On the 5.16 MeV and 7.56 MeV states of B^{10} 426

B. BREMOND, On the effective interaction in finite nuclei 434

S. E. DARDEN, T. R. DONOGHUE and C. A. KELSEY, The polarization of neutrons from the $Li^7(p, n)Be^7$ reaction (I) 439

S. M. AUSTIN, S. E. DARDEN, A. OKAZAKI and Z. WILHELMI, The polarization of neutrons from the $Li^7(p, n)Be^7$ reaction (II) 451

GÖSTA RUDSTAM and ALEXIS C. PAPPAS, Mass and charge distribution in high energy induced fission 468

I. C. NASCIMENTO, G. MOSCATI and J. GOLDEMBERG, Systematics of $(\gamma, 2n)$ reactions 484

L. COHEN, Matrix elements for the alpha-particle 492

B. MARGOLIS, Neutron polarization by Coulomb scattering 498

N. H. GALE, J. B. GARG and K. RAMAVATARAM, Neutron angular distributions for the reaction $^{16}O(^3He, n)^{18}Ne$ 500

T. ROTHEM, F. R. METZGER and C. P. SWANN, Lifetimes of the 668-keV and 961-keV excited states in Cu^{63} 505

I. BERGQVIST and N. STARFELT, Gamma-ray spectra from capture of fast neutrons 513

HIROSHI NAKAMURA and TOSHIYUKI TOYODA, Connection of spinor fields . 524

February 1961

NORTH-HOLLAND PUBLISHING COMPANY-AMSTERDAM

EDITORIAL BOARD

AUSTRALIA & NEW ZEALAND:	H. Messel (Sydney), M. L. Oliphant (Canberra)
AUSTRIA:	B. Karlik (Vienna), H. Thirring (Vienna)
BELGIUM:	M. de Hemptinne (Louvain), J. Verhaeghe (Ghent)
CANADA:	G. Volkoff (Vancouver)
DENMARK:	C. Møller (Copenhagen), S. Rozental (Copenhagen), G. E. Brown (Copenhagen)
FINLAND:	L. Simons (Helsinki)
FRANCE:	A. Berthelot (Saclay), S. Gorodetzky (Strasbourg)
GERMANY (DEM. REP.):	G. Hertz (Leipzig)
GERMANY (FED. REP.):	W. Gentner (Freiburg i. B.), J. H. D. Jensen (Heidelberg)
GREAT BRITAIN:	W. E. Burcham (Birmingham), T. H. R. Skyrme (Harwell)
HUNGARY:	L. Janossy (Budapest)
INDIA:	H. Bhabha (Bombay), R. Ramanna (Trombay)
IRISH REPUBLIC:	J. McConnell (Maynooth)
ISRAEL:	G. Racah (Jerusalem)
ITALY:	E. Amaldi (Rome)
JAPAN:	S. Kikuchi (Tokay), S. Tomonaga (Tokyo)
MEXICO:	M. Moshinsky (Mexico)
NETHERLANDS:	H. Brinkman (Groningen), S. R. de Groot (Leiden)
NORWAY:	E. Hylleraas (Oslo), A. Lundby (Oslo), H. Wergeland (Trondheim)
POLAND:	L. Infeld (Warsaw), J. Werle (Warsaw)
PORTUGAL:	J. M. Araújo (Porto), J. R. de Almeida Santos (Coimbra)
SOUTH AMERICA:	G. Beck (Saõ Paulo), J. Leite Lopes (Rio de Janeiro)
SPAIN:	J. M. Otero (Madrid), C. Sanchez del Rio (Madrid)
SWEDEN:	O. Klein (Stockholm), K. Siegbahn (Uppsala), I. Waller (Uppsala)
SWITZERLAND:	P. Huber (Basel), P. Scherrer (Zürich)
U.A.R. & ARAB COUNTRIES:	F. El Bedewi (Cairo), M. G. Nooh (Cairo)
U.S.A.:	H. H. Barschall (Madison, Wisconsin), S. Devons (New York), V. F. Weisskopf (Cambridge, Mass.)
U.S.S.R.:	M. A. Markov (Moscow), I. S. Shapiro (Moscow), D. V. Skobeltzyn (Moscow)
YUGOSLAVIA:	I. Supek (Zagreb)

CONTRIBUTIONS may be sent to the Editor, Professor L. Rosenfeld, NORDITA, Blegdamsvej 17, Copenhagen Ø, either directly, or preferably through the intermediary of one of the members of the Editorial Board of the country or region in which the author is working. They may be written in English, French or German.

NUCLEAR PHYSICS is published in fortnightly issues. The subscription price per volume of 700 pages is fl 57.00; 114s; $ 15.00. Post-free.

SUBSCRIPTIONS should be sent to the publishers, NORTH-HOLLAND PUBLISHING COMPANY P.O. Box 103, Amsterdam or to any subscription-agent.

BOOKS FOR REVIEW should be sent to Professor Rosenfeld.

No part of this issue may be reproduced in any form, by print, photoprint, microfilm or any ther means without permission from the publisher.

Printed in the Netherlands

3.B:4.E *Nuclear Physics* **22** (1961) 341—352; © *North-Holland Publishing Co., Amsterdam*
Not to be reproduced by photoprint or microfilm without written permission from the publisher

ON THE DECAY OF BARIUM 129

EDVIN ARBMAN and INGA BRITT HÄLLER
The Gustaf Werner Institute for Nuclear Chemistry, University of Uppsala, Sweden

Received 10 October 1960

Abstract: The internal conversion and positon spectra of Ba^{129} have been studied with a double focusing beta-ray spectrometer. Positons of energies 1425 ± 15keV, 1243 ± 35 keV and 975 ± 60 keV with relative intensities 780, 240 and 60, respectively, were found. More than 60 transitions are identified from internal conversion lines. The decay of positons and a large number of conversion lines was followed in the spectrometer. A half-life of 2.61 ± 0.02 hours was found for the positons, and half-lives ranging from 2.00 ± 0.10 to 2.37 ± 0.08 hours were measured for various conversion lines. About 6 % of Ba^{129} was found to decay by positons. The observations are interpreted as a consequence of isomerism in Ba^{129}.

1. Introduction

In connection with work on the Ba → Cs → Xe decay chains for mass numbers 128 and 129 performed by Novakov *et al.* [1]), the electron spectrum of the short-lived Ba^{129} activity has been investigated at this institute. Ba^{129} was first identified by R. W. Fink and D. H. Templeton [2]) from bombardments of CsCl with protons in the Berkeley synchrocyclotron. The mass assignment was made by mass spectrographic analysis of a purified barium sample and by identification of the 31 hour caesium daughter activity. Fink *et al.* found a half-life of 2.0 ± 0.1 hours. Independently C. C. Thomas Jr. and E. O. Wiig [3]) in spallation of caesium with protons found an 1.8 ± 0.2 hour barium isotope, which by milking methods was assigned Ba^{129}. Positons were found to be emitted in the decay and later, from studies of the Ba^{129} positon spectrum in a low resolution beta-ray spectrometer, R. W. Fink and E. O. Wiig [4]) reported a maximum positon energy of 1.6 ± 0.2 MeV.

Recently the radiations from Ba^{129} have been investigated with the scintillation spectrometer technique by W. Henkes [5]). The Ba^{129} activity was produced with the $Ba^{130}(n, 2n)Ba^{129}$ reaction. Henkes reported a positon half-life of 2.45 ± 0.05 hours. Gamma rays of energies 0.127, 0.182, 0.210 and 1.45 MeV were found. 19 % of the positons were in coincidence with the 0.210 MeV transition and 5.6 % with the 0.127 MeV transition. Coincidences were also found between the 0.182 MeV and the 1.45 MeV gamma transitions. Milking experiments showed 25 to 30 % of Ba^{129} to decay by positon emission, which was found compatible with the intensities of the X-rays, the positons, and the various gamma rays only if unobserved gamma-gamma coincidences are postulated.

2. Experimental Procedure

Ba^{129} was produced by the $Cs^{133}(p, 5n)Ba^{129}$ reaction by bombarding CsCl with protons of 45 MeV mean energy in the Uppsala synchrocyclotron. After a two hour irradiation the CsCl was dissolved in water and about 1 mg iron carrier was added. The iron and barium were precipitated as carbonates by the addition of Na_2CO_3. The precipitate was dissolved in HCl, reprecipitated, and thoroughly washed with water. The precipitate was then dissolved in a small volume 8 N

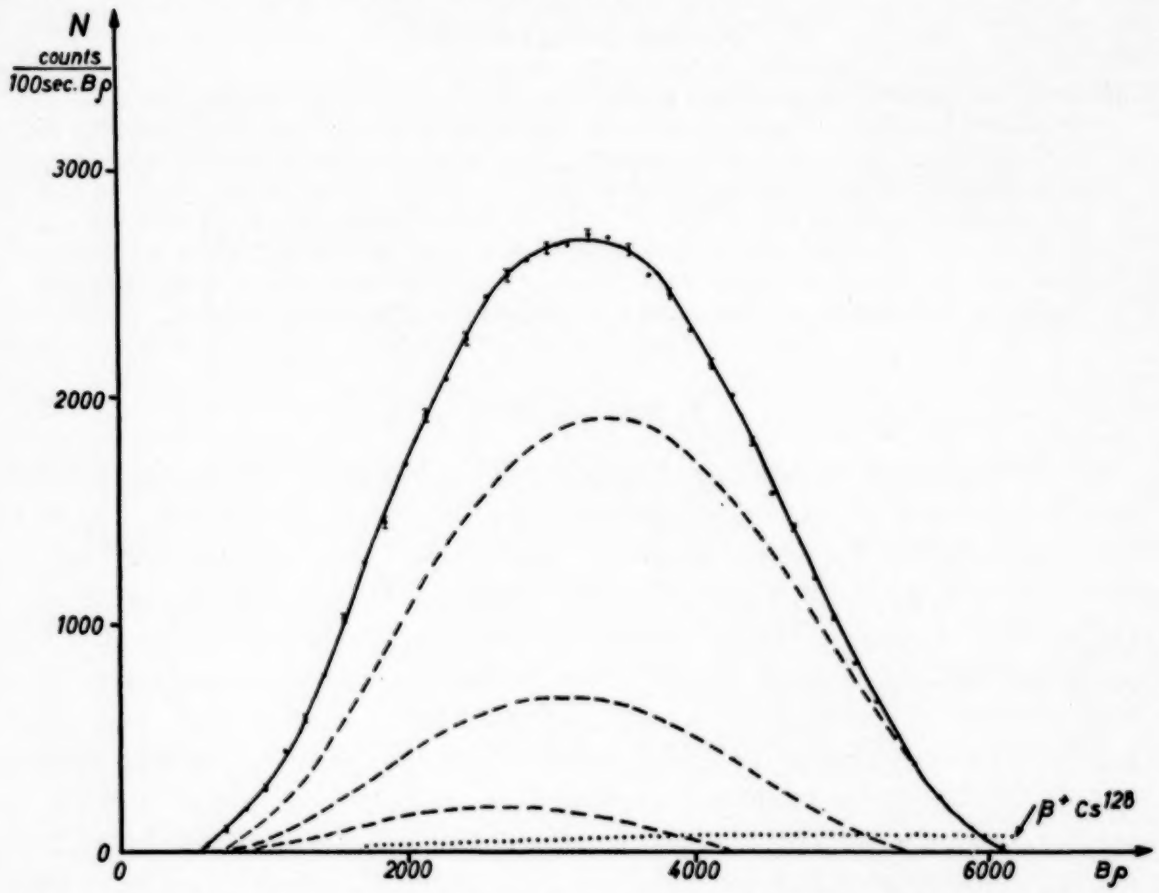

Fig. 1. Positon spectrum of Ba^{129}. The solid line represents the spectrum obtained in the double-focusing spectrometer at 1 % resolution corrected for decay and background. Source width 2 mm; activity vacuum evaporated onto 0.7 mg/cm² aluminium foil. The dotted lines indicate the partial spectra according to a Fermi analysis. At the bottom the subtracted background due to Cs^{128} is indicated.

HCl and the solution passed through a Dowex 1 ion exchange column saturated with 8 N HCl. The iron is adsorbed on the column whereas the barium remains in solution and passes through.

The positon distribution and conversion electron spectra were studied with the double focusing beta-ray spectrometer [6]). Sources for investigagtion of the positons and conversion electron lines of energies less than about 250 keV were prepared by evaporation in vacuum of the activity onto 0.7 mg/cm² aluminium

foils. For measuring the weak conversion lines of higher energies, the active barium solution was evaporated on 0.9 mg/cm² mylar strips of 1 mm width, which were then used as sources in the spectrometer.

The positon spectrum from the Ba^{129} decay, measured with the spectrometer adjusted for a resolution of 1 % and corrected for decay and the presence of a weak 2.4 day positon background due to Cs^{128} in equilibrium with Ba^{128}, is shown in fig. 1. By Fermi analysis (fig. 2), the positon spectrum decomposes

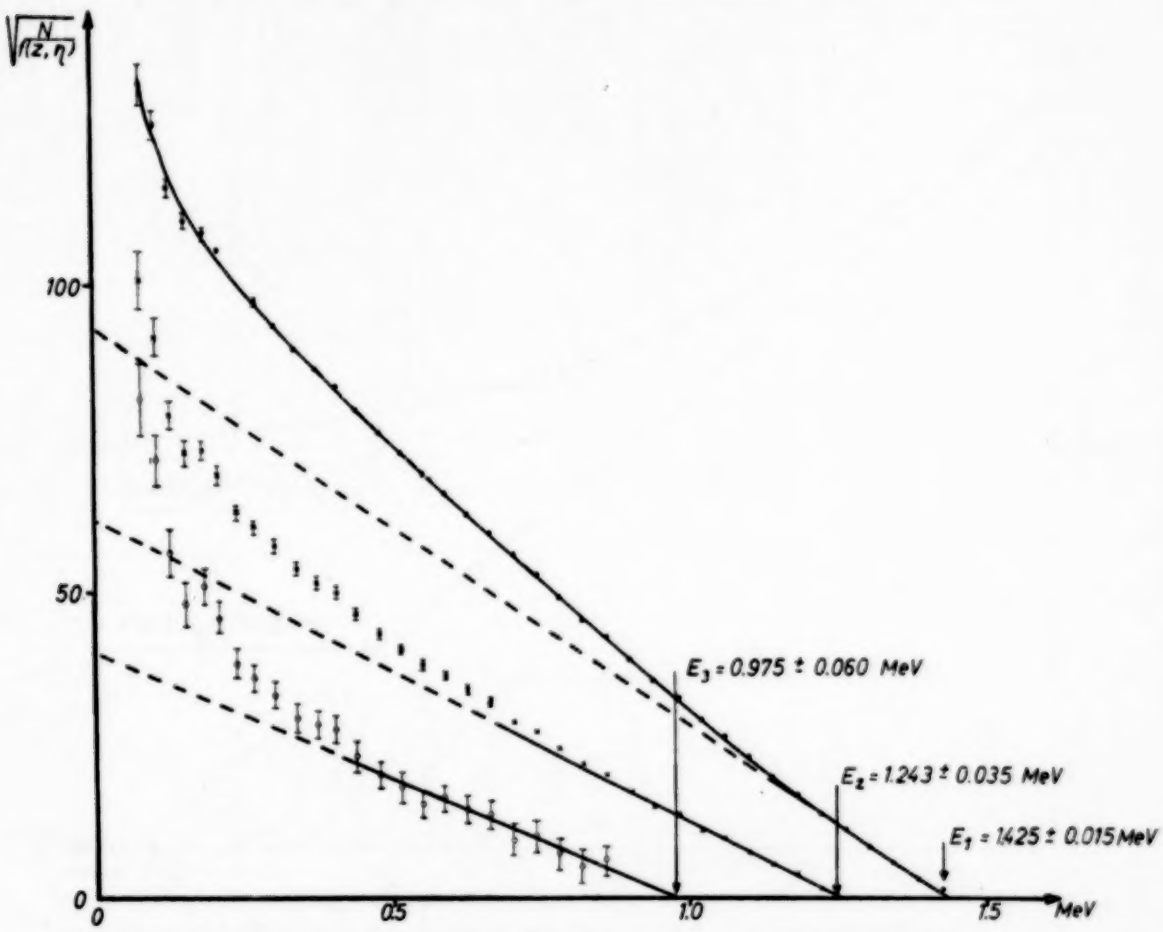

Fig. 2. Fermi analysis of the positon spectrum from fig. 1. Screening correction is applied. The Fermi line of the highest energy component was determined with a least squares fit to the 7 experimental points above 1175 keV. Similarly the line for the second component was determined by the 8 last points. Allowed shape is assumed.

into three components of energies 1425±15 keV, 1243±35 keV and 975±60 keV with the intensities 780, 240 and 60, respectively, expressed in the same relative intensity units as the conversion lines. In the analysis allowed shapes, i.e., straight Fermi lines have been assumed. Because of the rather small energy difference between the highest energy components, the error limits in energies and intensities are comparatively large. The Fermi line of the highest energy component was determined with the aid of the method of least squares [7]),

attributed to the seven experimental points above 1175 keV. It is seen from fig. 2 that there is a surplus of low energy electrons (about 1 % of the total positon intensity), which may indicate the presence of a positon component of about 250 keV maximum energy.

The positon half-life was followed from two different sources for about 5 days with the spectrometer set to focus positons of 700 keV energy. The decay curve showed a 2.6 hour activity, superimposed on the 2.4 day positon background

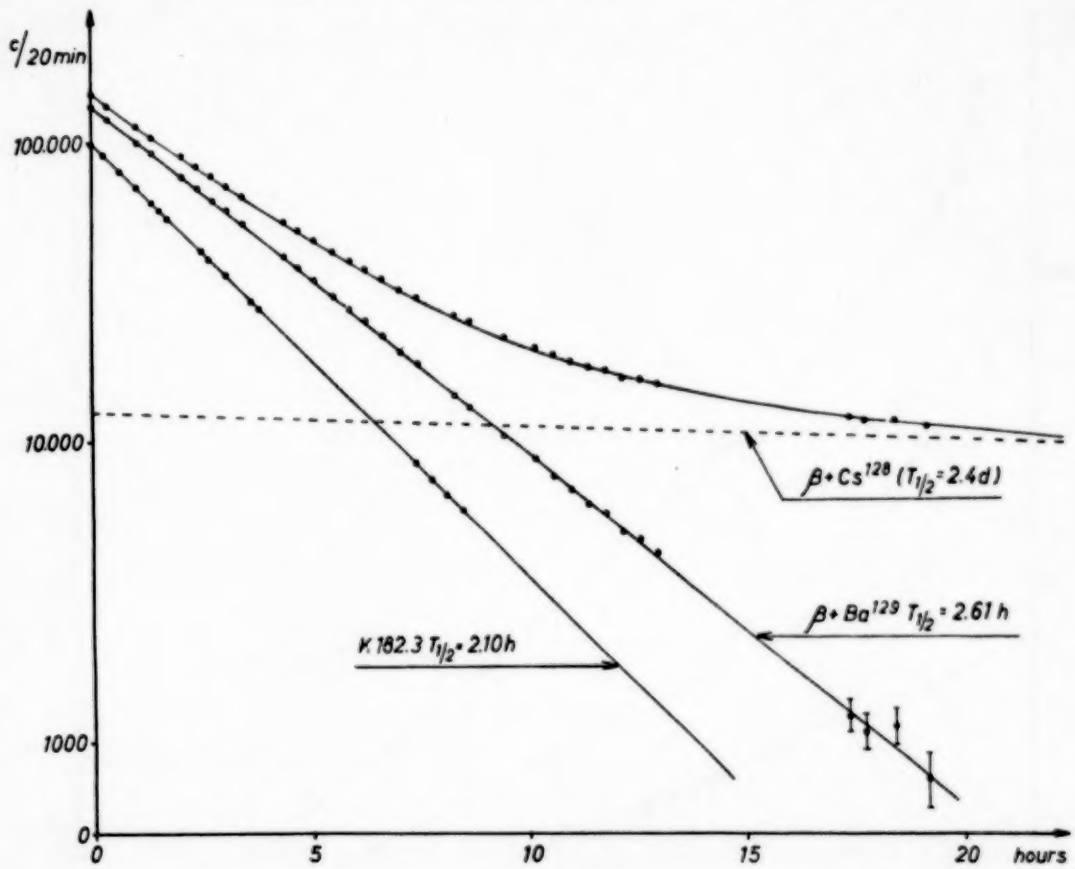

Fig. 3. Decay curves of positons ($T_{\frac{1}{2}} = 2.61$ h) and the K conversion line of the 182.3 keV transition ($T_{\frac{1}{2}} = 2.10$ h) of Ba^{129}, measured in the spectrometer. The decay of positons of about 700 keV energy was followed. The Ba^{129} positons are superimposed on a 2.4 day background due to Cs^{128} in equilibrium with Ba^{128} (dotted line).

from Cs^{128} in equilibrium with Ba^{128} (fig. 3). Application of the weighted least square method to the two sets of experimental data gave the half-lifes 2.62 ± 0.03 hours and 2.61 ± 0.02 hours, respectively, for the short-lived positon decay.

Conversion electrons of energies from 17 keV to 2 MeV were studied with a spectrometer resolution of about 0.4 %. The spectrum appeared to be very line-rich, most of the lines of energies above about 250 keV being weak (figs. 4 and 5). Rough half-lives on the lines in the low energy region were obtained from automatic records and at higher energies by measuring the spectrum twice.

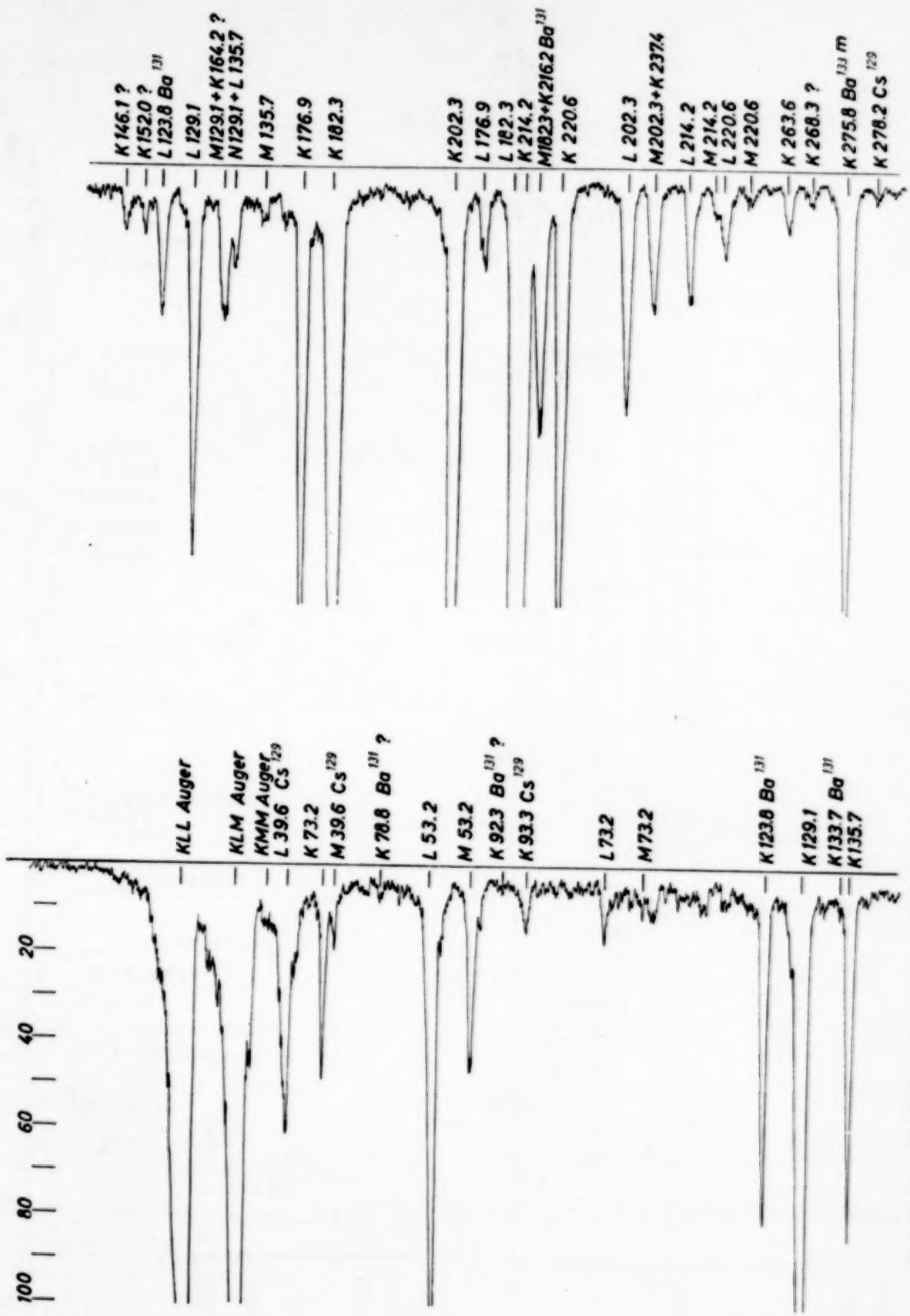

Fig. 4. Record of the low energy part of the internal conversion spectrum from a Ba^{129} source. Spectrometer resolution 0.4 %.

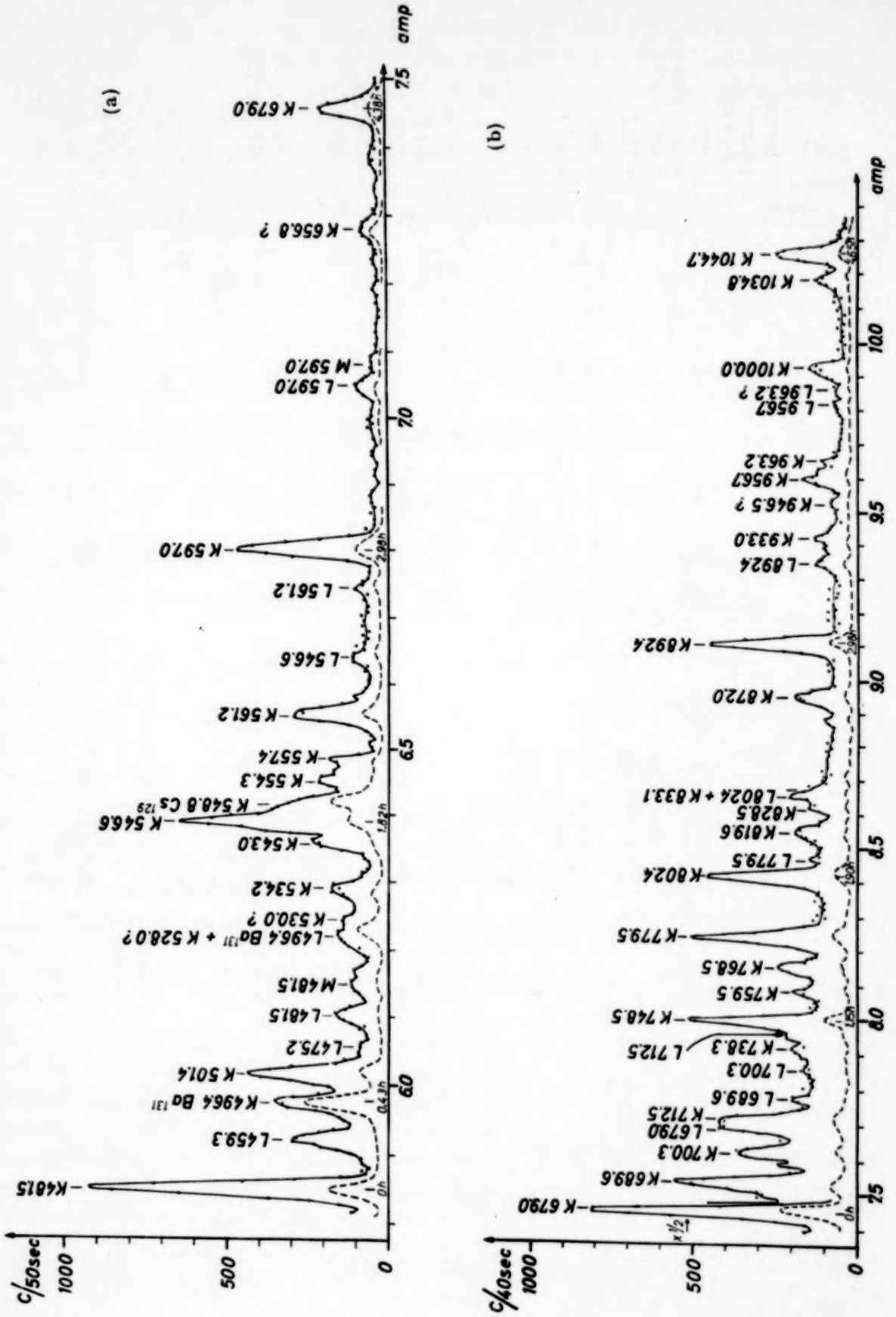
(a)
c/50sec
1000
500
0
amp
6.0
6.5
7.0
7.5
K 481.5
L 459.3
K 496.4 Ba 131
K 501.4
L 475.2
L 481.5
M 481.5
L 496.4 Ba 131 + K 528.0 ?
K 530.0 ?
K 534.2
K 543.0
K 546.6
K 548.8 Cs 129
K 554.3
K 557.4
K 561.2
L 546.6
L 561.2
K 597.0
L 597.0
M 597.0
K 656.8 ?
K 679.0
(b)
c/40sec
1000
500
0
amp
2.5
3.0
3.5
4.0
4.5
5.0
5.5
6.0
K 679.0
K 689.6
K 700.3
L 679.0
K 712.5
L 689.6
L 700.3
K 738.3
L 712.5
K 748.5
K 759.5
K 768.5
K 779.5
K 802.4
L 779.5
K 819.6
K 828.5
L 802.4 + K 833.1
K 872.0
K 892.4
L 892.4
K 933.0
K 946.5 ?
K 956.7
K 963.2
L 956.7
L 963.2 ?
K 1000.0
K 1034.8
K 1044.7

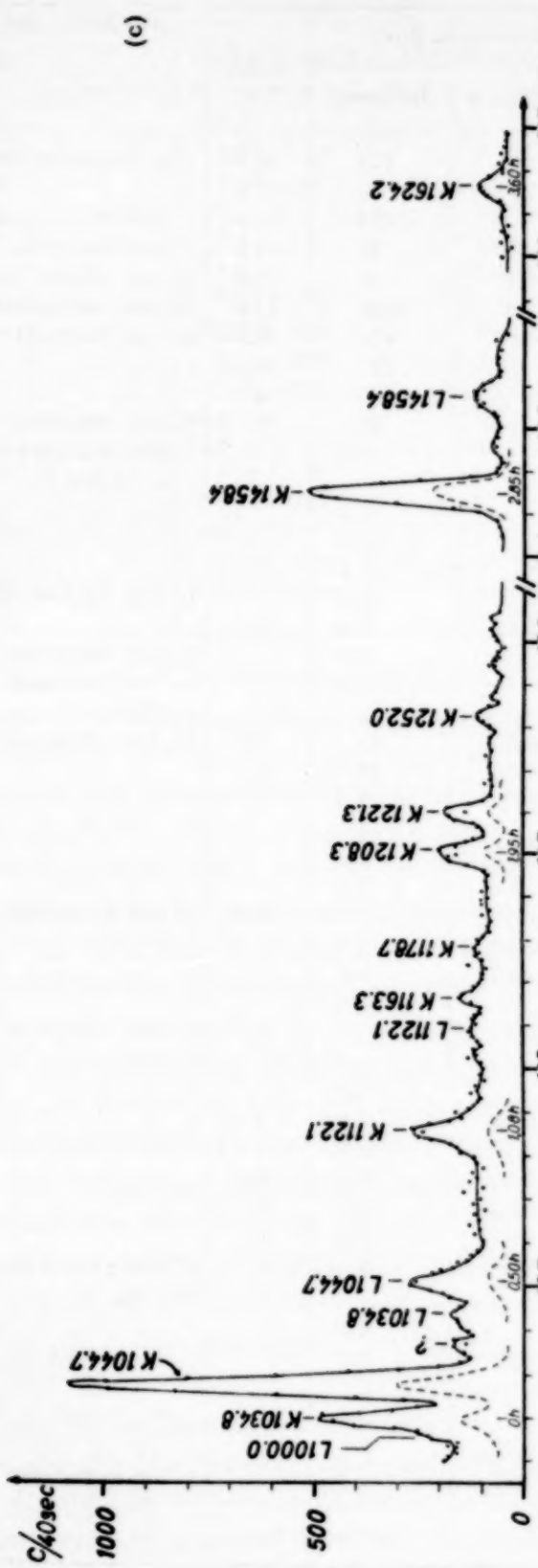

Fig. 5. High energy region of Ba^{129} conversion spectrum. The parts a, b and c are measured from different sources. Uncorrected for decay; instead the times are given at which the tops of some prominent lines were measured. Dotted lines represent remeasurements of the spectra after about 5 hours in the cases a and c and after 7 hours in the case b.

TABLE 1

Transitions in Ba^{129}

Transition energy (keV)	Lines observed	K conversion line		K/ΣL	Remarks
		Half-life hours	Intensity		
53.2	K, L_{1-3}, M_2, N_2	2.3	120	0.5	The intensity given is that of $L_1+L_2+L_3$
73.2	K, L_1, M_1	2.3	30	5.5	
129.1	K, L_1, M_1, N_1	2.22±0.05	420	>5.6	L and M lines composite with other lines
135.7	K, L_1, M_1	2.22±0.10	55	>6.1	L line composite with N 129.1
176.9	K, L_1	2.33±0.10	66	7.0	M line hidden by L 182.3
182.3	K, L_1, M_1	2.10±0.02	1000	7.0	M line composite with K 216.3 Ba^{131}
202.3	K, L_1	2.12±0.05	255	6.9	M line composite with K 237.4
214.2	K, L_1, M_1	≈2	137	6.9	
220.6	K, L_1, M_1	2.37±0.08	65	6.7	
237.4	K, L_1	≈2	19	9	K line composite with M 202.3
263.6	K	≈2	7.2		L line indicated on the high energy side of K 293.5
286.0	K	2.1	1.2		
293.5	K	2.2	1.2		
328.2	K	2.1	0.9		
333.6	K	2.22±0.10	2.3		L line on low energy side of K 365.6
337.5	K, L_1	2.11±0.08	3.3	6	
365.6	K	2.3	3.5		L line composite with K 392.0
386.3	K	2.1	3.4		L line indicated on low energy side of K 419.5
392.0	K, L_1	2.09±0.05	35	8.0	M line composite with K 425.8
419.5	K, L_1, M_1	2.11±0.05	27	6.4	
425.8	K	≈2	1.5		
433.8	K	≈2	1.5		
459.3	K, L_1	2.10±0.05	12		
475.2	K, L_1	2.13±0.08	3.2		
481.5	K, L, M	2.04±0.10	9.1	6.3	M line composite with other lines
501.4	K	2.14±0.10	4.2		
534.2	K	2.08±0.05	2.0		
543.0	K	2.1	2.8		
546.6	K, L	2.22±0.10	10	8	K line composite with K 548.8 Cs^{129}
554.3	K	2.1	2.5		
557.4	K	2.2	2.3		
561.2	K, L	2.15±0.05	4.8	8	
597.0	K, L, M	2.10±0.05	10.3	6	
679.0	K, L, M	2.08±0.05	6.5	6.5	
689.6	K, L	2.13±0.06	2.0	6	
700.3	K, L	2.1	1.2	6	
712.5	K, L	2.1	1.5	≈5	K line not resolved from 679.0 keV L and M lines
738.3	K	2.0	0.4		
748.5	K	2.13±0.05	2.5		L line hidden by K 779.5
759.5	K	2.2	0.5		
768.5	K	2.5	0.9		
779.5	K, L	2.07±0.10	2.8		
802.4	K	2.00±0.12	2.8		L line composite with K 833.1
819.6	K	2.0	0.9		
828.5	K	2.1	0.6		

TABLE 1 (continued)

Transition energy (keV)	Lines observed	K conversion line		K/ΣL	Remarks
		Half-life hours	Intensity		
833.1	K	2.2	1.1		
872.0	K	2.07±0.12	1.3		
892.4	K, L	2.16±0.08	4.2	6.4	
933.0	K	2.0	0.8		
956.7	K, L	2.1	1.4	5	
963.2	K	2.2	0.8		
1000.0	K, L	2.18±0.08	1.5	6	
1034.8	K, L	2.22±0.12	1.4	7.4	
1044.7	K, L	2.15±0.10	3.8	6.2	
1122.1	K, L	2.18±0.10	0.8	6.2	
1163.3	K	≈2	0.3		
1178.7	K	≈2	0.2		
1208.3	K	2.18±0.10	0.8		
1221.3	K	2.19±0.10	0.7		
1252.0	K	≈2	0.3		
1458.4	K, L	2.11±0.05	4.4	6.3	
1624.2	K	2.10±0.12	0.9		

Most of the conversion lines decayed with a half-life of about 2 hours. The longer lived lines could be identified as belonging to Ba^{133m}, Ba^{131} and Ba^{128} and the growing 31 hour Cs^{129} lines (cf. figs. 4 and 5). The measurements indicated somewhat shorter half-lives on the "2 hour" line group than the 2.6 hour period found for the positons, however, and also small divergences in half-lives between various conversion lines. The decay of a number of the most prominent lines was therefore followed in the spectrometer for about 12 hours. The half-lives obtained for these lines were found to differ considerably and are given to three significant figures in column 3 of table 1.

The energies of the conversion lines, which should be accurate to 1.5 parts in 1000 or better, are determined relative to the strong K-conversion lines of the 124 keV transition in Cs^{131} and the 276 keV isomeric transition from Ba^{133m} [8]), which were always present in the sources under investigation. The $B\rho$-values 1041.3±0.4 and 1828.2±0.7 gauss · cm respectively used for these two lines were determined in a separate run with the ThB F and I lines as reference lines from a barium source on which ThB had been electrostatically collected.

The results obtained from the study of internal conversion spectra are collected in tables 1 and 2. The conversion of all transitions in table 1 is assumed to occur in caesium as this was found to be the case for those transitions to which two or more conversion lines have been observed. In deriving the relative intensities the line and positon counting rates were extrapolated back to the end of bombardment with the use of the half-lives of the various lines given to three significant figures. For the rest of the lines, a half-life of 2.1 hours was assumed.

The weak lines collected in table 2 are less well established and interfere with other lines in several cases. They all seem to decay with a half-life of about 2 hours.

Conversion spectra also were studied from sources produced by 35 MeV and 65 MeV mean proton energy. From both these sources the same relative inten-

TABLE 2

Unassigned internal conversion lines with about 2 hours half-life

Line energy (keV)	Intensity (K 182.3 = 1000)	Line energy (keV)	Intensity (K 182.3 = 1000)
49.14	8	232.3	4
53.70	1.5	259.2	0.5
63.52	1.6	264.6	0.6
65.29	0.7	287.5	0.9
67.50	6.0	306.8	0.3
68.08	0.5	310.1	0.1
70.68	1.5	340.5	0.9
73.14	1.5	346.3	
79.48	1.2	348.2	1
83.01	0.7	358.7	1
86.05	2	380.7	1
90.35	1	419.5	1
92.00	3	481.4	0.5
113.1	2.8	483.7	0.5
116.0	5	494.1	
121.1	2.3	534.4	1
128.5	5	620.8	1.6
132.3	1	634.9	0.6
137.8	1	827.1	0.3
157.6	1	911.5	0.3
164.2	5	1021.7	0.2
194.9	4	1142.7	0.1
215.7	5		

sities for the prominent lines of the short-lived group were found as from the sources produced by 45 MeV protons. These measurements indicate that the lines do not belong to isotopes of different masses in spite of the observed divergences in half-lives. One must therefore assume that the observed 2.6 hour positons as well as the about 2.1 hour conversion lines follow from the decay of Ba^{129} and that the divergences in half-lives arises from isomerism.

3. Discussion

The 127 keV, 182 keV and 1.45 MeV gamma rays from the decay of Ba^{129} reported by Henkes [5]) are certainly identical with the 129.1, 182.3 and 1458 keV transitions found in the present investigation. The gamma-ray peak observed

by Henkes at 210 keV should then be composed of the gammas of the 202.3, 214.2 and 220.6 keV transitions. Also the weak gamma-rays of 0.67, 0.77, 0.89 and 1.04 MeV observed by Henkes but not unambiguously assigned to Ba^{129} by him can be indentified with transitions or groups of transitions of about these energies in table 1.

Our observed positon half-life 2.61 ± 0.02 hours is somewhat longer than the value 2.45 ± 0.05 hours obtained by Henkes. The discrepancy may however by explained in the light of the present results. Henkes measured the positons by coincidences between two scintillation detectors for the 510 keV annihilation radiation. According to table 1 there are a large number of gamma transitions with an energy of 500 keV or higher. It is quite plausible to assume that some of these gammas are mutually coincident. One may then expect a contribution of gamma-gamma coincidences in the coincidence counting rate. The gamma transitions, however, decay with shorter half-lives (about 2.2 hours) than the positons. With these considerations, therefore, the observed coincidence rate on the annihilation radiation would give too low a value for the positon half-life.

The existing data on the decay of Ba^{129} are not sufficient to establish the decay scheme, which seems to be rather complicated. Some main features of the decay are however discernible. Thus, the dominating positon branch of 1.42 MeV maximum energy must decay to the ground state of Cs^{129} because there is no transition observed of sufficient intensity and with appropriate half-life which could de-excite a level fed by this positon branch. The ground state of Cs^{129} has spin $\frac{1}{2}$ [8]) and the 1.42 MeV positon transition — judging from the positon half-life and energy — is very probably allowed with a spin change $\leqq 1$. The positon decaying state should then have a spin value $\leqq \frac{3}{2}$ and half-life of 2.61 hours.

The energy difference between the two most energetic positon components is 182 keV, which agrees with the energy of the intense 182.3 keV M1 transition. This energy agreement, however, may be fortuitous because coincidences were not observed between positons and the 182 keV gamma ray [5]). Furthermore, the half-life of the 182.3 keV transition is considerably shorter than the positon half-life. Other levels adjacent in energy and de-excited by the 176.9, 214.2 or 220.6 keV transitions could as well be fed by the 1243 keV positons.

The two intense transitions of energies 182.3 keV and 1458 keV, which both are converted in caesium and, according to Henkes' coincidence measurements, emitted in cascade but not coincident with the positons, very probably follow from the decay of a second excited state in Ba^{129}. In analogy with the isotopes Ba^{133}, Ba^{135}, and Ba^{137} the low-spin, 2.6 hour positon decaying level would then be the ground state, while the other level would be a high-spin isomeric state. This state would then have a half-live of about 2.1 hours decaying predominantly by electron capture to excited high-spin levels in Cs^{129}, since no isomeric transition to the ground state has been observed so far. The transitions

with intermediate half-lives can be explained as originating from excited levels in Cs^{129}, which are fed — directly or indirectly — partly from the ground state and partly from the isomeric state of Ba^{129}.

The interpretation ot the observed anomalous half-lives as due to the existence of an isomeric state in Ba^{129} and not to the presence of another barium isotope is supported by the fact that the internal conversion lines showed the same relative intensities in spectra from sources produced with different bombarding energies. This also seems reasonable with respect to the total number of the Cs^{129} daughter atoms and thus the total number of Ba^{129} atoms produced. This number can be estimated from the intensities of the growing Cs^{129} conversion lines if the Cs^{129} decay scheme is known. One can then find the fraction of Ba^{129} decaying by positon emission. In this manner it was found that about 6 % positon decay took place from a source prepared one hour after the end of the irradiation. For this estimate, the decay scheme for Cs^{129} proposed by Nijgh [9]) was used. Supposing the two isomers to be produced in about equal yield and the positons to follow from the decay of the ground state only, this state would decay 12 % by positon emission, which seems a reasonable figure with regard to the available decay energy.

As an aid for construction of a decay scheme a large number ot energy sum relations, where the sum of the energies of two transitions is equal to the energy of third transition, can be found. In order to propose a decay scheme, however, more data are required. Measurements of electron-electron coincidences and electron-positon coincidences would be very valuable. Also a thorough study of the gamma rays for transition intensities and multipole order assignments is desirable. One difficulty in these investigations would be the interference of other barium isotopes simultaneously produced in the cyclotron bombardment. A convenient way to avoid this difficulty would be to use mass-separated sources.

References

1) T. Novakov, S. Koički, M. Mladjenovič and E. Arbman, C. R. du Congr. Intern. de Phys. Nucl. (Paris 1958) p. 935
2) R. W. Fink and D. H. Templeton, J. Am. Chem. Soc. **72** (1950) 2818
3) C. C. Thomas, Jr. and E. O. Wiig, J. Am. Chem. Soc. **72** (1950) 2818
4) R. W. Fink and E. O. Wiig, Phys. Rev. **91** (1953) 194
5) W. Henkes, Phys. Rev. **113** (1959) 863
6) E. Arbman and N. Svartholm, Arkiv Fysik **10** (1955) 1
7) R. Mitchell and R. Madey, U.C.R.L. 2783
8) D. Strominger, J. M. Hollander and G. T. Seaborg, Rev. Mod. Phys. **30** (1958) 585
9) G. J. Nijgh, Thesis, Amsterdam 1955

8.A

Nuclear Physics **22** (1961) 353—409; ©*North-Holland Publishing Co., Amsterdam*

Not to be reproduced by photoprint or microfilm without written permission from the publisher

ANTIPROTON ANNIHILATIONS IN COMPLEX NUCLEI

A. G. EKSPONG, Å. FRISK, S. NILSSON † and B. E. RONNE

Institute of Physics, University of Uppsala

and

Institute of Physics, University of Stockholm

Received 26 September 1960

Abstract: An investigation of 356 antiproton annihilations in nuclear emulsion is reported. The results are generally analysed to yield information on primary processes, assumed to be annihilations with single protons or neutrons into a number of pions with or without a K-meson pair.

The average pion multiplicity is 4.68 ± 0.12 for annihilations at rest, and 5.11 ± 0.12 for annihilations in flight (the antiproton energy being on the average 166 MeV). This increase of 0.4 ± 0.2 pions is to be compared with an expected average increase of 0.1 pion. The pion energy distributions are given with mean values of 391 ± 10 MeV total energy (at rest) and 390 ± 9 MeV (in flight).

Emission of K-meson pairs is found to take place in 3 ± 2 % of the annihilation reactions. The average number of pions emitted together with K-mesons is 2.2 ± 0.5. The correction for K-meson pairs unobservable in usual emulsion experiments has been computed. The result that about 40 % of the K-meson pairs are undetectable, means that the correction for detection efficiency is larger than previously assumed. A recalculation of all published data using emulsion detectors results in a world average of 5.0 ± 1.1 % of the annihilations with K-meson pairs for annihilations at rest and in flight (antiproton energy below 250 MeV).

The annihilation probability at rest with neutrons is found to be less than that with protons on the basis of a determination of the number of stars with an odd number of charged pions relative to that with an even number. The ratio odd/even is 0.73 ± 0.09.

The reabsorption probability of the pions in complex emulsion nuclei is determined. It is found that 18 % of the pions are absorbed on the average (at rest) and 32 % (in flight). The difference is understood as a result of the movement of the centre-of-momentum and the penetration of the antiprotons into the nuclei for the cases produced in flight.

Comparison of our experimental results with the predictions of various theories is carried out. For the pion production, however, no decision in favour of a particular theoretical model can be made. As regards the production of K-mesons, all theories fail to predict the experimentally found production frequency.

The world data on antiproton annihilations are collected, reanalysed and discussed.

1. Introduction

Since the discovery of the antiproton [1]) some experiments have been devoted to the study of antiproton reactions in nuclear emulsions and bubble chambers. The present paper deals with the annihilation process in emulsion. The results on the antiproton cross sections have already been reported [2]).

The investigation is based on 356 antiproton captures at rest and in flight with kinetic energies of the antiprotons ranging from 0—250 MeV. The contents of the paper are given below.

† Now at CERN, Geneva.

Contents

1. Introduction 353

2. The sample of antiprotons 355

3. Measurements on the emitted particles 356

3.1. GENERAL CONSIDERATIONS. 356

3.2. PIONS 357

3.2.1. Energy distribution and average energy 357

3.2.2. Multiplicity and charge 362

3.2.3. Electron pairs from the decay of neutral pions 363

3.3. HEAVY PRONGS 364

3.4. STARS WITH CHARGED STRANGE PARTICLES 368

3.4.1. Details of the events 368

3.4.2. Conservation of strangeness 370

3.4.3. Evaluation of the relative abundance of K-*meson pairs and the average energy going into* K-*meson production* 370

3.4.4. Hyperons and hyperfragments. 371

4. Comparison with other experimental data 372

4.1. PIONS AND HEAVY PRONGS. 372

4.2. STRANGE PARTICLES 372

5. Annihilation into pions 375

5.1. CONSEQUENCES OF ENERGY CONSERVATION. 375

5.1.1. Excitation energy 376

5.1.2. Best fit average values of the primary pion multiplicity and energy, the number of interacting pions, and the energy given to the nucleus. 377

5.1.3. Discussion 379

5.2. TRANSFORMATION OF AN ISOTROPIC PION ANGULAR DISTRIBUTION FROM THE C.M.S. TO THE LABORATORY SYSTEM FOR ANTIPROTONS CAPTURED IN FLIGHT. 380

5.2.1. The antiproton annihilates directly. 381

5.2.2. The antiproton undergoes elastic scattering once 382

5.2.3. The resulting distribution. 382

5.3. ABSORPTION OF THE PIONS 383

5.4. COMPARISON OF EXPERIMENTAL AND EXPECTED ANGULAR DISTRIBUTION OF THE PIONS. ESTIMATION OF THE AVERAGE PRIMARY PION MULTIPLICITY 385

5.5. PROBABILITY OF CAPTURE OF AN ANTIPROTON BY PROTONS AND NEUTRONS 387

5.6. COMPARISON WITH STATISTICAL THEORIES 389

5.6.1. Introduction 389

5.6.2. Consequences of charge independence 391

5.6.3. Comparison of estimates and predictions 393

6. Annihilation into pions and K-mesons 397

7. Summary. 399

Appendix 1. The influence of distortion on energy determinations by multiple scattering measurements 401

Appendix 2. The efficiency of detection of tracks from annihilation stars 403

Appendix 3. Best fit method of solving an overdetermined system of equations 404

Appendix 4. Transformation of an isotropic pion angular distribution from C.M.S. to the laboratory system for antiprotons captured in flight 405

A.4.1. *The antiproton annihilates directly*. 405

A.4.2. *The antiproton undergoes elastic scattering once* 407

2. The Sample of Antiprotons

The scanning procedure and the method of identification of the antiproton tracks have been described in an earlier paper [2]).

A summary of the antiproton sample is given in table 1. The vertical headings divide the events into five phenomenological groups according to the appear-

TABLE 1

The sample of antiprotons [a])

Phenomenological groups	A. Total no. of anti-protons	B. Events > 20 μm from surface or glass; with pions and stabble particles only	C. Events < 20 μm from surface or glass	D. Events with charged strange particles
I. Particles which come to rest and give $\geqq 1$ prong	167	156	9	2
II. Particles which come to rest without giving any prongs	8	8		
III. Particles giving a star in flight with $\geqq 1$ prong	179 [b])	170 [b])	6	3
IV. Particles disappearing in flight	7 [c])	7 [c])		
V. Particles which leave the stack	16			

[a]) 10 stars from an earlier experiment [3]) are included

[b]) This figure includes an estimated number of 3 protons

[c]) This figure includes an estimated number of 2 charge exchange scatterings.

ance of the end of the track. The first column (A) shows the total number of antiprotons in each of the five groups, the second (B) gives an unbiassed sample of events without observed strange particles, the fourth (D) contains the events with strange particles, whereas the third (C) gives the number of events situated too close to an emulsion boundary to permit careful analysis. A prong is required to be longer than 5 μm, otherwise it is classified as a blob. About 20 % of the stars contain blobs in addition to the prongs taken into account.

The antiproton stars belonging to the unbiassed groups B I—IV in table 1 are analysed in subsections 3.1—3.3. At rest we have 164 annihilations, because the 8 events representing particles coming to rest without giving a star, are included. One would expect a small admixture of antiproton charge exchange scatterings in the groups B III and B IV. The charge exchange cross section is known to be 4—10 mb from counter experiments [4, 5]). We would thus expect about 2 events in the sample. These are taken from group B IV and the other 5 events are included in the annihilations in flight. The number of annihilations

in flight will consequently be 175, about 3 of which are proton stars as explained in ref. [2]). The proton contamination has been excluded when possible, e.g. in the calculation of the charged pion multiplicity.

Subsection 3.4 deals with the strange particle events in D I and D III.

The reason for excluding the events situated less than 20 μm from either surface or glass is the experimental loss of thin tracks in this region (see Appendix 2).

3. Measurements on the Emitted Particles

3.1. GENERAL CONSIDERATIONS

The prongs from the antiproton annihilation stars have been divided into two groups according to their ionization being above or below $g/g_0 = 1.4$ (corresponding to a pion energy of 80 MeV or a proton energy of 500 MeV).

Multiple scattering and ionization measurements were performed on all tracks with an ionization below the limit and a dip angle less than 17°. (Subsection 3.2.1.) In this sample all particles are consistent with pions.

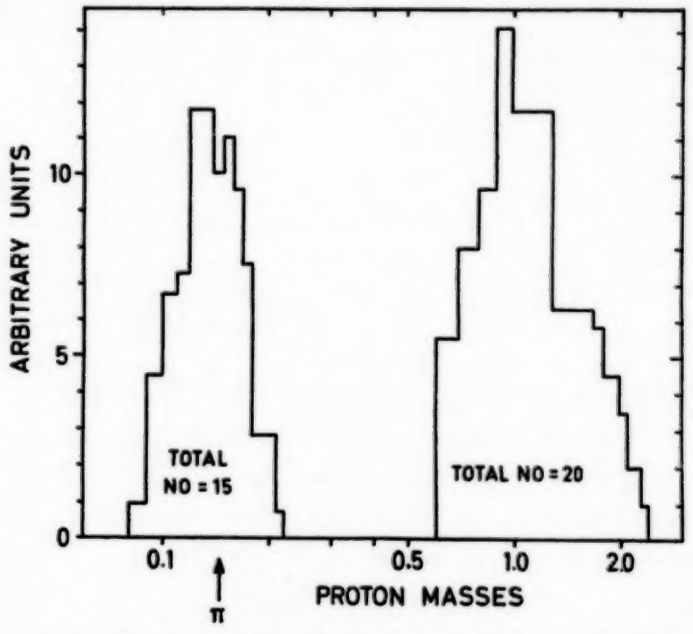

Fig. 1. Mass spectrum of particles which have $g/g_0 \geqq 1.4$, dip angles $\leqq 17°$ and either interact in flight or leave the stack.

Tracks with an ionization above the limit were followed until they stopped, interacted in flight or left the stack. These particles were identified as pions or protons by means of observations of grain density and range, change in grain density and range or, when necessary, grain density and multiple scattering. It is, in general, possible to determine the mass of stopping particles with a range of at least 1 cm in emulsion by grain counting. These measurements are

discussed in subsect. 3.3. In most cases, it is also possible to identify pions and protons among the particles which interact in flight or leave the stack. The measured mass distribution of particles which interact in flight or leave the stack and with dip angle less than 17° is shown in fig. 1. Each mass measurement is represented in a linear scale by a rectangle of constant area and with a base which is twice the estimated standard deviation of the measurement. The group consists of 35 particles, 15 of which were designated as pions and 20 as protons or deuterons. The K-mesons will be discussed in subsect. 3.4.

Tracks classified as due to protons include also tracks due to particles heavier than the proton. Short tracks which ended without any visible interaction were classified as protons.

In table 2 we give the total number and the identification of prongs with $g/g_0 \geqq 1.4$ from antiproton annihilations in groups B I and B III.

TABLE 2
Total number and identity of prongs with $g/g_0 \geqq 1.4$

Antiproton star	Particles identified as	Total number of prongs		
		Stopping in the stack	Interacting in flight	Leaving the stack
at rest group B I [a])	p	488	12	21
	π	46	5	7
in flight, group B III [a])	p	930	15	64
	π	60	4	14

[a]) see table 1

In addition to the tracks in table 2 there are 632 pions with $g/g_0 < 1.4$ in groups B I and B III. The number of interacting pions together with the observed length of pion tracks yields an interaction mean free path of 29 ± 6 cm, which is in good agreement with pion experiments.

3.2. PIONS

3.2.1. Energy distribution and average energy

In view of the importance of the determination of the pion mean energy we will discuss our measurements in some detail.

TABLE 3
Pions with kinetic energy below 80 MeV

Characteristics of the track	Number
(i) Stopping π^-	67
(ii) Stopping π^+	39
(iii) Leaving the stack	21
(iv) Interacting in flight	9
(v) Estimated additional number in 70 % of the solid angle (see text)	21
Total no. with $T_\pi \leqq 80$ MeV	157

All pions with kinetic energy below 80 MeV (corresponding to $g/g_0 \geqq 1.4$) are listed in table 3 according to what happens to the track.

The energy of pions belonging to (i) and (ii) has been obtained from the range. The pion energies of the groups (iii) and (iv) have been determined by means of ionization and/or multiple scattering measurements. A careful investigation of all tracks with low ionization and small dip angle has been performed and will be reported below. As a result of this investigation we found, in addition to pions classified by the scanners to have $g/g_0 \geqq 1.4$, 9 others with energy below

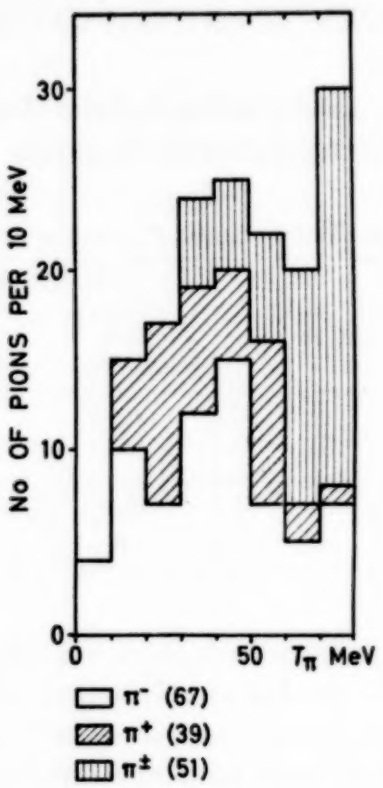

Fig. 2. The energy distribution of pions with kinetic energy less than 80 MeV.

80 MeV. As 30 % of the solid angle was investigated, we would expect an additional number of 21 in the total sample of pions with energy below 80 MeV. We assume that the 21 added pions have the same energy distribution as the 9 regrouped ones, that is, most of them have energies above 60 MeV.

An unbiassed energy distribution of all pions with energy below 80 MeV can thus be obtained. It is given in fig. 2.

The energy of particles with ionization $g/g_0 < 1.4$ and dip angle $\beta \leqq 17°$ was determined by multiple scattering measurements. A grain count, in addition, showed that all tracks in this sample were consistent with pion tracks. All particles were taken as pions although a slight admixture of electrons cannot be excluded (see subsect. 3.2.3.) Of the 159 tracks in the sample, 10 (7 with β

$< 11°.5$) interacted in flight or left the stack after too short a distance to permit a mass or an energy determination.

From earlier measurements [2]), it was known that the distortion in our stack was not negligible. For this reason the influence of the distortion on the energy determinations was carefully investigated and the distortion was eliminated as far as possible. The tracks were divided into three dip angle intervals: 0—5°.8, 5°.8—11°.5, and 11°.5—17°.0. The intervals correspond to equal solid angles (10 % of the total solid angle). The number of pions in each interval was 63, 58, and 28, respectively. The low number in the last group is explained by statistical fluctuations and the following considerations. The tracks were selected on the basis of dip angles, measured by the scanners. In the course of the accurate determination of dip angles, a number of tracks with a previous $\beta \lesssim 17°$ were found to have $\beta > 17°$. No influx came from $\beta > 17°$, since 17° was the limit

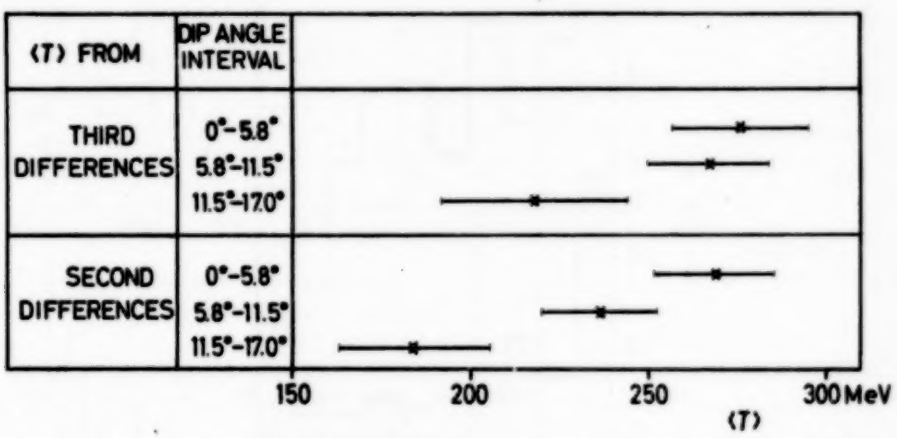

Fig. 3. The measured average pion kinetic energy as a function of the dip angle.

chosen. Depending on the energy of the particle, 60 to 120 cells were taken in the measurement of the multiple scattering. The momentum-velocity product $p\beta$ was calculated from second and third differences. Noise was eliminated by the subtraction method (between $t-2t$ and $t-3t$, where t is the cell length). The mean energies in each angular interval are shown in fig. 3. The mean energies increase when they are calculated from the third instead of the second differences. This is what one would expect because second order distortion is then eliminated. From the systematic trend of the mean values, even when third differences are used, one may suspect that there remains distortion of higher order. The geometrical correction discussed below can only account for a negligible part of the energy differences.

In order to minimize the influence of remaining distortion we have proceeded in the following way.

(i) The values of $p\beta$ are interpolated to zero dip. See Appendix 1.

(ii) Tracks with dip angles in the region 11°.5—17°.0 have been excluded in

the final energy distributions in order to obtain only a small correction to the measured $p\beta$-values.

The final distortion correction resulted in a 15 MeV increase of the mean energy of the pions with dip angles in the region 5°.8—11°.5. The mean energy for the whole distribution increased by 5.5 MeV.

In order to obtain an unbiassed energy distribution for annihilations in flight one has to make an important geometrical correction. The need for this correction arises because of the following two circumstances: first, the pion energies depend on the space angle between the pion and the antiproton tracks, and second, the measured fraction of the number of pions depends on the same

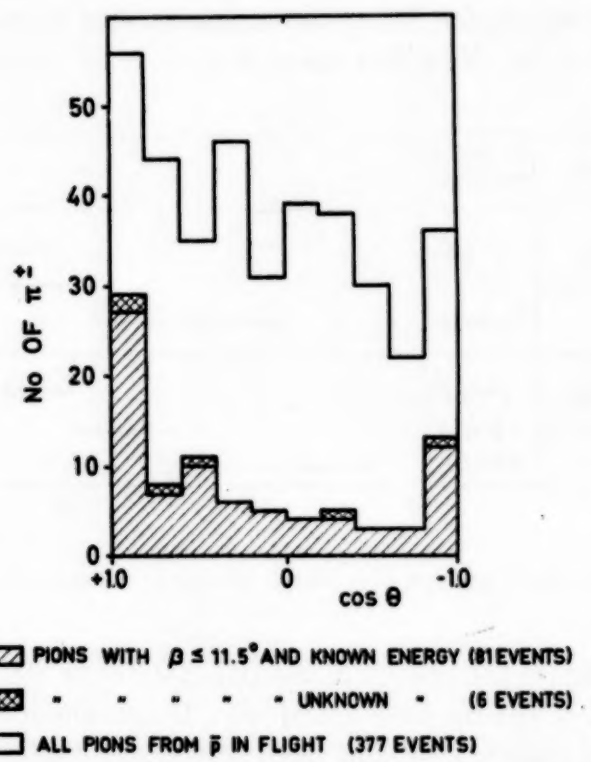

Fig. 4. The angular distribution of pions emitted from antiproton captures in flight. θ is the space angle between the pion track and the direction of the incoming antiproton.

angle. The measured sample is found to be biassed towards high pion energies. Fig. 4 gives the angular distribution for all pions emitted from the antiproton captures in flight. The angular distribution of the pions with dip angle $\beta \leqq 11°.5$ is also indicated. About 50 % of the pions in the forward direction ($0.8 < \cos\theta \leqq 1.0$) have been measured. In the other intervals, only about 18 % of the tracks conform to the dip angle criterium $\beta \leqq 11°.5$. This fact is quite obvious for geometrical reasons. A calculation starting from the total angular distribution shows that the number of pions with $\beta \leqq 11°.5$ in each space angle interval is in agreement with what one would expect. The average kinetic energy for

pions emitted forward ($0.8 < \cos\theta \leqq 1.0$) is 314 ± 37 MeV, while for those outside this forward cone it is 195 ± 20 MeV. If one takes the mean of the measured energies one will get a too high average energy and, moreover, the energy distribution will be wrong. The correct average pion energy is obtained by calculating the mean energy for each angular interval and multiplying by the actual fraction of pions in the interval. The correction is found to amount to a decrease of the average energy by 22 MeV.

The corrected average pion energy is

$$215 \pm 20 \text{ MeV}. \tag{1}$$

The geometrical correction discussed above is thus of importance. It has not been discussed in the literature earlier.

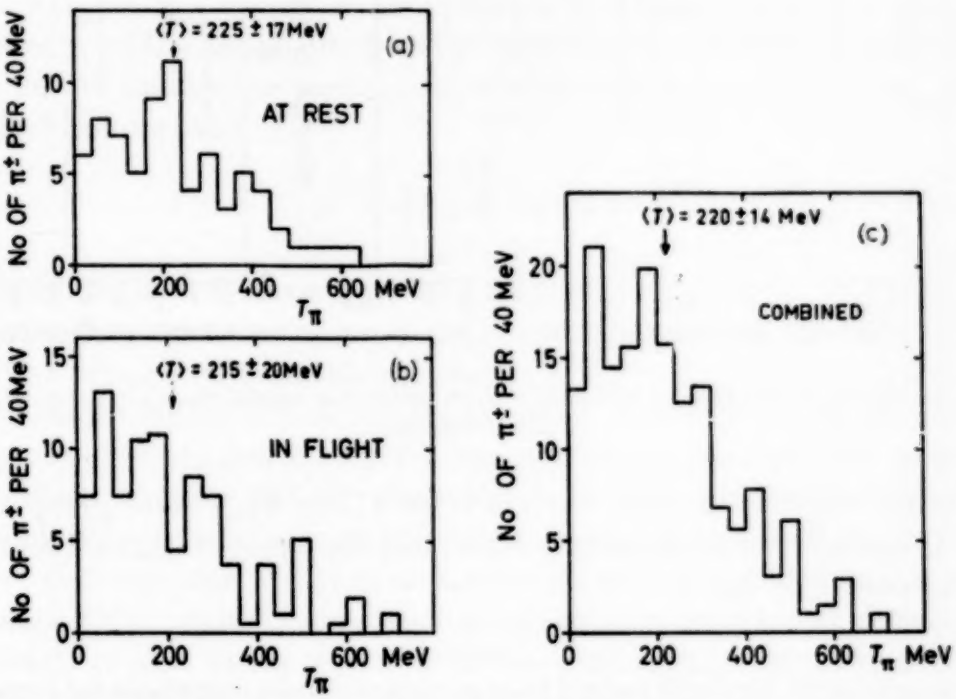

Fig. 5. The observed energy spectrum of charged pions from antiproton stars a) at rest, b) in flight and c) combined. Pions with dip angle $\leqq 11°.5$ were measured.

The corrected energy distributions of pions from annihilations at rest, in flight, and combined are plotted in figs. 5 a), b) and c). The total number of pions is 14 (below 80 MeV)+60 (above 80 MeV)+1 (not measured) = 75 at rest and 20.5+60.5+6 = 87 in flight. Fig. 2 gives a detailed picture of the part of the combined spectrum at energies below 80 MeV over the whole solid angle.

The average total energy of the charged pions $\langle E_{\pi^\pm} \rangle$ is found to be for antiprotons captured

$$\begin{aligned} &\text{at rest:} && \langle E_{\pi^\pm} \rangle = 365 \pm 17 \text{ MeV}, \\ &\text{in flight:} && \langle E_{\pi^\pm} \rangle = 355 \pm 20 \text{ MeV}, \\ &\text{combined:} && \langle E_{\pi^\pm} \rangle = 360 \pm 14 \text{ MeV}. \end{aligned} \tag{2}$$

3.2.2. Multiplicity and charge

The distributions of the number of charged pions emitted from the antiproton stars at rest, in flight and combined are shown in figs. 6a), b), and c), respectively.

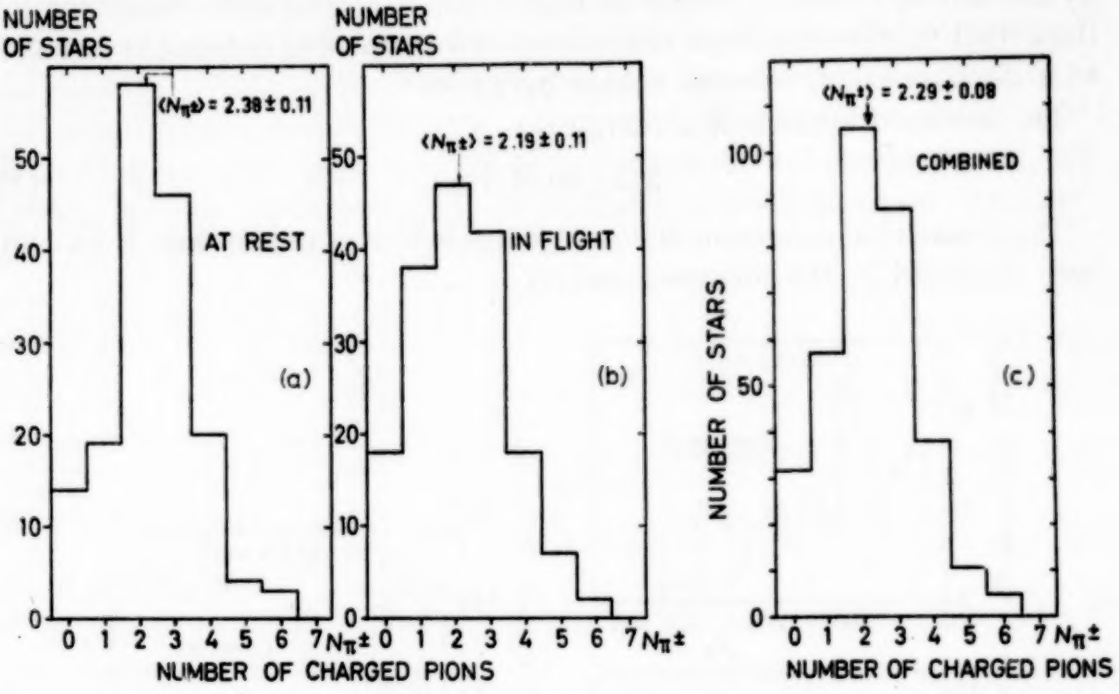

Fig. 6. Charged pion multiplicity distribution from antiproton annihilations a) at rest, b) in flight and c) combined.

The actual numbers are also given in table 4. The $8\,\bar{p}_\rho$ events (group B II in table 1) are included for the events at rest and the 3 proton stars are subtracted for the events in flight.

TABLE 4

The frequency of the number of charged pions per antiproton star (frequencies not corrected for reabsorption of pions)

	Number of charged pions per star							
	0	1	2	3	4	5	6	0—6
No. of stars at rest	14	19	58	46	20	4	3	164
in flight	18	38	47	42	18	7	2	172
combined	32	57	105	88	38	11	5	336

The average number of charged pions is for annihilations

$$\begin{aligned} &\text{at rest:} \quad \langle N_\pi\pm\rangle = 2.38\pm0.11, \\ &\text{in flight:} \quad \langle N_\pi\pm\rangle = 2.19\pm0.11, \\ &\text{combined:} \quad \langle N_\pi\pm\rangle = 2.29\pm0.08. \end{aligned} \tag{3}$$

The total number of pions (at rest and in flight) is 768. The number found within 20 % of the solid angle (162) agrees well with this figure taking into account the solid angle and the angular distributions (at rest and in flight).

In order to obtain an estimate of the true pion multiplicity it is necessary to correct for the experimental loss of pions. The detection efficiency e_π is defined as the ratio of the number of pions found to the true number of pions. In our case it has been estimated to be (Appendix 2).

$$e_\pi = 0.98 \pm 0.02. \tag{4}$$

In subsect. 3.2.3. it is pointed out that we would expect about 1 % electron contamination among tracks counted as pions. This will result in an increased multiplicity. The combined effect of electron contamination and detection efficiency (4) yields a negligible correction to the measured values. Therefore the figures in table 4 and (3) are taken as correct estimates of the true numbers.

The ratio of negative to positive pions in the energy interval 20 MeV $\leqq T_\pi \leqq$ 80 MeV is (fig. 2)

$$\frac{N_{\pi^+}}{N_{\pi^-}} = \frac{34}{53} = 0.64 \pm 0.10. \tag{5}$$

Chamberlain *et al.* [6]) have calculated the ratio one would expect to find in emulsions. They take into account the neutron/proton ratio in emulsion, the interaction cross sections and energy spectra of the positive and negative pions. Their estimated ratio is 0.58, a value based also on the fundamentally important assumption of equal probability for annihilation on neutrons and protons.

The ratio is, however, not very sensitive to changes in the relative importance of annihilation on neutrons. At this stage we therefore limit ourselves to say that our determination is not in disagreement with the assumption of equal probability for annihilation on neutrons and protons (see further subsec. 5.5).

The ratio of zero prong stars due to stopping negative pions to the total number of π^- stars is $20/67 = 0.30 \pm 0.07$, which is in agreement with other experiments. This adds strength to the assertation that the identification of stopping pions is certain.

3.2.3. Electron pairs from the decay of neutral pions.

The number of charged pions seen in the analysed stars is 768. Assuming charge independence we would expect 5 Dalitz pairs from about 385 decaying neutral pions. Only one electron pair has been found. The space angle between the electrons is 2°. One of the electrons disappears in flight after having traversed 26 mm.

It is not surprising if 4 electron pairs have been overlooked. It has only been possible to recognize pairs in the following two cases: (i) If the angle between two minimum tracks from a star is small. Then we suspected a pair and exam-

ined the tracks carefully. (ii) If an electron had a dip angle less than 17° (about 30 % of all tracks) $p\beta$ and g/g_0 were meaured. The identity of the particle is then in principle given, but as regards an electron it is only possible to distinguish electrons from pions for electrons with momentum less than 100 MeV/c.

For Dalitz pairs [7]) about 50 % of the angles between the electrons are larger than 15° and about 70 % are larger than 5° in the C.M.S. of the pion. In transforming the distribution to the laboratory frame of reference one has to consider both the energy spectrum of the neutral pions and the division of the available energy between the electrons. Simple estimations show that the angular distribution in the laboratory system will not be appreciably more peaked towards small separation angles. The result is that we would expect to find about 2 out of 5 Dalitz pairs which is in agreement with our observed single event.

A common feature of antiproton experiments with emulsion [6, 8]) is that the number of Dalitz electron pairs observed is low in comparison with the expected number. This could have been mistaken to imply an abnormally low number of neutral pions produced (i.e. charge independence violated) or an abnormally high reabsorption of neutral pions. However, the discussion above shows, that a special kind of experimental bias is involved. There is no reason to suspect anything abnormal about the neutral pions.

In view of these circumstances there ought to be 8 electrons in our sample recorded as fast pions. This means that the experimental pion multiplicity has to be decreased by about 1 %, as was referred to earlier (subsect. 3.2.2.)

3.3. HEAVY PRONGS

All prongs due to stable particles with mass equal to or larger than the proton mass have been classified as heavy prongs. In the energy determinations they are taken to be protons.

A sample of heavy prongs was selected for careful mass determinations. The prongs selected were required to (i) come to rest in the stack (ii) have a range longer than 8 mm and (iii) have a dip angle less then 17° (30 % of the total solid angle). The group contained 78 tracks. The masses were determined by a combination of range and ionization measurements. The mass distribution is plotted in fig. 7. The result of the measurements is that most of these "knock-on" particles are protons with a probable small admixture of deuterons.

A number of the short prongs are certainly due to deuterons, alpha-particles, etc. If one wants to compute the energy given to heavy prongs the assumption that all prongs are protons leads to a result which has a negligible systematic error.

Fig. 8 shows the percentage of the total available energy which is seen in heavy prongs for annihilations at rest and in flight.

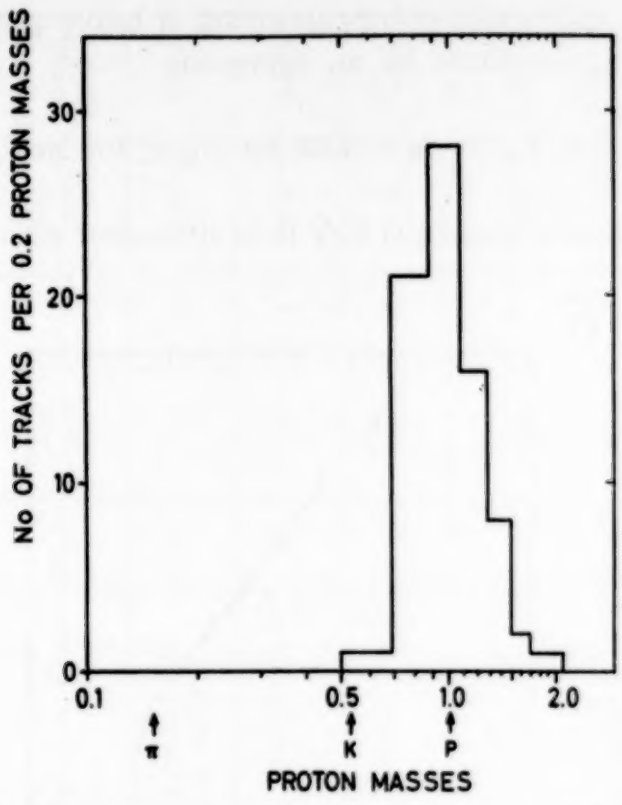

Fig. 7. Mass distribution of stopping heavy particles with range $\geqq 8$ mm and dip $\leqq 17°$.

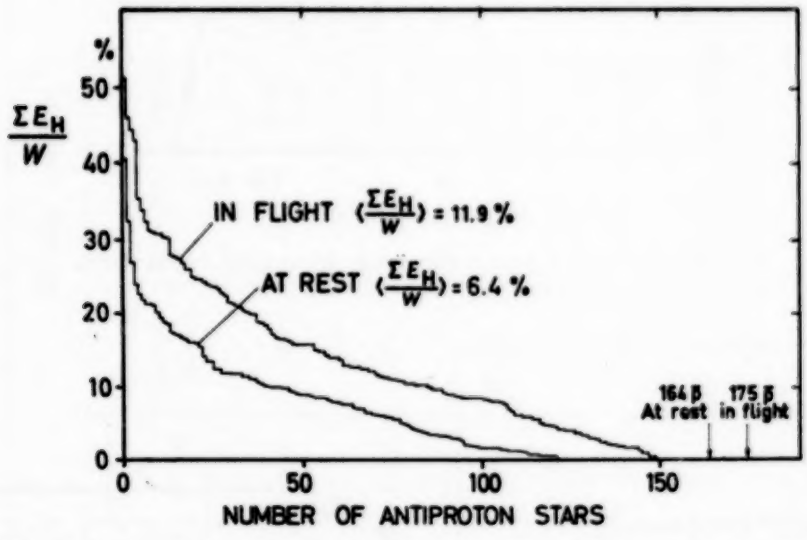

Fig. 8. Percentage of the total available energy W which is seen in heavy prongs.

The mean energy per star of the heavy prongs is for annihilations

$$\begin{aligned} &\text{at rest:} && \langle E_H \rangle = 120 \pm 13 \text{ MeV}, \\ &\text{in flight:} && \langle E_H \rangle = 242 \pm 25 \text{ MeV}, \\ &\text{combined:} && \langle E_H \rangle = 183 \pm 13 \text{ MeV}. \end{aligned} \tag{6}$$

Binding energy is included.

Fig. 9 gives the differential energy spectrum of heavy prongs for all stars. The distribution can be fitted by an expression

$$\frac{dN_H}{dT_H} \propto T_H^{-\alpha} \quad (\alpha = 1.22 \text{ for } T_H < 100 \text{ MeV}). \tag{7}$$

The change in slope at about 100 MeV is in agreement with the results of the

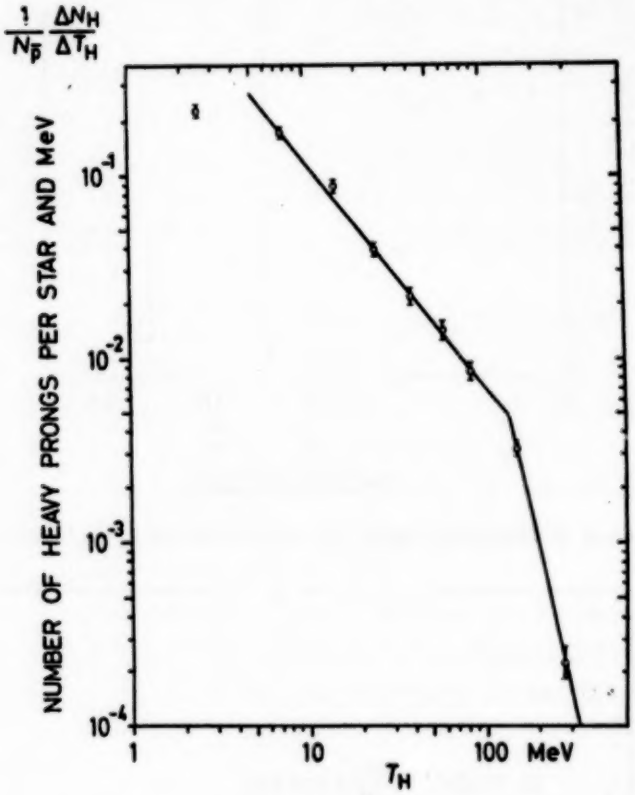

Fig. 9. The heavy prong spectrum from antiproton stars.

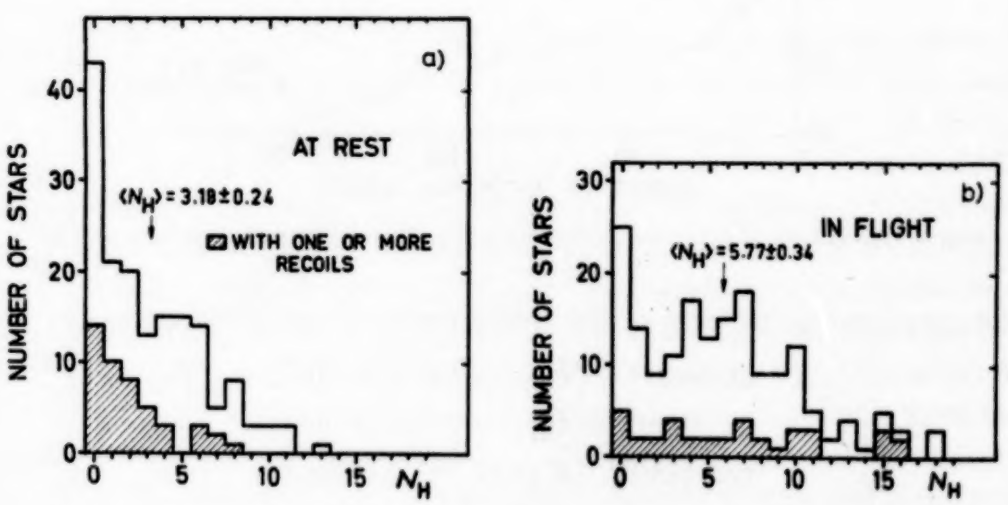

Fig. 10. The heavy prong distribution from antiproton stars a) at rest, b) in flight.

TABLE 5

Antiproton annihilation stars with charged strange particles

$\bar{P}$	$T_{\bar{P}}$ (MeV)	Strange particle					Parent star				
		Dipangle (degrees)	Observed range (mm)	Kinetic energy (MeV)	Identity	Terminal behaviour. Comments	$N_{\pi\pm}$	$\Sigma E_{\pi\pm}$ (MeV)	N_H	ΣE_H (MeV)	Total vis. energy (MeV)
6—58 (2)	188	42	8.3	59	K±	Decay in flight or nuclear reaction. Identification certain.	0	0	4	210	1423
6—58 (5)	188	73	62.9	166	K?	Leaves the stack. Identification uncertain.	0	0	4	210	1423
6—100	0	10	67.6	121	K^+	Decay at rest. $K^+_{\pi_2}$-mode. Identification certain.	3	802	2	74	1491
6—175	96	16	3.6	54	${}_{\Lambda}H^4$	Decay at rest. Details of this event have already been published [9])	1	158	9	559	979
6—295	58	20	7.4	39	K?	Leaves the stack. Identification uncertain.	1	382	5	523	1438
6—345	0	0	0.86	10	K^-	K^--absorption star at rest with 2 prongs. Identification certain.	3	>700	0	0	>1200

Berkeley group [6]), while the Rome group [8]) does not find any change for annihilations at rest. We investigated the data at rest and in flight separately but the results were the same in both cases.

The heavy prong distribution is given in fig. 10. The stars which have additional blobs, i.e. tracks shorter than 5 μm are shaded.

The mean number of heavy prongs is for annihilations

$$\begin{aligned} &\text{at rest:} && \langle N_H \rangle = 3.18 \pm 0.24, \\ &\text{in flight:} && \langle N_H \rangle = 5.77 \pm 0.34, \\ &\text{combined:} && \langle N_H \rangle = 4.51 \pm 0.22. \end{aligned} \tag{8}$$

3.4. STARS WITH CHARGED STRANGE PARTICLES

3.4.1. Details of the events

The information on the 5 events containing charged strange particles (table 1, column D I and III) is collected in table 5.

The events will now be discussed in more detail.

Event no. $\bar{P}-6-58$

The annihilation star consists of 6 prongs of which 4 are stable heavy prongs and 2 very probably due to a K^+K^--pair. One of the K-mesons is definite. It travels 8.3 mm in emulsion and gives in flight rise to a secondary track with

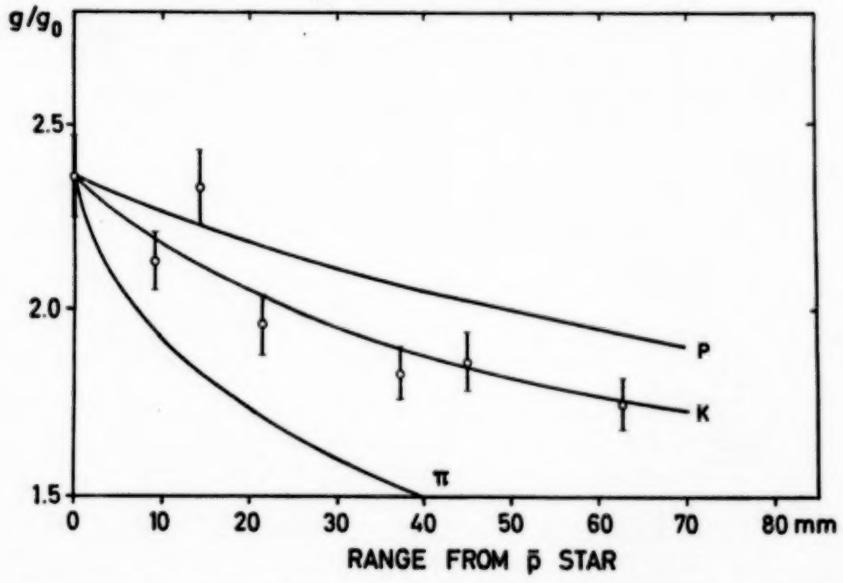

Fig. 11. Ionization vs range for track 5, star $\bar{p}-6-58$. The curves are normalized to the g/g_0-value at the point of disappearance from the stack of track 5.

$g/g_0 = 1.86 \pm 0.22$ corresponding to a pion with energy 42^{+11}_{-8} MeV or a proton with energy 280 ± 50 MeV. On the basis of measurements on the primary track one cannot with certainty establish its identity as a K-meson. The kinematics

of the whole event excludes, however, every interpretation of the primary prong except the K-meson interpretation. Thus we conclude that the track is consistent with a charged K-meson which undergoes a nuclear reaction or decays according to the $K'_{\pi 3}$-mode.

The other possible K-meson track is emitted with a dip angle of 73° and leaves the stack after 62.9 mm. Change of grain density versus range indicates a K-meson. Measurements are displayed in fig. 11. We do not claim, however, to be able to identify a track of 73° dip with certainty. Therefore, the identity is recorded as uncertain in table 5.

Event no. $\bar{P}-6-100$

The K-meson has a dip angle of 10° and goes 67.6 mm before it decays at rest. The secondary track has a dip of 25° and leaves the stack after 69.9 mm. Assuming it to be a pion, ionization measurement gives an energy of 107 ± 3 MeV. This is consistent with the unique pion energy of 108 MeV in the $K^+_{\pi 2}$ mode of decay. Other possibilities, for instance $K^+_{\mu 3}$ or a K^- interacting with a nucleus to give a pion (which by chance fits the $K^+_{\pi 2}$ kinematics) cannot be excluded, but are less likely.

Event no. $\bar{P}-6-175$

The antiproton star consists of 9 heavy prongs, one pion and one hyperfragment. Details of this event have been published in a separate paper [9]). A complete analysis shows that the unstable heavy prong is a ${}_{\Lambda}H^4$-fragment undergoing mesonic two-body decay, ${}_{\Lambda}H^4 \rightarrow \pi^- + He^4$.

Event no. $\bar{P}-6-295$

The K-meson track leaves the stack after 7.4 mm at a dip angle of 20°. Mass determination has been difficult because the track is located at the edge of the stack, where the distortion is considerable. The distortion has been checked by scattering measurements on beam pions in the actual region of the stack. In spite of this procedure we prefer to consider this K-meson as not quite certain.

Event no. $\bar{P}-6-345$

The K^--meson is brought to rest after 0.86 mm and gives rise to an absorption star. The absorption star consists of one negative pion and one heavy prong. A mass determination by the constant sagitta method excludes the interpretation of the event as being due to a hyperfragment. The other three tracks in the parent antiproton star were due to pions and no accompanying K^+ could be found.

3.4.2. Conservation of strangeness

The conservation of strangeness has not been positively proved in any of our events. In the first event of table 5, strangeness may very well be conserved, there being two charged K-mesons. In some other cases one may assume that the observed charged K-meson is accompanied by an unobserved neutral K-meson. In two of the events (events 6—100 and 6—295) the missing energy is, however, not sufficient for another K-meson. The missing energy being 377 MeV and 488 MeV, respectively. The conservation of strangeness requires that the observed unit of strangeness is balanced by another unobserved unit. In the cases with insufficient energy one may assume that the other strangeness unit was carried by a K-meson which was reabsorbed or by a neutral hyperon which escapes detection in emulsion. For this to be possible it is necessary that the observed strange particle carried a positive unit of strangeness. It is satisfactory to note that such is the case in event 6—100, where the K-meson was identified with positive charge.

3.4.3. Evaluation of the relative abundance of K*-meson pairs and the average energy going into* K*-meson production*

It is in many respects a difficult problem to deduce the percentage of annihilation stars containing $K\bar{K}$-pairs in a proper way. The number of K-mesons is small and large corrections have to be made.

The most important correction is for the number of $K\bar{K}$-pairs not seen in emulsion. Negative K-mesons may be reabsorbed by the nucleus and neutral K-mesons are in general not detected. By assuming charge independence the probabilities for different charge states $K^+\bar{K}^0$, K^+K^-, $K^0\bar{K}^0$ and K^0K^- with 0, 1, 2, or 3 pions can be calculated (subsect. 5.6.2). Given the probabilities for $K\bar{K}+n\pi$ for different numbers of pions (n) from a statistical theory, the frequencies in emulsion can be obtained. The result for the Fermi theory with the interaction volume $\Omega = 10\Omega_0$ is given in table 6. ($\Omega_0 = (4\pi/3)(\hbar/m_\pi c)^3$ where m_π is the mass of the pion).

TABLE 6

Probabilities of different charge configurations for $K\bar{K}$-pairs in nuclear emulsion. Calculations made on the basis of a Fermi statistical theory (with $\Omega = 10\Omega_0$)

Charge state	Frequency
$K^+\bar{K}^0$	16 %
K^+K^-	27 %
$K^0\bar{K}^0$	27 %
K^0K^-	30 %

The charged state frequencies are very stable for any reasonable relative

strength of the isospin $T = 0$ and $T = 1$ interaction channels and for variations of the interaction volume between $10\Omega_0$ and $20\Omega_0$. They differ only by one or two units in different cases.

$K^0\bar{K}^0$-pairs will escape detection in emulsion. Moreover, about 44 % of the K^- mesons will be reabsorbed. This percentage has been obtained by using eq. (35) and the value $R/\lambda = 4.55$ for the inverse mean free path of the K^--meson in nuclear matter [10]). The $K\bar{K}$-pairs not detectable in emulsion thus constitutes 40 % (=27 %+0.44×30 %). This estimate differs appreciably from the value 24 % used in analysing previous experiments [6]).

In order to estimate the percentage of $K\bar{K}$-pairs in antiproton stars the following procedure has been used. In 30 % of the total solid angle (dip $\leqq 17°$) all tracks with range of more than 8 mm have been identified, except for particles heavier than the proton, in which case the mass resolution was not sufficient. See figs. 1 and 7, and subsect. 3.2.1. One K^+-meson (event $\bar{P}-6-100$) was found in this sample.

The situation for particles with $\beta \leqq 17°$ and range less than 8 mm is not so clear. Measurements permit only a separation of pions and protons. Thus K^- giving rise to zero prong stars (K_ρ^-) and K^+ with a minimum ionizing secondary might be missed. In this group we found one K^- (event $\bar{P}-6-345$). It was identified on account of its absorption star. The fraction of K_ρ^- is known to be about 15 %. The number of negative K-mesons in the range interval should then be corrected by this figure. Within 30 % of the total solid angle 2 antiproton stars with K-mesons have been found. This means that 3 ± 2 % of the antiproton stars emit $K\bar{K}$-pairs.

We can also calculate the average energy per annihilation star which goes into K-mesons $\langle E_{K\bar{K}} \rangle$. In this experiment the average total energy of an emitted K-meson is $\langle E_K \rangle = 560\pm55$ MeV. Thus $\langle E_{K\bar{K}} \rangle = 33\pm22$ MeV. Only the certain K-mesons have here been included. This means that the estimate is slightly biassed. The probability for a K-meson to leave the stack increases with energy and a high energy K-meson is therefore more likely to be included in the category of uncertain events or to escape detection.

The results of this section are summarized below:

$$\begin{aligned} &\text{abundance of } K\bar{K}\text{-pairs } \langle N'_{K\bar{K}} \rangle = 3\pm2\ \%, \\ &\langle E_{K\bar{K}} \rangle = 33\pm22 \text{ MeV per antiproton star,} \\ &\text{percentage of K-meson pairs not detectable in emulsion is } 40\ \%. \end{aligned} \tag{9}$$

3.4.4. Hyperons and hyperfragments

The creation of hyperons is energetically possible in the annihilation process. However, so far only two definite cases of hyperons from antiproton stars in

emulsion have been reported. We have one case of a Λ^0 bound in a ${}_{\Lambda}H^4$-fragment. The Rome group [8]) has one definite case of Σ^-.

It is impossible to decide in these cases if the hyperon is produced in the primary process or if it is due to the secondary reaction

$$\bar{K}+N \rightarrow Y+\pi, \tag{10}$$

where N denotes a nucleon, Y a hyperon and the $\bar{K}$ is coming from a directly produced $K\bar{K}$-pair.

If the hyperon is primarily produced, because of baryon conservation, it must have been created in a two-nucleon absorption process

$$\bar{p}+N+N \rightarrow Y+K+n\pi. \tag{11}$$

4. Comparison with Other Experimental Data

4.1. PIONS AND HEAVY PRONGS

The main experiments on antiproton annihilations in nuclear emulsion have been done in Berkeley [6, 11]), Rome [8]), Saclay [12]) and Uppsala. The group at Oxford [13]) has not published a complete analysis of its events. There are also results based on less statistics from other laboratories [14, 15]).

For easy reference the main experimental quantities obtained by different groups are collected in table 7.

The combined values have been computed by taking the weighted average of the results from the different laboratories. The weight is the inverse square of the standard deviation stated by the respective authors.

The values of $\langle N_{\pi^\pm} \rangle$ are the measured values and do not include correction for detection efficiency. Apart from this, the experimental data can be directly compared. There is a fairly good overall agreement. No measurement deviates by more than about two standard deviations from the combined mean. All values are therefore compatible from a statistical point of view.

4.2. STRANGE PARTICLES

The experimental information from different laboratories on antiproton annihilations in emulsion with strange particles emitted is collected in tables 8 and 5.

Much more experimental work is needed before one can speak about any reliable data for annihilation stars containing strange particles. It is very difficult to obtain unbiassed identifications and energy distribution of the K-mesons. Each laboratory has tried to arrive at unbiassed results using various techniques. We have collected the results and applied our new estimate of 40 % for the fraction of K-meson pairs escaping detection, instead of the previously used figure (24 %). As explained in subsect. 3.4.3 we believe the earlier figure to be

TABLE 7

Summary of main experimental results concerning pions and heavy prongs

		Group				Combined [f]
		Uppsala	Berkeley	Rome	Saclay	
$N_{\bar{p}}$ [a]	a.r. [b]	175	126	349	104	754
	i.f.	183	95	304	101	683
$\langle T_{\bar{p}} \rangle$ MeV	i.f.	166	141	150	156	154
$\langle N_{\pi^\pm} \rangle$ [c]	a.r.	2.38± 0.11	2.50± 0.26	2.46± 0.14	2.54± 0.17	2.44± 0.07
	i.f.	2.19± 0.11	2.30± 0.28	2.18± 0.13	2.22± 0.17	2.20± 0.07
$\langle N_H \rangle$	a.r.	3.18± 0.24	3.33± 0.34	3.42± 0.19	3.22± 0.20	3.29± 0.11
	i.f.	5.77± 0.34	5.09± 0.60	4.80± 0.40	5.66± 0.28	5.46± 0.18
$\langle E_{\pi^\pm} \rangle$ MeV	a.r.	365 ±17	324 ±21	379 ±12	366 ±21	365 ± 8
	i.f. [d]	355 ±20	361 ±30	370 ±17	324 ±24	356 ±11
$\langle \Sigma E_H \rangle$ MeV	a.r.	120 ±13	144 ±15	121 ±10	140 ±13	129 ± 6
	i.f.	242 ±25	220 ±26	173 ±22	263 ±27	220 ±12
N_{π^+}/N_{π^-}; $20 \leqq T_\pi \leqq 80$ MeV		0.64± 0.10	0.45± 0.12	0.73± 0.20	0.66± 0.18 [e]	0.59± 0.07
e_π		0.98± 0.02	0.90± 0.10	0.93± 0.03		
Number of $\bar{p}_\rho$ per star		5 ± 2 %	2 $^{+3}_{-2}$ %	2.2%	4 %	

[a]) According to the criteria followed when analysing the stars, a few of them are not included at different stages of the analysis. We have included possible $\bar{p}_\rho$-events while the other groups have excluded them with the argument that they are uncertain. The Berkeley and the Rome groups have a small contamination of charge-exchange scatterings and proton stars in their statistics. We have, when possible, made corrections for these effects. The Saclay group has excluded all events with visible energy less than the kinetic energy of the antiproton in their calculations.

[b]) a.r. (at rest), i.f. (in flight).

[c]) Uncorrected for scanning efficiency.

[d]) $\langle E_\pi \rangle$ in flight is the value stated by the respective authors. In case the geometrical correction (sect. 3.2.1) has not been taken into account the energies should be decreased by about 20 MeV.

[e]) This figure probably includes some pions with kinetic energy less than 20 MeV.

[f]) The combined values are the weighted averages of the results of the different laboratories.

TABLE 8

Strange particles in antiproton annihilation stars analysed in Berkeley, Rome, Oxford and Saclay (See table 5 for the Uppsala events).

Group	$\bar{p}$	$T_{\bar{p}}$ (MeV)	Strange particle					Parent star				
			Dip. angle (degr.)	Obs. range (mm)	Kinetic energy (MeV)	Ident.	Terminal behaviour. Comments	$N_{\pi^\pm}$	$\Sigma E_{\pi^\pm}$ (MeV)	N_H	ΣE_H (MeV)	Tot. vis. energy (MeV)
B	3 —3	183	15	24.7	80	K	Disappears in flight. Definite K					
B	3 —25		30	53	104	K^+	Decay at rest. Definite K					
B	3s—59		29	83	235	K	Leaves the stack. Definite K					
B	3s—83		23	40	355	K?	Leaves the stack. Uncertain ident.					
B	3 —7	152	19	35	260	K?	Leaves the stack. Uncertain ident.					
B	2 —3	90	44	19	175	K?	Leaves the stack. Uncertain ident.					
B	3s—3		74	78	120	K?	Comes to rest. Nothing at end. Uncertain					
B	3s—71		67	15	102	K?	Star in flight. Uncertain ident.					
B	3s—86		64	17	195	K?	Star in flight. Uncertain ident.					
B	3 —3	183	74	40	195	K?	Leaves the stack. Uncertain ident.					
B			6	42	245	Σ?	Uncertain					
B					250	Σ^+?	Uncertain					
R	208	0	21	68.5	118	K^-	Star at rest with 2 prongs. Definite K	2	>280	1	>100	>991
R	96	0	45	8.5	36	K^+	Decay with a min. track. Definite K	0		3	105	634
R	143	0	6	63.7	105	K^-	Star at rest with 3 prongs. Definite K	0		2+(1)	>158	>756
R	462	0	45	57.0	205	Σ^-	Decay in flight. Definite Σ	0		2+(1)	>195	>659
R	48	205	27	4.4	25	K^-	Star at rest with 2 prongs. Definite K	0		0		>1057
R	48	205	49	45.0	45	K^+	Decay with a min. prong. Definite K	0		0		>1057
0					148	K^-	Capture star	3				
0					152	K^-	K_ρ close to surface	1				
0					115	K^+	Decay at rest	1				
0					215	$K^\pm$	Leaves the stack	1				
0					295	$K^\pm$	Interacts at surface	0				
0					280	$K^\pm$	Leaves the stack	2				
S	$\bar{p}_{13}$	0	6	0.6	8	K^+	Decay at rest	2	>476	4	>140	>1118
S	$\bar{p}_{79}$	0	32	36	83	K^+	Decat at rest	0		1	>104	>681
S	$\bar{p}_{132}$	0	5.5	76	≈220	$K^\pm$	Leaves the stack	0		0		714
S	$\bar{p}_{152}$	0	9.5	14.6	49	K^+	Decay at rest	1	>220	3	111	>873
S	$\bar{p}_{177}$	0	36	10	39	K^+	Decay at rest	0		5	172	705
S	$\bar{p}_{61}$	215	4.5	15	≈72	K?	Uncertain	0		11	422	988
S	$\bar{p}_{262}$	186	8	90	142	K^+	Decay at rest	3	>583	7	130	>1349
S	$\bar{p}_{234}$	0	25	0.06	?	K^-	Interaction in flight. 3-prong star	2	>395	2	36	>925
S	$\bar{p}_{245}$	0	27	1.38	94	K^+	Decay in flight	2	>400	0		>1495
S	$\bar{p}_{249}$	0	6	1.40	13	K^-	Interaction at rest. 1-prong star	2	>400	0		>1495

in error. It is then possible to deduce the abundance of $K\bar{K}$-pairs as well as $\langle E_{K\bar{K}} \rangle$ for each laboratory. The figures are given in table 9.

TABLE 9

Percentage of annihilation stars with K-meson pairs and average energy per star going into K-mesons [a])

Laboratory	Berkeley	Rome	Saclay	Oxford	Uppsala	Combined [b])
$\langle N'_{K\bar{K}} \rangle$ (%)	4.4± 1.9	5.1± 2.5	7.7± 2.7	13.3± 5.8	3.0± 2.0	5.0± 1.1
$\langle E_{K\bar{K}} \rangle$ (MeV)	56 ±24	57 ±29	87 ±32	185 ±73	33 ±22	57 ±13

[a]) The correction for events escaping detection is discussed in the text.
[b]) The combined average is the weighted mean of the different values.

5. Annihilation into Pions

5.1. CONSEQUENCES OF ENERGY CONSERVATION

We assume that the sample of antiproton stars in table 1, B I—IV, is drawn from a population where the primary process is

$$\bar{p}+N \rightarrow N'_{\pi}\pi+N'_{K\bar{K}}K\bar{K}. \tag{12}$$

Here, N stands for nucleon, N'_{π} is the number of primarily produced pions, $N'_{K\bar{K}}$ the number of primarily produced K-meson pairs.

The observable process in emulsion is, in principle,

$$\bar{p}+{}^{A}_{Z}X \rightarrow {}^{A'}_{Z'}X+N_{\pi}\pi+N_{K\bar{K}}K\bar{K}+N_{p}p+N_{n}n, \tag{13}$$

where emission of only protons and neutrons from the nucleus is assumed. In formula (13), ${}^{A}_{Z}X$ is the capturing nucleus in emulsion, N_{π} the number of pions outside the nucleus, $N_{K\bar{K}}$ the number of $K\bar{K}$-pairs outside the nucleus, N_{p} the number of protons emitted (can also be taken to include deuterons, α-particles etc.) and N_{n} the number of neutrons emitted.

Energy balance between the initial and final state gives

$$E_{\bar{p}}+E_{X} = E_{X'}+\sum E_{\pi}+\sum E_{K\bar{K}}+\sum E_{p}+\sum E_{n}, \tag{14}$$

where E denotes total energies in the laboratory system.

Assuming that the binding energies of the nucleons are equal, $E_{B}(p) = E_{B}(n) = E_{B}$, this equation can be rewritten as

$$W = \sum E_{\pi}+\sum E_{K\bar{K}}+U, \tag{15}$$

where

$$W = m_{\bar{p}}+m_{N}-E_{B}+T_{\bar{p}} = \sum E'_{\pi}+\sum E'_{K\bar{K}}, \tag{16}$$

$$U = \sum(T_{p}+E_{B})+\sum(T_{n}+E_{B}). \tag{17}$$

Further, W is the total energy available in the annihilation process for creation of pions and K-mesons, U the energy carried away by nucleons. E' denotes total energies inside the nucleus and T kinetic energies outside the nucleus. The residual nucleus is assumed to be in its ground state.

Eq. (15) expresses the conservation of energy in the process (13). When many processes (13) are observed with emission of different numbers of particles, average values over the processes are introduced and we will in the following use:

$$W = \langle \sum E_\pi \rangle + \langle \sum E_{K\bar{K}} \rangle + \langle U \rangle = \langle \sum E'_\pi \rangle + \langle \sum E'_{K\bar{K}} \rangle. \tag{18}$$

5.1.1. Excitation energy

In order to proceed further and arrive at the average primary pion multiplicity and energy it is necessary to make more assumptions and appeal to other experiments. We follow the procedure introduced by the Berkeley group [6]) and refer to this paper for detailed discussion. The following quantities are introduced:

the average number ν of interacting pions (absorbed or inelastically scattered),

the fraction a of the interacting pions which are absorbed.

Then,

$$\left.\begin{aligned} &a\nu = \text{the number of pions absorbed,} \\ &(1-a)\ \nu = \text{the number of pions inelastically scattered,} \\ &E_0 = \text{the average energy of the inelastically scattered pions.} \end{aligned}\right\} \tag{19}$$

The new assumption is then that the energy given to the nucleons equals the energy lost by the pions

$$\langle U \rangle = a\nu\{\langle E'_\pi \rangle + \omega_0\} + (1-a)\nu\{\langle E'_\pi \rangle + \omega_0 - E_0\}$$

or

$$\langle U \rangle = \nu\{\langle E'_\pi \rangle + \omega_0 - (1-a)E_0\}. \tag{20}$$

ω_0 is a constant which takes into account the energy dependence of the pion cross section.

Further

$$\langle \sum E_\pi \rangle = \langle N_\pi \rangle \langle E_\pi \rangle, \quad \langle \sum E'_\pi \rangle = \langle N'_\pi \rangle \langle E'_\pi \rangle. \tag{21}$$

The constant ρ is defined by the relation

$$\langle N_\pi \rangle = \rho \langle N_{\pi^\pm} \rangle. \tag{22}$$

It is further assumed that charge independence holds in the process (12). Then

$$\langle E_\pi \rangle = \langle E_{\pi^\pm} \rangle = \langle E_{\pi^0} \rangle \quad \text{and} \quad \rho = 1.5. \tag{23}$$

5.1.2. Best fit average values of the primary pion multiplicity and energy, the number of interacting pions and the energy given to the nucleus.

If a and E_0 are known, we are still left with 4 unknown quantities, namely $\langle N'_\pi \rangle$, $\langle E'_\pi \rangle$, ν and $\langle U \rangle$ and 3 eqs., viz. (20) and (18). Eq. (18), in fact, acts as two equations because the energy conservation can be written down in terms of primary or in terms of secondary quantities.

More relations are needed and from other experiments it is known that $\nu = \langle N_H \rangle / n_H$ and $\langle U \rangle = h \langle E_H \rangle$, where $n_H = 2.5$ and $h = 2.7$.

We are now able to write down the following system of equations:

$$
\begin{aligned}
f_1 &= \nu - \langle N_H \rangle / n_H = 0, \\
f_2 &= \langle U \rangle - h \langle \textstyle\sum E_H \rangle = 0, \\
f_3 &= \langle U \rangle - \nu \{ \langle E'_\pi \rangle + \omega_0 - (1-a) E_0 \} = 0, \\
f_4 &= \langle N'_\pi \rangle \langle E'_\pi \rangle - W + \langle \textstyle\sum E_{K\bar{K}} \rangle = 0, \\
f_5 &= (\langle N'_\pi \rangle - a\nu) \langle E_{\pi^\pm} \rangle - (\langle E'_\pi \rangle - \omega)(\langle N'_\pi \rangle - \nu) - (1-a)\nu E_0 = 0, \\
f_6 &= \langle N'_\pi \rangle - a\nu - \frac{1.5}{e_\pi} \langle N_{\pi^\pm} \rangle = 0.
\end{aligned}
\tag{24}
$$

f_1 and f_2 are empirical relations; f_3 is eq. (20), f_4 and f_5 are obtained from (18) by means of a little manipulation, and f_6 comes from the use of eqs. (21) and (22). The assumption (23) has been made. In eqs. (24) we used

$$
\omega = \omega_0 \frac{\nu}{\langle N'_\pi \rangle - \nu}. \tag{25}
$$

The system (24) consists of 6 equations connecting 4 unknown quantities. In previous works [6, 12]) the procedure has been to obtain $\langle N'_\pi \rangle$ etc. from the first five equations by some "best fit" method. The quantity ρ is then decuced from the last equation as a check of the consistency of the approach.

We think it is more appropriate to include the last equation (f_6) when one wants to obtain the "best fit" solution of the system. The best fit solution is defined by the condition

$$
\sum_{i=1}^{6} p_i f_i^2 = \text{minimum}, \tag{26}
$$

where p_i is the weight to be attached to the equation f_i.

The best fit method is further discussed in Appendix 3.

The input data are collected in table 10.

The value of E_0 differs from the value $E_0 = 215 \pm 15$ MeV previously used [6]). Interactions of 560 MeV negative pions with emulsion nuclei have been investigated in this laboratory [16]). The average energy of the inelastically scattered pions was found to be higher than that measured by M. Blau *et al.* [17])

at 500 MeV primary energy. The new value of E_0 is obtained by taking our result and the result of Belovitskii [18]) at 300 MeV into account.

TABLE 10

Input data used for the best fit values (energies in MeV)

From other experiments	From this experiment		
	Quantity	at rest	in flight
$n_H = 2.5 \pm 0.2$	$\langle N_H \rangle$	3.18 ± 0.24	5.77 ± 0.34
$h = 2.7 \pm 0.2$	$\langle \Sigma E_H \rangle$	120 ± 13	242 ± 25
$a = 0.75 \pm 0.03$	W	1868	2034
$E_0 = 235 \pm 15$	$\langle \Sigma E_{K\bar{K}} \rangle$	40 ± 10	40 ± 10
$\omega_0 = 14 \pm 5$	$\langle E_{\pi^\pm} \rangle$	365 ± 17	355 ± 20
$\omega = 6 \pm 2$	$\langle N_{\pi^\pm} \rangle$	2.38 ± 0.11	2.19 ± 0.11

Our best fit method has also been applied to the data measured by other groups as well as to the combined world averages (table 7).

The values of the derived quantities $\langle N'_\pi \rangle$, $\langle E'_\pi \rangle$, ν and $\langle U \rangle$ are given in table 11.

TABLE 11

Best fit solution. $\langle N'_\pi \rangle$ is the average primary pion multiplicity, $\langle E'_\pi \rangle$ the average primary pion total energy, ν the average number of interacting pions, $\langle U \rangle$ the average energy given to the nucleus

Quantity		Laboratory				Combined [c])
		Uppsala	Berkeley [b])	Rome [b])	Saclay [b])	
$\langle N'_\pi \rangle$	a.r. [a])	4.68 ± 0.12	5.34	4.71	4.82	4.77 ± 0.09
	i.f. [d])	5.11 ± 0.12	5.24	4.97	5.32	5.12 ± 0.15
$\langle E'_\pi \rangle$	a.r.	391 ± 10	340	386	376	380 ± 7
(MeV)	i.f.	390 ± 9	373	395	370	384 ± 11
ν	a.r.	1.13 ± 0.11	1.33	1.11	1.22	1.16 ± 0.08
	i.f.	2.19 ± 0.17	1.90	1.66	2.38	2.01 ± 0.14
$\langle U \rangle$	a.r.	386 ± 34	392	376	403	385 ± 19
(MeV)	i.f.	750 ± 42	624	576	747	673 ± 41

[a]) a.r. (at rest), i.f. (in flight)

[b]) calculated by our best fit method

[c]) calculated by means of the combined values in table 7 (last column)

[d]) if 20 MeV is subtracted from $\langle E_{\pi^\pm} \rangle_{\text{i.f.}}$ in the Berkeley, Rome, and Saclay data the effect is that the values should be replaced by $\langle N'_\pi \rangle + 0.1$, $\langle E'_\pi \rangle - 10$ and $\nu + 0.1$. $\langle U \rangle$ is almost unaffected. See table 7, note [d]), for comments.

The errors are statistical ones arising from the errors in the input values. They have been obtained by the following Monte Carlo method. Each input value C_k with its standard deviation is known. The C_k's were assumed to be independent and to have a Gaussian distribution (with the experimentally obtained mean and corresponding s.d. in each case). Six equally probable values of C_k were chosen and numbered from 1 to 6. By throwing a die, carefully tested for randomness, 12 times, a random set of the 12 input values was obtained. These input quantities are $\langle N_H \rangle$, n_H, h, $\langle \sum E_H \rangle$, ω_0, a, E_0, W, $\langle \sum E_{K\bar{K}} \rangle$, $\langle E_{\pi^\pm} \rangle$, e_π, and $\langle N_{\pi^\pm} \rangle$. In all, 80 sets were simulated (Uppsala a.r. and i.f., combined a.r. and i.f., each consisting of 20 sets). The errors indicated in table 11 are the standard deviations of the derived distributions. The mean values of these distributions, and the derived values calculated by means of the experimental average values directly, agreed well.

All calculations were done on an electronic computer, Facit EDB.

The distribution of N'_π for our data at rest is shown in fig. 12 as an example.

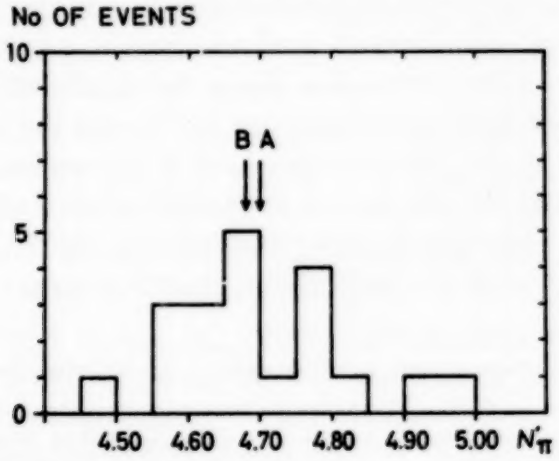

Fig. 12. The distribution of N'_π at rest obtained by a Monte Carlo method. *A*. $\langle N'_\pi \rangle = 4.70$ is the mean of the distribution. The standard deviation = 0.12. *B*. $\langle N'_\pi \rangle = 4.68$ was obtained directly from the input values.

5.1.3. Discussion

The results of subsect. 5.1.2 are based on the main assumptions (i) that only pions and K-mesons are emitted in the annihilation of the antiproton, (ii) that the energy given to the nucleons can be written in the form (20), and (iii) that charge independence holds in the reactions. Apart from this some empirical relations had to be introduced.

The values for the Berkeley set of data agree well with the values derived in ref. [6]). A slight difference can be expected since we have imposed the condition $\rho = 1.5$. The Rome data [8]) were not treated in this way earlier. As regards the Saclay data [12]) our results do not agree with the "best fit" values derived in the reference.

at 500 MeV primary energy. The new value of E_0 is obtained by taking our result and the result of Belovitskii [18]) at 300 MeV into account.

TABLE 10

Input data used for the best fit values (energies in MeV)

From other experiments	From this experiment		
	Quantity	at rest	in flight
n_H = 2.5 ± 0.2	$\langle N_H \rangle$	3.18± 0.24	5.77± 0.34
h = 2.7 ± 0.2	$\langle \Sigma E_H \rangle$	120 ±13	242 ±25
a = 0.75± 0.03	W	1868	2034 ± 5
E_0 = 235 ±15	$\langle \Sigma E_{K\bar{K}} \rangle$	40 ±10	40 ±10
ω_0 = 14 ± 5	$\langle E_{\pi^\pm} \rangle$	365 ±17	355 ±20
ω = 6 ± 2	$\langle N_{\pi^\pm} \rangle$	2.38± 0.11	2.19± 0.11

Our best fit method has also been applied to the data measured by other groups as well as to the combined world averages (table 7).

The values of the derived quantities $\langle N'_\pi \rangle$, $\langle E'_\pi \rangle$, ν and $\langle U \rangle$ are given in table 11.

TABLE 11

Best fit solution. $\langle N'_\pi \rangle$ is the average primary pion multiplicity, $\langle E'_\pi \rangle$ the average primary pion total energy, ν the average number of interacting pions, $\langle U \rangle$ the average energy given to the nucleus

Quantity		Laboratory				Combined [c])
		Uppsala	Berkeley [b])	Rome [b])	Saclay [b])	
$\langle N'_\pi \rangle$	a.r. [a])	4.68± 0.12	5.34	4.71	4.82	4.77± 0.09
	i.f. [d])	5.11± 0.12	5.24	4.97	5.32	5.12± 0.15
$\langle E'_\pi \rangle$ (MeV)	a.r.	391 ±10	340	386	376	380 ± 7
	i.f.	390 ± 9	373	395	370	384 ±11
ν	a.r.	1.13± 0.11	1.33	1.11	1.22	1.16± 0.08
	i.f.	2.19± 0.17	1.90	1.66	2.38	2.01± 0.14
$\langle U \rangle$ (MeV)	a.r.	386 ±34	392	376	403	385 ±19
	i.f.	750 ±42	624	576	747	673 ±41

[a]) a.r. (at rest), i.f. (in flight)

[b]) calculated by our best fit method

[c]) calculated by means of the combined values in table 7 (last column)

[d]) if 20 MeV is subtracted from $\langle E_{\pi^\pm} \rangle_{\text{i.f.}}$ in the Berkeley, Rome, and Saclay data the effect is that the values should be replaced by $\langle N'_\pi \rangle + 0.1$, $\langle E'_\pi \rangle - 10$ and $\nu + 0.1$. $\langle U \rangle$ is almost unaffected. See table 7, note [d]), for comments.

The errors are statistical ones arising from the errors in the input values. They have been obtained by the following Monte Carlo method. Each input value C_k with its standard deviation is known. The C_k's were assumed to be independent and to have a Gaussian distribution (with the experimentally obtained mean and corresponding s.d. in each case). Six equally probable values of C_k were chosen and numbered from 1 to 6. By throwing a die, carefully tested for randomness, 12 times, a random set of the 12 input values was obtained. These input quantities are $\langle N_H \rangle$, n_H, h, $\langle \sum E_H \rangle$, ω_0, a, E_0, W, $\langle \sum E_{K\bar{K}} \rangle$, $\langle E_{\pi^\pm} \rangle$, e_π, and $\langle N_{\pi^\pm} \rangle$. In all, 80 sets were simulated (Uppsala a.r. and i.f., combined a.r. and i.f., each consisting of 20 sets). The errors indicated in table 11 are the standard deviations of the derived distributions. The mean values of these distributions, and the derived values calculated by means of the experimental average values directly, agreed well.

All calculations were done on an electronic computer, Facit EDB.

The distribution of N'_π for our data at rest is shown in fig. 12 as an example.

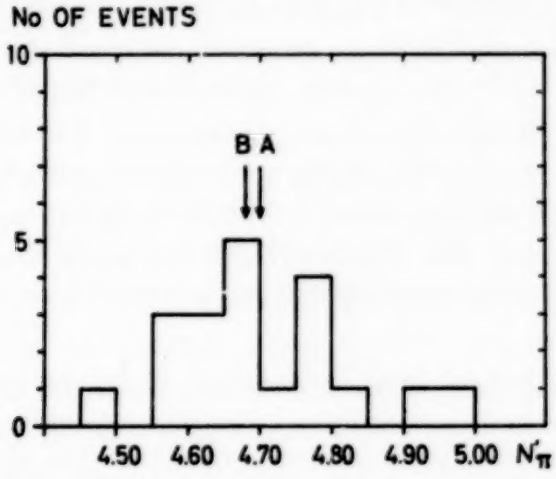

Fig. 12. The distribution of N'_π at rest obtained by a Monte Carlo method. *A*. $\langle N'_\pi \rangle = 4.70$ is the mean of the distribution. The standard deviation = 0.12. *B*. $\langle N'_\pi \rangle = 4.68$ was obtained directly from the input values.

5.1.3. Discussion

The results of subsect. 5.1.2 are based on the main assumptions (i) that only pions and K-mesons are emitted in the annihilation of the antiproton, (ii) that the energy given to the nucleons can be written in the form (20), and (iii) that charge independence holds in the reactions. Apart from this some empirical relations had to be introduced.

The values for the Berkeley set of data agree well with the values derived in ref. [6]). A slight difference can be expected since we have imposed the condition $\rho = 1.5$. The Rome data [8]) were not treated in this way earlier. As regards the Saclay data [12]) our results do not agree with the "best fit" values derived in the reference.

Our data (which are supported by the combined data) give that the average primary pion energy is the same at rest and in flight while the average multiplicity increases with 0.4 ± 0.2. One would expect the latter to increase slowly with the available energy, $\langle N'_\pi \rangle \propto W^{\frac{1}{4}}$ [19]), which relation is given by the statistical theory of antiproton annihilation. Thus a 9 % change in the available energy W can only account for a change of about 0.1 in the multiplicity. A lower but less certain value for the multiplicity in flight, namely 4.2 ± 0.5, has been derived with a different method described in subsect. 5.4. Apart from this it can be concluded that the difference between an increase of 0.4 and of 0.1 is at present not statistically significant.

Bubble chamber experiments give $\langle N'_\pi \rangle = 4.94 \pm 0.31$, $\langle E'_\pi \rangle = 380 \pm 12$ MeV [22]) and $\langle N'_\pi \rangle = 4.7 \pm 0.5$, $\langle E'_\pi \rangle = 390 \pm 14$ MeV [24]) in hydrogen. This is in excellent agreement with the emulsion data. The carbon annihilations in a propane bubble chamber [24]) yield $\langle E_{\pi^\pm} \rangle = 368 \pm 9$ MeV. The corresponding combined (at rest+in flight) result in our experiment is $\langle E_{\pi^\pm} \rangle = 360 \pm 14$ MeV.

The philosophy of the present approach was to consider pions and K-mesons as the only primary annihilation products and to assume that part of the energy was transferred to the nucleus where the annihilation took place by the mechanism of pion absorption and scattering. One of the quantities derived in the best fit solution was U, the energy given to the nucleus. It is of interest to see how this together with the energy of emitted pions and K-mesons accounts for the available energy. The results given below show that the unaccountable energy is consistent with the hypothesis that it is zero.

The division of the available energy on different particles

	at rest	in flight
Energy to charged pions	$47 \pm 3\%$	$38 \pm 3\%$
neutral pions	$23 \pm 2\%$	$19 \pm 2\%$
nucleons	$21 \pm 2\%$	$37 \pm 2\%$
K-mesons	$2 \pm 1\%$	$2 \pm 1\%$
Unaccountable energy	$7 \pm 4\%$	$4 \pm 4\%$

(27)

It follows from these figures that a larger proportion of the available energy goes to the nucleons for annihilations in flight than at rest. This means that more pions are absorbed by the nucleus when the antiproton is captured in flight than when it is absorbed at rest. A model for pion reabsorption is described in subsect. 5.3. which gives a good account for this behaviour.

5.2. TRANSFORMATION OF AN ISOTROPIC PION ANGULAR DISTRIBUTION FROM C.M.S. TO THE LABORATORY SYSTEM FOR ANTIPROTONS CAPTURED IN FLIGHT

The angular distribution of pions from antiproton captures in flight will be

peaked forward even if the pions are emitted isotropically in the C.M.S. of the antiproton and the capturing nucleon due to the movement of the centre-of-momentum. In this section the transformation from C.M.S. to the labòratory system will be performed.

5.2.1. The antiproton annihilates directly

We treat first the case when the antiproton does not undergo elastic scattering inside the nucleus before being captured.

We ask for the probability of the following event occurring: an incoming antiproton with momentum in the interval $\mathbf{p}_1$ to $\mathbf{p}_1+\mathrm{d}\mathbf{p}_1$ is captured by a nucleon with momentum between $\mathbf{p}_2$ and $\mathbf{p}_2+\mathrm{d}\mathbf{p}_2$ and a pion with momentum $\mathbf{p}_\pi{}^*$ to $\mathbf{p}_\pi{}^*+\mathrm{d}\mathbf{p}_\pi{}^*$ (in the C.M.S. of the pions) is subsequently emitted.

$\mathbf{p}_1$, $\mathbf{p}_2$ and $\mathbf{p}_\pi{}^*$ are independent random variables. Thus in momentum space the joint probability for the event is

$$\mathrm{d}^9\sigma = w(\mathbf{p}_1)\mathrm{d}^3p_1 w(\mathbf{p}_2)\mathrm{d}^3p_2 w(\mathbf{p}_\pi{}^*)\mathrm{d}^3p_\pi{}^*. \tag{28}$$

Here, $w(\mathbf{p})$ is the frequency function in momentum space, d^3p the volume element in momentum space.

The following assumptions are now made:

(i) The nuclear potential of the antiproton is zero. Then $w(\mathbf{p}_1)$ is the measured momentum distribution of the antiprotons.

(ii) The momentum distribution of the nucleon is that of a Fermi gas, i.e. $w(\mathbf{p}_2) = 3/4\pi p_F{}^3$; p_F = the maximum Fermi momentum = 250 MeV/c.

(iii) The pions are emitted isotropically in the C.M.S. i.e. $w(\mathbf{p}_\pi{}^*) = \text{const.}$

(iv) $E_2 = \sqrt{m_2{}^2+p_2{}^2}$ varies very little with p_2 and the numerical value $E_2 = E_F = m_2+\frac{3}{5}T_F$ will be used. The nucleon kinetic energy $T_F = 33$ MeV corresponds to the momentum $p_F = 250$ MeV/c.

Starting from expression (28) and using the assumptions (i)—(iv) it is then possible to calculate the expected angular distribution, $\mathrm{d}\sigma/\mathrm{d}(\cos\theta_\pi)$. Details of the computation are given in Appendix A.4.1.

The result of this section is

$$\frac{\mathrm{d}\sigma}{\mathrm{d}(\cos\theta_\pi)} = \tfrac{1}{2}(A+B\cos\theta_\pi+C\cos^2\theta_\pi), \tag{29}$$

where θ_π is the angle between the pion and the incoming antiproton, and A, B and C are given by

$$\begin{aligned} A &= 1-\frac{1}{2}\left\{1+\left\langle\frac{1}{\beta_\pi{}^2}\right\rangle\right\}\left\langle\left(\frac{p_1}{E_1+E_F}\right)^2\right\rangle, \\ B &= 2\left\langle\frac{1}{\beta_\pi}\right\rangle\left\langle\frac{p_1}{E_1+E_F}\right\rangle, \\ C &= \frac{3}{2}\left\{1+\left\langle\frac{1}{\beta_\pi{}^2}\right\rangle\right\}\left\langle\left(\frac{p_1}{E_1+E_F}\right)^2\right\rangle. \end{aligned} \tag{30}$$

Here, $\langle\ \rangle$ means average value, β_π is the velocity of the pion in C.M.S., p_1 and E_1 are momentum and total energy of the antiproton, and $E_F = 959$ MeV.

5.2.2. *The antiproton undergoes elastic scattering once*

An estimate of the cross section for elastic scattering of antiprotons in nuclear matter gives $\sigma_{sc} = \frac{1}{3}\,\sigma_{tot}$ [20]). One third of the antiprotons will therefore undergo elastic scattering inside the nucleus before being captured. The change in direction thus introduced tends to smear out the pion angular distribution in the laboratory system and make it less peaked forward.

The effect is found to be relatively minor and we, therefore, limit the calculations to the case, where the antiproton has been elastically scattered only once. The effect of elastic scattering twice or more is negligible.

The calculation starts from the expression (29), which obviously is valid with respect to the direction of the scattered antiproton. The momentum distribution $w(\mathbf{p}_x)$ of the incoming antiproton is, however, no longer the measured momentum distribution $w(\mathbf{p}_1)$. The new antiproton momentum $\mathbf{p}_x$ can be expressed in terms of $\mathbf{p}_1$, the transferred momentum $\mathbf{g}$ and the angle η between $\mathbf{p}_1$ and $-\mathbf{g}$ during the collision.

The joint distribution of $\mathbf{g}$ and $\cos\eta$ can be found using a Fermi gas model of the nucleus [20]). The required average values can thus be calculated.

In this case the coefficients A, B and C are of the form

$$
\begin{aligned}
A' &= 1-\frac{1}{4}\left\{1+\left\langle\frac{1}{\beta_\pi^2}\right\rangle\right\}\left\{3\left\langle\left(\frac{p_1-g\cos\eta}{E_1+E_F}\right)^2\right\rangle-\left\langle\frac{p_1^2+g^2-2gp_1\cos\eta}{(E_1+E_F)^2}\right\rangle\right\},\\
B' &= 2\left\langle\frac{1}{\beta_\pi}\right\rangle\left\langle\frac{p_1-g\cos\eta}{E_1+E_F}\right\rangle, \qquad (31)\\
C' &= \frac{3}{4}\left\{1+\left\langle\frac{1}{\beta_\pi^2}\right\rangle\right\}\left\{3\left\langle\left(\frac{p_1-g\cos\eta}{E_1+E_F}\right)^2\right\rangle-\left\langle\frac{p_1^2+g^2-2gp_1\cos\eta}{(E_1+E_F)^2}\right\rangle\right\}.
\end{aligned}
$$

Details are given in Appendix A.4.2.

5.2.3. *The resulting distribution*

We need an estimate of $\langle 1/\beta_\pi\rangle$ and $\langle 1/\beta_\pi^2\rangle$ in order to obtain the numerical value of the constants A, B and C. If the energy distribution of pions from antiprotons at rest (fig. 5a) is taken at its face value then $\langle 1/\beta_\pi\rangle = 1.20\pm0.03$. This agrees with the combined Uppsala+Berkeley+Rome data, $\langle 1/\beta_\pi\rangle = 1.19\pm0.02$. This estimate of $\langle 1/\beta_\pi\rangle$ is an upper limit since the spectrum contains pions, which have been scattered and therefore lost energy before leaving the nucleus.

A lower limit is provided by the bubble chamber data from $\bar{p}$–p annihila-

tions at rest. A combination of the results of Horwitz *et al.* [22]) and Agnew *et al.* [23, 24]) yields $\langle 1/\beta_\pi \rangle = 1.15 \pm 0.01$. It is a lower limit because the bubble chamber data "at rest" include events which are effectively not a rest. This fact can, however, be expected to influence the average value very little.

We therefore adopt as an estimate of the average values

$$\left\langle \frac{1}{\beta_\pi} \right\rangle = 1.15, \quad \left\langle \frac{1}{\beta_\pi^2} \right\rangle = 1.40. \tag{32}$$

The final value of the coefficients A, B and C will consist of $\frac{2}{3}$ of (30) and $\frac{1}{3}$ of (31). With the average values (32) put in, the final result is

$$\frac{\mathrm{d}\sigma}{\mathrm{d}(\cos\theta_\pi)} = \tfrac{1}{2}(0.92 + 0.58\cos\theta_\pi + 0.24\cos^2\theta_\pi). \tag{33}$$

The correction for elastic scattering of the antiproton as described in subsection 5.2.2 resulted in a 10 % decrease of the asymmetry coefficient B which is 0.58 in (33).

5.3. ABSORPTION OF THE PIONS

In the notation of subsect. 5.1 the fractions of pions absorbed and inelastically scattered are

$$\varepsilon_a = \frac{a\nu}{N'_\pi}, \quad \varepsilon_{\mathrm{inel}} = \frac{(1-a)\nu}{N'_\pi}. \tag{34}$$

We want to relate this to an average mean free path of the pions in nuclear matter of constant density.

Assuming an isotropic emission of the pions for an antiproton captured at rest on the surface of the nucleus the following expression is obtained

$$\varepsilon(\xi) = \frac{1}{2}\left\{1 - \frac{1}{\xi}(1 - \mathrm{e}^{-\xi})\right\}, \tag{35}$$

where ξ is $2R/\lambda$, R the radius of the nucleus, λ the mean free path of the pion.

The total mean free path of the antiproton in nuclear matter is about $(0.5-0.6)\times 10^{-13}$ cm [2, 25]) and the absorption mean free path is about 0.8×10^{-13} cm. The captures in flight will be investigated on the basis of a model in which the nucleus is assumed to be spherical (radius R) with constant density and the antiproton is assumed to penetrate on an average a distance $\lambda_{\bar{\mathrm{p}}} = 0.7\times 10^{-13}$ cm into the nucleus (measured along the direction of flight and from the nuclear surface). The distance is somewhat shorter than the absorption mean free path due to elastic scattering of the antiproton.

If the angular distribution of the pions at the capture point is $\mathrm{d}\sigma/\mathrm{d}(\cos\theta) = \frac{1}{2}(A + B\cos\theta + C\cos^2\theta)$ one obtains the fraction absorbed per

$\frac{1}{2}\mathrm{d}(\cos\theta)$;

$$\varepsilon(\xi, \cos\theta) = (A + B\cos\theta + C\cos^2\theta)\iint (1 - \mathrm{e}^{-l\xi})2b\,\mathrm{d}b\,\frac{1}{2\pi}\,\mathrm{d}\varphi, \qquad (36)$$

where l is the distance from the capture point to the nuclear surface (in units of R), and b the impact parameter (in units of R).

A z-axis along the direction of the antiproton is introduced and a direction is described by the angles θ and φ.

Further

$$\varepsilon(\xi) = \int_{-1}^{+1} \varepsilon(\xi, \cos\theta)\tfrac{1}{2}\mathrm{d}(\cos\theta). \qquad (37)$$

The relation (36) can be integrated numerically. It contains the factor $\lambda_{\bar{\mathrm{p}}}/R$, where $\lambda_{\bar{\mathrm{p}}} \approx 0.7 \times 10^{-13}$ cm and $R \approx 4.2 \times 10^{-13}$ cm for a mean nucleus in emulsion. We use the value $\lambda_{\bar{\mathrm{p}}}/R = 0.17$ in the calculations. Further the numerical values of A, B and C in eq. (33) are used.

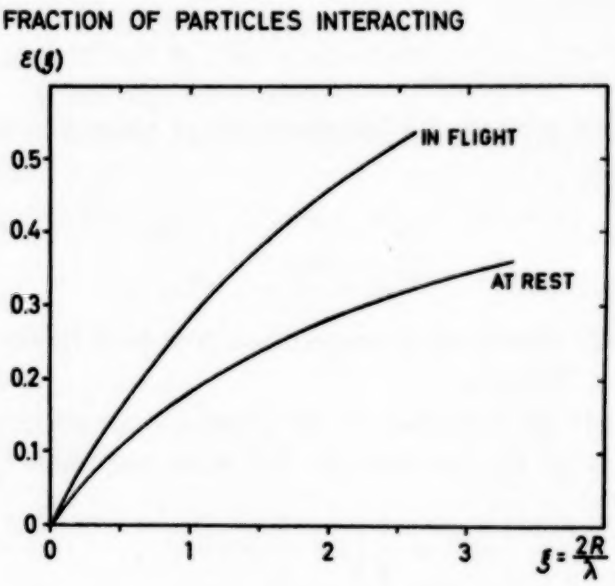

Fig. 13. The fraction of particles $\varepsilon(\xi)$ as a function of $\xi = 2R/\lambda$, where R is the nuclear radius and λ the mean free path of the particle in nuclear matter.

The above relations also hold for the inelastic process if $\xi = 2R/\lambda_{\mathrm{inel}}$.

The probabilities of interaction as a function of $\xi = 2R/\lambda$ for pions emitted from captures at rest and in flight, eqs. (35) and (37), are shown in fig. 13.

The best fit data in table 11 gives the fraction of pions absorbed (assumed to be equal for π^+, π^-, and π^0)

$$\begin{aligned} &\text{at rest} \quad \varepsilon_{\mathrm{a}} = 0.18 \pm 0.02, \\ &\text{in flight} \quad \varepsilon_{\mathrm{a}} = 0.32 \pm 0.03. \end{aligned} \qquad (38)$$

According to fig. 13 the value $\varepsilon = 0.32$ in flight should correspond to $\varepsilon = 0.20$ at rest, if the pion mean free path is the same.

The same comparison for the fraction of inelastically scattered pions (calculated by means of the best fit values) yields

$$\begin{aligned} &\text{at rest} \quad \varepsilon_{\text{inel}} = 0.06 \pm 0.01, \\ &\text{in flight} \quad \varepsilon_{\text{inel}} = 0.11 \pm 0.02. \end{aligned} \tag{39}$$

Fig. 13 shows that $\varepsilon = 0.11$ in flight should correspond to $\varepsilon = 0.07$ at rest.

There is good agreement between the expected and measured differences in flight and at rest. This indicates that the picture of the captures in flight can account for these features of the real process.

The fraction per $\frac{1}{2}\mathrm{d}(\cos\theta)$ of particles interacting, eq. (36), is given in fig. 14. Curves for $\varepsilon(\xi) = 0.30$ and $\varepsilon(\xi) = 0.10$ are shown.

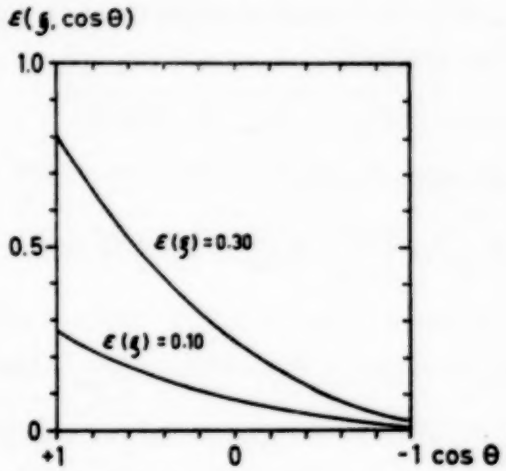

Fig. 14. $\varepsilon(\xi, \cos\theta)$ as a function of $\cos\theta$ for antiproton captures in flight. $\varepsilon(\xi) = \int_{-1}^{+1}\varepsilon(\xi, \cos\theta)\frac{1}{2}\mathrm{d}(\cos\theta)$.

The curves are very insensitive to variations of $\lambda_{\bar{p}}$ in the region $(0.5-0.8)\times 10^{-13}$ cm.

5.4. COMPARISON OF EXPERIMENTAL AND EXPECTED ANGULAR DISTRIBUTION OF THE PIONS. ESTIMATION OF THE AVERAGE PION MULTIPLICITY

The results of subsections 5.2 and 5.3 will now be used to compare the experimental and expected angular distribution of pions from captures in flight.

Let $\Delta\sigma$ be defined by

$$\Delta\sigma = \int_{\cos\theta_1}^{\cos\theta_2} \mathrm{d}\sigma, \tag{40}$$

where $\mathrm{d}\sigma$ is given by eq. (33).

If $\langle N'_\pi \rangle$ is the average number of pions per star emitted isotropically in the primary process, then $\frac{2}{3}\langle N'_\pi \rangle \Delta\sigma$ is the number of charged pions we would

frequencies (P_{n^c}) and the observed frequencies (P_{N^c}), which are

$$P_{N^c} = \sum_{n^c} \alpha_{N^c n^c} P_{n^c}, \tag{47}$$

where $\alpha_{N^c n^c}$ is the probability to obtain the number N^c charged pions emitted from the nucleus when the number of charged pions created is n^c.

The coefficients $\alpha_{N^c n^c}$ will be derived on the basis of certain assumptions:

(i) the primarily created charged pions are distributed at random in various directions;

(ii) the probability for absorption (ε_a) is a function of the direction in which the pion travels. It is assumed to be independent of the pion charge and is a mean for all energies;

(iii) it is assumed that the absorption can be described in terms of a mean emulsion nucleus.

We define an average absorption probability ε_a which is obtained by averaging over the directions of pion emission. Then it can be shown that the probabilities α are related to ε_a in the following manner:

$$\alpha_{N^c n^c} = \binom{n^c}{N^c} \varepsilon_a^{\,n^c - N^c} (1-\varepsilon_a)^{N^c}. \tag{48}$$

The observed average multiplicity of charged pions $\langle N^c \rangle$ is related to the corresponding primary multiplicity $\langle n^c \rangle$ through

$$\langle N^c \rangle = (1-\varepsilon_a)\langle n^c \rangle. \tag{49}$$

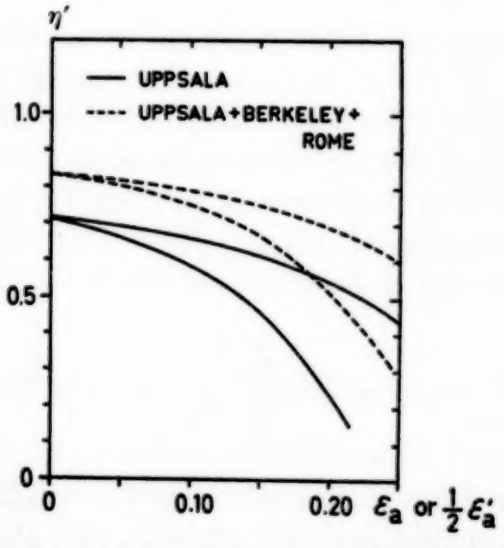

Fig. 16. The ratio η' (number of reactions with an odd number of charged pions to that with an even number) corrected for pion absorption. Upper curve: model with no pion correlation ($\varepsilon_a = 0.18 \pm 0.02$ is the experimentally determined average absorption probability). Lower curve: model with strong pion correlation. ($\frac{1}{2}\varepsilon'_a = 0.18 \pm 0.02$).

In the calculations, the average absorption probability (ε_a) is obtained from the best fit solution, where (49) enters. By means of (48) and (47) a value for the odd/even ratio (η') is obtained. Fig. 16 shows this ratio as a function of the average absorption probability. Two sets of experimental frequencies for stars at rest P_{N^c} were used, (i) the frequencies in table 4, and (ii) the frequencies obtained by a combination of Uppsala, Berkeley, and Rome data (corrected for detection efficiency).

Fig. 16 also contains two lower curves, one for each set of experimental frequencies. These curves were obtained by relaxing one of the assumptions above, namely that with random pion emission. The new assumption made was that half the number of charged pions are emitted with direction away from the nuclear surface where the annihilations at rest are pictured to occur. This half is thus not subject to absorption, whereas the other half, emitted in directions towards the nucleus are strongly absorbed. The average absorption probability for a pion passing through the nucleus is ε'_a, and $\frac{1}{2}\varepsilon'_a$ is identical with the previously used ε_a. This can be seen from the expression for the average observed pion multiplicity which now reads

$$\langle N^c \rangle = (1-\tfrac{1}{2}\varepsilon'_a)\langle n^c \rangle. \tag{50}$$

This model overemphasizes the importance of a correlation among the charged pions, imposed by e.g. momentum conservation. This extreme model, therefore, only serves the purpose to show that the resulting odd/even ratio will be lowered by taking correlation effects into account. The real correlation among charged pions is, however, much smaller, which means that the first model is the better one.

Using the value $\varepsilon_a = 0.18 \pm 0.02$ obtained in the best fit solution, eq. (38), we estimate

$$\eta' = \frac{\sum_{\text{odd } n^c} P_{n^c}}{\sum_{\text{even } n^c} P_{n^c}} = 0.6 \pm 0.2. \tag{51}$$

This value is in agreement with the results obtained by the Rome group [8]). If the annihilation probability on neutrons equals that on protons, one expects a ratio odd/even of 1.2, since the number of neutrons exceeds the number of protons by 20 % in emulsion nuclei.

The problem is further discussed in subsect. 5.6.3.

5.6. COMPARISON WITH STATISTICAL THEORIES

5.6.1. Introduction

The features of the antiproton annihilation process to be understood theoretically are

(i) the high average multiplicity of the pions,

(ii) the energy distribution of the pions,

(iii) the ratio of annihilations on protons and neutrons respectively in complex nuclei,

(iv) the percentage of K-mesons,

(v) the energy distribution of the K-mesons,

(vi) the large cross section for annihilation.

Most experiments on $\bar{p}$—N annihilation have been compared with Fermi's statistical theory [30]) and its modifications [31, 32, 33]).

The average pion multiplicity and the energy distribution are in fair agreement with the predictions provided the free parameter of the theory, the interaction volume Ω is taken to be $10\Omega_0$, where

$$\Omega_0 = \frac{4\pi}{3}\left(\frac{\hbar}{m_\pi c}\right)^3.$$

The theory fails completely to account for the percentage of K-mesons which is 5.0 ± 1.1 %. With $\Omega = 10\Omega_0$ the theory gives 18 % K-mesons. Apart from this the large value of Ω is unsatisfactory. One would expect $\Omega \approx \Omega_0$ since the interaction range between an antinucleon and a nucleon should be of the order of the Compton wave length of the pion.

Various suggestions have been put forward to improve the situation.

In the theory of Koba and Takeda [34]), the pion cloud and the core are treated separately. The theory successfully accounts for the high pion multiplicity. It predicts, however, a second maximum in the energy spectrum of the pions in the region of 400—500 MeV, which is not borne out by experiments.

Ball and Chew [35]) have treated the problem of cross sections. They were able to fit the low-energy experimental data for the cross sections without attaching special characteristics to the nuclear core and the pion cloud.

L. F. Cook [36]) has developed a theory of multiple meson production in nucleon-antinucleon annihilations in flight, which includes the approximate energy dependence of the matrix elements and the results of Ball and Chew with respect to the partial waves involved in annihilation. He was able to obtain fair agreement with multiplicities and energy spectra of the pions. The strange particle production was not treated.

F. Cerulus [37]) has recently attempted to include a strong π—π interaction in the final state in the statistical theory of $\bar{p}$—N annihilation. In this way it is possible to retain the plausible value $\Omega = \Omega_0$. The properties of the π—π isobar were taken from speculations on the magnetic moment of the neutron [38]). The theory also introduces a separate K-meson interaction volume (Ω_K).

The probabilities P_n of obtaining n pions will be needed in the following sections. The predictions by theories of Fermi (applied by W. H. Barkas *et al.* [11])), Cerulus and Cook are given in table 12.

TABLE 12

Probabilities P_n to obtain n pions given by different theories

No. of pions	Fermi [11] $\Omega_\pi = 10\Omega_0$	Cerulus [a] [37] $\Omega_\pi = \Omega_0$ $\Omega_K = 1/10\Omega_0$	Cook [b] [38] $\Omega_\pi = \Omega_0$ $G^2 = 6$ [c]
2	0.001	0.009	0.018
3	0.056	0.090	0.216
4	0.216	0.326	0.198
5	0.440	0.389	0.236
6	0.236	0.184	0.144
7	0.051	0.000	0.107
8			0.060
9			0.020
$\langle n \rangle$	5.00	4.65	4.90

[a] For $\bar{p}$—p annihilation. In charge analysis, for instance, these figures cannot be used since the different subsystems of π—π isobars and π-mesons must be taken into account separately. $K\bar{K}$ pairs account for 0.17 % of the stars.

[b] For $\bar{p}$—p-annihilations. The values are calculated for annihilations in flight at $T_{\bar{p}} = 200$ MeV.

[c] G is the coupling strength.

The values of the parameters are chosen to give an average multiplicity $\langle n \rangle$ in agreement with experiments (table 11 and eq. (45)).

We have used the frequencies of the Fermi theory calculated in the Antiproton Collaboration Experiment [11]. The solution was done by an approximation method. A Monte Carlo calculation of the phase space integrals [37] shows that the ACE solution is sufficiently accurate.

It should be noted that Cerulus' theory contains more parameters than indicated in table 12. The properties of the π—π isobar are important in the theory. The probabilities P_n are calculated for angular momentum $J = 1$, isospin $T = 1$ and mass $m = 4m_\pi$ of the pion isobar. The average pion multiplicity is not sensitive to changes in Ω_K but sensitive to changes in the mass of the isobar.

5.6.2. Consequences of charge independence

The nucleon N is assigned an isospin $T = \frac{1}{2}$; $(TT_3) = |\frac{1}{2}\frac{1}{2}\rangle$ is the state spinor in isospace for the proton and $|\frac{1}{2}\ -\frac{1}{2}\rangle$ the isospinor for the neutron. From the total isobaric spin operator of the quantized nucleon-antinucleon field it follows that the antinucleon ($\bar{N}$) states are $-|\frac{1}{2}\ -\frac{1}{2}\rangle$ for $\bar{p}$ and $|\frac{1}{2}\frac{1}{2}\rangle$ for $\bar{n}$.

An initial $\bar{p}p$- or $\bar{p}n$-state consists of [39]

$$|\bar{p}p\rangle = \frac{1}{\sqrt{2}}\{|00\rangle - |10\rangle\}, \quad |\bar{p}n\rangle = -|1-1\rangle. \tag{52}$$

The charge states are labelled ($\bar{p}p$) etc. and the isospin states $|TT_3\rangle$.

If the total isospin is conserved the final state will consist of $T = 1$ and $T = 0$ states only. By assuming charge independence it is possible to calculate the different charge configurations of a number n of pions in a $|10\rangle$, $|00\rangle$ or $|1{-}1\rangle$ state. Since a pion system consisting of more than two mesons is not uniquely specified by its total isospin T and third component T_3, a further assumption is made, viz. that all ways of arriving at a certain (TT_3) combination are equally probable.

Given the probabilities for different charge configurations in definite isospin states the final state charge distribution from an initial $\bar{p}p$-system will depend on the transition probabilities of the two isospin channels $T = 1$ and $T = 0$. With regard to the composition of the initial states (52), the transition rates ω_n for the reactions $\bar{p}+N \to n\pi$ can, in a statistical theory, be written

$$\omega_n(\bar{p}p) = \tfrac{1}{2}\{\omega_n(1)+\omega_n(0)\}\rho_n, \quad \omega_n(\bar{p}n) = \omega_n(1)\rho_n, \tag{53}$$

where $\omega_n(T)$ = the weight of the state T. ρ_n includes all other factors (integrals over momentum space etc.). It is independent of isospin. See also the work of B. Desai [40]) in this connection.

Let $C_{nn^c}(TT_3)$ be the probability of obtaining n^c charged pions out of a total of n pions in the state (TT_3). Taking into account the average neutron excess of 20 % in emulsion one obtains

$$C_{nn^c}(\mathrm{em}) = \frac{\{C_{nn^c}(10)+2.4\,C_{nn^c}(1-1)\}\omega_n(1)+C_{nn^c}(00)\omega_n(0)}{3.4\omega_n(1)+\omega_n(0)}. \tag{54}$$

The normalization is such that

$$\sum_{n^c} C_{nn^c} = 1. \tag{55}$$

If P_n is the frequency of n pions we get the frequency of charged pions P_{n^c} by

$$P_{n^c} = \sum_n C_{nn^c}(\mathrm{em})P_n. \tag{56}$$

The probabilities C_{nn^c} depend on the weights $\omega_n(T)$ which will be chosen in three different ways as discussed below.

(i) In the spirit of the statistical theory, $\omega_n(T)$ should be equal to the number of independent isospin combinations for given T and T_3. For n non-interacting pions

$$\omega_n(T) = (2T+1)\sum_{i=T}^{n} \frac{(-1)^{i+n}}{2i+1}\binom{n}{i}\binom{2i+1}{i-T}, \tag{57}$$

where $\omega_n(T)$ in this case is Yeivin and de Shalit's coefficients [41]).

Since the P_n's are only slightly affected by different choices of $\omega_n(T)$ the

effects of different relative weights will be investigated in case of the Fermi theory by putting

(ii) $\omega_n(1) = \omega_n(0)$. This means equal probability for annihilation on protons and neutrons. This is in accordance with the theory of Ball and Chew which is supported by measurements on the cross sections.

(iii) $\omega_n(0) = 3\omega_n(1)$, which implies $\omega_{\bar{p}n} = \frac{1}{2}\omega_{\bar{p}p}$, will also be chosen.

The coefficients C_{nnc} have been calculated for $n = 2$ to 8 as well as for different $(\pi—\pi^*)$ states in Cerulus' theory. π^* denotes the $(\pi—\pi)$ isobar. Some of the coefficients can be found in the literature [19, 42]).

The P_n's are given in table 12. The relative frequencies P_{nc} are given in table 13.

TABLE 13

The expected frequencies of charged pions in emulsion [a])

No. of pions	Fermi theory			Cerulus [b])	Cook
	Statistical weights	$\omega(0)=\omega(1)$	$\omega(0) = 3\omega(1)$	Statistical weights	$\omega(0) = \omega(1)$
0	0.006	0.009	0.012	0.004	0.016
1	0.071	0.062	0.042	0.056	0.095
2	0.138	0.168	0.229	0.176	0.203
3	0.375	0.326	0.224	0.478	0.298
4	0.203	0.249	0.344	0.200	0.185
5	0.179	0.154	0.106	0.078	0.135
6	0.024	0.029	0.041	0.008	0.048
7	0.004	0.003	0.002		0.018
8					0.002
η' [c])	1.70	1.20	0.60	1.57	1.20

[a]) Not corrected for absorption of the pions.

[b]) Ref. [43]). The figures in the reference are corrected by a factor $\frac{1}{2}$. C.f. eq. (53).

[c]) $\eta' = \sum_{\text{odd } n^c} P_{nc} / \sum_{\text{even } n^c} P_{nc}$.

The frequencies in table 13 are not yet corrected for pion absorption.

5.6.3. *Comparison of estimates and predictions*

The experiment will now be compared with the theoretical predictions. Fermi's statistical theory [11]), Cerulus' version of the statistical theory and Cook's theory will be discussed. The free parameters of the theories are adjusted to fit the experimental average pion multiplicity. Tables 11 and 12 give the relevant data. We have:

$$\text{Theory} \begin{cases} \langle N'_\pi \rangle = 5.00, & \text{Fermi: } \Omega_\pi = 10\Omega_0; \\ \langle N'_\pi \rangle = 4.65, & \text{Cerulus: } \Omega_\pi = \Omega_0,\ \Omega_K = \frac{1}{10}\Omega_0; \\ \langle N'_\pi \rangle = 4.90, & \text{Cook: } \Omega_\pi = \Omega_0,\ G^2 = 6; \end{cases} \tag{58}$$

$$\text{Experiment } \{\langle N'_\pi \rangle = 4.9 \pm 0.1 \text{ (data at rest and in flight combined).}$$

Next the relative frequencies of charged pions can be compared with the experiment. The combined data at rest and in flight will be used in order to obtain enough statistics. The expected frequencies of charged pions in emulsion have been given in table 13. These figures must be corrected for pion absorption. This is done by means of eqs. (47) and (48). The mean values of the theoretical distributions were adjusted to agree with the average pion multiplicity $\langle N_{\pi^\pm} \rangle = 2.29$ of the experimental histogram.

The different versions of the weights of the isospin channels for the Fermi theory do not give any noticeable difference in the final distribution in this case.

The experimental and the corrected theoretical relative frequencies of charged pions are shown in fig. 17.

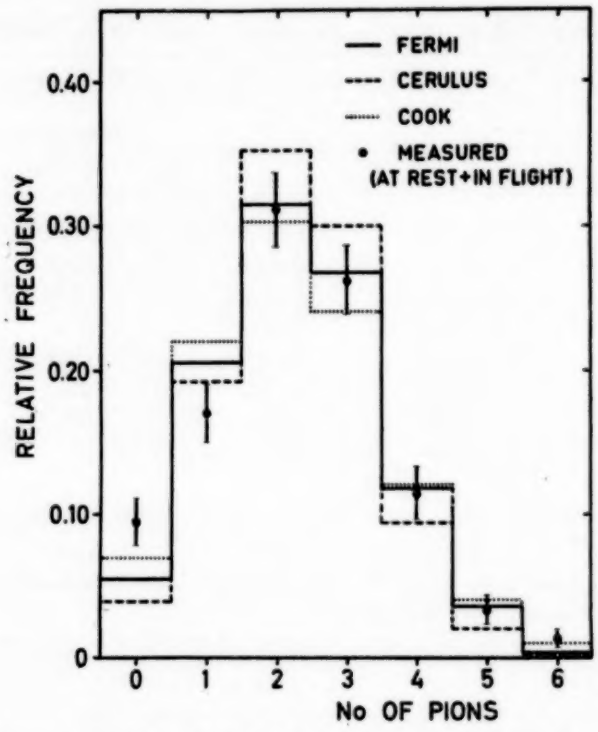

Fig. 17. Observed and predicted charged pion multiplicity distributions.

The experimental distribution is compatible with the distributions of Fermi and Cook as judged by a χ^2-test. In the case of Cerulus' distribution the probability of obtaining a larger χ^2 is $\ll 0.1$ % and the deviation is significant. Three-fourths of the contribution to χ^2 comes, however, from $N_{\pi^\pm} = 0$. It is experimentally very difficult to get an unbiassed estimate of the number of zero prong stars and there might be systematic errors. In view of this we still consider the Cerulus' results to be compatible with the experimental distribution.

The theories also predict the energy distribution of the pions. The theoretical distributions must be corrected [44]) for absorption and inelastic scattering of the

primary pions and for the effect of scanning efficiency. The effect of the correction is shown in fig. 18 where the original and corrected Fermi distributions are compared.

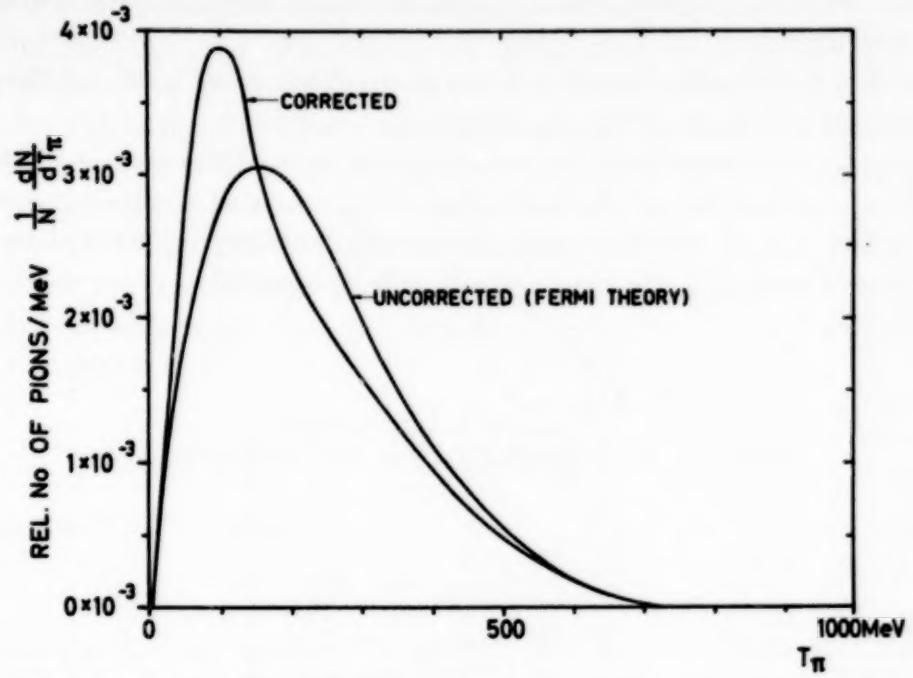

Fig. 18. The effect of correcting the pion energy distributions for detection efficiency, pion absorption, and inelastic scattering. Uncorrected curve: the distribution given by the Fermi theory. Corrected curve: the distribution expected in emulsion.

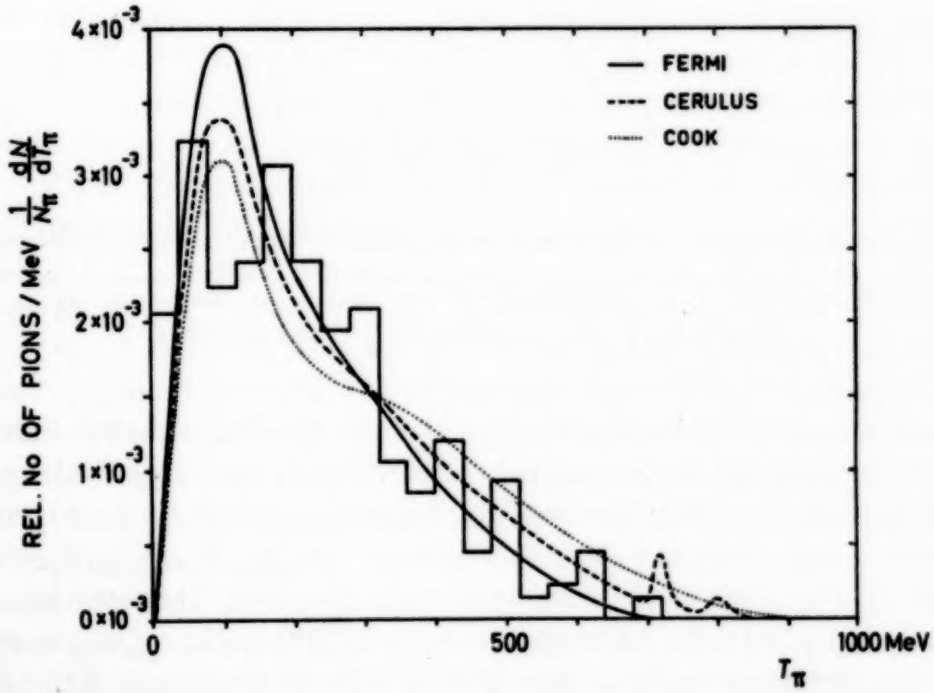

Fig. 19. Observed and predicted charged pion energy distributions.

The corrected theoretical curves and the combined experimental distribution (at rest and in flight) are given in fig. 19. According to a χ^2-test the three theoretical distributions are compatible with the hypothesis that they are the population from which the experimental sample is drawn. Moreover the χ^2-values are about the same.

Thus, it is not possible to rule out any of the theories by means of the charged pion multiplicity and energy distributions.

Finally, the predicted and the experimental ratio of the sum of the frequencies of an odd number of charged pions to the sum of the frequencies of an even number of pions will be compared. The effect of varying the relative weights of the $T = 1$ and $T = 0$ isospin states will be studied.

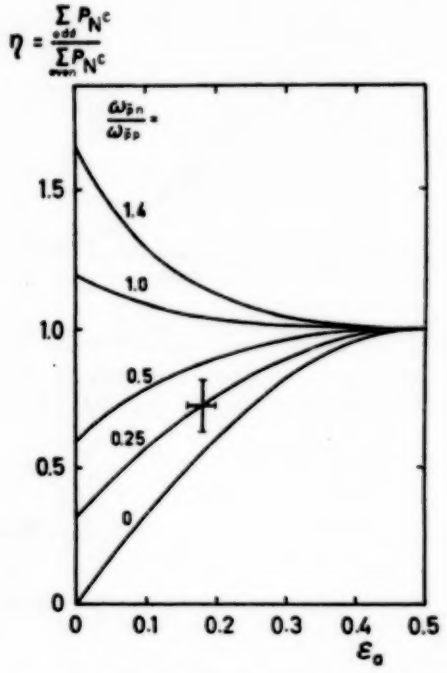

Fig. 20. Predicted ratio η of the number of stars with an odd number to stars with an even number of charged pions as a function of the average fraction ε_a of the pions absorbed. $\omega_{\bar{p}n}$ and $\omega_{\bar{p}p}$ denote the probabilities for annihilation on neutron and proton, respectively. P_{N^c} is the frequency of N^c charged pions. The measured value is also indicated.

The starting point is the different versions of the Fermi theory (table 13), i.e. $\omega(T)$ proportional to the number of independent states available, $\omega(0) = \omega(1)$ and $\omega(0) = 3\omega(1)$. The expected frequencies in emulsion are computed by means of eqs. (47) and (48). In this way $\eta = \sum_{odd} P_{N^c} / \sum_{even} P_{N^c}$ can be obtained as a function of the fraction of pions absorbed. The resulting curves are shown in fig. 20 with the annihilation probability ratio $\omega_{\bar{p}n}/\omega_{\bar{p}p}$ as a parameter. The measured ratio at rest $\eta^{meas} = 0.73 \pm 0.09$ at $\varepsilon_a = 0.18 \pm 0.02$ is also indicated.

The present approach is the reverse of the analysis in subsect. 5.5. It is very instructive, however, to see how the correction for absorption works either way. If we compare the values outside the nucleus we have $\eta = 0.73 \pm 0.09$ (measured) and $\eta = 1.16$ (expected; Fermi theory, statistical weights).

We conclude that the probability for antiproton annihilation at rest on neutrons is less than one would expect from a statistical theory. The results in subsect. 5.5 and in fig. 20 indicate that $\omega_{\bar{p}n} < \omega_{\bar{p}p}$. This result for annihilations at rest differs from the result in an earlier paper [2]) giving an annihilation cross section on neutrons at least as large as that on protons at an average kinetic energy of 166 MeV of the antiproton.

In terms of the relative strengths of the two isospin interaction channels, the result here could indicate that the isospin $T = 0$ channel predominates over the $T = 1$ channel.

6. Annihilations into Pions and K-Mesons

In this section the process

$$\bar{p} + N \rightarrow N'_{\pi}\pi + N'_{K\bar{K}}K\bar{K} \tag{59}$$

will be discussed. This was also the subject of sect. 5 but there the stars containing K-mesons were eliminated and the dominant process, viz. annihilation into pions, was analysed.

The experimental data on stars with charged K-mesons are still very scanty. Some information will, however, be extracted. In subsect. 4.2 the average charged pion multiplicity for stars with K-mesons was obtained, $\langle N_{\pi^{\pm}} \rangle = 1.24 \pm 0.25$. This figure must be corrected for the number of pions (≈ 0.15) coming from absorbed $\bar{K}$-mesons. The events occur at rest and in flight. A reasonable value of the fraction of pions absorbed is therefore $\varepsilon_a = 0.25 \pm 0.05$. Assuming that charge independence holds the average pion multiplicity in the primary process is then obtained.

$$\langle N'_{\pi} \rangle = 2.2 \pm 0.5. \tag{60}$$

The Fermi theory with K-meson production included predicts that K-meson pairs are produced in 18 % of the stars for $\Omega_{\pi} = 10\Omega_0$ [11]). Cerulus' theory predicts 0.17 % for $\Omega_{\pi} = \Omega_0$, $\Omega_K = \frac{1}{10}\Omega_0$. This should be compared with the experimental figure of 5.0 ± 1.1 %. One can conclude that the theories are unable to cope with the production of K-meson pairs. The reason for this might be that the K-mesons cannot be treated within the frame work of a statistical theory.

It may still be meaningful to compare with the theoretical K-meson energy distributions, since the energy distributions are mainly governed by the momentum space integrals. It is impossible to arrive at an unbiassed experi-

mental K-meson energy distribution at the present stage. We will, however, tentatively use the 26 identified K-mesons in tables 5 and 8. A lower limit of the average K-meson energy is $\langle T_K \rangle = 107 \pm 16$ MeV.

The energy spectrum for the K-mesons is compared with the predictions of Fermi's theory, calculated by Sandweiss [45]), in fig. 21 and Cerulus' theory in fig. 22. Sandweiss' curves give $\langle T_K \rangle = 66$ MeV for $2K+3\pi$, 116 MeV for

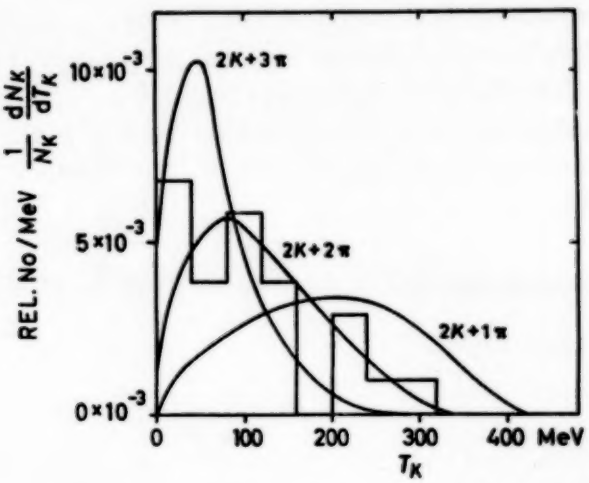

Fig. 21. Observed and predicted energy spectrum of the K-mesons (Fermi's theory).

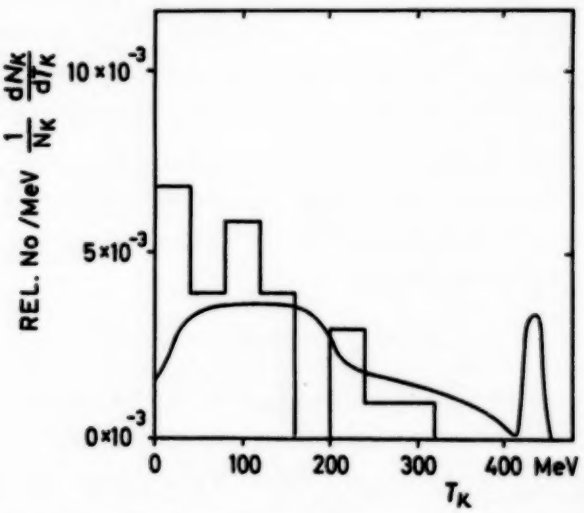

Fig. 22. Observed and predicted energy spectrum of the K-mesons (Cerulus' theory).

$2K+2\pi$ and 218 MeV for $2K+\pi$. The value $\langle N'_\pi \rangle = 2.2$ will give an energy distribution in agreement with the experimental histogram. Cerulus' theory gives $\langle T_K \rangle = 184$ MeV and $\langle N'_\pi \rangle = 1.41$. The peak at $T_K \approx 440$ MeV is due to the reaction $\bar{p}+N \rightarrow K+\bar{K}$.

7. Summary

Some of the main results of this work will be summarized and discussed in this section.

(i) The average total energy per pion outside the nucleus is for annihilations

$$\text{at rest:} \quad \langle E_{\pi^\pm} \rangle = 365 \pm 17 \text{ MeV},$$
$$\text{in flight:} \quad \langle E_{\pi^\pm} \rangle = 355 \pm 20 \text{ MeV}.$$

(average antiproton energy = 166 MeV.) The correction of the average energy in flight due to the anisotropic angular distribution of the pions was found to be important.

(ii) The average charged pion multiplicity outside the nucleus is

$$\text{at rest:} \quad \langle N_{\pi^\pm} \rangle = 2.38 \pm 0.11,$$
$$\text{in flight:} \quad \langle N_{\pi^\pm} \rangle = 2.19 \pm 0.11.$$

(iii) If one assumes that the primary annihilation process is

$$\bar{\text{p}} + \text{nucleon} \rightarrow N'_{\pi}\pi + N'_{\text{K}\bar{\text{K}}}\,\text{K}\bar{\text{K}}$$

and further assumes energy conservation and charge independence the primary average pion multiplicity and total energy can be deduced by means of a best fit method. Some information from pion experiments are also used in the analysis. The results are

$$\text{at rest:} \quad \langle N'_{\pi} \rangle = 4.68 \pm 0.12 \quad (4.77 \pm 0.09),$$
$$\langle E'_{\pi} \rangle = 391 \pm 10 \text{ MeV} \quad (380 \pm 7) \text{ MeV},$$
$$\text{in flight:} \quad \langle N'_{\pi} \rangle = 5.11 \pm 0.12 \quad (5.12 \pm 0.15),$$
$$\langle E'_{\pi} \rangle = 390 \pm 9 \text{ MeV} \quad (384 \pm 11) \text{ MeV}.$$

The figures within brackets are the combined world averages deduced by our method of best fit.

(iv) The percentage of K-meson pairs and average energy going into K-mesons per antiproton star is

$$\langle N_{\text{K}\bar{\text{K}}} \rangle = 3 \pm 2\,\% \quad (5.0 \pm 1.1)\,\%,$$
$$\langle E_{\text{K}\bar{\text{K}}} \rangle = 33 \pm 22 \text{ MeV/star} \quad (57 \pm 13) \text{MeV/star}.$$

The figures within brackets are obtained by combining all available information from different laboratories.

The percentage of undetectable K-meson pairs in emulsion is 40 %.

(v) A ${}_{\Lambda}\text{H}^4$ hyperfragment from an antiproton capture star has been identified.

(vi) The available energy can be accounted for in the following way:

	at rest	in flight
Energy to: $\pi^{\pm}$	47±3%	38±3%
π^0	23±2%	19±2%
nucleons	21±2%	37±2%
$K\bar{K}$-pairs	2±1%	2±1%
Unaccountable energy	7±4%	4±4%

This is for stars without observed charged strange particles.

(vii) The average fractions of pions absorbed and inelastically scattered are, respectively,

$$\text{at rest: } \varepsilon_a = 0.18 \pm 0.02, \quad \varepsilon_{\text{inel}} = 0.06 \pm 0.01,$$
$$\text{in flight: } \varepsilon_a = 0.32 \pm 0.03, \quad \varepsilon_{\text{inel}} = 0.11 \pm 0.02.$$

The differences between the values at rest and in flight are well accounted for by a model in which the pions are emitted isotropically. The antiproton at rest is assumed to annihilate on the nuclear surface and the antiproton in flight is assumed to travel a mean free path in the nucleus before annihilating. The effect of the movement of the C.M.S. in flight on the pion angular distribution in the laboratory system is calculated.

(viii) The observed angular distribution of pions emitted from captures in flight together with the model mentioned above also furnishes an estimate of the average pion multiplicity

$$\langle N'_\pi \rangle = 4.2 \pm 0.5.$$

(ix) The charged pion multiplicity and energy distributions have been compared with the predictions of Fermi's statistical theory, Cook's interaction model and Cerulus' version of the statistical theory (strong $\pi-\pi$ interaction in the final state). Our results do not permit a decision in favour of a particular theory.

(x) The experimental ratio η of the number of stars at rest with an odd number of charged pions to the number of stars with an even number of charged pions is

$$\eta = 0.73 \pm 0.09.$$

This is at variance with what one would expect theoretically, viz. $\eta = 1.16$ (Fermi theory).

(xi) The above ratio can be shown to indicate that the probability for annihilation on neutrons is less than that on protons.

(xii) The agreement between experiment and theory as regards K-meson

production is extremely poor. It may be that the K-mesons cannot be treated within the frame work of a statistical theory.

The analysis of the capture stars in this work rests on two basic assumptions, namely that only pions and $K\bar{K}$-pairs are emitted in the primary process and that charge independence holds. These assumptions are well supported by the bubble chamber experiments, which deal with the primary process directly.

We express our deep gratitude to Dr. E. J. Lofgren, Professor G. Goldhaber and Professor E. Segrè for their help in planning and carrying out of the successful exposure. Thanks are due to Mr. J. F. Garfield, Brookhaven, who developed the stack.

The facilities put at our disposal by Professor Kai Siegbahn are gratefully acknowledged as is his continued interest in this work.

We thank our scanners Mrs I. Nilsson, Mrs. S Eklund, Miss I. Durén, Miss B. Lundkvist, Miss M. Källsten and Miss V. Braun for their excellent work.

Thanks are due to the Swedish Board for Computing Machinery, Stockholm, for free machine time at the Facit EDB computer.

The research was partly sponsored by the Air Research and Development Command through its European Office. Support was also obtained from the Swedish Atomic Research Council.

Appendix

A.1. THE INFLUENCE OF DISTORTION ON ENERGY DETERMINATIONS BY MULTIPLE SCATTERING MEASUREMENTS

Introduce a coordinate system (xyz) with (xy) in the emulsion plane and the z-direction from glass to surface ($z = 0$ is at glass). If the emulsion is distorted the displacement of a grain at the point (x, y, z) can be written

$$\mathbf{K}z = \sum_{i=1}^{\infty} \mathbf{K}_i \frac{z^i}{z_0^{i-1}}, \tag{1}$$

where z_0 is the thickness of the emulsion.

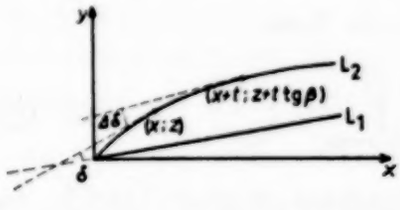

Fig. 23. Notation used in Appendix 1.

The vectors $\mathbf{K}_i$ represent different orders (i) of distortion. $\mathbf{K}_1$ means shear, $\mathbf{K}_2$ c-shaped and $\mathbf{K}_3$ s-shaped distortion. The projection in the (xy)-plane of an

undistorted track, $y = Ax$, (fig. 23, L_1), has after distortion the form (L_2)

$$y - \sum_{i=1}^{\infty} K_i \frac{z^i}{z_0^{i-1}} \sin \varphi_i = A \left\{ x - \sum_{i=1}^{\infty} K_i \frac{z^i}{z_0^{i-1}} \cos \varphi_i \right\}, \tag{2}$$

where φ_i is the angle between the x-axis and the direction of $\mathbf{K}_i$.

The track to be measured is lined up along the x-axis ($y \approx 0$). After some approximations for small angles one can compute the change $\Delta\delta$ in the angle between the tangents at the two points (x, z) and $(x+t, z+t \operatorname{tg} \beta)$,

$$\Delta\delta = \left\{ \frac{2t}{z_0} \sum_{i=2}^{\infty} \binom{i}{2} \left(\frac{z}{z_0}\right)^{i-2} K_i \sin \varphi_i \right\} \operatorname{tg}^2 \beta, \tag{3}$$

where β is the dip angle of the track and t the cell length.

The angle

$$\delta = \sum_{i=1}^{\infty} i K_i \left(\frac{z}{z_0}\right)^{i-1} \sin \varphi_i \operatorname{tg} \beta \tag{4}$$

is shown in fig. 23.

When third differences are used to calculate $p\beta$ it is seen from (3) that the remaining distortion can be written as the mean value of

$$\Delta^2\delta = \left\{ \frac{6t^2}{z_0^2} \sum_{i=3}^{\infty} \binom{i}{3} \left(\frac{z}{z_0}\right)^{i-3} K_i \sin \varphi_i \right\} \operatorname{tg}^3 \beta. \tag{5}$$

The expression within the brackets will be approximately constant and the contribution from distortion α_d to the true mean scattering angle $\bar{\alpha}_s$ will vary as $\operatorname{tg}^2\beta$.

Assuming α_s to be Gaussian and α_d small compared to $\bar{\alpha}_s$ it is possible to show that

$$\bar{\alpha}_s = \bar{\alpha}_m - \text{const.} \frac{\alpha_d^2}{\bar{\alpha}_s}, \tag{6}$$

where $\bar{\alpha}_m$ is the measured mean scattering angle.

As $p\beta = \text{const.}/\bar{\alpha}$ we then have

$$\left(\frac{1}{p\beta}\right)^2_{\text{meas}} = \left(\frac{1}{p\beta}\right)^2_{\text{true}} + \text{const. } \operatorname{tg}^6 \beta. \tag{7}$$

The constant is determined by plotting $(1/p\beta)^2_{\text{meas}}$ versus $\operatorname{tg}^6\beta$ for all tracks. The correction is then applied to each track separately.

The distortion correction resulted in a 15 MeV higher average energy for the tracks with $\beta = 5°.8$—$11°.5$. The average energy for all pions increased by 5.5 MeV.

A.2. THE EFFICIENCY OF DETECTION OF TRACKS FROM ANNIHILATION STARS

The detection efficiency of tracks $e = e(z, p, T, \beta)$ is a function of the distance of the star from glass or surface z, a factor p which takes into account the emulsion and microscope properties, the energy T of the particle, and the dip angle β of the track.

1) $e(z)$

We have examined the variation of the charged pion multiplicity of antiproton stars of groups I and III (table 1) as a function of the distance of the star from glass or surface in unprocessed emulsion. The results are given below.

$z(\mu m)$	No. of stars	$\langle N_{\pi^\pm} \rangle$
0—10	10	1.70 ± 0.42
10—20	5	1.40 ± 0.63
20—30	10	2.70 ± 0.42
30—50	23	2.30 ± 0.27
>50	293	2.34 ± 0.07

5 stars with K-mesons have been excluded. The decrease of the multiplicity at the top and bottom layers makes it necessary to exclude stars situated $< 20\ \mu m$ from either surface or glass in the analysis.

2) $e(p)$

The influence of emulsion and microscope properties on the detection efficiency may be determined by looking at $\mu^+ \rightarrow e^+$ decays. We have 42 π^+ decaying at rest. In all these cases the scanners recognized the electron from the μ^+ decay. It is therefore assumed that this part of the total efficiency is close to 100 %.

3) $e(T, \beta)$

The dependence on energy and dip angle has been examined by comparing the number of tracks found by two scanners observing the same stars. All stars have been carefully examined twice. The secondary tracks from the stars were divided into six groups; three dip angle intervals corresponding to equal solid angles and two ionization intervals one above and one below the value $g/g_0 = 1.4$. The results for $e(T, \beta)$ are given below.

β^0 \ g/g_0	<1.4	$\geqq 1.4$
0—19	0.89	0.99
19—42	0.89	0.98
42—90	0.85	0.95

As all stars were investigated twice the resulting efficiency for the two ionization groups is 0.98 ± 0.02 and 1.00 respectively. These figures should then represent the total detection efficiency. The Rome group [8]) (0.93) and the Berkeley group [6]) (0.90) have arrived at considerably lower estimates. We find $\approx 90\,\%$ of the pions the first time. The second time with the same efficiency also $\approx 90\,\%$ of the overlooked 10 % are found. This is how the resulting efficiency was deduced.

As one would expect, tracks with low ionization and large dip angles are most likely to be missed.

The influence of the missed high energy pions on the average pion energy is less than 1 MeV and can be neglected.

A.3. BEST FIT METHOD OF SOLVING AN OVERDETERMINED SYSTEM OF EQUATIONS

Let the system of equations be

$$f_i(x_1 x_2 \ldots x_n, C_1 C_2 \ldots C_m) = 0 \quad (i = 1, 2 \ldots l), \tag{1}$$

where x_j denotes unknowns to be determined by the above conditions and the quantities C_k are experimentally determined input data.

In the overdetermined case $l > n$ one can define a best fit solution by requiring that

$$\sum p_i f_i^2 = \text{min.} \tag{2}$$

The weight p_i of the equation f_i is defined by the relation

$$\frac{1}{p_i} = \sum_k \left(\frac{\delta f_i}{\delta C_k}\right)^2 \text{var } C_k. \tag{3}$$

One notices that the weights are functions of the unknown variables $(x_1 x_2 \ldots x_n)$.

The condition (2) can be written

$$\sum_i \left\{2 p_i f_i \frac{\delta f_i}{\delta x_j} + f_i^2 \frac{\delta p_i}{\delta x_j}\right\} = 0 \quad (j = 1, 2 \ldots n). \tag{4}$$

This gives n equations for solving the n unknowns. The system (4) has to be solved by successive approximations.

In this way $\langle N'_\pi \rangle$, $\langle E'_\pi \rangle$, ν and $\langle U \rangle$ in table 11 have been obtained from eqs. (24), subsect. 5.1.2.

The error in $x_j = x_j(C_1, C_2, \ldots C_m)$ is

$$\sigma_{x_j}^2 = \text{var } x_j = \sum_k \left(\frac{\delta x_j}{\delta C_k}\right)^2 \text{var } C_k. \tag{5}$$

In our case this expression is, however, not suitable for obtaining numerical

results. Therefore a Monte Carlo method has been used for deriving the standard deviations. It is described in subsect. 5.1.2.

A.4. TRANSFORMATION OF AN ISOTROPIC PION ANGULAR DISTRIBUTION FROM C.M.S. TO THE LABORATORY SYSTEM FOR ANTIPROTONS CAPTURED IN FLIGHT IN COMPLEX NUCLEI

A.4.1. The antiproton annihilates directly.

The expression

$$\mathrm{d}^9\sigma = w(\mathbf{p}_1)\mathrm{d}^3p_1 w(\mathbf{p}_2)\mathrm{d}^3p_2 w(\mathbf{p}_\pi{}^*)\mathrm{d}^3p_\pi{}^* \tag{1}$$

is explained in the text, eq. (28), subsect. 5.2.1.

Introduce a laboratory coordinate system with z-axis in the direction of $\mathbf{p}_1$. Spherical polar coordinates in momentum space will consistently be used, i.e. p is the magnitude of a vector $\mathbf{p}$, θ is the space angle between $\mathbf{p}$ and the z-axis and φ is the azimuthal angle. We have $\mathrm{d}^3p = p^2\mathrm{d}p \sin\theta\, \mathrm{d}\theta\, \mathrm{d}\varphi$.

The velocity $\boldsymbol{\beta}_{\mathrm{CM}}$ of the centre-of-momentum is along the vector $\mathbf{p}_1+\mathbf{p}_2$ and is

$$\boldsymbol{\beta}_{\mathrm{CM}} = \frac{\mathbf{p}_1+\mathbf{p}_2}{E_1+E_2}. \tag{2}$$

E is the total energy of the particle.

Five coordinate transformations are now performed. The first one is

(i) $$(p_2\theta_2\varphi_2) \rightarrow (\beta_{\mathrm{CM}}\theta_{\mathrm{CM}}\varphi_{\mathrm{CM}}).$$

The other variables are kept constant. The transformation equations are

$$\begin{aligned} &\beta_{\mathrm{CM}}(E_1+E_2)\sin\theta_{\mathrm{CM}} = p_2\sin\theta_2, \\ &\beta_{\mathrm{CM}}(E_1+E_2)\cos\theta_{\mathrm{CM}} = p_1+p_2\cos\theta_2, \\ &\varphi_{\mathrm{CM}} = \varphi_2. \end{aligned} \tag{3}$$

The Jacobian of the transformation is

$$J^1 = \frac{\delta(p_2\theta_2\varphi_2)}{\delta(\beta_{\mathrm{CM}}\theta_{\mathrm{CM}}\varphi_{\mathrm{CM}})} = \frac{\beta_{\mathrm{CM}}(E_1+E_2)^2}{p_2}, \tag{4}$$

apart from a factor $1-\beta_{\mathrm{CM}}(p_2/E_2)\,(\cos\theta_{\mathrm{CM}}\cos\theta_2+\sin\theta_{\mathrm{CM}}\sin\theta_2)$ in the denominator. With $(p_2)_{\max} = 250$ MeV/c and $\beta_{\mathrm{CM}} \approx 0.3$ the factor is always close to one and it has been replaced by this number.

The second one is

(ii) $$(p_\pi{}^*\theta_\pi{}^*\varphi_\pi{}^*) \rightarrow (\beta_\pi\theta_\pi{}^*\varphi_\pi{}^*),$$

where

$$p_\pi{}^* = m_\pi\beta_\pi/\sqrt{1-\beta_\pi{}^2}, \tag{5}$$

$$J^{II} = \frac{\delta p_\pi^*}{\delta \beta_\pi} = m_\pi (1-\beta_\pi^2)^{-\frac{3}{2}}. \tag{6}$$

The third transformation is

(iii) $$(\theta_\pi^* \varphi_\pi^*) \to (\theta'_\pi \varphi'_\pi).$$

The coordinate system $(x^* y^* z^*)$ is chosen with the z^*-axis long $\boldsymbol{\beta}_{CM}$. The transformation equations are [21])

$$\cos\theta_\pi^* = \frac{1}{1-\beta_{CM}^2 \cos^2\theta'_\pi}\left\{-\frac{\beta_{CM}}{\beta_\pi}\sin^2\theta'_\pi + (1-\beta_{CM}^2)\cos\theta'_\pi \times \sqrt{1-\frac{\beta_{CM}^2}{\beta_\pi^2}\frac{1-\beta_\pi^2}{1-\beta_{CM}^2}\sin^2\theta'_\pi}\right\}, \qquad \varphi_\pi^* = \varphi'_\pi. \tag{7}$$

The Jacobian is

$$J^{III} = \frac{\delta(\theta_\pi^* \varphi_\pi^*)}{\delta(\theta'_\pi \varphi'_\pi)} = \frac{\sin\theta'_\pi}{\sin\theta_\pi^*} Q, \tag{8}$$

where

$$Q = \frac{1-\beta_{CM}^2}{(1-\beta_{CM}^2\cos^2\theta'_\pi)^2} \frac{\left\{\frac{\beta_{CM}}{\beta_\pi}\cos\theta'_\pi + \sqrt{1-\frac{\beta_{CM}^2}{\beta_\pi^2}\frac{1-\beta_\pi^2}{1-\beta_{CM}^2}\sin^2\theta'_\pi}\right\}^2}{\sqrt{1-\frac{\beta_{CM}^2}{\beta_\pi^2}\frac{1-\beta_\pi^2}{\beta_{CM}^2}\sin^2\theta'_\pi}}$$

Here, $(x'y'z')$ is a coordinate system in the laboratory frame of reference rotated with respect to (xyz).

The fourth transformation is

(iv) $$(\theta'_\pi \varphi'_\pi) \to (\theta_\pi \varphi_\pi).$$

θ and φ are the angles of the π-meson in the original (xyz)-system. The Jacobian of the transformation can be shown to be

$$J^{IV} = \frac{\sin\theta_\pi}{\sin\theta'_\pi}. \tag{9}$$

The transformation equation needed for later purposes is

$$\cos\theta'_\pi = \cos\theta_\pi \cos\theta_{CM} + \sin\theta_\pi \sin\theta_{CM} \cos(\varphi_\pi - \varphi_{CM}). \tag{10}$$

The last transformation is

(v) $$(\varphi_{CM}, \varphi_\pi) \to (\varphi_{CM}, \varphi_\pi - \varphi_{CM}),$$

with

$$J^{V} = \frac{\delta(\varphi_{CM}, \varphi_\pi)}{\delta(\varphi_{CM}, \varphi_\pi - \varphi_{CM})} = 1. \tag{11}$$

The results of the transformations can be summarized as

$$\begin{aligned}
&\mathrm{d}p_2\mathrm{d}\theta_2\mathrm{d}\varphi_2 = J^{\mathrm{I}}\mathrm{d}\beta_{\mathrm{CM}}\mathrm{d}\theta_{\mathrm{CM}}\mathrm{d}\varphi_{\mathrm{CM}},\\
&\mathrm{d}p_\pi{}^*\mathrm{d}\theta_\pi{}^*\mathrm{d}\varphi_\pi{}^* = J^{\mathrm{II}}\mathrm{d}\beta_\pi\mathrm{d}\theta_\pi{}^*\mathrm{d}\varphi_\pi{}^*,\\
&\mathrm{d}\theta_\pi{}^*\mathrm{d}\varphi_\pi{}^* = J^{\mathrm{III}}\mathrm{d}\theta'_\pi\mathrm{d}\varphi'_\pi,\\
&\mathrm{d}\theta'_\pi\mathrm{d}\varphi'_\pi = J^{\mathrm{IV}}\mathrm{d}\theta_\pi\mathrm{d}\varphi_\pi,\\
&\mathrm{d}\varphi_{\mathrm{CM}}\mathrm{d}\varphi_\pi = J^{\mathrm{V}}\mathrm{d}\varphi_{\mathrm{CM}}\mathrm{d}(\varphi_\pi-\varphi_{\mathrm{CM}}).
\end{aligned} \tag{12}$$

J^{I} to J^{V} are given in eqs. (4), (6), (8), (9) and (11).

Substitution of (12) into (1) yields

$$\begin{aligned}
\mathrm{d}^7\sigma = {}& w(\mathbf{p}_1)\mathrm{d}p_1 w(\mathbf{p}_2)(E_1+E_2)^3\beta_{\mathrm{CM}}^2\mathrm{d}\beta_{\mathrm{CM}}\sin\theta_{\mathrm{CM}}\mathrm{d}\theta_{\mathrm{CM}}\mathrm{d}\varphi_{\mathrm{CM}}\\
&\times w(p_\pi{}^*)m_\pi(1-\beta_\pi{}^2)^{-\frac{3}{2}}\mathrm{d}\beta_\pi Q\sin\theta_\pi\mathrm{d}\theta_\pi\mathrm{d}(\varphi_\pi-\varphi_{\mathrm{CM}}).
\end{aligned} \tag{13}$$

The term in (13) which will cause troubles is Q. β_{CM} is on an average ≈ 0.3 and β_π will in general be 0.7 to 1.0. Therefore Q is expanded in powers of β_{CM} and terms of the third and higher orders are neglected. Q will be a second degree expression in $\cos\theta'_\pi$.

Making use of the assumptions (i)—(iv), subsect. 5.2.1. the expression (13) can now be integrated. The integration limits are in order of integration:

$$\varphi_\pi-\varphi_{\mathrm{CM}} \text{ and } \varphi_{\mathrm{CM}},\ 0\to 2\pi,$$

$$(\cos\theta_{\mathrm{CM}})_{\mathrm{min}} = \frac{p_1{}^2+\beta_{\mathrm{CM}}^2(E_1+E_{\mathrm{F}})^2-p_{\mathrm{F}}{}^2}{2p_1\beta_{\mathrm{CM}}(E_1+E_{\mathrm{F}})},\quad (\cos\theta_{\mathrm{CM}})_{\mathrm{max}} = 1,$$

$$(\beta_{\mathrm{CM}})_{\mathrm{min}} = \frac{p_1-p_{\mathrm{F}}}{E_1+E_{\mathrm{F}}},\quad (\beta_{\mathrm{CM}})_{\mathrm{max}} = \frac{p_1+p_{\mathrm{F}}}{E_1+E_{\mathrm{F}}}.$$

The final result is given in eq. (29), subsect. 5.2.1. The numerical values to be applied in this paper are

$$\left\langle\frac{p_1}{E_1+E_{\mathrm{F}}}\right\rangle = 0.277,\quad \left\langle\left(\frac{p_1}{E_1+E_{\mathrm{F}}}\right)^2\right\rangle = 0.078.$$

A.4.2. The antiproton undergoes elastic scattering once.

The notation is shown in fig. 24.

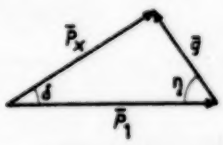

Fig. 24. Notation used in Appendix 4.2.

$\mathbf{p}_1$ is the momentum of the incident antiproton, $\mathbf{p}_x$ the momentum of the antiproton after the collision, $\mathbf{g}$ the momentum transferred during the collision, δ the angle of scattering in the lab. system, η the angle between $\mathbf{p}_1$ and $-\mathbf{g}$.

With reference to $\mathbf{p}_x$ the angular distribution is given by eq. (29), subsect. 5.2.1. but with p_1 in the expression for the coefficients A, B and C, eq. (30), replaced by p_x.

Before averaging over $\mathbf{p}_1$ we have

$$A = 1-\tfrac{1}{2}\left\{1+\left\langle\frac{1}{\beta_\pi{}^2}\right\rangle\right\}\left(\frac{p_x}{E_x+E_F}\right)^2,$$
$$B = 2\left\langle\frac{1}{\beta_\pi}\right\rangle\frac{p_x}{E_x+E_F}, \qquad (1)$$
$$C = \tfrac{3}{2}\left\{1+\left\langle\frac{1}{\beta_\pi{}^2}\right\rangle\right\}\left(\frac{p_x}{E_x+E_F}\right)^2.$$

A transformation from the direction $\mathbf{p}_x$ to the direction $\mathbf{p}_1$ gives new coefficients (after integrating over φ) in front of $\cos^n\theta_\pi$ ($n = 0$, 1 and 2):

$$A' = A+\tfrac{1}{2}C(1-\cos^2\delta), \quad B' = B\cos\delta, \quad C' = \tfrac{1}{2}C(3\cos^2\delta-1). \qquad (2)$$

The values of p_x and $\cos\delta$ are distributed in a way that is determined by the differential scattering cross section. We take an average in the following manner. The factor E_x+E_F in the denominator is replaced by its average, which is a very good approximation in the range of energies considered. From fig. 24 we obtain

$$p_x{}^2 = p_1{}^2+g^2-2p_1 g\cos\eta,$$
$$p_x\cos\delta = p_1-g\cos\eta, \qquad (3)$$
$$(p_x\cos\delta)^2 = p_1{}^2+g^2\cos{}^2\eta-2p_1 g\cos\eta.$$

Substitution of (3) and (1) into (2) gives the expression (31), subsect. 5.2.2, for the coefficients A', B' and C'.

In order to compute the averages of the three quantities g^2, $g\cos\eta$, and $g^2\cos^2\eta$ needed in (3), the joint distribution of g and η given in an earlier paper[20]) (eq. (9) in this ref.) was used. In the paper quoted, the scattering of antiprotons in nuclear matter was treated using a strongly anisotropic cross section for free particles and observing the limitations imposed by the Pauli exclusion principle.

The results of the tedious calculations are

$$\langle g^2\rangle = 1.354\,p_F{}^2, \qquad \langle g\cos\eta\rangle = 0.612\,p_F,$$
$$\langle g^2\cos^2\eta\rangle = 0.611\,p^2{}_F, \quad \langle p_1 g\cos\eta\rangle = 1.405\,p_F{}^2.$$

References

1) O. Chamberlain, E. Segrè, C. Wiegand and T. Ypsilantis, Phys. Rev. **100** (1955) 947
2) A. G. Ekspong and B. E. Ronne, Nuovo Cim. **13** (1959) 27
3) A. G. Ekspong, S. Johansson and B. E. Ronne, Nuovo Cim. **8** (1958) 84
4) J. Button, T. Elioff, E. Segrè, H. M. Steiner, R. Weingart, C. Wiegand and T. Ypsilantis, Phys. Rev. **108** (1957) 1557

5) C. A. Coombes, B. Cork, W. Galbraith, G. R. Lambertson and W. A. Wenzel, Phys. Rev. **112** (1958) 1303
6) O. Chamberlain, G. Goldhaber, L. Jauneau, T. Kalogeropoulos, E. Segrè and R. Silberberg, Phys. Rev. **113** (1959) 1615
7) R. H. Dalitz, Proc. Phys. Soc. A **64** (1951) 667
8) E. Amaldi, G. Baroni, G. Bellettini, C. Castagnoli, M. Ferro-Luzzi and A. Manfredini, Nuovo Cim. **14** (1959) 977
9) A. G. Ekspong, Å. Frisk and B. E. Ronne, Phys. Rev. Letters **3** (1959) 103
10) S. Nilsson and Å. Frisk, Ark. f. Fysik **14** (1958) 277
11) W. H. Barkas, R. W. Birge, W. W. Chupp, A. G. Ekspong, G. Goldhaber, S. Goldhaber, H. H. Heckman, D. H. Perkins, J. Sandweiss, E. Segrè, F. M. Smith, D. H. Stork, L. Van Rossum, E. Amaldi, G. Baroni, C. Castagnoli, C. Franzinetti and A. Manfredini, Phys. Rev. **105** (1957) 1037
12) A. Berthelot, C. Choquet, A. Daudin, O. Goussu and F. Lévy, Nuclear Physics **14** (1960) 545
13) G. B. Chadwick and P. B. Jones, Phil. Mag. **3** (1958) 1189;
A. Engler, P. B. Jones and J. H. Mulves, Proc. Roy. Soc. A **254** (1960) 425
14) A. H. Armstrong and G. M. Frye, Bull. Am. Phys. Soc. **2** (1957) 379
15) J. Dyer, H. H. Heckman, F. M. Smith, Y. Eisenberg, W. Koch, M. Nikolič, M. Schneeberger and H. Winzeler, Helv. Phys. Acta **32** (1959) 559
16) Å. Frisk, S. Nilsson, B. E. Ronne and W. Schneider, Ark. f. Fysik (to be published)
17) M. Blau and M. Caulton, Phys. Rev. **96** (1954) 150
18) G. E. Belovitskii, Soviet Phys. JETP **8** (1959) 581
19) S. Z. Belenkij, V. M. Maksimenko, A. I. Nikišov and I. L. Rozental, Usp. Fiz. Nauk **62** (1957) 1;
Fortschr. d. Phys. **6** (1958) 524
20) A. G. Ekspong, Ark. f. Fysik **16** (1959) 129
21) J. Blaton, Mat. Fys. Medd. Dan. Vid. Selsk. **24**, No. 20
22) N. Horwitz, D. Miller, J. Murray and R. Tripp, Phys. Rev. **115** (1959) 472
23) L. E. Agnew, T. Elioff, W. B. Fowler, L. Gilly, R. Lander, L. Oswald, W. Powell, E. Segrè, H. Steiner, H. White, C. Wiegand and T. Ypsilantis, Phys. Rev. **110** (1958) 994
24) L. E. Agnew, (thesis) UCRL 8785 (1959)
25) J. R. Fulco, Phys. Rev. **114** (1959) 374
26) G. Goldhaber and S. Goldhaber, Phys. Rev. **91** (1953) 467
27) B. A. Nikolskii, L. P. Kudrin and S. A. Ali-Zade, Soviet Phys. JETP **5** (1957) 93
28) A. H. Morrish, Phys. Rev. **90** (1953) 674; Phil. Mag. **45** (1954) 47
29) M. Blau and A. R. Oliver, Phys. Rev. **102** (1956) 489
30) E. Fermi, Progr. Theor. Phys. **5** (1950) 570
31) R. Gatto, Nuovo Cim. **3** (1956) 468
32) G. Sudarshan, Phys. Rev. **103** (1956) 777
33) S. Z. Belenkii and I. S. Rozental, JETP **3** (1956) 786
34) Z. Koba and G. Takeda, Progr. Theor. Phys. **19** (1958) 269
35) J. S. Ball and G. F. Chew, Phys. Rev. **109** (1958) 1385
36) L. F. Cook, (thesis) UCRL 8841 (1959)
37) F. Cerulus, Nuovo Cim. **14** (1959) 827; CERN 60–10; and private communication
38) W. R. Frazer and J. R. Fulco, Phys. Rev. Letters **2** (1959) 365
39) B. J. Malenka and H. Primakoff, Phys. Rev. **105** (1956) 338
40) B. R. Desai, UCRL–9024 (1960)
41) Y. Yeivin and A. de Shalit, Nuovo Cim. **1** (1955) 1146
42) F. Cerulus, Suppl. Nuovo Cim. **15** (1960) 402
43) F. Cerulus, CERN internal report
44) T. Kalogeropoulos, (thesis) UCRL 8677 (1959)
45) J. Sandweiss, Thesis, UCRL 3577 (1956)

8.B

Nuclear Physics **22** (1961) 410—425; ©*North-Holland Publishing Co., Amsterdam*

Not to be reproduced by photoprint or microfilm without written permission from the publisher

$\pi\pi$ INTERACTIONS IN πN-COLLISIONS AT HIGH PION ENERGIES

D. I. BLOKHINTSEV and WANG YUNG

Joint Institute for Nuclear Research, Moscow, USSR

Received 9 September 1960

Abstract: In this paper the role of the peripheral $\pi\pi$ interaction in πN collisions is studied when the momentum of the primary pion is about 7 GeV. It has been shown that in elastic πN scattering the contribution of the peripheral $\pi\pi$ interaction is not great, and that it is fully camouflaged by the diffraction scattering from the nucleon core. In the case of inelastic collisions the contribution of the $\pi\pi$ interaction is already quite noticeable and, therefore, it is possible to determine the cross sections for $\pi\pi$ interaction from the experimental data on multiple pion production. The distribution of the transverse momentum of the recoil nucleon has been calculated in the processes $\pi+N\to N+2\pi$ and of Λ^0 for the process $\pi+N\to\Lambda^0+K+\pi$. It has been shown also that this distribution is in agreement with the experimental data.

1. Elastic Collisions

At high energies elastic pion scattering on nucleons reduces essentially to diffraction scattering. Therefore, the possibility of detecting the $\pi\pi$ interaction from the measurements of elastic pion scattering on nucleons depends upon the relative role of the peripheral elastic $\pi\pi$ interactions and diffraction scattering induced by central opaque parts of the nucleon (core) [1]. In this section we are going to consider the relative role of these two contributions to elastic scattering.

We represent the wave function of the pion-nucleon system $\phi(x, y)$ (x are the nucleon coordinates, y, the pion coordinates) as a sum

$$\phi(x, y) = p(x, y)+q(x, y). \tag{1}$$

At the same time $q(x, y)$ satisfies the equation

$$q(x, y) = \phi^0(x, y)+K_c q(x, y)+K_\pi q(x, y). \tag{2}$$

Here $\phi^0(x, y)$ is the primary wave, $p(x, y)$ is the contribution of the renormalized diagram which may be divided into two parts connected only by one nucleon line (see fig. 1a), K_π and K_c are the renormalized integral operators. The operator K_π represents the peripheral $\pi\pi$ interaction (diagram fig. 1b), the operator K_c gives the contribution of all the remaining diagrams (see, e.g. fig. 1c) †.

† The theory of eq. (2) is developed by W. Zimmermann [2]. We give it here in somewhat changed notations.

If we divide $q(x, y)$ into two parts

$$q(x, y) = q_c(x, y)+q_\pi(x, y), \tag{3}$$

where $q_c(x, y)$ is due to the core scattering and satisfies the equation

$$q_c(x, y) = \phi^0(x, y)+K_c q_c(x, y), \tag{4}$$

then the wave $q_\pi(x, y)$ is due to the $\pi\pi$ interaction and satisfies the equation

$$q_\pi(x, y) = K_\pi q_c(x, y)+K_c q_\pi(x, y)+K_\pi q_\pi(x, y). \tag{5}$$

In this equation the second term represents the diffraction on the core of the wave scattered by the pion, while the third term, the reaction of the wave scattered by the pion. Therefore, the main term will be the first one, and, approximately, one may set

$$q_\pi(x, y) \approx K_\pi q_c(x, y). \tag{6}$$

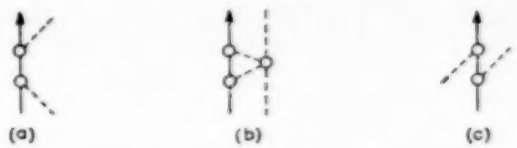

Fig. 1. Diagrams of elastic collisions.

At high pion energies the influence of the nucleon core can be approximately described by the optical model. Therefore,

$$p(x, y)+q_c(x, y) = \phi^0(x, y)+\phi_d(x, y) \tag{7}$$

where $\phi_d(x, y)$ is the wave of the diffraction scattering. Thus, our task, since we are interested only in the influence of the peripheral $\pi\pi$ interaction, reduces to the integration of the expression

$$q_\pi(x, y) \approx K_\pi(\phi^0(x, y)+\phi_d(x, y)-p(x, y)). \tag{8}$$

The similarity of integral (8) and the one of Feynman makes it possible to determine approximately $q_\pi(x, y)$ in terms of the corresponding Feynman integral, if instead of an incident plane wave we use the wave distorted by the core $\phi^0(x, y)+\phi_d(x, y)-p(x, y)$.

Thus, we get from (1), (3), (7)

$$\phi(x, y) = \phi^0(x, y)+\phi_d(x, y)+q_{\pi_1}(x, y)+q_{\pi_2}(x, y)+q_{\pi_3}(x, y), \tag{9}$$

where $\phi^0(x, y) = \phi_1{}^0(x)\phi_2{}^0(y)$ is a plane incident wave, while

$$\phi_d(x, y)+q_{\pi_1}(x, y)+q_{\pi_2}(x, y)+q_{\pi_3}(x, y)$$

is a scattered wave. At the same time $q_{\pi_1}(x, y)$, $q_{\pi_2}(x, y)$, $q_{\pi_3}(x, y)$ are due to the terms $\phi^0(x, y)$, $\phi_d(x, y)$, $p(x, y)$ respectively (see (8)). The diffraction wave

$\phi_d(x, y)$ in the pion and nucleon centre-of-mass-system, in accordance with ref. [3]), must be put as

$$\phi_d(x, y) = \frac{e^{-iE_m x_0 - ik_0 y_0}}{4\pi} \int_S \left(\gamma \frac{\partial}{\partial \mathbf{r}} - \gamma_4 E_m - m\right) \gamma_3 \frac{e^{ip|\mathbf{r}-\boldsymbol{\rho}|}}{|\mathbf{r}-\boldsymbol{\rho}|} \{1-\Omega(\rho)\} u_{\mathbf{p}_i} d\bar{\rho}$$

$$\equiv \frac{e^{-iE_m x_0 - ik_0 y_0}}{(2\pi)^3} \int_S \int (ip'_\mu \gamma_\mu - m) \frac{e^{i\mathbf{p}'\cdot\mathbf{r} - i\mathbf{p}'\cdot\boldsymbol{\rho}}}{p'^2+m^2-E^2-i\varepsilon} \gamma_3 u_{\mathbf{p}_i} d^3\mathbf{p}' \{1-\Omega(\rho)\} d\bar{\rho}. \quad (10)$$

Here, m is the nucleon mass, μ the pion mass, $\mathbf{r} \equiv \mathbf{x}-\mathbf{y}$, $\mathbf{p}' = (p \sin\theta \cos\phi, p \sin\theta \sin\phi, p \cos\theta)$ is the scattered momentum in the c.m.s., $\mathbf{p}_i = (0, 0, p)$ is the initial momentum, $E_m = \sqrt{p^2+m^2}$, $k_0 = \sqrt{p^2+\mu^2}$, $d\bar{\rho} = \rho d\psi d\rho$; the integration is carried out over all the plane S, perpendicular to $\mathbf{p}_i$ and passing through the centre of the core. Further we have

$$\Omega(\rho) = \begin{cases} 1 & \text{at} \quad \rho > R_0, \\ e^{-K\sqrt{R_0^2-\rho^2}} & \text{at} \quad \rho \leqq R_0 \end{cases} \quad (R_0 = \text{the radius of the core}).$$

At $r \gg R_0$ we have

$$\phi_d(x, y) \approx \frac{1}{4\pi} (i\gamma \cdot \mathbf{p}' - \gamma_4 E_m - m) \frac{e^{ipr}}{r} \int_S e^{-ip\rho \cos\psi \sin\theta} \{1-\Omega(\rho)\} \gamma_3 u_{\mathbf{p}_i} d\bar{\rho}. \quad (10a)$$

In these formulae, θ is the angle between the directions $\mathbf{p}'$ and $\mathbf{p}_i$; it coincides with the direction $\mathbf{r}$.

The calculation of the first integral in (8) leads to the result

$$q_{\pi 1}(x, y) = \frac{e^{ipr}}{r} \sum_{\sigma=\pm\frac{1}{2}} u_{\mathbf{p}'\sigma} \frac{3}{8\pi^3} \frac{p}{k_0} \frac{1}{v} g_0^2 \lambda_0 (\bar{u}_{\mathbf{p}'\sigma} u_{\mathbf{p}_i}) I_1(\theta), \quad (11)$$

where σ is the spin index, v is the relative velocity in the c.m.s., θ is defined as before, whereas $mI_1(\chi)$ is equal to

$$mI_1(\chi) = \int_0^1 \int_0^1 \frac{m^2 xy^2 dx dy}{\mu^2 - xy\mu^2 + x^2y^2m^2 + 4(1-x)(y-y^2)\sin^2 \frac{1}{2}\chi p^2}. \quad (12)$$

Similarly

$$q_{\pi 2}(x, y) = \frac{e^{ipr}}{r} \sum_{\sigma=\pm\frac{1}{2}} u_{\mathbf{p}'\sigma} \frac{3}{8\pi^3} \frac{p}{k_0} \frac{1}{v} g_0^2 \lambda_0 (\bar{u}_{\mathbf{p}'\sigma} I_2(\theta) u_{\mathbf{p}_i}), \quad (13)$$

where

$$mI_2(\theta) = \int_{-\frac{1}{2}\pi}^{\frac{1}{2}\pi} d\psi \int_{-1}^{+1} d(\cos\theta') \int_0^{2\pi} d\phi' \int_0^{R_0} \left[\rho' d\rho' mI_1(\chi) p e^{ip\rho' \sin\theta' \cos\psi} \right.$$

$$\left. \times \frac{(-p \cos\theta' - p\gamma_1\gamma_3 \sin\theta' \sin\phi' - p\gamma_2\gamma_3 \sin\theta' \cos\phi' - p)}{2(2\pi)^2} \{1-\Omega(\rho')\}\right]. \quad (14)$$

Here χ is the angle between the directions $\mathbf{r}$ and (θ', ϕ'). The time-dependent phases are identical for $\phi_d(x, y)$, $q_{\pi_1}(x, y)$, $q_{\pi_2}(x, y)$ and we omit them.

Neglecting $q_{\pi_2}(x, y)$ and $q_{\pi_3}(x, y)$, we obtain the expressions for the scattered wave (spinor)

$$\frac{e^{ipr}}{r}[A_\theta(i\gamma\cdot\mathbf{p}'-\gamma_4 E_m-m)\gamma_3 u_{\mathbf{p}_i}+\sum_{\sigma=\pm\frac{1}{2}} BI_1(\theta)(\bar{u}_{\mathbf{p}'\sigma}u_{\mathbf{p}_i})u_{\mathbf{p}'\sigma}],$$
$$A_\theta=\frac{1}{4\pi}\int_S e^{-ip\rho\cos\psi\sin\theta}\,d\bar{\rho}\{1-\Omega(\rho)\},\quad B=\frac{p}{k_0}\frac{1}{v}g_0^2\lambda_0\frac{3}{8\pi^3}. \tag{15}$$

From here we find for the differential scattering cross section

$$\left(\frac{d\sigma}{d\Omega}\right)_{\text{elas}}=\left(\frac{d\sigma}{d\Omega}\right)_{\text{diffra}}+\left(\frac{d\sigma}{d\Omega}\right)_{\pi_1}. \tag{16}$$

It is worth noting that the interference terms are wholly absent. After averaging over the initial polarizations and summing over the finite ones, the cross section $(d\sigma/d\Omega)_{\pi_1}$ is found to be

$$\left(\frac{d\sigma}{d\Omega}\right)_{\pi_1}=\frac{1}{2E_m^2}B^2(I(\theta))^2[(1-\cos\theta)p^2+2m^2]. \tag{17}$$

In the following table are listed the values $(d\sigma/d\Omega)_{\pi_1}$ in the c.m.s. for the momentum of the incident meson $p_{\text{lab}} = 6.8$ GeV/c:

θ^0	0^0	12^0	24°	36°
$\left(\frac{d\sigma}{d\Omega}\right)_{\pi_1}$ mb/sr	2.96	1.74	1.02	0.62

It was assumed that the renormalized interaction constant $g_0^2/4\pi = 15$, whereas the pion interaction constant $|\lambda_0|$ is equal to $4\pi\times 0.3$ †.

In fig. 2 the calculated cross section is compared with the experimental one.

As is seen, $(d\sigma/d\Omega)_{\pi_1}$ increases for forward scattering, but not at all so sharply as the experimental curve. Further, at $p_{\text{lab}} = 6.8$ GeV/c, $(d\sigma/d\Omega)_{\pi_1}$ is much smaller than the experimental value. In general, at $p \to \infty$, $(d\sigma/d\Omega)_{\pi_1}$ decreases as $1/p^2$ at $\theta = 0$, and as $1/p^4$ at $\theta \neq 0$.

Hence, for high energies ($\gtrsim$ 5—6 GeV lab. system) the contribution of the peripheral $\pi\pi$ interaction to elastic πN collision is not great and within the experimental error [4]).

† This value is given by Mandelstam and Chew for low energies. If the momentum of the incident pion in the lab. system is equal to 6.8 GeV/c, then in the rest system of the incident and virtual pions the momentum is only 680 MeV/c. Therefore, it seems that the given value of $|\lambda_0|$ can be used without a large error (see section 2).

The contrary is the case for smaller pion momenta $p_{\text{lab}} \leqq 1$ to 2 GeV/c. For instance, for $p_{\text{lab}} = 1.1$ GeV/c, $(d\sigma/d\Omega)_{\pi_1,\,\theta=0} \approx 10$ mb. At the same energy the experimental value $(d\sigma/d\Omega)_{\text{exp},\,\theta=0}$ is less than 10 mb/sr. It should be concluded from here that the role of $\pi\pi$ interaction in elastic πN scattering at $p_{\text{lab}} < 1$—2 GeV/c is very appreciable.

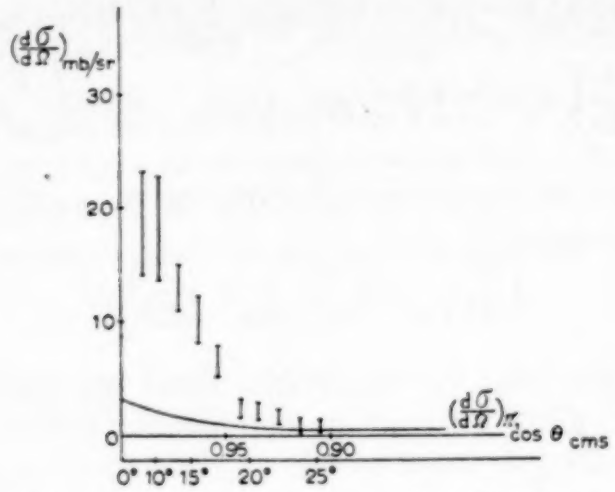

Fig. 2. Comparison of the calculated cross section with the experimental one.
I Experimental data of π—p collisions with $p_{\text{lab}} = 6.8$ GeV/c (see ref. [4])).
— Theoretical curve of $(d\sigma/d\Omega)_{\pi_1}$ with $\lambda_0 = 4\pi \times 0.3$.

Consider now the importance of some simplifications we made. First of all, let us note that if in the core besides the absorption there is a refraction, then the quantity $\{1-\Omega(\rho)\}$ would have an imaginary part. Under this condition the interference term in (16) would not have vanished. Estimation has shown that if the imaginary part $\{1-\Omega(\rho)\}$ amounts to 5 % of the real one, then $(d\sigma/d\Omega)_{\text{interf}} < 0.5$ mb/sr (at $\theta = 0$), that is also very small if compared with the scattering from the core.

Further, we neglected the waves $q_{\pi_2}(x, y)$ and $q_{\pi_3}(x, y)$. If we retain the term $q_{\pi_2}(x, y)$, then the scattered wave has the form

$$\frac{e^{ipr}}{r}\left[A_\theta(i\boldsymbol{\gamma}\cdot\mathbf{p}-\gamma_4 E_m-m)\gamma_3 u_{\mathbf{p}_i}+\sum_{\sigma=\pm\frac{1}{2}} B(\bar{u}_{\mathbf{p}'\sigma}[I_1(\theta)+I_2(\theta)]u_{\mathbf{p}_i})u_{\mathbf{p}'\sigma}\right]. \quad (18)$$

To estimate the influence of $I_2(\theta)$ we put $\Omega(\rho) = 0$ for $\rho \leqq R_0$ and $\Omega(\rho) = 1$ for $\rho > R_0$; then

$$I_2(\theta) = \int_{-1}^{+1} d(\cos\theta') \int_0^{2\pi} d\phi' I_1(\chi)\,\frac{R_0 J_1(pR_0\sin\theta')}{\sin\theta'} \times \frac{(-p\cos\theta' - p\gamma_1\gamma_3\sin\theta'\sin\phi' - p\gamma_2\gamma_3\sin\theta'\cos\phi' - p)}{8\pi} \quad (19)$$

$+$ imiginary part

(χ is the angle between the directions (θ, φ) and (θ', φ')).

Since a) $I_1(\chi)$ is maximum at $\chi = 0$, and decreases rapidly for $\chi \neq 0$, and b) $|J_1(pR_0 \sin\theta')|/\sin\theta'$ is maximum at $\theta' = 0$ and decreases rapidly for $\theta' \neq 0$, then it is easy to see that $|\mathrm{Re}I_2(\theta)|_{\max} = |\mathrm{Re}I_2(0)|$ (if $\theta = 0$, then $\chi = \theta'$) and decreases rapidly for θ deviating from $\theta = 0$. The imaginary part is of the same order of Re $I_2(\theta)$.

The value $|\mathrm{Re}I_2(0)|$ in (19) amounts to $\approx 0.4 \times I_1(0)$ (for $R_0 = 0.7\hbar/\mu c$ and $p_{\mathrm{lab}} = 6.8$ GeV/c) and the sign of $\mathrm{Re}I_2(0)$ is opposite to $I_1(0)$. In this case the contribution of peripheral $\pi\pi$ interaction to elastic πN scattering is

$$\left(\frac{\mathrm{d}\sigma}{\mathrm{d}\Omega}\right)_{\pi_1+\pi_2,\,\theta=0} \approx 1 \text{ mb/sr},$$

i.e. taking into account $q_{\pi_2}(x, y)$ does not change the above-mentioned conclusions.

The imaginary part also gives an interference term, but is of the same order of $(\mathrm{d}\sigma/\mathrm{d}\Omega)_{\pi_1+\pi_2,\,\theta=0}$.

For the isobaric state $T = \frac{3}{2}$ we have $p(x, y) = 0$, whereas for $T = \frac{1}{2}$ we have $p(x, y) \neq 0$. The module $p(x, y)$ is somewhat smaller than $\phi_d(x, y)$. Hence, the above conclusions for elastic collision also remain unchanged with account of the influence of both $q_{\pi_2}(x, y)$ and $q_{\pi_3}(x, y)$.

Thus, it is confirmed that the contribution of peripheral $\pi\pi$ interaction to elastic πN-scattering at an energy of > 5—6 GeV is not great. Therefore, from the data on elastic πN scattering at high energy of pions it is difficult to determine the $\pi\pi$ interaction.

2. Inelastic Collision of the $\pi + \mathrm{N} \to \mathrm{N} + 2\pi$ Type

Now we show that the contribution of the $\pi\pi$ interaction to inelastic πN scattering is not small and may be used to obtain data on $\pi\pi$ interaction.

In order to take into account the contributions from different factors at arbitrary momenta of final pions q_1 and q_2 we adopt the representation similar to Mandelstam's (see fig. 3).

$$s = -(p+q)^2,\ t = -(p-p')^2,\ \bar{s} = -(q-p')^2,\ \mathscr{M}^2 = -(q_1+q_2)^2 = -Q^2, \quad (20)$$

i.e. we consider the two final mesons as a single particle with the mass $\mathscr{M}$ †. For each value of $\mathscr{M}^2$ different $q_1, q_2 (q_1+q_2 = Q)$ may be possible. Below are

† Here we have neglected that diagram, in which the nucleon firstly emits a pion, then absorbs the incident pion, and finally emits another pion. But the contribution of this diagram is of the same order of contribution of pole $\bar{s} = m^2$; therefore it is small (see below).

treated the matrix elements as functions of the variables s, t, $\bar{s}$, at any fixed values of the other parameters. Here

$$s+\bar{s}+t = 2m^2+\mu^2+\mathscr{M}^2 = M^2. \tag{21}$$

When $\mathscr{M}^2$ is fixed, then only two of s, $\bar{s}$, t are free. We know from dispersion relations for $A(s, \bar{s}, t)$ (one of the invariant parts of the amplitude of the process shown in fig. 3) with $s = \text{const.}$, $t = \text{const.}$ and $\bar{s} = \text{const.}$ that $A(s, \bar{s}, t)$ has three poles: $t = \mu^2$, $s = m^2$, $\bar{s} = m^2$ and the cuts $t \geqq 9\mu^2$, $s \geqq (m+\mu)^2$ and $\bar{s} \geqq (m+\mu)^2$.

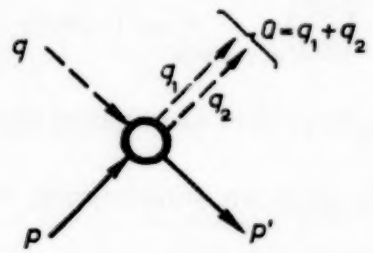

Fig. 3. The momenta of the initial and final particles.

Thus, following Mandelstam, we suppose that $A(s, \bar{s}, t)$ is representable as follows [5]).

$$A(s, \bar{s}, t) = \frac{\alpha}{\mu^2-t} + \frac{\beta}{m^2-s} + \frac{\gamma}{m^2-\bar{s}} + \frac{1}{\pi^2}\int_{9\mu^2}^{\infty}\int_{(m+\mu)^2}^{\infty} \frac{A_{23}(\bar{s}', t')\mathrm{d}t'\mathrm{d}\bar{s}'}{(t'-t)(\bar{s}'-\bar{s}')}$$

$$+ \frac{1}{\pi^2}\int_{9\mu^2}^{\infty}\int_{(m+\mu)^2}^{\infty} \frac{A_{31}(t', s')\mathrm{d}t'\mathrm{d}s'}{(t'-t)(s'-s)} + \frac{1}{\pi^2}\int_{(m+\mu)^2}^{\infty}\int_{(m+\mu)^2}^{\infty} \frac{A_{12}(s', \bar{s}')\mathrm{d}s'\mathrm{d}\bar{s}'}{(s'-s)(\bar{s}'-\bar{s})}, \tag{22}$$

where the spectral functions $A_{23}(\bar{s}', t')$, $A_{31}(t', s')$, $A_{12}(s', \bar{s}')$ do not vanish only in the regions $\{t' > 9\mu^2, \bar{s}' > (m+\mu)^2\}$, $\{t' > 9\mu^2, s' > (m+\mu)^2\}$, $\{s' > (m+\mu)^2, \bar{s}' > (m+\mu)^2\}$ respectively.

From (22) (when $\mathscr{M}^2$ is fixed)

$$A_{\mathscr{M}^2}(s, \bar{s}, t) = \frac{\alpha}{\mu^2-t} + \frac{\gamma}{m^2-\bar{s}} + \frac{1}{\pi}\int_{9\mu^2}^{\infty}\mathrm{d}t' \frac{\mathscr{A}_3(t', s)}{t'-t} + \frac{1}{\pi}\int_{(m+\mu)^2}^{\infty}\mathrm{d}\bar{s}' \frac{\mathscr{A}_2(\bar{s}', s)}{\bar{s}'-\bar{s}}, \tag{23}$$

where

$$\mathscr{A}_3(t', s) = \frac{1}{\pi}\int_{(m+\mu)^2}^{\infty}\mathrm{d}s' \frac{A_{31}(t', s')}{s'-s} - \frac{1}{\pi}\int_{-\infty}^{M^2-(m+\mu)^2-t'}\mathrm{d}s' \frac{A_{23}(\bar{s}', t')}{s'-s},$$

$$\mathscr{A}_2(\bar{s}', s) = \frac{1}{\pi}\int_{(m+\mu)^2}^{\infty}\mathrm{d}s' \frac{A_{12}(s', \bar{s}')}{s'-s} - \frac{1}{\pi}\int_{-\infty}^{M^2-9\mu^2-\bar{s}'}\mathrm{d}s' \frac{A_{23}(\bar{s}', t')}{s'-s}.$$

Eq. (23) is just the dispersion relation for $A(s, \bar{s}, t)$ with fixed s. In the c.m.s. the kinematic consideration yields [6])

$$p^2 = \frac{[s-(m+\mu)^2][s-(m-\mu)^2]}{4s}, \quad (p = |\mathbf{p}| = |\mathbf{q}|),$$
$$p'^2 = \frac{[s-(m+\mathscr{M})^2][s-(m-\mathscr{M})^2]}{4s}, \quad (p' = |\mathbf{p}'| = |\mathbf{Q}|), \tag{24}$$

$$2t = M^2 - s + 4pp'z - \frac{(m^2-\mathscr{M}^2)(m^2-\mu^2)}{s},$$
$$2\bar{s} = M^2 - s - 4pp'z + \frac{(m^2-\mathscr{M}^2)(m^2-\mu^2)}{s}. \tag{25}$$

Here, $z = \cos\theta$, with θ being the angle between $\mathbf{p}$ and $\mathbf{p}'$. It is seen from here that possible values of $\mathscr{M}^2$ lie within the limits $4\mu^2 \leqq \mathscr{M}^2 \leqq (\sqrt{s}-m)^2 = (E-m)^2$. ($E$ = the total energy), z lies in $-1 \leqq z \leqq 1$.

We see from (24) that $p' = 0$ when $\mathscr{M}^2 = (E-m)^2$. Besides, at definite values of s and $\mathscr{M}^2$ the physically possible t lie within the limits

$$t_1 = \tfrac{1}{2}\left\{M^2 - s + 4pp' - \frac{(m^2-\mathscr{M}^2)(m^2-\mu^2)}{s}\right\} \quad (z = 1),$$
$$t_2 = \tfrac{1}{2}\left\{M^2 - s - 4pp' - \frac{(m^2-\mathscr{M}^2)(m^2-\mu^2)}{s}\right\} \quad (z = -1).$$

In fig. 4 two extreme cases with $\mathscr{M}^2 = (E-m)^2$ and $\mathscr{M}^2 = 4\mu^2$ are shown, when $s = (26.6)^2\mu^2 = 707.6\ \mu^2$ (the pion momentum in the lab. system is ≈ 6.8 GeV/c.)

It is seen if $\mathscr{M}^2$ increases from $4\mu^2$ up to $(E-m)^2$, then

a) the lines $\bar{s} = m^2 = 46.3\mu^2$ and $\bar{s} = (m+\mu)^2 = 61$ are gradually displaced to the right,

b) the physically possible interval (t_1, t_2) on the line $s = 707.6\ \mu^2$ decreases gradually from ($t_1 \approx -0.26\ \mu^2$, $t_2 \approx -612.4\ \mu^2$) up to ($t_1 \approx -100.1\ \mu^2$, $t_2 \approx -100.1\ \mu^2$),

c) the distances of the interval (t_1, t_2) on the line $s = \text{const.}$ from the poles and from the cuts increase gradually.

From here one can draw the following qualitative conclusions:

a) the main contribution is in the region of the value of $\mathscr{M}^2$ not very far from $4\mu^2$, and the value of t not very far from $t = \mu^2$. Indeed, the closeness from the pole $t = \mu^2$ makes it very probable that p' has the backward direction ($z = 1$);

b) the next important contribution is made by the cut $t \geqq 9\mu^2$, which also gives the contribution essentially to the scattering in the backward direction;

c) the contributions of the pole $\bar{s} = m^2$ and of the cut $\bar{s} \geqq (m+\mu)^2$ are very small, i.e., the probability that p' is directed in the forward direction ($z = -1$) is very small.

We can also see from fig. 4 that the smallest values of the denominators of the terms of the pole $t = \mu^2$, of the cut $t \geqq 9\mu^2$, of the pole $\bar{s} = m^2$ etc. to eq.

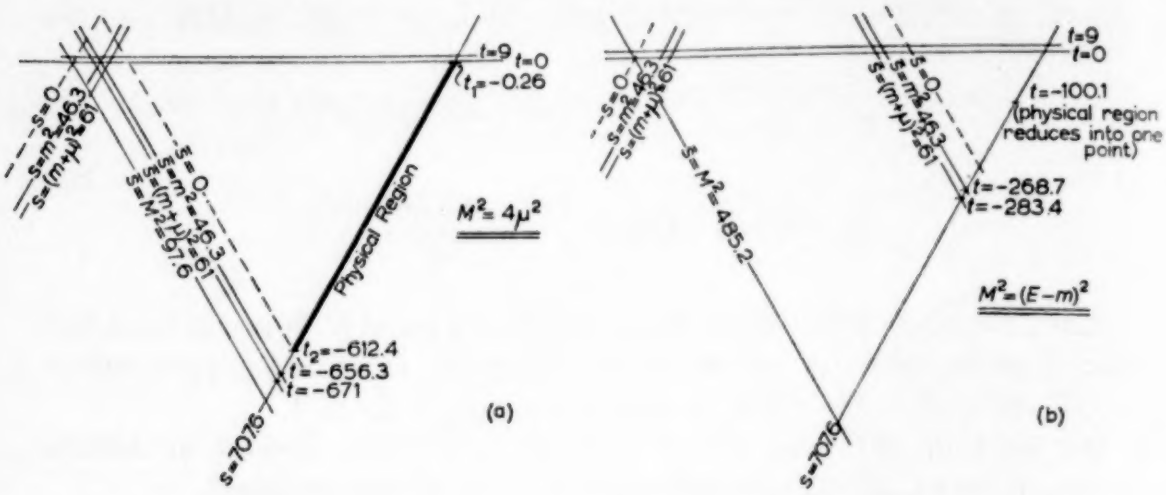

Fig. 4. The physical region (a) when $M^2 = 4\mu^2$, (b) when $M^2 = (E-m)^2$.

(23) are equal to $|t-\mu^2| \approx 1$, $|t-9\mu^2| \approx 10$, $|\bar{s}-m^2| \approx 50$ etc., respectively.

Therefore, for the first approximation it is sufficient to take into account the contribution of the pole $t = \mu^2$ only, i.e.,

$$\langle \mathrm{f}|S|\mathrm{i}\rangle = \frac{(2\pi)^4}{2^{\frac{3}{2}}}\,\delta^4(p+q-p'-q_1-q_2)\,\frac{g_0(\bar{u}_1\gamma_5 u_1)}{(p'-p)^2+\mu^2}\,\frac{(\pi_1\pi_2|\pi\pi')}{\sqrt{\omega_1\omega_2\omega}}.$$

After summing over the finite nucleon polarizations and averaging over the initial ones, we get for the cross section

$$\sigma_{\pi+\mathrm{N}\to\mathrm{N}'+\pi_1+\pi_2} = \frac{g_0^2}{(2\pi)^5}\,\frac{1}{16 v_{\pi\mathrm{N}}}\int \delta^4(p+q-p'-q_1-q_2)\,|(\pi_1\pi_2|\pi\pi')|^2$$
$$\times\,\frac{1}{p_0 p'_0}\,\frac{p_0 p'_0 - pp'\cos\theta - m^2}{[2p_0 p'_0 - 2pp'\cos\theta - 2m^2+\mu^2]^2}\,\frac{\mathrm{d}^3p'\,\mathrm{d}^3q_1\,\mathrm{d}^3q_2}{\omega_1\omega_2\omega}. \quad (26)$$

Here, p, p_0 are the momentum and the energy of the initial nucleon, p', p'_0 the momentum and the energy of the recoil nucleon, $v_{\pi\mathrm{N}}$ is the relative velocity between the initial pion and the nucleon, q_1, ω_1, q_2, ω_2 are the momenta and the energy of final pions π_1, π_2, and ω is the energy of an incident pion; all those quantities are defined in the c.m.s. Further, m, μ are the nucleon and pion masses and θ is the angle between $\mathbf{p}$ and $\mathbf{p}'$.

$(\pi_1\pi_2|\pi\pi')$ resembles the invariant factor in the matrix element

$$\langle\pi_1\pi_2|S|\pi\pi'\rangle = \frac{(2\pi)^4}{4}\frac{(\pi_1\pi_2|\pi\pi')}{\sqrt{\omega\omega'\omega_1\omega_2}}\,\delta^4(q+q'-q_1-q_2). \tag{27}$$

We shall consider the amplitude $(\pi_1\pi_2|\pi\pi')$ to be constant and later on discuss this assumption. Under this assumption we have

$$\sigma_{\pi+N\to N'+\pi_1+\pi_2} \approx \frac{g_0^2}{(2\pi)^4}\frac{1}{16v_{\pi N}}\frac{1}{p_0\omega}\int\frac{1}{p'_0}\frac{(p_0p'_0-pp'\cos\theta-m^2)}{[2p_0p'_0-2pp'\cos\theta-2m^2+\mu^2]^2}f(p')\mathrm{d}^3p', \tag{28}$$

$$\begin{aligned} f(p') &= \frac{|(\pi_1\pi_2|\pi\pi')|^2}{2\pi}\int\delta^4(p+q-p'-q_1-q_2)\,\frac{\mathrm{d}^3q_1\mathrm{d}^3q_2}{\omega_1\omega_2} \\ &= |(\pi_1\pi_2|\pi\pi')|^2\sqrt{1-\frac{4\mu^2}{(E-p'_0)^2-p'^2}}, \quad (E=\omega+p_0), \end{aligned} \tag{29}$$

where

$$\frac{f(p')}{f(0)} = \sqrt{1-\frac{4\mu^2}{(E-p'_0)^2-p'^2}} \approx 1 \quad (0<p'<p'_{\max})$$

and suddenly falls down to zero at $p'\approx p'_{\max}$, with

$$p'_{\max} = \frac{1}{2E}\sqrt{(E+m+2\mu)(E+m-2\mu)(E-m+2\mu)(E-m-2\mu)}.$$

From (28) it is possible to show that

1) $$\frac{\partial\sigma_{\pi+N\to N'+\pi_1+\pi_2}}{\partial\Omega_{p'}} \approx \frac{g_0^2|(\pi_1\pi_2|\pi\pi')|^2}{(2\pi)^4 16v_{\pi N}}\frac{1}{p_0\omega} \cdot\int\frac{p'^2}{p'_0}\frac{(p_0p'_0-pp'\cos\theta-m^2)}{[2p_0p'_0-2pp'\cos\theta-2m^2+\mu^2]^2}\sqrt{1-\frac{4\mu^2}{(E-p'_0)^2-p'^2}}\,\mathrm{d}p' \tag{30}$$

has a sharp maximum at $\theta=0$, i.e., the recoil nucleons are directed sharply in the backward direction. Further,

2) the distribution of the total p' in the πN c.m.s.

$$\begin{aligned} \frac{\partial\sigma_{\pi+N\to N'+\pi_1+\pi_2}}{\partial p'} &= \frac{g_0^2|(\pi_1\pi_2|\pi\pi')|^2}{(2\pi)^3 16v_{\pi N}}\frac{1}{p_0\omega}\frac{p'^2}{p'_0} \\ &\times\sqrt{1-\frac{4\mu^2}{(E-p'_0)^2-p'^2}}\left[\frac{1}{4pp'}\log\left(1+\frac{4pp'}{(2p_0p'_0-2pp'-2m^2+\mu^2)}\right)\right. \\ &\left.-\frac{\mu^2}{(2p_0p'_0-2m^2+\mu^2)^2-4p^2p'^2}\right] \end{aligned} \tag{31}$$

has its maximum near $p' \approx p'_{max}$ (see fig. 5). (If we take into account the contribution of the cut $t > q\mu^2$, then the maximum of the distribution in fig. 5 will be somewhat displaced to the left).

3) The distribution of the transverse momentum of the recoil nucleon $p'_\perp$ is expressed by the formula (in the πN c.m.s.)

$$\frac{\partial\sigma_{\pi+N\to N'+\pi_1+\pi_2}}{\partial p_\perp'} = \frac{g_0^2|(\pi_1\pi_2|\pi\pi')|^2}{(2\pi)^3\,16 v_{\pi N}}\,\frac{1}{p_0\omega}$$
$$\times\int_{\sqrt{p'^2_{max}-p'^2_\perp}}^{\sqrt{p'^2_{max}-p'^2_\perp}} \frac{p'_\perp}{p'_0}\,\frac{(p_0p'_0-pp'_z-m^2)}{(2p_0p'_0-2pp'_z-2m^2+\mu^2)^2}\sqrt{1-\frac{4\mu^2}{(E-p'_0)^2-p'^2}}\,dp'_z \quad (32)$$
$$(p'^2 = p'^2_\perp + p'^2_z)$$

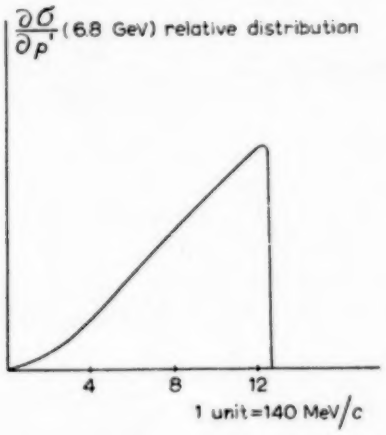

$E = 26.6\mu$ $\quad p'_{max} = 12.34\mu c$ $\quad p = 12.4\mu c$ $\quad$ (c.m. syst)

Fig. 5. Total momentum distribution in the πN c.m.s.

The transverse momentum of the recoil nucleon $p'_\perp$ corresponding to the distribution maximum of $p'_\perp$ almost does not change with the pion energy: $p'_{\perp\,opt} \approx 330$—$350$ MeV/c (see the distribution curves in fig. 6).

4) The total cross section for the reaction $\pi+N \to N'+\pi_1+\pi_2$, according to (28), is equal to (in the πN c.m.s.)

$$\sigma_{\pi+N\to N'+\pi_1+\pi_2} = \frac{g_0^2|(\pi_1\pi_2|\pi\pi')|^2}{(2\pi)^3\,16 v_{\pi N}}\,\frac{1}{p_0\omega}\int_0^{p'_{max}}\frac{p'^2}{p'_0}\sqrt{1-\frac{4\mu^2}{(E-p'_0)^2-p'^2}}$$
$$\times\left[\frac{1}{4pp'}\log\left(1+\frac{4pp'}{(2p_0p'_0-2pp'-2m^2+\mu^2)}\right)-\frac{\mu^2}{(2p_0p'_0-2m^2+\mu^2)^2-4p^2p'^2}\right]dp'$$
$$= \frac{g_0^2|(\pi_1\pi_2|\pi\pi')|^2}{(2\pi)^3\,16 v_{\pi N}}\,\frac{1}{p_0\omega}\times 0.5. \quad (33)$$

(Momentum of incident π is $p_{lab} \approx 6.8$ GeV/c.)

In this integral the main contribution is from the region p' near p'_{max}.

Therefore, it will be reasonable in formula (33) to take the value of $|(\pi_1\pi_2|\pi\pi')|^2$ near $p' = p'_{\max}$. This corresponds to $\pi\pi$ scattering when $|q| = 12.4\mu^2$, $|q'| \approx 0$ in the lab. system, or $|q| = |q'| = 680$ MeV/c in the centre-of-mass system of π and π'.

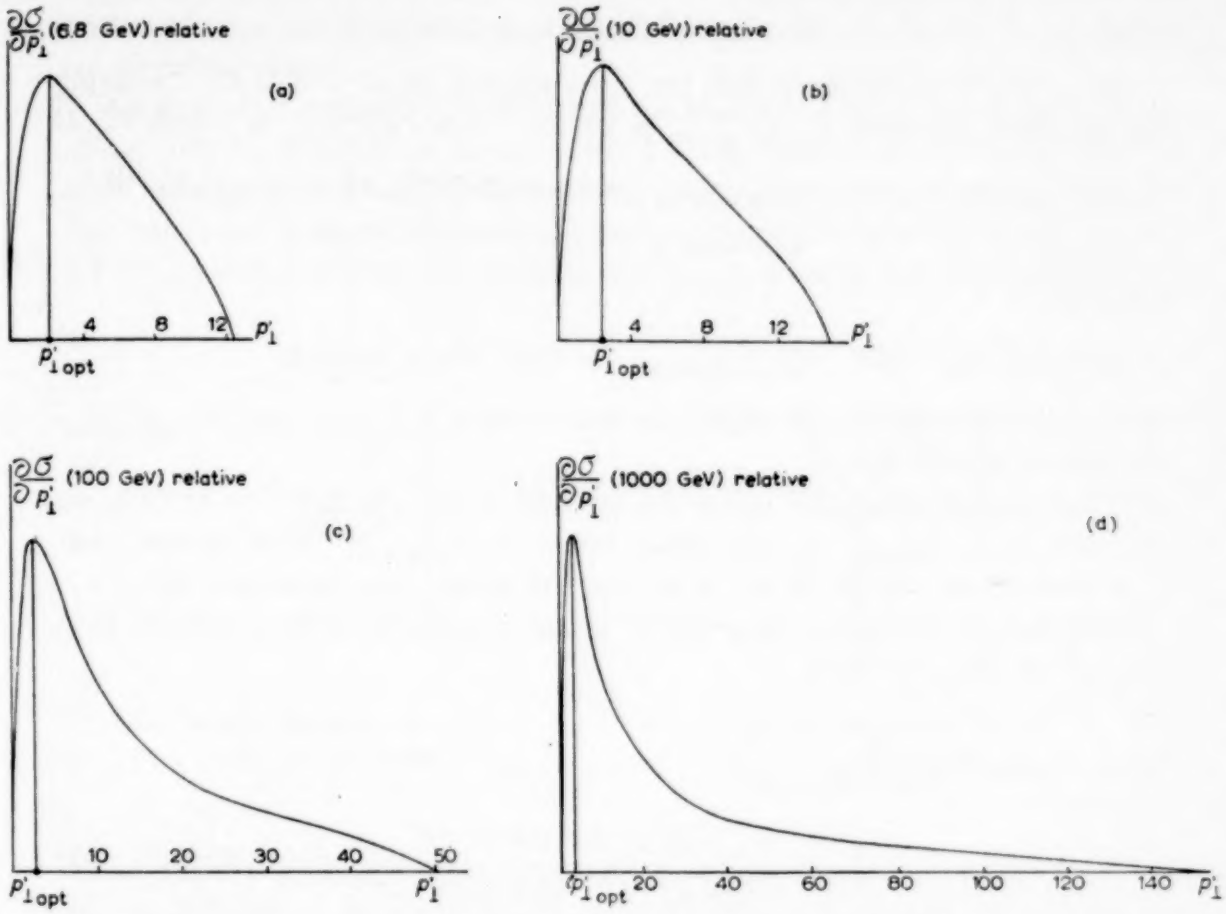

Fig. 6. Transverse momentum distributions. (a) $p_{\perp\,\mathrm{opt}} = 2.39$ units $= 335$ MeV/c; momentum of the pion ≈ 6.8 GeV/c (lab. syst.). (b) $p'_{\perp\,\mathrm{opt}} = 2.37$ units $= 332$ MeV/c; momentum of the pion ≈ 10 GeV/c (lab. syst.). (c) $p'_{\perp\,\mathrm{opt}} \approx 2.5$ units $= 350$ MeV/c; momentum of the pion ≈ 100 GeV/c (lab. syst.). (d) $p'_{\perp\,\mathrm{opt}} \approx 2.5$ units $= 350$ MeV/c; momentum of the pion ≈ 1000 GeV/c (lab. syst.). (1 unit $= 140$ MeV/c).

Further (in the c.m.s.),

$$\sigma_{\pi+\pi'\to\pi_1+\pi_2} = \frac{1}{v_{\pi\pi}^2}\,\frac{1}{16}\,\frac{1}{(2\pi)^2}\int \frac{|(\pi_1\pi_2|\pi\pi')|^2}{\omega^4}\,q^2\,\mathrm{d}\Omega \approx \frac{1}{64\pi\omega^2}\,|(\pi_1\pi_2|\pi\pi')|^2 \tag{34}$$

(considering $|(\pi_1\pi_2|\pi\pi')|^2$ to be independent of angle). Therefore, the ratio of the cross sections $\sigma_{\pi+\pi'\to\pi_1+\pi_2}/\sigma_{\pi+\mathrm{N}\to\mathrm{N}'+\pi_1+\pi_2}$, when the momentum of the primary pion is ≈ 6.8 GeV, is found to be ≈ 3.

On the other hand, the cross section for $p_\perp \leqq 1\mu c (\approx 140$ MeV/c) turns out to be

$$\sigma^{(p_\perp \leqq \mu c)}_{\pi+N\to N'+\pi_1+\pi_2} \approx \frac{1}{20}\sigma_{\pi+N\to N'+\pi_1+\pi_2},$$

when the momentum of the primary pion is ≈ 6.8 GeV/c; therefore

$$\sigma_{\pi+\pi'\to\pi_1+\pi_2}/\sigma^{(p_\perp \leqq \mu c)}_{\pi+N\to N'+\pi_1+\pi_2} \cong 60.$$

According to preliminary data the cross sections for $\pi^- p$ inelastic scattering for all final channels is $\sigma_{\pi^- p(\text{total})} \approx 25$ mb † and $\sigma^{(p_\perp \leqq \mu c)}_{\pi^- p(\text{total})} \approx 2.6$mb ††. If

$\sigma_{\pi^-+p\to n+\pi^++\pi^-}$ and $\sigma_{\pi^-+p\to p+\pi^0+\pi^-}$ are about 20 % of $\sigma_{\pi^- p(\text{total})}$, i.e. if
$\sigma_{\pi^-+p\to n+\pi^++\pi^-}$ and $\sigma_{\pi^-+p\to p+\pi^0+\pi^-}$ are both about 5 mb,

whereas

$\sigma^{(p_\perp \leqq \mu c)}_{\pi^-+p\to n+\pi^++\pi^-}$ and $\sigma^{(p_\perp \leqq \mu c)}_{\pi^-+p\to p+\pi^0+\pi^-}$ are both about 0.5 mb

then the cross sections for elastic $\pi\pi$ scattering $\sigma_{\pi^-+\pi^+\to\pi^-+\pi^+}$ and $\sigma_{\pi^-+\pi^0\to\pi^-+\pi^0}$ are about 15—30 mb.
(Taking $\lambda_0 = 4\pi\times 0.3$ and using the method of the perturbation theory, we also get $\sigma_{\pi+N\to N'+\pi_1+\pi_2}$ in the same order as $\sigma_{\pi^- p(\text{total})}$. This means that $\lambda_0 = 4\pi\times 0.3$ is correct in an order for the given case in section 1).

Note that if the factor $|(\pi_1\pi_2|\pi\pi')|^2$ is not considered to be constant, then instead of (28), we have

$$\sigma_{\pi+N\to N'+\pi_1+\pi_2} \approx \frac{g_0^2}{(2\pi)^4\, 16 v_{\pi N}}\,\frac{1}{p_0\omega} \cdot\int \frac{1}{p'_0}\,\frac{p_0p'_0 - pp'\cos\theta - m^2}{(2p_0p'_0 - 2pp'\cos\theta - 2m^2+\mu^2)^2}\,F'(p',\theta')\,\mathrm{d}^3p', \quad (35)$$

where

$$F'(p',\theta) = \int \frac{1}{2\pi}\,|(\pi_1\pi_2|\pi\pi')|^2\,\delta^4(p+q-p'-q_1-q_2)\,\frac{\mathrm{d}^3q_1\,\mathrm{d}^3q_2}{\omega_1\omega_2}. \quad (36)$$

In this case the conclusions 1), 2), 3) remain correct. Indeed, $f(p')$ in (29) is the first approximation for $F'(p',\theta)$ in (36), the conclusions 1), 2) and 3) are mainly determined by the factor

$$\frac{1}{p'_0}\,\frac{p_0p'_0 - pp'\cos\theta - m^2}{(2p_0p'_0 - 2pp'\cos\theta - 2m^2+\mu^2)^2}$$

and are not very sensitive to $f(p')$ and to $F'(p',\theta)$.

† According to measurements in the propane cloud chamber in the meson beam with the momentum 6.8 GeV/c (private communication of Wang Kan-chang, Lab. of High Energies, JINR).
†† According to emulsion-measurements, in the meson beam with the momentum 6.8 GeV/c (private communication of R. M. Lebedev, Lab. of High Energies, JINR).

It follows from this consideration that if we also take into account the processes of multiple pion production in the pion-pion interaction corresponding to diagram in fig. 7, then the conclusions 1) and 3) on the distribution of the recoil momentum remain valid, since they are not sensitive to the vertex of the $\pi\pi$ interaction (vertex λ_0). Besides, in this case the maximum of the distribution of total recoil momentum in fig. 5 shifts further to the left according to conservation laws.

We have also made the calculation of the transverse recoil momentum of the Λ^0-particle for the process shown in fig. 8. This diagram gives the momentum of Λ^0 sharply in the backward direction. At the same time it turned out that the transverse momentum is found to be too large for the pseudoscalar vertex (Λ^0NK) and too low for the scalar one. For a mixture of the pseudoscalar and

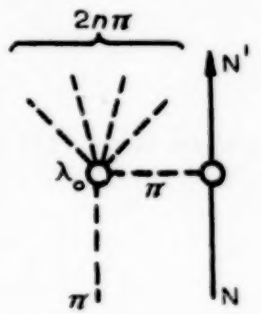

Fig. 7. Diagram of multiple pion production.

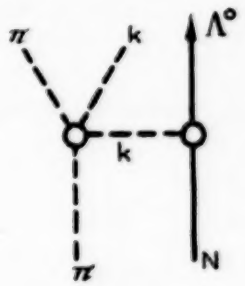

Fig. 8. Diagram of KΛ production.

scalar type ($1\pm\gamma_5$) when the momentum of the primary pion is 6.8 GeV/c, $p_{\Lambda\perp\,\mathrm{opt}}$ is found to be $\approx$ 410 MeV/c, whereas the experimental value is $p_{\Lambda\perp\,\mathrm{opt}}$ $\approx 410\pm42$ MeV/c †. We have

$$\frac{\partial\sigma}{\partial p'_{\Lambda\perp}} \propto \int_{-\sqrt{p'^2_{\max}-p'^2_{\Lambda\perp}}}^{\sqrt{p'^2_{\max}-p'^2_{\Lambda\perp}}} \frac{p'_{\Lambda\perp}}{p'_{\Lambda 0}} \sqrt{\left(1-\frac{(m_K+\mu)^2}{(E-p'_{\Lambda 0})^2-(p'^2_\Lambda)}\right)\left(1-\frac{(m_K-\mu)^2}{(E-p'_{\Lambda 0})^2-p'^2_\Lambda}\right)} \times \frac{p_0 p'_{0\Lambda}-pp'_{\Lambda z}}{(2p_0p'_{0\Lambda}-2pp'_{\Lambda z}-m^2-m_\Lambda{}^2+m_K{}^2)^2}\,\mathrm{d}p'_{\Lambda z}, \quad (37)$$

where m, m_Λ, m_K, μ are the masses of the nucleon, Λ^0-particle, K-meson and π-meson, p_0 and E are defined as earlier, and

$$p'_{\max} = \frac{1}{2E}\sqrt{[(E+m_\Lambda)^2-(\mu+m_K)^2]\,[(E-m_\Lambda)^2-(\mu+m_K)^2]}, \quad (38)$$

$$p'^2_{\Lambda 0} = p'^2_\Lambda + m_\Lambda{}^2 = p'^2_{\Lambda z} + p'^2_{\Lambda\perp} + m_\Lambda{}^2.$$

† Ding Da-tsao (private communication).

In fig. 9 is given the distribution $p'_{\Lambda\perp}$ in the generation of Λ^0 and K particles. Note that the interactions of the type $1\pm\gamma_5$ will lead to the polarization of Λ_0 particles.

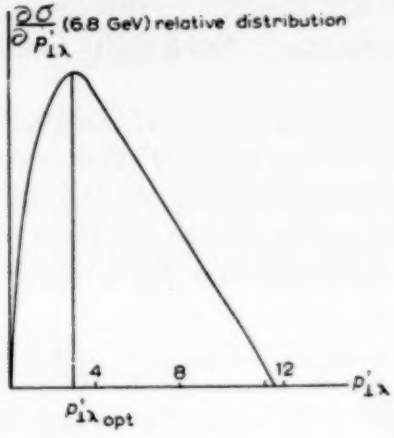

Fig. 9. Transverse momentum distribution. $p'_{\perp\Lambda\,\mathrm{opt}} \approx 2.9$ units = 410 MeV/c (1 unit = 140 MeV/c).

3. Summary

1. The contribution of the peripheral $\pi\pi$ interaction to elastic pion scattering by a nucleon at pion energies > 5—6 GeV is not great; it is essential at energies $\leqq 1$—2 GeV.

2. In the same region of pion energies (> 5—6 GeV) the contribution of the $\pi\pi$-interaction to inelastic pion scattering is quite appreciable. From the preliminary data on $\pi+\mathrm{N} \to \mathrm{N}'+\pi_1+\pi_2$ processes one can estimate the cross section for $\pi\pi$-interaction to be ≈ 15—30 mb (at momentum $\cong 680$ MeV/c in c.m.s. of $\pi\pi$).

3. The transverse momentum of the recoil nucleon in the πN-collision is weakly dependent upon the incident pion energy; $p_{\perp\mathrm{opt}} \approx 330$—350 MeV/$c$ in the interval 7—1000 GeV/c.

4. For the generation of Λ^0 particles the transverse momentum of the Λ^0-particle is in agreement with experiment under the assumption that the vertex (Λ_0NK)-interaction has the structure $(1\pm\gamma_5)$. In this case one should expect the polarization of the generated Λ^0 particles.

The authors express their gratitude to Kim Ze-phen for the numerical calculations. One of the authors (Wang Yung) thanks A. V. Efremov, Tzu Hun-yuan, Chou Kuang-chao, and Ho Tso-hsiu for helpful discussions and valuable advices.

References

1) D. I. Blokhintsev, V. S. Barashenkov and B. M. Barbashov, Uspekhi fiz. nauk **68** (1959) 417–447
2) W. Zimmermann, Suppl. Nuovo Cim. **11** (1954) 106–117
3) A. I. Akhiezer and I. Ya. Pomeranchuk, Uspekhi fiz. nauk **65** (1958) 593–630
4) Wang Kan-chang *et al.*, JETP **38** (1960) 426–431
5) S. Mandelstam, Phys. Rev. **112** (1958) 1344–1360
6) T. W. B. Kibble, Phys. Rev. **117** (1960) 1159–1162

1.D.1

Nuclear Physics **22** (1961) 426—433; © *North-Holland Publishing Co., Amsterdam*

Not to be reproduced by photoprint or microfilm without written permission from the publisher

ON THE 5.16 MeV AND 7.56 MeV STATES OF B^{10}

W. W. TRUE † and E. K. WARBURTON

Palmer Physical Laboratory, Princeton University, Princeton, New Jersey ††

Received 19 September 1960

Abstract: The methods developed by Talmi and co-workers are used to calculate the binding energies of the two B^{10} levels formed by coupling $2s_{\frac{1}{2}}^2$ to the Be^8 ground state. The calculated energies are found to be in excellent agreement with those of the B^{10} 5.16 and 7.65 MeV levels for which the most probable spin-parity and isobaric-spin assignments are $J^\pi = 1^+$, $T = 0$ and $J^\pi = 0^+$, $T = 1$, respectively. The strong γ-transition connecting these levels is also consistent with the proposed identification with double-particle excitation into the 2s—1d shell. The excitation energies of $2s_{\frac{1}{2}}^n$ levels in Be^{10}, B^{11} and C^{12} are also calculated assuming that the Be^8 ground state forms an inert core.

1. Introduction

A great deal of experimental work has been done recently on the B^{10} states between 4.5 and 8 MeV, in particular on the 5.16 and 7.56 MeV levels [1–3]). The most recent work [3]) confirms the strong γ-transition between these two states and supports the well-established spin-parity assignment of $J^\pi = 0^+$ for the 7.56 MeV level. The strength of the γ-transition, if it is M1, is 4.5 ± 0.4 Weisskopf units [2]). Such a strong γ-transition could only be dipole, and since B^{10} is self-conjugate, the dipole selection rules [4–6]) indicate $\Delta T = 1$ for this transition as well as $J = 1$ for the 5.16 MeV level. Other evidence [1]) indicates even parity for this level and from a review of the experimental data it appears that the most likely assignments for these two states are $(J^\pi, T) = (1^+, 0)$ and $(0^+, 1)$ for the 5.16 and 7.56 MeV levels, respectively. It should be emphasized that these assignments are far from conclusive since the data are inconsistent. Also, there is the mystery of the missing $(2^+, 1)$ analog of the Be^{10} first-excited state which is expected at about 5 MeV in B^{10} and which was previously thought to be the B^{10} 5.16 MeV level. However, the purpose of this note is not to attempt to resolve the ambiguities in the spin-parity and isobaric-spin assignments of B^{10}, but only to show that if the B^{10} 5.16 and 7.56 MeV levels are $(J^\pi, T) = (1^+, 0)$ and $(0^+, 1)$, respectively, then they most probably arise from the

† Now at Department of Physics, University of California, Davis, California.

†† This work was supported by the U. S. Atomic Energy Commission and the Higgins Scientific Trust Fund.

group of levels $1s^4\,1p^4(2s, 1d)$ †; that is, to the group of states formed by raising two nucleons from the 1p-shell into the degenerate, or nearly degenerate, 2s and 1d shells. The point here is that it is quite unlikely that these two levels belong to the 1p-shell if these spin-parity and isobaric-spin assignments are correct. This follows from the intermediate-coupling calculations of Kurath [7]) in the p-shell, which indicate that there are no unaccounted for $(0^+, 1)$ p-shell states below at least 10 MeV in B^{10}, and none with $(J^\pi, T) = (1^+, 0)$ below 9 MeV. So that, if these assignments are correct, the B^{10} 5.16 and 7.56 MeV states are quite sure to arise from excited configurations.

In N^{14} the $(0^+, 1)$ 8.62 MeV level and the (1,0) 6.23 MeV level have been assigned [8,9]) to the group of levels formed by $s^4p^8(s, d)$. The M1 γ-transition connecting these states is extremely strong, 7.3 Weisskopf units, and the separation between them is 2.39 MeV. If, then, the B^{10} 7.56 and 5.16 MeV levels are $(0^+, 1)$ and $(1^+, 0)$, respectively, they bear a strong resemblance to these N^{14} states; the γ-transition between them having an energy of 2.40 MeV and a strength, if it is M1, of 4.5 ± 0.4 Weisskopf units [2,3]).

Unna and Talmi [8]) obtained good agreement between the excitation energies of these two N^{14} levels and the excitation energies calculated for the two levels formed by coupling $2s^2$ to the C^{12} ground state. The C^{12} core was assumed to be $s^4p_{\frac{3}{2}}^8$. The extreme jj-coupling assumption of $s^4p_{\frac{3}{2}}^8$ was fundamental to their work since they considered the general problem of the binding energies of states formed by adding $p_{\frac{1}{2}}^m 2s^n$ to the $p_{\frac{3}{2}}^8$ core. However, for states formed by adding 2s or 1d nucleons to the C^{12} ground state, the weaker assumption of an inert spin-zero core would give the same results. In the next section, the excitation energies of the $(0^+, 1)$ and $(1^+, 0)$ levels formed by adding $2s^2$ to an inert spin-zero Be^8 ground-state core will be calculated using the method of Talmi and co-workers [8,10]).

2. Calculations

In the work of Unna and Talmi [8]), it was assumed that there was no mixing of the 2s and 1d shells so that it is proper to speak of the $p^m 2s^n$ configuration. This assumption will be made in the present work. The validity of this assumption will be discussed in sect. 3. Furthermore, it will be assumed that for $m = 4$ or 8 the $1s^4p^m$ configuration forms an inert spin-zero core, the Be^8 or C^{12} ground state, for which the kinetic energy and interaction energy with a single 2s nucleon are independent of the number of nucleons in the 2s shell and their mode of coupling. This assumption was made by Unna and Talmi for a C^{12} core for both $2s_{\frac{1}{2}}$ and $1p_{\frac{1}{2}}$ nucleons and seems to be justified by the excellent over-all agreement they obtained with experiment. The further assumption, made here,

† This notation is intended to suggest that these levels belong to the configurations $s^4p^4s^2+s^4p^4d^2+s^4p^4sd$. When no confusion should arise, we shall leave off the principal quantum numbers and the closed $1s^4$ shell.

of an inert Be^8 core seems reasonable since the Be^8 nucleus is quite tightly bound, more so than any other nucleus between He^4 and C^{12}, and has only two excited states below 15 MeV, the lowest at 2.9 MeV [1]).

For $j = \frac{1}{2}$ particles, the binding energy of a j^n configuration can be written as [8, 10])

$$\text{B.E.} = n_n A_N + n_p A'_N + \tfrac{1}{2}n(n-1)a + [T(T+1) - \tfrac{3}{4}n]b - \text{C.E.}, \qquad (1)$$

where n_n is the number of neutrons, n_p the number of protons, n is $n_n + n_p$, the quantity T is the isobaric-spin of the j^n configuration, and C.E. is the Coulomb energy of the extra-core protons. A_N (or A'_N) represents the interaction of a neutron (or proton) with the inert core of N nucleons, and a and b are parameters which can be determined in principle if the interaction potential and the single-particle radial wave functions are known [10]). In this work, the parameters A_N, A'_N, a and b in eq. (1) will be determined by comparison with experiment. Note that the parameter c of Talmi and Thieberger [10]) does not appear in eq. (1) as it is not needed for configurations involving nucleons with $j = \frac{1}{2}$.

If the $p^8(s, d)N^{14}$ levels at 8.62 and 6.23 MeV [9]) are assumed to be $2s^2$ coupled to the C^{12} ground state, and the C^{13} and N^{13} first-excited states are assumed to be formed by coupling a 2s nucleon to the C^{12} ground state, then the parameters A_{12}, A'_{12}, a and b for 2s nucleons can be determined from the binding energies of these states. The result is †

$$A_{12} = 1.86 \text{ MeV}, \quad A'_{12} = -0.42 \text{ MeV}, \qquad (2a)$$

and

$$a = 3.04 \text{ MeV}, \quad b = -1.20 \text{ MeV}. \qquad (2b)$$

These values of A_{12}, A'_{12}, a and b are different from those obtained by Unna and Talmi [8]) (see table 1). The A_{12}, A'_{12}, a and b were determined by Unna and Talmi from energy levels of mass 17, 18, and 19. We do not believe that these parameters give a good representation of the effective 2s interaction for $2s^2$ outside a Be^8 or C^{12} core. In brief, our arguments are based on the evidence[11, 12]) for configuration interaction between the 2s and 1d shells. This question will be discussed in more detail in sect. 3.

In order to study 2s particles outside the Be^8 core, it is necessary to determine A_8 and A'_8, the neutron and proton interaction energies with the Be^8 core. A_8 was found by using eq. (1) and assuming that the 1.75 MeV, $J^\pi = \frac{1}{2}^+$, level [1]) in Be^9 is formed by coupling a 2s neutron to the Be^8 core. Eq. (1) yields

$$A_8 = -0.083 \text{ MeV}. \qquad (3)$$

A'_8 is not so readily determined since the 2s state has not been identified in B^9.

† All binding energies used in this work are taken from ref. [1]).

To estimate the excitation energy of the $s^4p^4 2s$ state in B^9 the difference in Coulomb energy between a p-state proton and an s-state proton coupled to the Be^8 core was estimated in the following way. The Be^8 core was replaced with a uniform charge distribution which had a radius of $R = 1.20\, A^{\frac{1}{3}} \times 10^{-13}$ cm $= 2.40 \times 10^{-13}$ cm. The p (or s) proton was described by an harmonic oscillator wave function with the parameter ν_p (or ν_s) appearing in the oscillator wave function taken from the work of Talmi and Thieberger [10]). The Coulomb energy between the core and the extra-core proton was found to be 2.38 MeV for the p state and 2.07 MeV for the 2s state. This result would indicate that the 2s state in B^9 should be at an excitation of about 1.44 MeV. There is some experimental evidence for a level in B^9 at about 1.4 MeV [1]).

Using 1.44 MeV for the excitation energy of the $J^\pi = \frac{1}{2}^+$, $B^9 p^4 2s$ state leads to

$$A'_8 = +1.63 \text{ MeV}. \tag{4}$$

From eq. (1) and the parameters in eqs. (2), (3) and (4), the excitation energies of the two $2s^2$ states in B^{10} are calculated to be

$$E(0, 1) = 7.52 \text{ MeV}, \quad E(1, 0) = 5.12 \text{ MeV}. \tag{5}$$

These energies are to be compared with the positions of the two levels at 7.56 MeV and 5.16 MeV in B^{10}. The remarkably good agreement (40 keV difference) gives good support to an identification of the 7.56 MeV and 5.16 MeV levels in B^{10} with the $(0^+, 1)$ and $(1^+, 0)$ levels formed by coupling $2s^2$ to the Be^8 ground state. The agreement is, in actual fact, somewhat better than expected even if the assumption of extreme *jj* coupling is valid. This is so because of the uncertainties due to such things as the Thomas shift [13]) as well as the uncertainty in the Coulomb energy calculations. We expect an uncertainty of several hundred keV or so from these effects.

In this calculation, we used the A_{12} and A'_{12} obtained from the experimental binding energies of the mass 13, 2s states. If we had used the A_{12} and A'_{12} given by Unna and Talmi [8]) to determine the parameters a and b, the calculated B^{10} excitation energies would both have been 320 keV lower. We feel that the A_{12} and A'_{12} obtained from the mass 13, 2s states are the better ones to use for two reasons. First of all, the A_{12} and A'_{12} of Unna and Talmi were obtained from a least squares fit to 13 $p_{\frac{1}{2}}^n 2s$ states between C^{13} and F^{17} and these do not necessarily represent the effective interaction of a $2s_{\frac{1}{2}}$ nucleon with the C^{12} core in the absence of $p_{\frac{1}{2}}^n$. Secondly, we expect the Thomas shift and the Coulomb corrections in mass 9 to be somewhat the same as in mass 13 so that using the mass 13 states to obtain A_{12} and A'_{12} corrects to some extent for these effects.

3. Discussion of Calculation

As was pointed out in the last section, it is possible to get A_{12} and A'_{12} from

the positions of the 2s levels in C^{13} and N^{13}. In the same manner, A_{16} and A'_{16} can be obtained from the positions of the 2s levels in O^{17} and F^{17}. With these additional parameters, it is now possible to calculate the position of the $2s^n$ levels with a C^{12} or O^{16} core, as well as with a Be^8 core. Table 1 gives a comparison

TABLE 1

Comparison of the parameters in MeV of this paper with those of Unna and Talmi

Parameters	This paper	Unna and Talmi
a	3.04	3.57
b	−1.20	−1.91
A_8	−0.08	−0.08 [a])
A'_8	−1.63	−1.63 [a])
A_{12}	1.86	1.64
A'_{12}	−0.42	−0.52
A_{16}	3.28	3.28 [b])
A'_{16}	0.10	0.10 [b])

[a]) These parameters were not calculated by Unna and Talmi.
[b]) These parameters were not given explicitly by Unna and Talmi but are presumed to be as given.

TABLE 2

Calculated excitation energies of $s^4p^m2s^n$ configurations

Core	State (nucleus; J^π, T)	Energy (MeV) [a])	Energy (MeV) [b])	Experimental levels [c]) (energy (MeV); J^π, T)
Be^8	B^{10}; 1^+, 0	5.12	3.52	5.16; (1^+, 0)
	B^{10}; 0^+, 1	7.52	7.35	7.56; (0^+, 1)
	Be^{10}; 0^+, 1	6.20	6.03	6.18; ?
	B^{11}; $\frac{1}{2}^+$, $\frac{1}{2}$	10.59	7.93	?
	C^{12}; 0^+, 0	18.10	12.79	17.77; (0^+, 0) 10.1; 0^+, 0 7.66; 0^+, 0
C^{12}	N^{14}; 1^+, 0	6.23 [d])	4.95	6.23; (1^+, 0) [d])
	N^{14}; 0^+, 1	8.62 [d])	8.76	8.62; 0^+, 1 [d])
	O^{16}; 0^+, 0	11.57	6.90	11.25; 0^+, 0 6.06; 0^+, 0
O^{16}	F^{18}; 1^+, 0	1.54	0.00 [e])	1.70; 1^+, 0 0.00; 1^+, 0 [e])
	F^{18}; 0^+, 1	3.94	3.8	?
	F^{19}; $\frac{1}{2}^+$, $\frac{1}{2}$	2.60	0.00 [e])	? 0.00; $\frac{1}{2}^+$, $\frac{1}{2}$ [e])
	Ne^{20}; 0^+, 0	5.30	0.05	6.75; 0^+, 0 0.00; 0^+, 0

[a]) Calculated with the parameters of this paper (see table 1).
[b]) Calculated with the parameters of Unna and Talmi (see table 1).
[c]) Possible levels for assignment to the $2s^n$ states, this list is not necessarily complete. Uncertain J^π, T assignments are enclosed in parenthesis.
[d]) Used in this paper to fix the parameters a and b.
[e]) Used by Unna and Talmi to fix the parameters a and b.

of the parameters as determined above with the parameters of Unna and Talmi.

Table 2 gives a comparison of the calculated positions of some of the $2s^n$ configurations outside of a Be^8, C^{12} and O^{16} core with the parameters of table 1. For the calculations in table 2 which used the parameters of this paper, the Coulomb interactions for four $2s_{\frac{1}{2}}$ particles outside a core was assumed to be 0.85 MeV in all cases. This value for the Coulomb interaction is approximately that used by Unna and Talmi, although their Coulomb energy varied slightly with the various nuclei. The experimental levels given in table 2 are not unique but are given for comparison with the calculated values.

The B^{10} levels have been discussed in the previous section. The Be^{10} 6.18 MeV level seems to be the most likely candidate for the Be^{10} analog of the B^{10} 7.56 MeV level, it is the only Be^{10} level in the energy region near 6 MeV in Be^{10} for which $(0^+, 1)$ is possible. The calculated Be^{10}, $2s^2$ energy of 6.20 MeV lends support to this assignment. There are many B^{11} levels with unknown spin and parity about 10 MeV excitation and so no conclusions can be drawn regarding an identification of the $2s^3$ level in B^{11}. For $2s^4$ any errors in the parameters a and b are greatly magnified. Therefore, no conclusions are drawn regarding the $2s^4$ level in C^{12} except that it is quite unlikely that the $(0^+, 0)$ 7.66 MeV level is predominantly $2s^4$.

The calculations of Elliott and Flowers [11]) and of Redlich [12]) indicate considerable configuration mixing in F^{18} and F^{19}. Their calculations also indicate that the $(1^+, 0)$ F^{18} ground state contains less $2s^2$ than the next higher $(1^+, 0)$ level and that the F^{19} ground state contains less than 50 % $2s^3$. Thus the parameters a and b which Unna and Talmi obtained from the 2s states of F^{17} and O^{17} and the F^{18} and F^{19} ground states, assuming $2s^2$ and $2s^3$ for the two latter states, would seem to be liable to considerable error. It is perhaps significant that our parameters give best agreement with the F^{18} second highest $(1^+, 0)$ level (presumed to be the 1.70 MeV level) and the second highest $(0^+, 1)$ level which is not identified but presumed to be in the region 3 to 5 MeV in F^{18}. These two states are the mass 18 $(1^+, 0)$ and $(0^+, 1)$ states which have the most $2s^2$ according to the results of Redlich [12]). However, because of the configuration mixing between the 2s and 1d shells, we feel that the parameters a and b determined for Be^8 and C^{12} cores are not applicable for calculations using an O^{16} core and vice versa. This follows from the reversal of the relative positions of the $2s_{\frac{1}{2}}$ and $1d_{\frac{5}{2}}$ single-particle shells at O^{16}. That is, the method of Talmi and co-workers appears to be taking configuration mixing into account in a quantitative way as long as the relative positions of the $2s_{\frac{1}{2}}$ and $1d_{\frac{5}{2}}$ single-particle levels are the same; but the effect of configuration mixing on level position is very likely different outside the O^{16} core than outside the Be^8 or C^{12} core †.

† Because of the reversal of the $2s_{\frac{1}{2}}$ and $1d_{\frac{5}{2}}$ single-particle levels at O^{16}, the argument given in footnote 47 of ref. [9]) is in error.

A brief qualitiative argument can be given as to why the method of Talmi and co-workers works so well outside a given core, in spite of the presence of considerable configuration mixing. Consider two particles outside of an O^{16} core interacting with each other with a central two-body potential. These two particles could be in either the 2s or 1d shells. The positions of the resulting levels for a given spin will depend on the diagonal matrix elements and the amount of configuration mixing. Now suppose one assumed that the positions of the resulting energy levels arose from pure configurations (i.e., diagonal matrix elements only) due to some "pseudo" potential. It is then possible to calculate the energy levels of the three-particle configurations outside of the O^{16} core from these "pseudo" two-body diagonal matrix elements. This method has been discussed by Backer and Goudsmit [14]) and used in atomic physics calculations concerning the electronic configurations of an atom. Preliminary calculations indicate that this approach gives energy levels which are very close to those obtained by doing a three-particle calculation in detail with configuration mixing. Further calculations are being done on this aspect of the problem. This "pseudo" potential calculation has recently been put on a much firmer theoretical basis by de Shalit [15]).

For the reasons given above we consider the results of the present calculation to be more significant for the case of a Be^8 or C^{12} core than are the results using the parameters a and b of Unna and Talmi. Also, we believe that the present results are not very significant for the case of an O^{16} core.

4. Conclusions

The excitation energies of the lowest $(0^+, 1)$ and $(1^+, 0)$ levels of s^4p^4(s, d) were predicted from the measured positions of the 2s states in mass 9 and 13 and the excitation energies of the analogous s^4p^8(s, d) states in N^{14}. The calculation was made using the procedure developed by Talmi and co-workers with the additional assumption of an inert Be^8 ground-state core for the mass 9 and 10 levels. This procedure assumes $2s^2$ for these double-excited states in B^{10} and N^{14}; however, it is argued that the method gives effective parameters which correct, to a good approximation, for the effects of the expected mixing of the 2s and 1d shells and for other effects such as the Thomas shift.

The result of the calculation gives support to an identification of the B^{10} 5.16 and 7.56 MeV levels with $(1^+, 0)$ and $(0^+, 1)$ of s^4p^4(s, d). These assignments also offer an explanation for the strong M1 γ-transition connecting these states (assuming even parity for both). For an inert Be^8 core, the γ-transition is between two states with the shell-model wave functions

$$\Psi(J, T) = \alpha\psi(2s^2)+\beta\psi(2s1d)+\gamma\psi(d^2),$$

and, as discussed by Warburton and Pinkston [9]) for the case of N^{14}, the strength of the M1 transition between these states is expected to be extremely

strong. For instance, if both states were pure $2s^2$, the calculated strength is 8.6 Weisskopf units.

Both the 5.16 and 7.56 MeV states of B^{10} have extremely small α-widths for the Li^6 ground state [1]). This is expected for the 7.56 MeV level if it has $T = 1$; however, if the 5.16 MeV level is $(1^+, 0)$ then an explanation other than the isobaric-spin selection rule must be found for its small α-width. A tentative explanation can be made which is most easily stated from the viewpoint of the cluster model [16–18]). If the B^{10} 5.16 MeV level belongs to $s^4p^4(s, d)$ then the cluster model would describe it as a deuteron plus a Be^8 ground-state core, and in this case a large deuteron width but a small width for break up into the Li^6 ground state plus an α-particle is indicated [18]). However, this point should be checked by a quantitative calculation.

The authors wish to thank Carl Levinson for several discussions and for suggesting an investigation of the procedure of Talmi and co-workers using the method of Bacher and Goudsmit.

References

1) F. Ajzenberg-Selove and T. Lauritsen, Nuclear Physics **11** (1959) 1
2) W. E. Meyerhof, N. W. Tanner and C. M. Hudson, Phys. Rev. **115** (1959) 1227
3) N. W. Tanner, R. E. Meads, J. E. G. McIldowie and S. S. Hanna, Bull. Am. Phys. Soc. **5** (1960) 45
4) D. H. Wilkinson, Proceedings of the Rehovoth Conference on nuclear structure, ed. by H. J. Lipkin (North-Holland Publishing Company, Amsterdam 1958) Session IV, p. 175
5) G. Morpurgo, Phys. Rev. **110** (1958) 721
6) E. K. Warburton, Phys. Rev. **113** (1959) 595
7) D. Kurath, Phys. Rev. **101** (1956) 216
8) I. Unna and I. Talmi, Phys. Rev. **112** (1958) 452
9) E. K. Warburton and W. T. Pinkston, Phys. Rev. **118** (1960) 733
10) I. Talmi and R. Thieberger, Phys. Rev. **103** (1956) 718
11) J. P. Elliott and B. H. Flowers, Proc. Roy. Soc. A **229** (1955) 536
12) M. G. Redlich, Phys. Rev. **110** (1958) 468
13) R. G. Thomas, Phys. Rev. **88** (1952) 1109
14) R. F. Bacher and S. Goudsmit, Phys. Rev. **46** (1934) 948
15) A. de Shalit, private communication
16) K. Wildermuth and Th. Kanellopoulos, Nuclear Physics **7** (1958) 150
17) K. Wildermuth and Th. Kanellopoulos, The application of the cluster model to nuclear physics (CERN, June 1959)
18) B. Roth and K. Wildermuth, Bull. Am. Phys. Soc. **5** (1960) 271

1.D.1

Nuclear Physics **22** (1961) 434—438; ©*North-Holland Publishing Co., Amsterdam*

Not to be reproduced by photoprint or microfilm without written permission from the publisher

ON THE EFFECTIVE INTERACTION IN FINITE NUCLEI

B. BREMOND

Laboratoire de Physique Théorique et Hautes Energies Faculté des Sciences, Orsay (S et O.), France †

Received 8 August 1960

Abstract: The expectation values of the two nucleons interaction are calculated using Brueckner's matrix and shell model wave functions. These values are compared with phenomenological ones. The discrepancies can be explained by the effected approximations.

1. Introduction

A method of analysis of nuclear energy levels by the shell model in *jj* coupling was first and especially used by I. Talmi [1–4]). This method does not make any assumption about the form of the wave function and of the interaction between nucleons; it consists essentially in expressing the energies of the nuclei with the same open shells in terms of parameters, some of which are the expectation values of the nucleon-nucleon interaction in states with fixed kinetic momentum and isobaric spin. Adjusting these parameters makes it possible then to determine the energies to a high accuracy.

We shall here determine the 'phenomenological' parameters from the nucleon-nucleon potential. We use the method of Brueckner and look for the expectation value of the effective interaction, that is the value of a matrix K for a 'model' wave function. Two approximations are made:

1) the use of Brueckner's K matrix, describing the infinite nuclear matter, for finite nuclei,

2) the use as model wave functions of harmonic oscillator wave functions. The energy parameters are calculated for the $1s_{\frac{1}{2}}$, $d_{\frac{3}{2}}$ shells †† and for nuclei with open shells $1s_{\frac{1}{2}}$ and $p_{\frac{1}{2}}$ or $d_{\frac{3}{2}}$ and $1s_{\frac{1}{2}}$; *jj* coupling in this case seems to be a good approximation.

2. General Form of the Effective Interaction

The method of Brueckner for the calculation of the binding energy of a system of nucleons consists essentially in replacing the two-body interaction by a reaction matrix K. The matrix elements are then calculated, as in first-order perturbation theory, using a model wave function.

† Work supported in part by the United States Air Force through the European Office, Air Research and Development Command.

†† A nucleon is specified by the quantum numbers nlj, n being equal to zero in the lowest state.

This K matrix has been determined, for the nfinite nuclear matter, by imposing a requirement of self consistency, with the two-body potential of Gammel and Thaler [5]).

For a finite nucleus, the self-consistency condition should determine simultaneously the K matrix, the nucleon wave function and the value of the density everywhere inside the nucleus. We do not treat the self-consistency problem here, but rather start from a phenomenological determination of the density, make a simple assumption for the wave function and use for each density Brueckner's K matrix for that density.

The interaction energy for two nucleons 1 and 2 in i and j states is then

$$\langle i\gamma|K|i\gamma\rangle = \int \psi^*_{1i}(\mathbf{r}_1)\psi^*_{2j}(\mathbf{r}_2)K_{12}(\mathbf{r}_1, \mathbf{r}_2, \mathbf{r}'_1, \mathbf{r}'_2) \psi_{1i}(\mathbf{r}'_1)\psi_{2j}(\mathbf{r}'_2)\mathrm{d}^3r_1\mathrm{d}^3r_2\mathrm{d}^3r'_1\mathrm{d}^3r'_2 + \text{exchanges}. \tag{1}$$

The effective interaction is split into two parts:

a) a non local attractive part K_A practically independent of the nucleon density and function only of the relative distance between the nucleons $\mathbf{r} = \mathbf{r}_1 - \mathbf{r}_2$, of their relative angular momentum l and of their total spin S;

b) a repulsive part K_c due to the core of the two-body potential and depending both on rlS and on the density at the position $\mathbf{R} = \frac{1}{2}(\mathbf{r}_1 + \mathbf{r}_2)$ of the centre of mass of the two nucleons.

Brueckner has not calculated the odd angular momentum terms nor the tensor terms of the effective interactions. We use for these ones the simple first order perturbation theory with the Gammel and Thaler potential.

This approximation can be partially justified: these terms have a non zero angular momentum, so that the relative distance is never small and hence the effective interaction will not be very different in this case from the twobody potential.

The local approximation

In order to evaluate the importance of the non local character of the K matrix, in addition to the exact computation with the non local attractive term K_A, we also perform the calculation with the equivalent local potential

$$K_{A_{loc}}(\mathbf{r}) = \int \mathrm{d}\mathbf{r}' K_A(\mathbf{r}, \mathbf{r}').$$

3. The Model Wave Functions

We use harmonic oscillator wave functions. Their radius is phenomenologically adjusted for each shell to account for the Coulomb interaction energy terms as determined by the Talmi method.

The effective potential is a function of $\mathbf{r}l\mathbf{R}S$, and the wave functions depend

on the coordinates of the nucleons $\mathbf{r}_i l_i j_i$. We simplify the integrand, eq. (1), by performing two linear transformations:

a) a $jjLS$ transformation;

b) we express the two nucleon wave function $\psi(\mathbf{r}_1, \mathbf{r}_2)$ as a linear combination of products of wave function describing their relative motion and the motion of the centre of mass. The coefficients are calculated by a method due to A. Arima [6,7].

We then obtain the coefficients c of the total transformation *

$$|n_1 l_1 j_1, n_2 l_2 j_2, T, JM\rangle = \sum c(NL, nl, \mathscr{L}S, T, JM)\cdot$$

4. The Interaction Energy

The expectation value of the interaction between two nucleons in a state of angular momentum J and isobaric spin T

$$\langle n_1 l_1 j_1, n_2 l_2 j_2, T, JM|K|n_1 l_1 j_1, n_2 l_2 j_2, T, JM\rangle$$

can be expressed, by the above-mentioned transformations, as a linear expression of terms of the form

$$\langle NL, nl, \mathscr{L}S; TJM|K|NL, nl, \mathscr{L}S; TJM\rangle\cdot$$

The attractive term of the K matrix

It can be decomposed into a central, a spin orbit, and a tensor part. The angular variables integration is performed by the usual method and the evaluation of the matrix elements is thus reduced to the integration of its radial part.

The repulsive term of the K matrix

This term is important only when $l = 0$. Hence only the central part exists,

$$K_c = \frac{A}{4\pi r_c^2}\frac{1}{1-\dfrac{b}{r_0}}\,\delta(r-r_c)\delta(r'-r_c),$$

where r_c is the core radius and r_0 the mean distance of the nucleons to the centre of mass of the two nucleons: r_0 is related to the density d by

$$d = \frac{3}{4\pi r_0^3}\cdot$$

The integration over $\mathbf{r}$ is trivial.

But this term depends strongly on the value of the density at the position of

* n, l are relative quantum numbers, N, L quantum numbers of the motion of the centre of mass and $\mathscr{L}$, S, J respectively total angular momentum, spin and kinetic momentum.

the centre of mass of the two nucleons. We approximate the nucleus by a sphere of radius R_0 and uniform density d_0.

For these nuclei, around Ca^{40}, we choose $r_0 = 1.32 \times 10^{-13}$ cm. We show the interaction energies thus calculated and the phenomenological ones in table 1.

TABLE 1

Expectation values of the nucleon-nucleon interaction (in MeV). We have also given the linear combinations of expectation values determined in the Talmi method by the fundamental energy states (these combinations are determined more accurately in this method)

	T	J	Phenomenological determinations			Theoretical determinations	
						Local	Non local
$((1s_{\frac{1}{2}})^2 TJ)$	1	0	1.820 [1]		2.132 [4]	2.683	2.304
	0	1	2.452 [1]		2.278 [4]	3.253	2.379
$((d_{\frac{3}{2}})^2 TJ)$	1	0	2.729 [1]		2.796 [4]	0.801	0.520
	0	1			0.980 [4]	0.247	−0.232
	1	2	−0.085 [1]		−0.089 [4]	0.584	0.529
	0	3			2.654 [4]	1.831	1.315
$\frac{3}{10}(T=0,\ J=1)+\frac{7}{10}(T=0,\ J=3)$			2.152 [1]		2.152 [4]	1.356	0.851
$(1s_{\frac{1}{2}}, d_{\frac{3}{2}}; TJ)$	0	1			1.525 [4]	1.967	1.415
	0	2			2.864 [4]	1.171	0.836
	1	1			1.204 [4]	0.338	0.338
	1	2			−1.203 [4]	0.866	0.803
$\frac{1}{2}(T=0,\ J=1)+\frac{1}{2}(T=1,\ J=1)$			1.12 [2]	0.98 [2]	1.364 [4]	1.152	0.876
$\frac{1}{2}(T=0,\ J=2)+\frac{1}{2}(T=1,\ J=2)$			1.05 [2]	0.97 [2]	0.830 [4]	1.018	0.856
$(1s_{\frac{1}{2}}, p_{\frac{1}{2}}; TJ)$	0	0	3.09 [3]			2.962	2.040
	0	1	1.817 [3]			2.108	1.492
	1	0	−0.77 [3]			0.690	0.690
	1	1	0.011 [3]			0.709	0.614
$\frac{1}{2}(T=0,\ J=0)+\frac{1}{2}(T=1,\ J=0)$			1.162 [3]			1.826	1.365
$\frac{1}{2}(T=0,\ J=1)+\frac{1}{2}(T=1,\ J=1)$			0.914 [3]			1.408	1.053

5. Conclusion

The agreement between the theoretical and the phenomenological values of the energies is rather good for the $1s_{\frac{1}{2}}$ shell, not so good for the $d_{\frac{3}{2}}$ shell, and relatively good for the other shells. The discrepancies are of order 10 % for the $1s_{\frac{1}{2}}$ shell, 50 % for the other shells, except for the $d_{\frac{3}{2}}$ shell where the two results, are almost unrelated. This can be due partially to the fact that the theoretical values are obtained by subtracting two quantities which are nearly equal; in the $[(d_{\frac{3}{2}})^2 12]$ case for instance $\Delta = 0.52$ MeV $= 4$ MeV $- 3.5$ MeV.

Also one of the approximations made was poor: the substitution of the two-body potential for the odd l and tensor terms. This approximation is valid inasmuch as we are calculating the total energy of the nucleus, for then the

tensor terms cancel on complete shells and the singlet and triplet terms almost completely compensate each other. But this is not the case here since we are considering two nucleons in a state of given isobaric spin.

Unfortunately, it is not possible to find proper linear combinations of the energies that will eliminate the undesirable terms. For a given configuration, there are only two eigenvalues of the energy corresponding to a given isotopic spin, and no linear combination of these two eigenvalues eliminates the undesirable terms.

But there are some energy eigenvalues which do not contain any matrix element determined here in first Born approximation: the energies of the $(1s_{\frac{1}{2}})^2 JT$ configurations; for there the agreement between the theoretical determination (non local matrix) and the phenomenological one is excellent. For the $(1s_{\frac{1}{2}}, p_{\frac{1}{2}}, 00)$ and $(1s_{\frac{1}{2}}, d_{\frac{3}{2}}, 01)$ configurations, the proportion of energies coming from Born approximated matrix elements is rather weak so that the agreement is still good.

Another weak approximation is the local one; indeed the values so determined are twice as great.

The disagreement could be said as not being fundamental as regards the possibility of obtaining the energies from an effective interaction treatment, even when this effective interaction is beforehand computed in infinite nuclear matter.

It is also likely that the method of Talmi does not provide a unique accurate determination of the set of parameters; rather important changes in these parameters do not alter the overall agreement for the energies of the nuclei. Therefore it is not important to try to produce these parameters with a great accuracy.

We are indebted to Dr. B. Jancovici for suggesting the subject of this paper and for some criticism.

References

1) I. Talmi and R. Thieberger, Phys. Rev. **103** (1956) 718
2) S. Goldstein and I. Talmi, Phys. Rev. **105** (1957) 995
3) I. Unna and I. Talmi, Phys. Rev. **112** (1958) 452
4) A. Arima, Progr. Theor. Phys. **19** (1958) 421
5) K. A. Brueckner, J. L. Gammel and M. Weitzner, Phys. Rev. **110** (1958) 431
6) A. Arima, private communication
7) A. Arima and T. Terasawa, Progr. Theor. Phys. **23** (1960) 115

2.B

Nuclear Physics **22** (1961) 439—450; ©*North-Holland Publishing Co., Amsterdam*

Not to be reproduced by photoprint or microfilm without written permission from the publisher

THE POLARIZATION OF NEUTRONS FROM THE $Li^7(p, n)Be^7$ REACTION (I)

S. E. DARDEN, T. R. DONOGHUE and C. A. KELSEY

University of Notre Dame, Notre Dame, Indiana †

Received 13 October 1960

Abstract: Previous measurements on the polarization of neutrons from the $Li^7(p, n)Be^7$ reaction have been extended. Left-right asymmetries in the scattering of neutrons emitted from the reaction at a laboratory angle of 50° have been measured using scatterers of Li^6, Li^7, O and Mg. Measurements were carried out for laboratory scattering angles near 90°, and for neutron energies between 85 and 420 keV. Data obtained using the Li^7, O and Mg scatterers were analyzed to give the polarization of the neutrons emitted from the reaction. The measured polarizations are of the order of 0.4 down to 250 keV neutron energy, below which they decrease abruptly. Relatively small asymmetries observed using Li^6 as a scatterer suggest the antiparallel spin S-wave interaction may be the stronger for this nucleus.

1. Introduction

The $Li^7(p, n)Be^7$ reaction has been widely used as a neutron source for many years. As such, it has been the subject of considerable interest both from a practical standpoint and with a view towards understanding the reaction process itself. Extensive measurements on the reaction cross section were first carried out by Taschek and Hemmendinger [1]), who obtained the total and differential reaction cross section for proton bombarding energies from the threshold energy at 1.88 MeV up to 2.50 MeV. A pronounced peak in the total reaction cross section was observed at 2.25-MeV proton energy, superimposed on a relatively slowly varying background cross section. The angular distributions in the vicinity of this peak were found to be asymmetric about a neutron emission angle of 90° in the centre of mass system, indicating that states in the compound nucleus Be^8 of opposite parity are involved in the interaction. Although the angular distribution data were originally interpreted [2]) in terms of a resonant state at 2.25-MeV proton energy, formed by S-wave protons, and broad states formed by P-wave protons, it was subsequently shown by Adair [3]) that the resonance at 2.25-MeV proton energy most probably corresponds to a state having $J^\pi = 3^+$, $T = 1$, formed by P-wave protons, with the background cross section attributable to S-waves leading to states in the compound nucleus having $J^\pi = 2^-$ and 1^-. Since the initial and final states involved in the reaction are states having mirror symmetry, the reduced proton width γ_p^2 and neutron

† Work supported in part by the joint program of the Office of Naval Research and the United States Atomic Energy Commission.

width γ_n^2 for the states in Be^8 should be approximately equal if each state is characterized by a definite isobaric spin[4]). If in addition to charge symmetry, the charge independence of nuclear forces is assumed, the reduced widths of the 3^+ state in Be^8 should be simply related to the reduced neutron width of the 3^+ companion state in Li^8. Assuming this to be the case, and identifying the 3^+

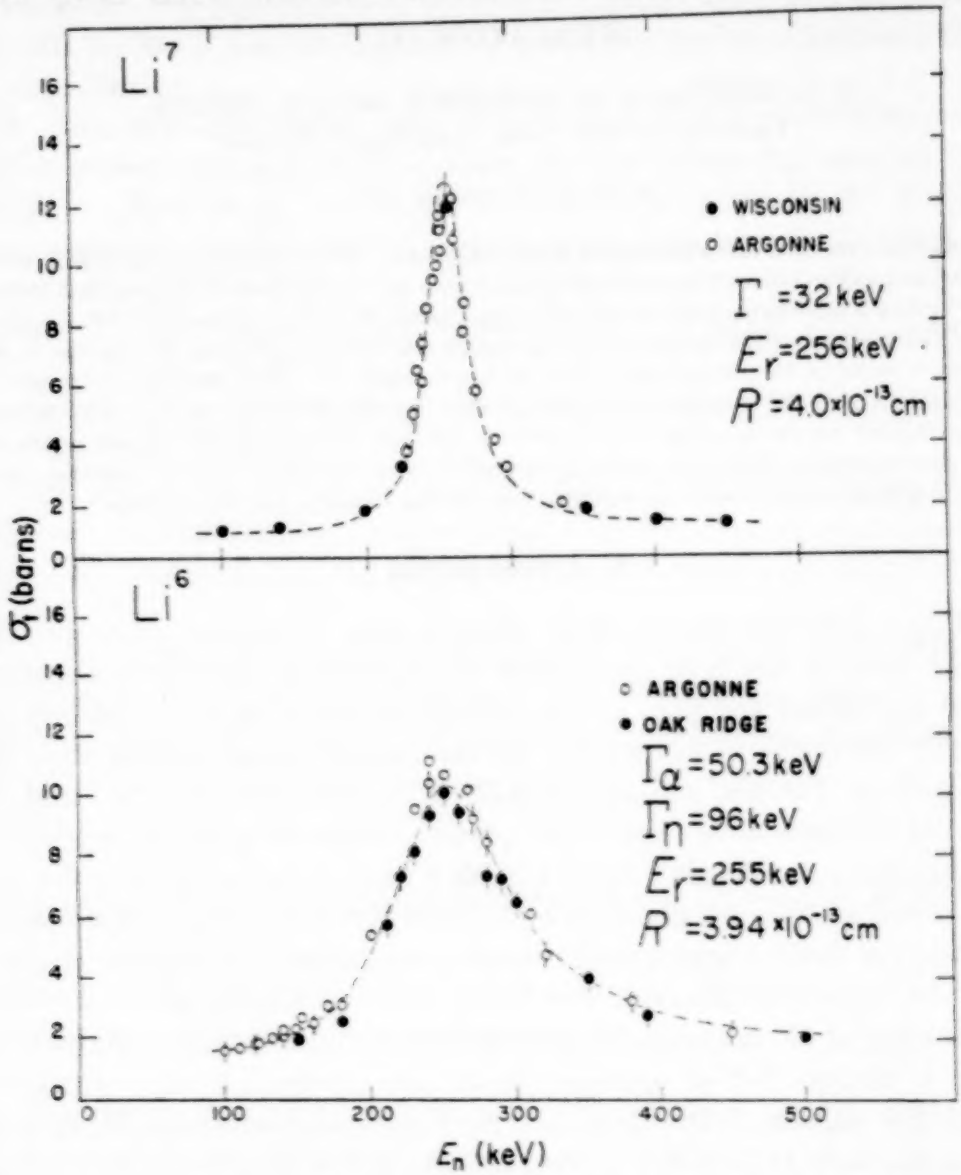

Fig. 1. Total cross-sections of Li^6 and Li^7. The data are from a number of sources as shown, and were taken from ref. [9]). The curves were calculated using the Breit-Wigner single-level formula with the parameters given in the figure. For Li^6 the resonance parameters were obtained from ref. [11]), and for Li^7 the parameters given in ref. [10]) were used. The non-resonant cross-section was assumed to involve only S-wave neutrons.

state in Li^8 with the resonance observed in the total neutron cross section of Li^7 at 256 keV neutron energy, Adair obtained reduced neutron and proton widths for the 3^+ level in Be^8 from the measured width of the resonance in the Li^7

total cross-section (fig. 1). Using these parameters, reasonably good agreement was obtained between calculated cross sections and the data of Taschek and Hemmendinger when the background cross section was assumed to involve broad 2^- states in Be^8 of zero isobaric spin, as well as some interaction in 1^- states. On the basis of these results Adair also predicted that the polarization of the neutrons emitted in the reaction should reach a value of about 0.5 † for proton energies near 2.25 MeV and decrease to a small value above and below the resonance energy.

A number of polarization measurements [5,6]) on the neutrons emitted from this reaction have been carried out for proton bombarding energies above 2.1 MeV. Most of the data were obtained for a neutron emission angle at or near 50° in the laboratory system. The experiments consisted in determining the left-right asymmetry in the scattering of the neutrons from samples of oxygen or helium. Since the scattering phase shifts of these nuclei are known for the energies involved in the measurements, the polarization of the incident neutrons can be inferred from the observed left-right asymmetry. Polarizations of the order of 0.35 were found over the region of proton energy between 2.1 and 4.0 MeV. These measured polarizations did not appear to vary strongly with energy, in disagreement with the predictions of Adair.

More recent measurements of the total reaction cross section have been performed by Newson *et al.* [7]) and by Macklin and Gibbons [8]). These authors have been unable to fit their data, which are considerably more precise than those of Taschek and Hemmendinger, using the equal reduced proton and neutron widths postulated by Adair for the 3^+ level in Be^8. A good fit to the measured reaction cross-section using 2^- and 3^+ levels is obtained only if γ_n^2 is taken to be several times larger than γ_p^2 for both states, and a contribution from higher energy states involving protons with $l > 0$ is included.

The investigations reported on in this and the following paper were undertaken to provide more complete polarization data for the $Li^7(p, n)Be^7$ reaction and to see whether the polarization and cross section data for the reaction can be fitted using just a few levels in Be^8. An extension of the previous polarization measurements to lower energies forms the subject of the present paper. The following paper concerns measurements of the angular dependence of the polarization and contains a discussion of attempts to understand the polarization and cross-section data in terms of a few levels in the Be^8 nucleus.

2. Polarization Analyzers

In the present experiment the general procedure followed in previous polarization experiments [5,6]) has been used to extend the measurements to lower energies with neutrons emitted from the reaction at a laboratory angle of 50°.

† The positive direction of the polarization is taken to be in the direction of the vector $\mathbf{k} \times \mathbf{k}'$, where $\mathbf{k}$ and $\mathbf{k}'$ are the propogation vectors of the incident and outgoing beams respectively.

Most of the measurements were carried out with a scatterer of Li^7. There is a pronounced resonance in the total cross section of Li^7 at 256 keV neutron energy. As shown in fig. 1, the measured total cross section [9]) in the vicinity of this resonance can be satisfactorily fitted by assuming the state in Li^8 has $J^\pi = 3^+$, being formed by P-wave neutrons in the parallel channel spin state, with the background cross section attributable entirely to S-wave scattering. The uniqueness of the spin and parity assignments to this level has been confirmed by angular distribution measurements [10, 11]) on the elastically scattered neutrons. On the basis of the measured angular distributions, together with the coherent and incoherent scattering cross sections for zero energy neutrons, Thomas *et al.* [10]) showed that the S-wave interaction in the vicinity of the resonance is almost entirely in the channel spin 2 state. As a consequence, the polarization $P(\theta)$ of the elastically scattered neutrons can be calculated with a fair degree of confidence using the resonance parameters shown in fig. 1 and the channel spin 2, S-wave phase shift obtained from the background cross-section. The sign of this S-wave phase shift is determined by the angular distribution data. For neutron energies between 240 keV and 450 keV, the calculated $P(\theta)$ is appreciable, indicating that Li^7 should be useful as a polarization analyzer in this energy region. Willard *et al.* [12]) have measured the asymmetry in the scattering of 280-keV polarized neutrons from Li^7 at c.m. scattering angles of 60° and 90° and found large effects to be present.

In the lower part of fig. 1 is shown the measured total cross section [9]) of Li^6. The dashed curve gives the cross section calculated from the single level dispersion formula [13]), again attributing the background cross section entirely to the interaction of S-wave neutrons with the nucleus. Although angular distribution measurements [11]) on Li^6 suggest that both channel spin states are equally important in the S-wave elastic scattering, the situation is complicated by the contribution of the $Li^6(n, \alpha)H^3$ reaction to the background cross section. The coherent scattering cross-section data [14]) for Li^6 are not sufficiently accurate to provide much information on the relative importance of the channel spin states in the S-wave scattering. In order to investigate this question further as well as to obtain data for the correction of the measured Li^7 asymmetries for the effect of Li^6 present in the Li^7 scatterers, asymmetry measurements were made using enriched Li^6 scatterers. An asymmetry measurement was also carried out with a magnesium scatterer using neutrons having an average energy of 85 keV. The predominant isotope of magnesium, Mg^{24}, has a resonance at 83 keV [15]), which makes it useful as a polarization analyzer in this energy region. In addition, asymmetries were measured with liquid oxygen scatterers at neutron energies of 350 and 420 keV.

3. Experimental Method

The experimental arrangement used to obtain the left-right asymmetries

was similar to that used in previous measurements [5]) and is illustrated schematically in fig. 2. Neutrons were produced by bombarding an evaporated lithium target with protons from the Notre Dame electrostatic accelerator. The neutrons emitted at a laboratory angle of 50° were collimated by the paraffin shield and scattered through the angle θ by cylindrical scattering samples. The average energy spread of the neutrons as determined from the target thickness at threshold was 44 keV. Periodic checks on the target thickness were obtained by measuring either a rise curve or a transmission curve for the Li^7 sample over the energy region around the resonance. When either of these

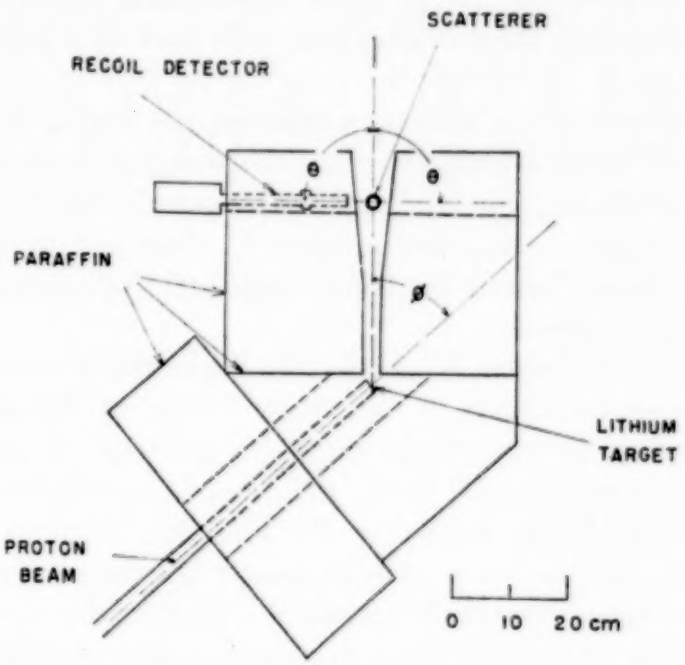

Fig. 2. Schematic diagram of the experimental arrangement used in measuring asymmetries.

methods indicated appreciable deterioration of the target, it was discarded and a fresh one evaporated. The lithium scatterers were encased in thin-walled aluminium containers 2.7 cm in diameter and 7.5 cm long. Natural lithium served as a Li^7 scatterer, and the Li^6 sample was enriched to 96 %. The scatterer used for the 85 keV measurement was a cylinder of magnesium metal (77 % Mg^{24}) 3.0 cm in diameter and 7.5 cm long. For the measurements with liquid oxygen, 2.2 cm diameter thin-walled brass containers insulated by styrofoam were used.

The scattered neutrons were detected by a hydrogen-filled recoil proportional counter 2.5 cm in diameter and having an active volume 9.0 cm long. The beginning of the active volume of the detector was 6.0 cm from the centre of the scatterer. Depending on the neutron energy, the gas pressure in the proportional counter was varied from 1.0 to 4.0 atm. Asymmetries in the scattering were obtained from the measured intensity of scattered neutrons with the

counter in the two positions shown in fig. 2, corresponding to scattering to the left and right through the angle θ. Background was determined in the usual manner by measuring the counting rate with the empty container in place. This background constituted a serious limitation on the accuracy of the measurements, since it generally amounted to 40—65 % of the counting rate with the scatterer in position. Pulse height discrimination on the amplified pulses from the neutron detector was employed such that in one scaler no pulses corresponding to neutrons having energies less than 40 % of the incident neutron energy were recorded, while in the other scaler a level of discrimination of 50 % was used. The variation with energy of the sensitivity of the recoil detector was measured by comparing its counting rate with that of a long counter as a function of energy.

In order to ensure that no unknown experimental asymmetries were being introduced, the left-right asymmetry in the scattering of neutrons from carbon was measured periodically. Since no appreciable polarization is produced in the scattering from carbon in this energy region [16]), there should be no measured asymmetry after corrections for the known small effects discussed in the following paragraph are applied.

The measured asymmetries are subject to a number of corrections. These arise from 1) small differences in the scatterer-detector distance on the two sides, 2) variation of neutron energy across the scatterer, 3) variation of neutron flux across the scatterer, 4) effects of isotopic impurities in the scatterers, and 5) the effect of multiple scattering. The first four corrections are generally small and can be applied in a straightforward manner. Effects of multiple scattering were taken into account by making a detailed numerical calculation. Briefly, this involved division of the cylindrical scattering volume into a number of zones into which the neutrons are scattered after their first collision. Using the known total and differential cross-sections for the first and second scatterings, the relative numbers of singly and doubly scattered neutrons entering the detector can be calculated for each measurement. The reduced detection efficiency of the recoil counter for the less energetic doubly scattered neutrons mitigates the effect of multiple scattering, especially for the lithium scatterers. Except for the oxygen measurements, which were subject to a somewhat larger multiple scattering correction, all of the corrections together changed the measured asymmetries on the average by about 4 % of their value. The estimated uncertainty introduced by the corrections is about one-third the value of the correction.

4. Results

All of the data obtained in the present experiment are summarized in table 1. The sixth column contains the corrected left-right asymmetries. These asymmetries are related to $P(\theta)$, the polarizing power of the scatterer, and P_n, the

TABLE I

Summary of data and results

Scatterer	Laboratory scattering angle	Mean proton energy (MeV)	Mean neutron energy (keV)	Energy spread (keV)	Corrected asymmetries L/R	$P_n P(\theta)$	P_n
Li^7	88°	2.042	190	50	0.887±0.082	−0.060±0.044	−1.00±0.73
		2.097	248	53	0.710±0.030	−0.170±0.018	0.54±0.055
		2.129	280	42	0.722±0.026	−0.162±0.015	0.38±0.043
		2.152	303	42	0.664±0.040	−0.202±0.024	0.46±0.055
		2.201	352	40	0.713±0.033	−0.167±0.019	0.45±0.051
		2.251	400	42	0.808±0.031	−0.106±0.018	0.36±0.060
		2.271	420	40	0.773±0.022	−0.128±0.012	0.48±0.048
Li^7	57°	2.229	380	42	0.748±0.043	−0.144±0.025	0.31±0.05
Li^6	88°	2.042	190	45	0.924±0.050	−0.040±0.025	−0.22±0.18
		2.097	248	53	1.143±0.039	0.066±0.021	
		2.152	303	42	1.184±0.044	0.084±0.020	
		2.201	352	40	1.139±0.042	0.065±0.020	
		2.251	400	45	1.008±0.043	0.004±0.022	
		2.271	420	40	1.122±0.050	0.058±0.025	
Mg	90°	1.950	85	40	0.966±0.035	−0.017±0.018	−0.04±0.042
O_2	87°	2.199	350	40	1.406±0.066	0.169±0.028	0.42±0.067
		2.271	420	36	1.527±0.059	0.208±0.023	0.22±0.024
C	88°	2.251	400	40	1.010±0.013		
		2.099	250	52	0.995±0.014		

polarization of the incident neutrons, by the expression

$$P_n P(\theta) = \frac{(L/R)-1}{(L/R)+1}, \tag{1}$$

in which (L/R) is the corrected experimental asymmetry. Values of $P_n P(\theta)$ obtained from the corrected asymmetries using eq. (1) are given in the seventh column of table 1, and, for Li^6 and Li^7, are presented in fig. 3. The c.m. scattering angles are 96° and 98° for Li^7 and Li^6 respectively. The horizontal bars indicate

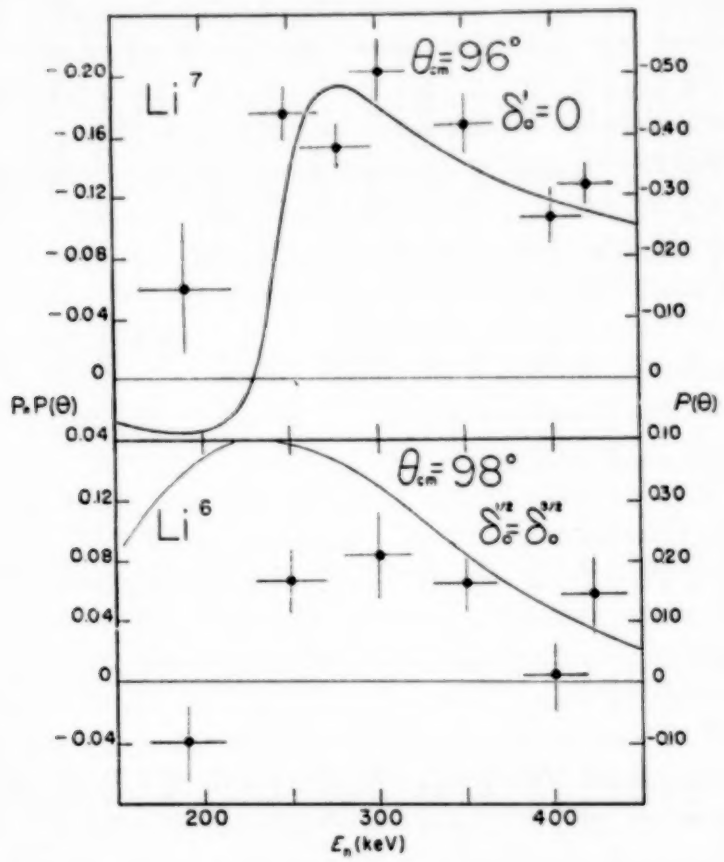

Fig. 3. Values of $P_n P(\theta)$ obtained from the Li^6 and Li^7 data. The ordinate scale on the right refers to the curves, which were calculated using the resonance parameters given in fig. 1. The parallel spin S-wave phase shift used in the calculations was obtained from the non-resonant total elastic cross section. For Li^7, the antiparallel spin phase shift, δ_0^1, was assumed to be zero, while for Li^6 both S-wave phase shifts were assumed to be of equal magnitude.

the neutron energy spread for the various measurements, while the vertical bars give the uncertainty introduced by counting statistics and the corrections applied to the data. Also shown in fig. 3 are the $P(\theta)$ calculated using the level earameters given in fig. 1 and the S-wave phase shifts obtained from the total plastic scattering cross section. If only the resonant phase shift δ_1^3 and the parallel spin S-wave phase shift δ_0^2 need be considered, $P(\theta)$ for Li^7(n, n)Li^7 is

given by [17])

$$P(\theta) = \frac{\frac{7}{8}\sin\delta_0{}^2 \sin\delta_1{}^3 \sin(\delta_0{}^2-\delta_1{}^3)\sin\theta}{\frac{5}{8}\sin^2\delta_0{}^2+\frac{7}{8}\sin^2\delta_1{}^3+\frac{7}{4}\sin\delta_0{}^2\sin\delta_1{}^3\cos(\delta_0{}^2-\delta_1{}^3)P_1(\theta)+\frac{21}{50}\sin^2\delta_1{}^3 P_2(\theta)} \quad (2)$$

where $P_1(\theta)$ and $P_2(\theta)$ are the first and second order Legendre polynomials. In the last column of table 1 are given the neutron polarizations P_n. These were obtained from the measured $P_n P(\theta)$ for Li^7 given in column seven of the table by dividing by the $P(\theta)$ computed using eq. (2). For this calculation, $P(\theta)$ was averaged over the energy spread of the neutrons, and weighted by the differential elastic scattering cross section. The same procedure was used in analyzing the data obtained with the oxygen and magnesium scatterers. For both of these elements, the elastic scattering and polarization at the energies used in the measurements can be calculated using a resonant ($J^\pi = \frac{3}{2}^-$) phase shift and an S-wave potential phase shift, both of which can be obtained from the total cross-section and angular distribution data [5, 15]). For magnesium, an uncertainty of about 15 % in the calculated $P(\theta)$ is introduced by the presence of the isotopes Mg^{25} and Mg^{26} in the scatterer.

Two typical asymmetries obtained with a carbon scatterer are also given in table 1. These asymmetries have been corrected only for the effect of the variation of neutron flux and energy across the scatterer. It is evident from the results that no appreciable unexpected experimental asymmetry was present in the measurements.

5. Discussion

In the lower part of fig. 3 is shown the calculated $P(\theta)$ for Li^6. This curve was obtained from an expression similar to eq. (2), but which takes into account the effect of the $Li^6(n, \alpha)H^3$ reaction, as well as the effect of the antiparallel spin S-wave phase shift. In computing $P(\theta)$ for Li^6, it was assumed that the two S-wave phase shifts were of equal magnitude. The magnitude of $P(\theta)$ is a measure of the relative importance of the two channel spin states in the S-wave scattering. If the parallel spin interaction predominates, $P(\theta)$ will be larger than shown in fig. 3, while a smaller polarization will result if the antiparallel spin interaction is stronger.

From a comparison of the left and right side ordinates of the upper part of fig. 3, it is evident that P_n is of the order of 0.4 down to a neutron energy of about 250 keV. The same relation between the left and right ordinate scales is used in the bottom half of fig. 3, hence the fact that the measured $P_n P(\theta)$ for Li^6 at 250 keV and higher energies lie on the average below the calculated $P(\theta)$ curve suggests that the antiparallel channel spin state may be more important in the S-wave interaction. In order that the calculated $P(\theta)$ pass through these points, it must be assumed that the antiparallel spin phase shift, $\delta_0{}^{\frac{1}{2}}$, is three or

four times as large as the parallel spin phase shift $\delta_0^{\frac{3}{2}}$. The curve in fig. 3 has been computed assuming that the S-wave elastic scattering from Li^6 can be described, at least in the spin $\frac{3}{2}$ state, completely in terms of real potential phase shifts. If $\frac{3}{2}^+$ states in Li^7 having comparable neutron and alpha widths are involved in the interaction, then the polarizations calculated using simple potential phase shifts may be in error. This may well be the case, since the background $Li^6(n, \alpha)H^3$ cross-section arises at least partially through $\frac{3}{2}^+$ states in Li^7, as indicated by the asymmetry about 90° of the angular distribution data [18]) for neutron energies below the resonance. The level involved may be a mirror state to the 6.35—MeV $\frac{3}{2}^+$ state in Be^7 which has been postulated to explain the measured $Li^6(p, \alpha)He^3$ angular distributions [19]). In any case, it is clear from the measurements that $P(\theta)$ for Li^6 is of the order of 0.15 in the energy region under consideration. From the shape of the calculated polarization curves, and the angular distribution data [11]), it can be shown that $P(\theta)$ cannot change violently between 190 keV and 250 keV so that the negative value of $P_n P(\theta)$ found for 190 keV neutron energy must arise from a small, or negative value of P_n at this energy. If $P(\theta)$ is taken to be 0.18 ± 0.10 at 190 keV, a value of P_n of -0.22 ± 0.18 results.

Column eight of table 1 contains all the results for P_n. Except for the Li^7 measurement at 420 keV neutron energy, the results of the present work are in good agreement with previous measurements. The value of 0.48 ± 0.048 found for P_n at 420 keV neutron energy is about a factor of two larger than the value resulting from the oxygen asymmetry measurement at the same energy. The reason for this discrepancy is not clear. The polarizing power of oxygen is rather large at this energy, and the estimated uncertainty in $P(\theta)$ introduced by uncertainties in the scattering phase shifts for oxygen [5]) is less than 5 %. Multiple scattering in the oxygen sample will tend to reduce the left-right asymmetry, but this effect is lessened at this energy, since the first collision in general lowers the neutron energy to a below-resonance value, for which the cross-section is sharply reduced. The multiple scattering correction has the effect of increasing the measured $P_n P(\theta)$ by 16 %. For these reasons it is difficult to see how the value of P_n obtained from oxygen data at this energy could be substantially in error. It would appear, rather, that the Li^7 measurement yields a value of P_n which is too large. An appreciable thickening of the lithium target during the course of the measurement of this point would give rise to a lower average energy for the neutrons and consequently a larger average polarization. There was no evidence that this was the case, however, as the measurement was repeated at a later time with a fresh target, with essentially the same results. Since the value of $P(\theta)$ used to obtain P_n from the Li^7 data at this energy was calculated assuming all of the background cross section to arise from the S-wave parallel spin interaction, the inclusion of some S-wave anti-parallel spin interaction would require a decreased parallel spin phase shift, and

therefore a decrease in $P(\theta)$, which would result in an even larger value of P_n. It thus seems unlikely that $\delta_0{}^1$ is appreciable at this energy. This is in disagreement with the results of Willard *et al.* [11]), who concluded from measurements on the asymmetry of $\sigma(\theta)$ about 90° that both S-wave phase shifts are of roughly equal magnitude. Although a small amount of channel spin 1 interaction may be present, a value of $\delta_0{}^1$ comparable to that of $\delta_0{}^2$ appears to be excluded by the agreement between the Li^7 and oxygen results [5]) for P_n below 420 keV as well as by the zero energy cross-section data. The existence of a small P-wave potential phase shift in this energy region cannot be excluded on the basis of either the total cross-section or angular distribution data. In fact the observed increase in the total cross section [9]) above 500 keV neutron energy may be taken as an indication that neutron orbital angular momenta larger than zero are contributing. However, the presence of an additional P-wave phase shift large enough to resolve the discrepancy between the two measured values of P_n at 420 keV appears unlikely on the basis of the total cross-section data †. Below 380 keV, the estimated uncertainty in $P(\theta)$ introduced by uncertainties in the Li^7 phase shifts is about $\pm 12\,\%$.

From the values of P_n in the last column of table 1, it is clear that P_n does indeed vary appreciably with energy, reaching a maximum for a proton energy near 2.10 MeV. Such a pronounced energy dependence would seem to be related to the resonance in the Li^7(p, n)Be^7 reaction cross section at 2.25 MeV proton energy. Further discussion of the results of this experiment is contained in section 4 of the following paper, where the polarization and cross-section data are considered in terms of states in Be^8.

† More recent measurements [20]) of $P_n P(\theta)$ between 450 keV and 600 keV yield values of $P(\theta)$ substantially larger than those given by the smooth curve in fig. 3. It appears therefore, that the uncertainties in the scattering phase shifts above 400 keV are too large to permit the use of Li^7 as a polarization analyzer in the energy region above 400 keV.

References

1) R. Taschek and N. Hemmendinger, Phys. Rev. **74** (1948) 373
2) G. Breit and I. Bloch, Phys. Rev. **74** (1948) 397
3) R. K. Adair, Phys. Rev. **96** (1954) 709
4) R. K. Adair, Phys. Rev. **87** (1952) 1041
5) Adair, Darden and Fields, Phys. Rev. **96** (1954) 503;
   A. Okazaki, Phys. Rev. **99** (1955) 55;
   Striebel, Darden and Haeberli, Nuclear Physics **6** (1958) 188
6) Willard, Bair and Kington, Phys. Rev. **95** (1954) 1359;
   L. Cranberg, Phys. Rev. **114** (1959) 174;
   Baicker, Jones and Tell, Bull. Am. Phys. Soc. **4** (1959) 62
7) Newson, Williamson, Jones, Gibbons and Marshak, Phys. Rev. **108** (1957) 1294
8) R. L. Macklin and J. H. Gibbons, Phys. Rev. **109** (1958) 105
9) Neutron Cross Sections, BNL 325, 2nd Ed. (1958)
10) Thomas, Walt, Walton and Allen, Phys. Rev. **101** (1956) 759
11) Willard, Bair, Kington and Cohn, **101** (1956) 765
12) Willard, Bair, Cohn and Kington, Bull. Am. Phys. Soc. 1, (1956) 54

13) J. M. Blatt and L. C. Biedenharn, Rev. Mod. Phys. **24** (1952) 258
14) C. G. Shull and E. O. Wollan, Phys. Rev. **81** (1951) 527
15) Newson, Block, Nichols, Taylor, Furr and Merzbacher, Annals of Physics **8** (1959) 211; H. W. Newson, Proc. Intern. Conf. on the Neutron Interactions with the Nucleus, Columbia University (1957)
16) Willard, Bair and Kington, Phys. Rev. **98** (1955) 669
17) A. Simon and T. A. Welton, Phys. Rev. **90** (1953) 1036
18) S. J. Bame and R. L. Cubitt, Phys. Rev. **114** (1959) 1580
19) Marion, Weber, and Mozer, Phys. Rev. **104** (1956) 1402
20) S. E. Darden, C. A. Kelsey and T. R. Donoghue, Proc. Intern. Conf. on the Polarization Phenomena of Nucleons, Helv. Phys. Acta, Supplementum, to be published

2.B *Nuclear Physics* **22** (1961) 451—467; © *North-Holland Publishing Co., Amsterdam*

Not to be reproduced by photoprint or microfilm without written permission from the publisher

THE POLARIZATION OF NEUTRONS FROM THE $Li^7(p, n)Be^7$ REACTION (II)

S. M. AUSTIN †, S. E. DARDEN ††, A. OKAZAKI ‡ and Z. WILHELMI ‡‡

University of Wisconsin, Madison, Wisconsin *

Received 13 October 1960

Abstract: The polarization of the $Li^7(p, n)Be^7$ neutrons has been deduced from measurements of the left-right asymmetry in the scattering of these neutrons from a liquid oxygen analyzer. Angular distributions of the polarization (P_n) were measured at 2.2, 2.6 and 3.0 MeV covering angular ranges (laboratory system) of from 30° to 70°, 30° to 115° and 30° to 70°, respectively. For neutrons emitted at 50°, additional measurements were made at proton energies between 2.1 and 3.1 MeV. At 2.6 MeV P_n is close to zero at 105° and 115°, suggesting that at least two states formed by the same initial channel spin and having $l_1+l_2 \geqq 2$ contribute to the reaction. The polarization at 50° as a function of energy decreases rapidly from about 0.5 at 2.15 MeV to a broad minimum centered at 2.45 MeV where the polarization is about 0.2 and then increases to a constant value near 0.3 at bombarding energies above 2.7 MeV. Polarizations and differential cross sections calculated assuming that the reaction is described by the levels in Be^8 which were postulated by Macklin and Gibbons to account for their measured total cross sections are not consistent with the experimental data. The results of calculations based on several other sets of level parameters are discussed. The unequal values of the reduced widths for emission of protons and neutrons observed for at least one level in Be^8 are explained in terms of the mixing by electromagnetic effects of states in Be^8 with the same spin and parity, but different isobaric spin.

1. Introduction

Because it has been widely used as a source of both polarized and unpolarized neutrons, the $Li^7(p, n)Be^7$ reaction has been the subject of much experimental and theoretical investigation. The results of previous measurements of the total cross section σ_T the differential cross section $\sigma(\varphi)$** and the neutron polarization $P_n(\varphi)$ for this reaction have been summarized in the preceding paper [1]). On the basis of the cross-section data several authors [2, 3]) have suggested that for proton energies between threshold and 2.3 MeV the $Li^7(p, n)Be^7$ reaction could be

† Now at the Clarendon Laboratory, Oxford University, Oxford, England.

†† On leave from the University of Notre Dame, Notre Dame, Indiana. Some of the calculations described in this paper were performed while the author was at the University of Notre Dame and were supported in part by the joint program of the Office of Naval Research and the U. S. Atomic Energy Commission.

‡ On leave from Atomic Energy of Canada, Limited, Chalk River, Ontario.

‡‡ On leave from the Institute for Nuclear Research of the Polish Academy of Science, Warsaw, Poland.

* Work supported in part by the U. S. Atomic Energy Commission and by the Graduate School from funds supplied by the Wisconsin Alumni Research Foundation.

** Unless specifically noted in the text all angles and energies are given in the laboratory system

13) J. M. Blatt and L. C. Biedenharn, Rev. Mod. Phys. **24** (1952) 258
14) C. G. Shull and E. O. Wollan, Phys. Rev. **81** (1951) 527
15) Newson, Block, Nichols, Taylor, Furr and Merzbacher, Annals of Physics **8** (1959) 211; H. W. Newson, Proc. Intern. Conf. on the Neutron Interactions with the Nucleus, Columbia University (1957)
16) Willard, Bair and Kington, Phys. Rev. **98** (1955) 669
17) A. Simon and T. A. Welton, Phys. Rev. **90** (1953) 1036
18) S. J. Bame and R. L. Cubitt, Phys. Rev. **114** (1959) 1580
19) Marion, Weber, and Mozer, Phys. Rev. **104** (1956) 1402
20) S. E. Darden, C. A. Kelsey and T. R. Donoghue, Proc. Intern. Conf. on the Polarization Phenomena of Nucleons, Helv. Phys. Acta, Supplementum, to be published

2.B

Nuclear Physics **22** (1961) 451—467; © *North-Holland Publishing Co., Amsterdam*

Not to be reproduced by photoprint or microfilm without written permission from the publisher

THE POLARIZATION OF NEUTRONS FROM THE $Li^7(p, n)Be^7$ REACTION (II)

S. M. AUSTIN †, S. E. DARDEN ††, A. OKAZAKI ‡ and Z. WILHELMI ‡‡

University of Wisconsin, Madison, Wisconsin •

Received 13 October 1960

Abstract: The polarization of the $Li^7(p, n)Be^7$ neutrons has been deduced from measurements of the left-right asymmetry in the scattering of these neutrons from a liquid oxygen analyzer. Angular distributions of the polarization (P_n) were measured at 2.2, 2.6 and 3.0 MeV covering angular ranges (laboratory system) of from 30° to 70°, 30° to 115° and 30° to 70°, respectively. For neutrons emitted at 50°, additional measurements were made at proton energies between 2.1 and 3.1 MeV. At 2.6 MeV P_n is close to zero at 105° and 115°, suggesting that at least two states formed by the same initial channel spin and having $l_1+l_2 \geqq 2$ contribute to the reaction. The polarization at 50° as a function of energy decreases rapidly from about 0.5 at 2.15 MeV to a broad minimum centered at 2.45 MeV where the polarization is about 0.2 and then increases to a constant value near 0.3 at bombarding energies above 2.7 MeV. Polarizations and differential cross sections calculated assuming that the reaction is described by the levels in Be^8 which were postulated by Macklin and Gibbons to account for their measured total cross sections are not consistent with the experimental data. The results of calculations based on several other sets of level parameters are discussed. The unequal values of the reduced widths for emission of protons and neutrons observed for at least one level in Be^8 are explained in terms of the mixing by electromagnetic effects of states in Be^8 with the same spin and parity, but different isobaric spin.

1. Introduction

Because it has been widely used as a source of both polarized and unpolarized neutrons, the $Li^7(p, n)Be^7$ reaction has been the subject of much experimental and theoretical investigation. The results of previous measurements of the total cross section σ_T the differential cross section $\sigma(\varphi)$ ** and the neutron polarization $P_n(\varphi)$ for this reaction have been summarized in the preceding paper [1]). On the basis of the cross-section data several authors [2, 3]) have suggested that for proton energies between threshold and 2.3 MeV the $Li^7(p, n)Be^7$ reaction could be

† Now at the Clarendon Laboratory, Oxford University, Oxford, England.

†† On leave from the University of Notre Dame, Notre Dame, Indiana. Some of the calculations described in this paper were performed while the author was at the University of Notre Dame and were supported in part by the joint program of the Office of Naval Research and the U. S. Atomic Energy Commission.

‡ On leave from Atomic Energy of Canada, Limited, Chalk River, Ontario.

‡‡ On leave from the Institute for Nuclear Research of the Polish Academy of Science, Warsaw, Poland.

• Work supported in part by the U. S. Atomic Energy Commission and by the Graduate School from funds supplied by the Wisconsin Alumni Research Foundation.

** Unless specifically noted in the text all angles and energies are given in the laboratory system

described primarily in terms of two levels in Be^8: a broad $J^\pi = 2^-$ level located near threshold and a 220-keV wide $J^\pi = 3^+$ level at 2.25 MeV. The orbital angular momenta of both the incident and outgoing particles were taken to be zero for the 2^- level and one for the 3^+ level. It was necessary to choose the ratio, γ_n^2/γ_p^2, of the reduced widths for neutron and proton emission to be near five for both of these levels in disagreement with the value of unity predicted by arguments [4]) based on the charge independence of nuclear forces.

On the other hand, the measured polarizations at 50° were consistent with a constant value of the polarization for bombarding energies between 2.1 and 4.5 MeV and showed no structure which could be associated with a resonance at 2.25 MeV. On the basis of this fact Striebel, Darden and Haeberli [5]) suggested that the reaction might not proceed only through the formation of a compound nucleus but that some direct interaction process might also contribute to the reaction. The present experiments were performed in the hope of clarifying this situation.

2. Experimental Method

The experimental arrangement and the method used to determine the left-right asymmetry in the scattering of the $Li^7(p, n)Be^7$ neutrons and the polarization of these neutrons were essentially the same as that used in previous experiments. Further details are given in the preceding paper [1]). Neutrons emitted from a metallic lithium target at an angle φ with respect to the direction of the incident protons were collimated by a paraffin shield and then scattered to the left or right through an angle θ by a cylindrical liquid-oxygen analyzer. The liquid oxygen was contained in a thin-walled (0.2 mm) brass can 2 cm in diameter and 22 cm in length which was held with its axis perpendicular to the scattering plane. At the scatterer the neutron beam was 7 cm high and 5 cm wide.

Neutrons were detected in a proton-recoil proportional counter filled with 6 atm of hydrogen at neutron energies of 700 keV or less and with 3 atm of propane at higher energies. The pulses from the proportional counter were amplified and fed to two scalers operated in parallel. One scaler was biased to discriminate against neutrons with less than 40 % of the incident neutron energy or against neutrons from the $Li^7(p, n)Be^{7*}$ reaction when these neutrons were present. The second scaler was biased to give about half the counting rate of the first scaler. Background counting rates measured with the empty sample can in position ranged from 20 % to 60 % of those obtained with the filled container. The target thickness was measured by the rise curve method [6]). The targets used were from 30 to 60 keV thick to 1.9-MeV protons.

In order to insure that no large instrumental asymmetries were present a measurement of the L-R ratio for scattering of neutrons from a carbon analyzer

at a neutron energy less than 500 keV was made whenever θ or φ were changed. The splitting of the p- and d-wave phase shifts describing the scattering of neutrons from C^{12} has been measured by Haeberli [7]) at 1.37 MeV. From a reasonable extrapolation of these phase shifts to 500 keV one can estimate the asymmetry in the scattering of Li^7(p, n)Be^7 neutrons through either 60° or 90° to be the order of or less than 1 %. The measured carbon asymmetries were unity within statistical errors which were between 1 % and 2 %.

It was necessary to correct the measured left-right asymmetries for several effects associated with the finite geometry: (1) the variation of neutron flux across the sample caused by the angular dependence of the Li^7(p, n)Be^7 differential cross section; (2) the finite height of the sample; (3) multiple scattering of neutrons in the oxygen analyzer. The first two corrections were small, could be made with reasonable accuracy and introduced an uncertainty which was much smaller than the statistical error. The quantity $P_n\bar{P}(\theta)$ was then calculated from the measured left-right asymmetries using the relation

$$P_n(\varphi)\bar{P}(\theta) = \frac{(L/R)-1}{(L/R)+1}, \tag{1}$$

where $\bar{P}(\theta)$ is the analyzing power of the oxygen scatterer averaged over the neutron energy spread.

The multiple-scattering correction was made by an approximate method, assuming: (1) the scattering takes place in a plane perpendicular to the axis of the scatterer; (2) the angular distribution of the multiply-scattered neutrons lies half-way between an isotropic angular distribution and the angular distribution of the singly scattered neutrons; (3) the polarization of the multiply scattered neutrons is zero. This correction increased $P_n\bar{P}(\theta)$ by 9 % to 30 % with a typical correction being 15 %. The uncertainty in the multiple scattering correction introduced by the above assumptions was checked by calculating the error caused by them in a typical case and is estimated to be one-third of the value of the correction.

In order to obtain $P_n(\varphi)$ it is necessary to ascertain the analyzing power $P(\theta)$ of oxygen for neutrons. This quantity was taken from the calculations of Striebel *et al.* [5]) at neutron energies above 700 keV. At lower energies the polarizations were calculated from phase shifts obtained from the total neutron cross-section measurements of Okazaki [8]) and Striebel *et al.* [5]) Resonances in the total neutron cross section of O^{16} occur at 442 keV, 1000 keV and 1312 keV; the corresponding levels in O^{17} are known to have total angular momenta and parities of $\frac{3}{2}^-$, $\frac{3}{2}^+$ and $\frac{3}{2}^-$ [5, 9]). The widths at resonance of these levels are 48 keV, 123 keV, and 44 keV, respectively. The width of the 442-keV level was taken from Okazaki's fit to the total cross section in which the level shift was taken into account and the widths of the latter two levels were calculated from the observed [10]) widths measured by Striebel *et al.* [5]) assuming that the level shift

depended linearly [10]) on the neutron energy. The nuclear radius was taken to be $5.5f$, where $f = 10^{-13}$ cm.

The s-wave potential scattering phase shifts were determined by assuming that the potential scattering cross section decreased linearly from 3.6 barns at 200 keV to 2.65 barns at 700 keV. The potential scattering phase shifts for angular momenta greater than zero were set equal to zero [5, 8]).

The analyzing power calculated from these phase shifts for scattering angles of 60° and 90° in the c.m. system is shown in fig. 1. Striebel *et al.* [5]) estimated that uncertainties in the phase shifts introduce a maximum error in $P(60°)$ of

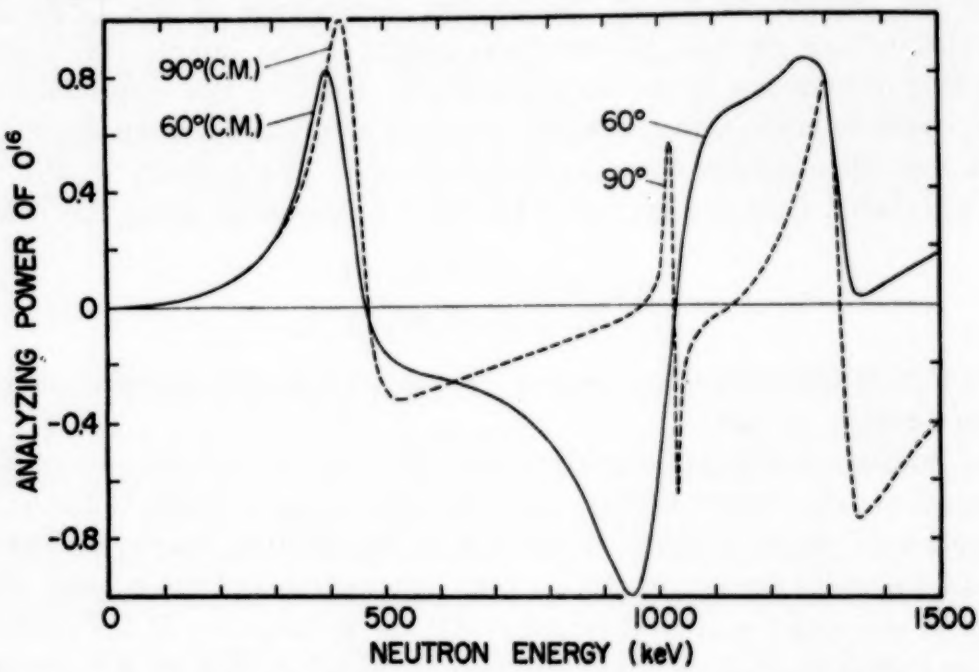

Fig. 1. The analyzing power of O^{16} for neutrons as a function of neutron energy for scattering angles of 60° and 90° in the centre-of-mass system. These correspond to laboratory scattering angles of 57° and 86.5°, respectively.

± 0.1 near 700-keV neutron energy and of ± 0.15 near 1200 keV with probable errors somewhat less than half as large. These uncertainties become appreciably smaller near 950 keV. Errors in $P(90°)$ are estimated to be less than 5 % near 400 keV and less than 10 % near 350 keV.

The values of $\bar{P}(\theta)$ were obtained by weighing $P(\theta)$ with $\sigma(\varphi)$ and $\sigma_s(\theta)$, the differential cross sections for production of these neutrons in the Li^7(p, n)Be^7 reaction and for elastically scattering them from the oxygen analyzer, respectively, and then numerically integrating over the neutron energy spread.

Table 1 shows the experimental results. Since the asymmetries measured on the high and low biased scalers did not differ by a significant amount in any case, the asymmetry with the smaller statistical error was chosen. The error given for the measured L/R asymmetries is the statistical standard deviation based on the number of counts. In other cases the error quoted includes the

TABLE 1

Summary of data and results

Mean proton energy $\bar{E}_p$ (MeV)	Mean neutron energy $\bar{E}_n$ (keV)	Neutron energy spread (keV)	φ (degrees)	θ (degrees)	Measured left-right asymmetry	$P_n \bar{P}(\theta)$ (corrected)	$\bar{P}(\theta)$	$P_n(\varphi)$
Oxygen asymmetries								
2.194	411	48	30	86.5	1.595±0.025	0.277 ±0.018	0.914	0.303±0.020
2.600	827	50	30	57	0.874±0.019	−0.0732±0.0109	−0.538	0.136±0.020
2.983	1209	44	30	57	1.252±0.050	0.134 ±0.027	0.763	0.175±0.036
2.144	295	19	50	86.5	1.151±0.041	0.0807±0.0218	0.209	0.386±0.104
2.199	350	35	50	57	1.639±0.056	0.284 ±0.028	0.495	0.573±0.057
2.200	351	19	50	86.5	1.326±0.038	0.161 ±0.020	0.419	0.385±0.047
2.235	385	19	50	86.5	1.555±0.052	0.251 ±0.026	0.685	0.367±0.038
2.271	419	19	50	86.5	1.691±0.056	0.318 ±0.032	0.980	0.324±0.032
2.400	543	33	50	86.5	0.900±0.023	−0.0623±0.0148	−0.318	0.196±0.047
2.500	637	32	50	86.5	0.917±0.028	−0.0470±0.0160	−0.250	0.188±0.064
2.600	731	31	50	57	0.904±0.029	−0.0542±0.0164	−0.343	0.158±0.048
2.836	950	29	50	57	0.557±0.033	−0.320 ±0.027	−0.992	0.323±0.027
3.040	1138	41	50	57	1.509±0.082	0.241 ±0.041	0.683	0.353±0.060
2.201	277	20	70	86.5	1.170±0.027	0.0906±0.0148	0.177	0.512±0.084
2.600	617	54	70	86.5	0.911±0.024	−0.0509±0.0140	−0.265	0.192±0.052
3.000	953	34	70	57	0.532±0.026	−0.346 ±0.023	−0.990	0.349±0.023
2.599	533	28	85	86.5	0.897±0.022	−0.0659±0.0146	−0.323	0.204±0.045
2.572	420	34	105	86.5	1.035±0.031	0.0225±0.020	0.980	0.023±0.021
2.522	386	36	105	86.5	1.039±0.049	0.0245±0.030	0.680	0.036±0.045
2.600	400	32	115	57	1.019±0.048	0.0130±0.033	0.810	0.016±0.041
Carbon asymmetries								
2.199	350	35	50	57	0.997±0.016			
2.600	400	32	115	57	1.001±0.022			
2.400	543	33	50	86.5	0.986±0.020			

statistical standard deviation and the error associated with the multiple scattering corrections discussed previously. From the many individual runs made in measuring each angle-energy point one could calculate a root-mean-square deviation; this quantity agreed well with the statistical standard deviation.

Several typical values of the asymmetry measured with a carbon analyzer are also given in table 1. These asymmetries are unity within their statistical errors; it appears that no large instrumental asymmetries were present.

3. Results

The values † of $P_n(50°)$ measured in this experiment and in the experiment described in the preceding paper [1]) are shown as a function of energy in fig. 2. There is reasonable agreement among the polarizations measured with the

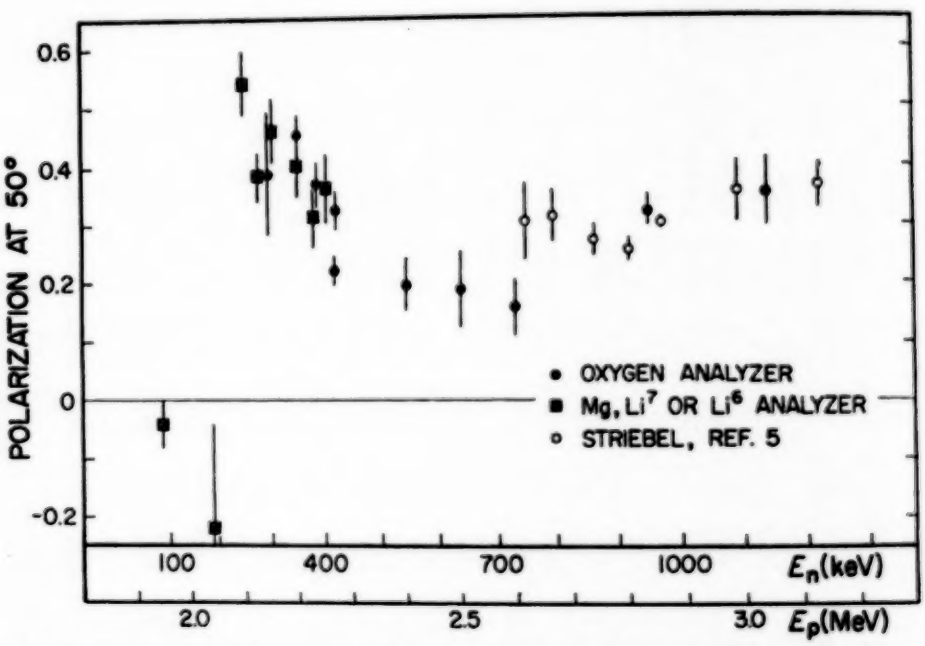

Fig. 2. The polarization of neutrons emitted by the $Li^7(p, n)Be^7$ reaction at $\varphi = 50°$ as a function of the proton and neutron energies. The data taken with O^{16} analyzers and Li^7, Li^6 or Mg^{24} analyzers are shown as solid circles and squares, respectively. The earlier data of Striebel *et al.* [5]) are shown as open circles at energies above 2.6 MeV. The point measured with a Li^7 analyzer at 2.270 MeV is not shown because of the uncertainty (see ref. [1])) in the analyzing power of Li^7 at this energy.

various analyzers, with the data of Okazaki [8]) and with the data of Striebel *et al.* [5]), shown at higher energies.

The angular distributions of polarization measured in the present experiment are shown in fig. 3. The range of energy and angle over which measurements could be made was limited by regions in which $P(\theta)$ was either small or varying

† The positive direction of the polarization is taken to be that of the vector $\mathbf{k} \times \mathbf{k}'$ where $\mathbf{k}$ and $\mathbf{k}'$ are the wave numbers of the incoming and outgoing particles, respectively.

rapidly and therefore unusable. At 2.6 MeV the polarization is close to zero at 105° and 115° in the laboratory system.

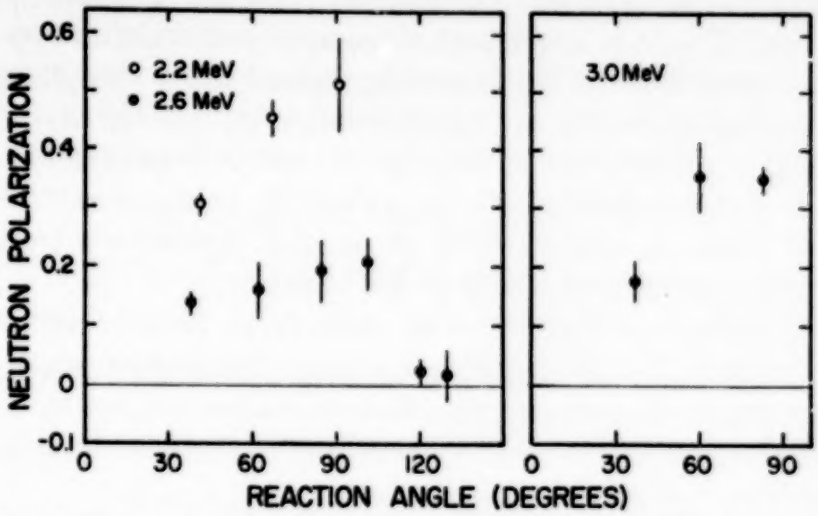

Fig. 3. The polarization of neutrons emitted by the $Li^7(p, n)Be^7$ reaction at an angle Φ in the c.m. system. These polarizations were measured using an oxygen analyzer.

4. Discussion

The value of $P_n(50°)$ as a function of energy varies rapidly in the region of 2.2 MeV, an effect which might be associated with the resonance in the reaction occurring at 2.25 MeV. In view of this fact an attempt was made to determine whether the observed polarizations and the cross section data could be fitted in terms of a reaction proceeding through a compound nucleus Be^8 in which only a few levels were important.

The expressions necessary for calculation of the cross sections and polarizations were obtained from the general formulas given by Blatt and Biedenharn [11]) and Simon and Welton [12]), respectively. Several assumptions were made to simplify these expressions while still retaining a physically reasonable model. It was assumed that: (1) at a particular energy only a single level of a given J^π is important; that is, the single-level approximation to the scattering matrix is valid; (2) incident and outgoing orbital angular momenta greater than $l = 1$ can be neglected; (3) both the orbital angular momentum l and the channel spin s associated with the incident particles are conserved in the reaction (that is, $l = l'$ and $s = s'$, where the primes denote these quantities after the reaction); (4) the level shift varies linearly with energy.

The single level approximation was based on the facts that in light nuclei one does not expect to find close level spacings and that no interference phenomena are observed in the total cross section.

The neglect of orbital angular momenta greater than one unit can be justified by noting that over the energy range of greatest interest (1.88 to 2.6 MeV) the

penetrability of the Coulomb-and-centrifugal barrier is higher by at least an order of magnitude for formation and decay of a level by s-waves rather than d-waves and by p-waves rather than f-waves. Over the same energy range the p-wave penetrabilities are larger than the d-wave penetrabilities by at least a factor of five. Thus states in Be^9 formed by higher l-waves must have relatively large reduced widths if they are to contribute significantly to the reaction.

That l equals l' follows from assumption (2) and conservation of parity. For the 2^- and 3^- levels postulated [2-6]) to explain the total-cross-section data for the $Li^7(p, n)$ reaction, conservation of angular momentum together with assumption (2) implies that s and s' are equal.

In the approximation that the level shift varies linearly with energy one proceeds as though the level shift were zero. The widths which one then obtains from fitting the data are the observed widths defined by Thomas [10]. Unless otherwise noted in the text all widths quoted should be interpreted as observed widths.

Expressions for the polarization and differential cross section were derived for the case where only three levels of the same channel spin in the Be^9 compound nucleus contribute to the reaction. These levels were chosen to facilitate comparison of the data with results of calculations based on the $J^\pi = 2^-$ and 3^- levels which were postulated by Macklin and Gibbons [2]) and which fit the total $Li^7(p, n)Be^7$ cross section at low energies, with the $J^\pi = 2^-$ level postulated [15]) to explain the $Li^7(p, \alpha)\alpha$ data [16]) and the $J^\pi = 1^-$ level suggested [17]) to explain the $Li^7(p, p)$ data [18]). In particular, formulas were derived for $J^\pi = 3^-$, 2^- and 2^- levels and for $J^\pi = 3^-$, 2^- and 1^- levels. The channel spin of the 2^- (or 1^-) level was taken to be two (see discussion below).

With these assumptions the formulas for the differential cross section and polarization [19]) are

$$\begin{aligned}
\sigma(\Phi) &= a_0 - a_1 P_1(\cos\Phi) + a_2 P_2(\cos\Phi),\\
a_0 &= \pi\lambda_p^2 \tfrac{1}{4}\{|S^{2-}|^2 + \tfrac{7}{6}|S^{3-}|^2 + \tfrac{5}{8}|S^{2-}|^2\} + \tfrac{3}{8}|S^{1-}|^2\},\\
a_1 &= \pi\lambda_p^2 \tfrac{7}{4}\,\mathrm{Re}\,(S^{2-})^* S^{3-} + \tfrac{5}{4}\,\mathrm{Re}\,(S^{2-})^* S^{2-}\{ + \tfrac{3}{4}\,\mathrm{Re}\,(S^{2-})^* S^{1-}\},\\
a_2 &= \pi\lambda_p^2 \tfrac{7}{24}|S^{2-}|^2\{ + \tfrac{3}{400}|S^{1-}|^2\} + \tfrac{21}{50}|S^{3-}|^2\\
&\qquad + \tfrac{7}{5}\,\mathrm{Re}\,(S^{3-})^* S^{2-}\{ + \tfrac{63}{50}\,\mathrm{Re}\,(S^{2-})^* S^{1-}\}.
\end{aligned} \tag{2}$$

$$\begin{aligned}
P_n(\Phi) &= \left(\frac{l'-1}{2}\right)^2 \frac{dP_n(\Phi)}{\sigma(\Phi)} = \frac{\lambda_p^2}{\sigma(\Phi)}\Big[\{0.078\,\mathrm{Im}\,(S^{2-})^* S^{2-}\{ + 0.1406\,\mathrm{Im}\,(S^{2-})^* S^{1-}\}\\
&\quad - 0.219\,\mathrm{Im}\,(S^{2-})^* S^{3-}\}\sin\Phi\\
&\quad + \{0.266\,\mathrm{Im}\,(S^{2-})^* S^{2-}\{ + 0.390\,\mathrm{Im}\,(S^{3-})^* S^{1-}\}\}\sin\Phi\cos\Phi\Big].
\end{aligned} \tag{3}$$

[19]) Ohlsen, quoted in Newson *et al.* [3]).

[20]) The factor $(l'-1)!^2$ occurring in eq. (3) did not appear in the formula given in ref. [19]). This omission was pointed out in a private communication from T. A. Welton.

The terms enclosed in the curly brackets are omitted if one is considering 3^+, 2^+ and 2^- levels and are substituted for the preceding terms if one is considering 3^+, 1^+ and 2^- levels. The P_l are the Legendre polynomials, Φ is the reaction angle in the centre-of-mass system and i' is the neutron spin. The reduced wavelength of the relative motion of the incident system is given by $\lambda\!\!\!^{-}_{\mathrm{p}}$. The combinations of the scattering matrices $S^{J\pi}$ which appear in eqs. (2) and (3) are given by

$$\begin{aligned} |S^{J\pi}|^2 &= (f^{J\pi})^2 \sin^2\delta^{J\pi}, \\ \mathrm{Re}\,(S^{J_1\pi_1})^* S^{J_2\pi_2} &= f^{J_1\pi_1} f^{J_2\pi_2} \sin\delta^{J_1\pi_1} \sin\delta^{J_2\pi_2} \\ &\quad \times \cos(\delta^{J_2\pi_2} - \delta^{J_1\pi_1} + \xi^{J_2\pi_2} - \xi^{J_1\pi_1}), \qquad (4) \\ \mathrm{Im}\,(S^{J_1\pi_1})^* S^{J_2\pi_2} &= f^{J_1\pi_1} f^{J_2\pi_2} \sin\delta^{J_1\pi_1} \sin\delta^{J_2\pi_2} \\ &\quad \times \sin(\delta^{J_2\pi_2} - \delta^{J_1\pi_1} + \xi^{J_2\pi_2} - \xi^{J_1\pi_1}). \end{aligned}$$

Here we have

$$\xi^{J\pi} = \sigma_l - \sigma_{l=0} - \zeta_{\mathrm{n}}{}^l - \zeta_{\mathrm{p}}{}^l, \qquad (5)$$

where σ_l is the Coulomb phase shift and $\zeta_{\mathrm{n}}{}^l$ and $\zeta_{\mathrm{p}}{}^l$ are the hard-sphere phase shifts for neutrons and protons, respectively, for the channel with angular momentum and parity equal to $J\pi$. The quantities $\delta^{J\pi}$ and $f^{J\pi}$ are given as

$$f^{J\pi} = \pm \frac{2(\Gamma_{\mathrm{n}}{}^{J\pi}\Gamma_{\mathrm{p}}{}^{J\pi})^{\frac{1}{2}}}{\Gamma^{J\pi}}, \quad \delta^{J\pi} = \tan^{-1}\frac{\Gamma^{J\pi}}{2(E_{\mathrm{R}} - E_{\mathrm{p}})}, \quad \Gamma^{J\pi} = \Gamma_{\mathrm{n}}{}^{J\pi} + \Gamma_{\mathrm{p}}{}^{J\pi} + \Gamma_{\alpha}{}^{J\pi}. \qquad (6)$$

The quantities $\Gamma_{\mathrm{n}}{}^{J\pi}$, $\Gamma_{\mathrm{p}}{}^{J\pi}$ are the partial widths for the emission of a neutron or proton from the compound state of Be^8 characterized by $J\pi$ and $\Gamma_{\alpha}{}^{J\pi}$ is the sum of the partial widths for the decay of this state through other open channels ($\Gamma_{\alpha}{}^{J\pi}$ is taken to be a constant). The resonance energy is E_{R} and E_{p} is the bombarding energy. The partial widths are related to the reduced widths † through the equation

$$\Gamma_{\mathrm{c}}{}^{J\pi} = 2P_{\mathrm{c}}{}^{J\pi}(\gamma_{\mathrm{c}}{}^{J\pi})^2. \qquad (7)$$

The penetrability P_{c} is defined by

$$P_{\mathrm{c}}{}^{J\pi} = \frac{k_{\mathrm{c}} R_{\mathrm{c}}}{F_l{}^2 + G_l{}^2}, \qquad (8)$$

where R_{c} is the channel radius, F_l and G_l are the regular and irregular Coulomb functions evaluated at the channel radius and k_{c} is the wave number of the relative motion in channel c. The values of the penetrabilities and hard-sphere phase shifts for protons were taken from the tables of Bloch *et al.* [18]), and the graphs of Sharp, Gove and Paul [19]). Corresponding quantities for neutrons

† The definition of $\gamma_{\mathrm{c}}{}^2$ used here is that given by Lane and Thomas [16]), in which $\gamma_{\mathrm{c}}{}^2$ has the dimension of energy. This reduced width is equal to the reduced width defined by Wigner and Eisenbud [17]), divided by the channel radius R_{c}.

were taken from the tables of Monahan, Biedenharn and Schiffer[20]). The channel radius R_c was chosen to be 4.0 f in both entrance and exit channels for calculation of the hard-sphere phase shifts except where otherwise noted in the text.

The $(\pm)$ sign appears in eq. (6) because dispersion theory determines the scattering amplitude only within a relative phase of 180°. These phases were chosen to provide the proper sign for a_1 and $P_n(50°)$ and are tabulated with the other level parameters.

TABLES 2—5

Parameters of levels in Be^8

E_R(MeV-lab)	J^π	Channel spin	Relative phase	γ_n^2/γ_p^2	γ_n^2(MeV-lab)	Γ_α(MeV-lab)
TABLE 2						
1.9	2^-	2	−	5.0	4.3	0
2.25	3^+	2	+	5.2	0.83	0
TABLE 3						
1.9	2^-	2	−	5.0	4.3	0
2.25	3^+	2	+	5.2	0.83	0
3.0	1^+	2	−	1.0	1.14	0
TABLE 4						
1.9	1^-	1	+	5.0	0.5	0
2.25	3^+	2	+	3.75	0.60	0
3.2	2^+	2	−	1.0	0.28	0.57
3.4	2^-	2	−	1.0	1.7	0
TABLE 5						
1.9	2^-	2	−	5.0	4.3	0
2.25	3^+	2	+	5.2	0.83	0
3.2	2^+	2	−	1.0	0.28	0.57

The results of a calculation using the parameters suggested by Macklin and Gibbons [2]) and tabulated in table 2 are shown in fig. 4a where they are compared with the experimental data. Although there is some similarity between the measured and calculated values the agreement with the polarization and angular distribution data is unsatisfactory even for proton energies below 2.2 MeV where the levels account for nearly all of the total cross section. A discrepancy between the measured angular distributions and calculations based on parameters similar to those of table 2 has been noted by Monahan and Mooring [25]).

Because of the rather poor agreement of these calculations with the experimental data at low energies, additional calculations were made assuming somewhat different sets of levels in Be^8. Several experimental criteria were used to guide the choice of these levels.

First, it was noted that the quantity σ_T/k_n does not approach a constant value as the $Li^7(p, n)$ threshold is approached from above [2]). This implies that there must be at least one level near threshold.

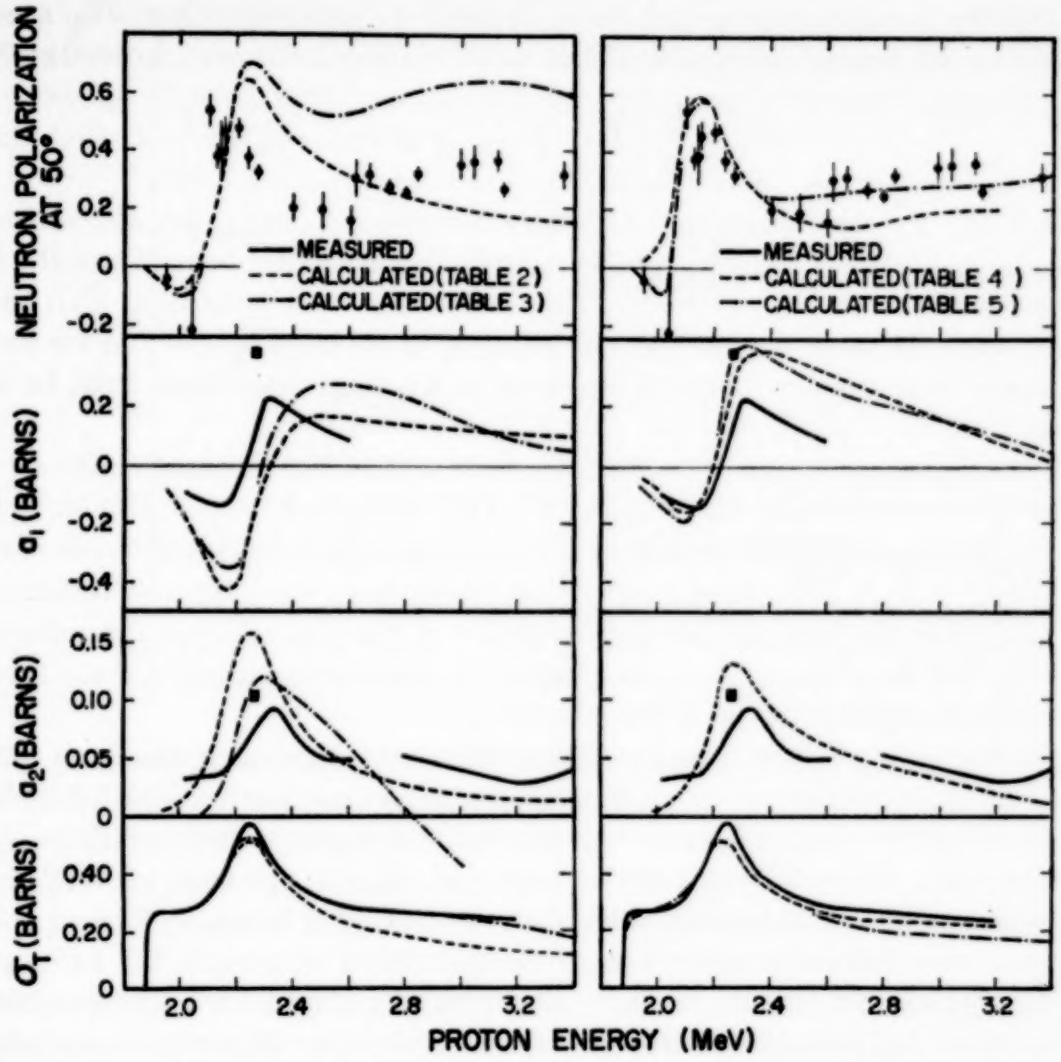

Fig. 4. Cross sections and polarizations calculated from the parameters of tables 2 to 5. In this figure the experimental values of the total cross section are those of Macklin and Gibbons [2]), corrected for the second neutron group using the data of Bevington *et al.* [21, 22]). The values of a_1 and a_2 were taken from Taschek and Hemmendinger [6]), at energies below 2.5 MeV and were obtained from the data of Bevington *et al.*, at higher energies. The point shown at 2.27 MeV was obtained from a measurement made by Gabbard, Davis and Bonner [24]). The polarization data shown include the results of the present experiments, the results of Striebel *et al.* [5]), and Baicker *et al.* [23]). Results calculated from the parameters of tables 2 and 3 are shown in fig. 4a; those calculated from tables 4 and 5 are shown in fig. 4b.

Secondly, if one is to reproduce the measured values of the polarization at proton energies above 2.6 MeV (where the level at 2.25 MeV is no longer important) at least one level involving orbital angular momenta greater than zero must contribute to the reaction in this energy region (in our approximation this level will be formed and will decay through p-waves). Further, since levels

must be formed by the same incident channel spin if they are to interfere and contribute to dP_n (as defined in eq. (3)) this level must be formed by the same channel spin as at least one of the other postulated levels.

Thirdly, we note that at 2.6 MeV, $P_n(105°)$ is near zero. Thus, dP_n must pass through zero at angles other than 0° or 180°. The quantity dP_n is given by [12])

$$dP_n = \sum_{i=1}^{L} b_i \overline{P_i^1} \quad (l_1+l_2 \geqq L \geqq |l_1-l_2|), \tag{9}$$

where the $\overline{P_i^1}$ are normalized Legendre functions, l_1 and l_2 are the orbital angular momenta by which any two contributing levels are formed and the b_i depend only on the proton energy. Thus at 2.6 MeV there must be at least two levels with the same channel spin contributing to the cross section and the sum of the orbital angular momenta involved in forming these levels must be at least two.

The assignment [2–4]) of $J^\pi = 3^+$ to the level at 2.25 MeV is based on the s—p interference observed in $\sigma(\varphi)$ and on the height of the peak in σ_T at 2.25 MeV. If one wishes to explain the peak in σ_T in terms of a single level it is also necessary to set $\gamma_n^2 \approx 5\gamma_p^2$. This violates the ordinary notions of the charge independence of nuclear forces [4]); a possible interpretation of this inequality of the reduced widths will be given below. The evidence for the assignment of these level parameters appears to be quite convincing.

On the basis of these considerations calculations were made assuming that in addition to the levels given in table 2 a third level located near 3.0 MeV, with a J^π of 2^- or 1^+ and formed by channel spin equal to two contributed to the reaction. The total width of this level was taken to be about 1.0 MeV and the neutron and proton reduced widths were chosen to be equal. These parameters were chosen to agree with levels postulated to explain the Li^7(p, p) and Li^7(p, n) data. Figure 4a shows the results for the 1^+ level. These results were calculated from the parameters tabulated in table 3. Neither this calculation nor a calculation made with the 2^+ level agreed well with the data.

The results of calculations performed for the rather different set of levels tabulated in table 4 are shown in fig. 4b. The major change has been to add a narrow s-wave 1^- level near threshold and to move the broad 2^- level to higher energies. The addition of the $J^\pi = 1^-$ level does not complicate eqs. (2) and (3) very much because this level is formed by a channel spin of one and thus does not interfere with the other levels which all are formed by channel spins of two. While the 1^- state is not suggested by other experiments involving Be^8 there is also no evidence denying its existence.

Also shown in fig. 4b are the results for still another set of levels. The parameters of these levels are given in table 5 and are similar to those given in table 2. However, the hard-sphere phase shift for neutrons ζ_n^0 has been drastically altered above threshold. This phase shift was taken to be that which would

arise from a hard sphere with a radius which was $12f$ immediately above threshold, and decreased smoothly to $4.0f$ above 2.3 MeV. This was done with no good theoretical justification but solely to fit the data. However, it is known that far-away levels can add to the apparent hard-sphere phase shift through the effect of a constant diagonal term in the R-matrix. Thus it would not be surprising if phase shifts calculated from a reasonable channel radius such as $1.4\ (A^{\frac{1}{3}}+1)\ f$ were incorrect.

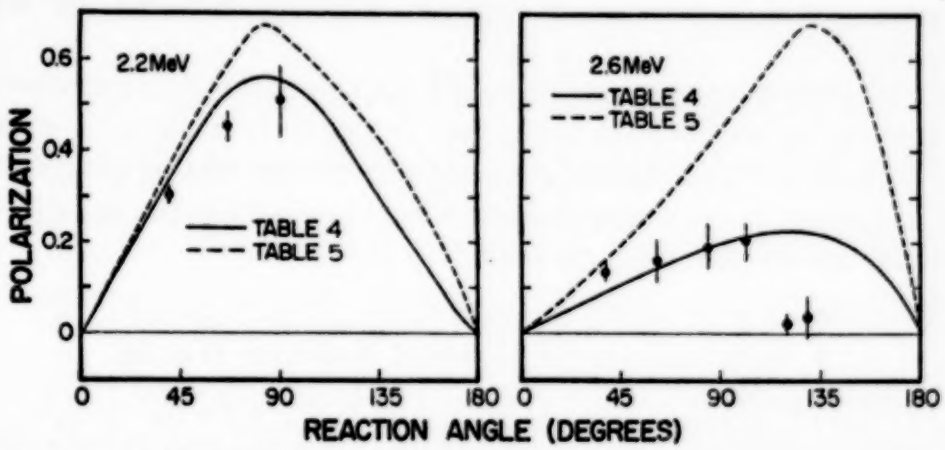

Fig. 5. Angular distributions of the polarization calculated from the parameters of tables 4 and 5. The experimental data are the same as those shown in fig. 3.

Fig. 5 shows a comparison of the angular distribution of the polarizations calculated from the levels of tables 4 and 5 and the results of the present experiment. At 2.2 MeV the levels of table 4 provide a reasonable fit to the data but neither set of levels is satisfactory at 2.6 MeV.

At energies below 2.6 MeV either of the sets of parameters tabulated in tables 4 and 5 provides a satisfactory qualitative fit to the data. The angular distribution of the polarization and the fact that there is no justification for the alteration of phases performed in the calculations with the levels of table 5 favor the levels of table 4. On the other hand, the experimental evidence shows that $P_n(50°)$ probably becomes negative at energies slighly above threshold while the polarizations calculated from the levels of table 4 are positive in this energy region. It does not appear possible at present to state definitely whether either or neither of these sets of levels provides a correct description of the Li^7(p, n) reaction at energies below 2.6 MeV. In particular one cannot exclude the possibility that some direct interaction contributes to the reaction. However, one can explain the dominant features of the reaction in terms of the formation of a compound nucleus.

It would probably be possible to improve these fits somewhat by further adjustments of the parameters or by relaxing some of the restrictions made in deriving eqs. (2) and (3). However, a large variety of level parameters have been tried and it seems unlikely that such changes would result in a great improve-

ment in the overall fit at the lower energies. Further, the experimental data are not particularly consistent at present. A recent measurement of $\sigma(\varphi)$ at 2.27 MeV made by Gabbard, Davis and Bonner [24]) yielded a cross section which differs from that which was measured by Tashek and Hemmendinger [6]) by about 50 % at the forward angles and which is much more sharply peaked in the forward direction. A discrepancy also appears when the differential cross sections of Taschek and Hemmendinger [6]) are integrated over solid angles and the resulting total cross section is compared with that measured by Macklin and Gibbons [2]).

Since the analysis of this reaction is difficult in any case because some of the states involved appear to be so broad that neither their position nor width can be well defined, it did not appear worthwhile to attempt further analysis at this time. It is perhaps worth noting that any levels postulated to fit the Li^7(p, n)Be^7 data must also fit the Li^7(p, p) data [15]).

5. Implications of Unequal Reduced Widths

Adair's proof [4]) of the equality of the reduced widths for the emission of protons and neutrons from the states of Be^8 contributing to the Li^7(p, n)Be^7 reaction involved the assumption that nuclear forces are charge symmetric, that is, if one neglects the Coulomb forces the n—n and p—p interactions are identical. This assumption is weaker than that of charge independence, which involves the additional condition that the n—n and n—p interactions are equal in corresponding states of relative motion, but is sufficient when one is dealing with the decay of a self-conjugate nucleus such as Be^8 into charge-mirror states such as (Be^7+n) and (Li^7+p).

There is a large amount of experimental evidence [26, 27]) that nuclear forces are, at least to a good approximation, charge independent. If this is so one can show that to the extent that Coulomb forces can be neglected states of nuclei are eigenstates of definite total isobaric spin T and that T as well as T_3, the third component of the isobaric spin, must be conserved in nuclear interactions. On the other hand it is possible for Coulomb forces to mix states of the same J^π and different T. If mixing between two such states occurs, the wave function for a given state of the nucleus can be written as

$$\Psi(J,\pi) = [\psi(J,\pi,T)\mathcal{S}_T{}^{T_3} + \alpha(T')\psi(J,\pi,T')\mathcal{S}_{T'}{}^{T_3}]\,\frac{1}{(1+\alpha^2)^{\frac{1}{2}}}, \qquad (10)$$

where $\psi(J,\pi,T)$ and $\psi(J,\pi,T')$ are the space-spin parts of the wave functions which would describe the states of the nucleus in the absence of Coulomb forces. The $\mathcal{S}_T{}^{T_3}$ are the isobaric spin wave functions. The $\Psi(J,\pi)$ are no longer characterized by a definite isobaric spin.

It has been shown that for the ground states of light nuclei α is small

($\approx 1\,\%$) [28, 29]) so that Li^7 and Be^7 have definite isobaric spins. Wilkinson [30]) has predicted that in light nuclei of type $4n$, such as Be^8, one can expect large mixing of states of different isobaric spin at excitation energies between 14 MeV and 30 MeV. The excitation energies involved in (Li^7+p) are the order of 20 MeV in the present experiments so we may expect the states of Be^8 to be of the type of eq. (10) with α large. Assuming that the states in Be^8 are described by eq. (10), that Li^7 and Be^7 form an isobaric-spin doublet, and using the definition of the reduced width [16]) one can show that

$$\frac{\gamma_n^2}{\gamma_p^2} = \frac{\left(1+\frac{B}{A}\alpha\right)^2}{\left(1-\frac{B}{A}\alpha\right)^2}, \tag{11}$$

where

$$A = \int_S \varphi^* \psi(J, \pi, T = 1)\mathrm{d}S, \quad B = \int_S \varphi^* \psi(J, \pi, T' = 0)\mathrm{d}S. \tag{12}$$

The integral is taken over the channel surface [16]) and φ is the space-spin part of the channel wave function describing the decay of Be^8 into (Be^7+n) or (Li^7+p). It has been assumed that nuclear forces do not depend on the charge so that φ is the same for both the (Li^7+p) and the (Be^7+n) channels.

The squares of the integrals A and B have the form of reduced widths so the Wigner limit [31]) might be used to place limits on these quantities if they were large. The evidence for unequal reduced widths in Be^8 is strongest for the relatively narrow $J^\pi = 3^+$ level at 2.25 MeV, where γ_n^2/γ_p^2 is about five. In order to get a rough estimate of the magnitude of α it was assumed that $\psi(J, \pi, T = 1)$ is not appreciably different from $\psi(J, \pi, T' = 0)$. Then

$$\frac{\gamma_n^2}{\gamma_p^2} = \frac{(1+\alpha)^2}{(1-\alpha)^2}. \tag{13}$$

This relationship has been given previously by Barker and Mann [32]) and by MacDonald and Marion [33]). We note from eqs. (11) or (13) that if there is no mixing ($\alpha = 0$) then γ_n^2 and γ_p^2 are equal.

Setting γ_n^2/γ_p^2 equal to five one finds from eq. (13) that $|\alpha|$ is of the order of 0.4 so that the mixing is large. Baz [34]) has suggested that the large values of the reduced neutron widths and the large mixing might be explained in terms of "threshold" states of the nucleus. In these states the most important part of the wave function is that part describing a neutron outside a Be^7 core. In this situation the nuclear forces are strongly affected by the n—p mass difference and mixing of different isobaric spin states can occur. In any case it appears that at least one of the states in Be^8 with an excitation energy near 20 MeV is not characterized by a definite value of the isobaric spin.

6. Summary

For energies below 2.6 MeV the polarization and cross-section data from the $Li^7(p, n)Be^7$ reaction can be qualitatively fitted by assuming that the reaction proceeds through the formation of a compound nucleus. Suitable sets of level parameters are given in tables 4 and 5. The dominant effects are ascribed to the interference of a narrow 3^+ level at 2.25 MeV and a broad 2^- background level. At least one level must be located near the (p, n) threshold and at 2.6 MeV there must be at least two levels contributing to the reaction which are formed by the same channel spin and $l_1+l_2 \geqq 2$.

Polarizations and differential cross-sections calculated from parameters suggested by Macklin and Gibbons [2]) do not agree with the experimental data, even for energies below 2.2 MeV where these levels account for nearly all of the total cross-section, unless one drastically alters the hard-sphere phases in this energy region.

The considerations of section 5 show that electromagnetic effects probably cause mixing of states of the same J^π and different isobaric spin at excitation energies in Be^8 near 20 MeV. In this event the total isobaric spin is no longer a good quantum number and reduced widths for proton and neutron emission need not be equal.

The authors wish to thank Prof. H. H. Barschall for suggesting the experiment and for his continued interest in this work. Thanks are also due to the Computing Laboratory at the Bendix Products Division of Bendix Aviation Corporation for the use of their Bendix G-15 Computer in performing the calculations discussed in section 5 of this paper.

References

1) S. E. Darden, T. R. Donoghue and C. A. Kelsey, Nuclear Physics **22** (1960) 439 (preceding paper)
2) R. L. Macklin and J. H. Gibbons, Phys. Rev. **109** (1958) 105;
J. H. Gibbons and R. L. Macklin, Phys. Rev. **114** (1959) 571
3) H. W. Newson, R. M. Williamson, K. W. Jones, J. H. Gibbons and H. Marshak, Phys. Rev **108** (1957) 1294
4) R. K. Adair, Phys. Rev. **96** (1954) 709; Phys. Rev. **87** (1952) 1041
5) H. R. Striebel, S. E. Darden and W. Haeberli, Nuclear Physics **6** (1958) 188
6) R. Taschek and A. Hemmendinger, Phys. Rev. **74** (1948) 373
7) W. Haeberli (private communication)
8) A. Okazaki, Phys. Rev. **99** (1955) 55
9) R. K. Adair, Phys. Rev. **92** (1953) 1491
10) R. G. Thomas, Phys. Rev. **81** (1951) 148
11) J. M. Blatt and L. C. Biedenharn, Revs. Mod. Phys. **24** (1952) 258
12) A. Simon and T. A. Welton, Phys. Rev. **90** (1953) 1036
13) D. R. Inglis, Phys. Rev. **74** (1948) 21
14) N. P. Heydenburg, C. M. Hudson, D. R. Inglis and W. D. Whitehead, Jr., Phys. Rev. **74** (1948) 405; Phys. Rev. **73** (1948) 241

15) P. R. Malmberg, Phys. Rev. **101** (1956) 114
16) A. M. Lane and R. G. Thomas, Revs. Mod. Phys. **30** (1958) 257
17) E. P. Wigner and L. Eisenbud, Phys. Rev. **72** (1947) 29
18) I. Bloch, M. H. Hull, Jr., A. A. Broyles, W. C. Bouricius, B. E. Freeman and G. Breit, Revs. Mod. Phys. **23** (1951) 147
19) W. T. Sharp, H. E. Gove and E. B. Paul, Chalk River Report TPI-70 (1953)
20) J. E. Monahan, L. C. Biedenharn and J. P. Schiffer, Argonne Report 5846 (1958)
21) P. R. Bevington, G. E. Mitchell, W. W. Rolland, R. M. Wilenzick and H. W. Lewis, Bull. Am. Phys. Soc. **4** (1959) 218
22) P. R. Bevington (private communication)
23) J. A. Baicker, K. W. Jones and B. Tell, Bull. Am. Phys. Soc. **4** (1959) 62
24) F. Gabbard, R. H. Davis and T. W. Bonner, Phys. Rev. **114** (1959) 201
25) J. E. Monahan and F. P. Mooring, Nuclear Instruments and Methods **6** (1960) 343
26) W. E. Burcham, Progress in Nuclear Physics **4** (1955) 171
27) D. H. Wilkinson, Phil. Mag. **1** (1956) 1031
28) L. A. Radicati, Proc. Phys. Soc. A **66** (1953) 139; A **67** (1954) 39
29) W. M. MacDonald, Phys. Rev. **100** (1955) 51; **101** (1956) 271
30) D. H. Wilkinson, Phil. Mag. **1** (1956) 379
31) T. Teichmann and E. P. Wigner, Phys. Rev. **87** (1952) 123
32) F. C. Barker and A. K. Mann, Phil. Mag. **2** (1957) 5
33) W. M. MacDonald and J. B. Marion, Bull. Am. Phys. Soc. **5** (1960) 34
34) A. I. Baz, Advances in Physics **8** (1959) 349

2.J

Nuclear Physics **22** (1961) 468—483; © *North-Holland Publishing Co., Amsterdam*

Not to be reproduced by photoprint or microfilm without written permission from the publisher

MASS AND CHARGE DISTRIBUTION IN HIGH ENERGY INDUCED FISSION

GÖSTA RUDSTAM and ALEXIS C. PAPPAS †

Nuclear Chemistry Group, SC-Division, CERN, Geneva, Switzerland

Received 26 September 1960

Abstra .: Low energy fission data have been used to estimate the symmetric fission probability and its energy dependence. Using this function together with characteristics of symmetric and asymmetric fission modes the mass and charge distributions in high energy induced fission have been obtained. A numerical calculation of the mass distribution to be expected in the fission of uranium with 170 MeV protons gives reasonable agreement with experimental results, and the extrapolations from low energy data seem justified. The mass dependence of the apparent neutron-to-proton ratio of the most probable primary fission fragment and of the width of the charge distribution have therefore been estimated. A comparison with experimental data shows that neither the hypothesis of unchanged charge distribution nor that of equal charge displacement alone can explain the observed trends, but suggests a mass dependent mixture of both.

1. Introduction

The mass and charge distribution in low energy induced fission have been studied experimentally in considerable detail [1]), and theoretical explanations of these features have been offered [2–8]). These studies have, however, not resulted in a satisfying understanding of the fundamental features of fission and a unifying picture describing all aspects of this highly complex reaction is not yet available.

For high energy induced fission a large amount of experimental data have also been accumulated [9]), but mainly phenomenological treatment of these data is available. In heavier elements (thorium and higher) the most striking effect of raising the irradiation energy is that the deep valley between the asymmetric peaks of the yield mass curve characteristic for low energy induced fission gradually disappears. Furthermore, the isobaric charge distribution gets broader, and the most probable primary fission product of a given mass is generally closer to stability than the corresponding one in low energy induced fission. In spite of these differences it might be possible to account for the results obtained with higher irradiation energies merely by a simple extrapolation of low energy data.

As originally suggested by Turkevich and Niday [10]) the observed yield mass

† Permanent address: Department of Chemistry, University of Oslo, Blindern, Norway.

distribution at intermediate energies can be interpreted as the sum of contributions from different modes of fission: symmetric and asymmetric. This idea has found support in the triple peaked mass distribution curve observed in 11 MeV proton induced fission of Ra^{226} by Jensen and Fairhall [11]) †.

The present work carries the Turkevich-Niday hypothesis further in an attempt to predict the mass and charge distributions to be expected at high irradiation energies using the following hypotheses:

(a) For a given fissioning nucleus, two different modes of fission can occur, namely symmetric and asymmetric with the relative probabilities $P(E)$ and $1-P(E)$, respectively, at the excitation energy E.

(b) For any excitation energy, the mass and charge distributions of both symmetric and asymmetric fission are those of low energy fission.

Without aiming at a theoretical interpretation of high energy induced fission phenomenae it is felt that a study along these lines would be a contribution to our understanding of the distribution observed in high energy induced fission.

It may be pointed out that a recent analysis of high energy fission data by Pate [12]) also makes use of an essentially low energy charge distribution.

2. Calculations of Mass and Charge Distributions

2.1. LOW ENERGY FISSION DATA TO BE USED IN THE CALCULATION

For thermal neutron induced fission of U^{235} the charge distribution has a width †† of about 2.2 charge units [13]), and the width of the asymmetric peaks of the yield mass curve is about 16 mass units [1]). The latter value is approximately valid also for thermal neutron induced fission of U^{233} and Pu^{239} and for pile neutron induced fission of Th^{232} and U^{238} [1]). For bismuth bombarded with 15 MeV deuterons the fission yield mass curve seems to be purely symmetric, and the width is also here about 16 mass units [14]). Similar results are obtained for other light targets [15]). In accordance with hypothesis (b) above the width is therefore assumed to be 2.2 charge units for the charge distribution and 16 mass units for the mass distribution (each of the peaks in case of asymmetric fission) both independent of the excitation energy. Furthermore, both the charge and the mass distribution will be approximated by Gaussian distributions. These approximations simplify the numerical computations and will as shown later in this paper influence the final results only to a very low extent.

A very important concept in studies of high energy induced reactions in heavy nuclei is the competition between fission and neutron evaporation

† After the present paper was finished Ford [53]) has published an examination of the Turkevich-Niday hypothesis in terms of linear algebra and found the experimental yield mass curves for three of the four examined cases to be consistent with the hypothesis.

†† In this paper "width" always designates the total width at half maximum of the distribution curve in question.

(evaporation of charged particles is much less probable and can be disregarded provided that the excitation energy is below the 200 MeV region[16])). The probability G for fission is therefore given by

$$G = \frac{\Gamma_f}{\Gamma_f + \Gamma_n + \Gamma_\gamma} \tag{1}$$

where Γ_f is the fission width, Γ_n the neutron emission width and Γ_γ the radiation width (the latter is neglected if either Γ_f or Γ_n is > 0). The parameter G depends on the fissioning nucleus while its dependence on the excitation energy

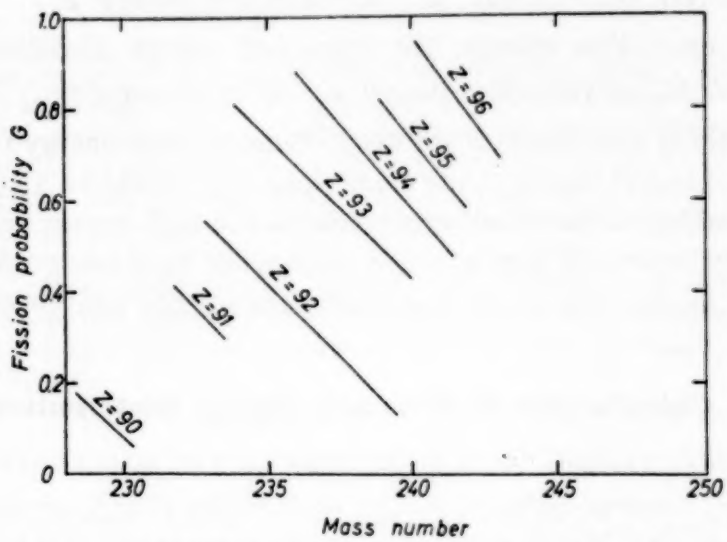

Fig. 1. Fission probability of heavy nucleides as function of mass number.

is not clear. According to some authors[17–19]) the influence of the excitation energy may be fairly slight for heavy elements although contradictory opinions have been put forward[8, 20–22]). For light elements, on the other hand, a rapid increase of G with increasing excitation energy has been clearly demonstrated[15]). The dependence of G on the fissioning nucleus is quite pronounced and has been the topic for several investigations[18, 19, 23, 24]). In the present paper use is made of the data by Vandenbosch and Huizinga[19]). The G curves thus obtained are plotted in fig. 1. These curves show that, for a given element, G decreases with increasing mass number.

2.2. PROBABILITY OF SYMMETRIC FISSION AS A FUNCTION OF EXCITATION ENERGY

The probability function for symmetric fission $P(E)$ depends strongly on the excitation energy and might also depend on the fissioning nucleus. It can be determined from the energy dependence of mass distributions by measuring the ratio between the yields at the symmetric and the asymmetric mass "peaks". These data should be taken only from experiments with irradiation energy

sufficiently low so that the formation of a compound nucleus N_0 with a definite excitation energy E_0 is a reasonable assumption. The compound nucleus may degrade its excitation energy by evaporation of neutrons. The excitation energy E_i of the nucleus N_i, after the evaporation of i neutrons, is given approximately by

$$E_i = E_{i-1} - B_{i-1} - \bar{E}_k \tag{2}$$

where the B_i's are neutron separation energies. The average kinetic energy $\bar{E}_k$ of the evaporated neutrons is here taken to be 2.5 MeV as determined by Skyrme and Harding [25]).

For the case in which a compound nucleus is formed (formation cross section: σ_{ln}), i neutrons are evaporated and the remaining nucleus undergoes symmetric fission, the cross section $\sigma_{s,i}$ can be written

$$\sigma_{s,i} = P(N_i, E_i)\sigma_{ln} G_i \prod_{j=0}^{i-1} (1-G_j). \tag{3}$$

Similarly, for asymmetric fission we have

$$\sigma_{a,i} = [1-P(N_i, E_i)]\sigma_{ln} G_i \prod_{j=0}^{i-1} (1-G_j). \tag{4}$$

The total cross sections for symmetric and asymmetric fission are obtained by summing over index i.

In order to obtain a relation between the cross sections and the "peak" value of the observed mass distribution, the symmetric and the asymmetric distribution are written as follows:

$$\begin{aligned} Y_{s,i}(A) &= K_{s,i} \exp[-k(A-A_{s,i})^2], \\ Y_{a,i}(A) &= K_{a,i}\{\exp[-k(A-A_{l,i})^2] + \exp[-k(A-A_{h,i})^2]\}, \end{aligned} \tag{5}$$

where the mass number $A_{s,i}$ corresponds to the symmetric peak, and $A_{l,i}$ and $A_{h,i}$ correspond to the light and heavy asymmetric peaks, respectively. Evidently we have

$$\begin{aligned} \sigma_s &= \sum_i \sigma_{s,i} \approx \tfrac{1}{2} \sum_i \int Y_{s,i} \mathrm{d}A \approx \tfrac{1}{2} \sqrt{\frac{\pi}{k}} \sum_i K_{s,i}, \\ \sigma_a &= \sum_i \sigma_{a,i} \approx \tfrac{1}{2} \sum_i \int Y_{a,i} \mathrm{d}A \approx \sqrt{\frac{\pi}{k}} \sum_i K_{a,i}. \end{aligned} \tag{6}$$

For a given excitation energy of the nucleus the total number of evaporated neutrons (prior to and after fission) is approximately independent of when fission actually takes place. This is due to the fact that the neutron separation energies concerned are comparable. Therefore, all the final symmetric mass distributions will have their maxima very close to the same mass number.

The same applies to asymmetric fission. Furthermore, as the distributions are narrow the contribution from asymmetric fission at the symmetric peak can be neglected, and *vice versa*.

Then

$$\sum_i K_{s,i} \Big/ \sum_i K_{a,i} = R(E_0), \tag{7}$$

where $R(E_0)$ is the ratio between the yield at the symmetric peaks and the yield at one of the asymmetric peaks. This ratio is directly obtained from the experimental yield mass distribution †.

The position of the symmetric peak is given by the expression

$$A_s = \tfrac{1}{2}(A_c - \nu - n), \tag{8}$$

with A_c equal to the mass number of the compound nucleus, ν equal to the average number of neutrons (2—3) emitted from the fragments in low energy induced fission and n equal to the maximum number of neutrons evaporated before fission. Taking the fission barrier into account the latter number can be approximated by the expression

$$n = \frac{E_0}{B + \bar{E}_k} - 1, \tag{9}$$

where B is the average separation energy of the neutrons. For asymmetric fission of heavy elements of interest to the present problem the position of the two asymmetric peaks in the yield mass curve are, according to Swiatecki [26]), given by the empirical relation

$$A_{h,l} = A_s \pm 0.045(40.2 - Z_c^2/A_c)\tfrac{1}{2}A_c, \tag{10}$$

with Z_c equal to the atomic number of the compound nucleus and A_s the mass number corresponding to a fictitious symmetric division.

Eqs. (3), (4), (6) and (7) give

$$P(N_0, E_0)G_0 + \sum_i P(N_i, E_i)G_i \prod_{j=0}^{i-1}(1-G_j) = \frac{R(E_0)}{2+R(E_0)}\left\{G_0 + \sum_i G_i \prod_{j=0}^{i-1}(1-G_j)\right\}. \tag{11}$$

This relation can be used for the evaluation of the probability function $P(N, E)$. At first E_0 is chosen so low that the excitation energy E_1, after the emission of one neutron, is below the fission barrier. In this case we have $G_i = 0$ for $i \geqq 1$, and

$$P(N_0, E_0) = R(E_0)/(2+R(E_0)). \tag{12}$$

† The inverse of $R(E_0)$ is the well known "peak-to-valley" ratio.

The next excitation energy E_0^1 is conveniently chosen so that

$$E_0^1 = E_0 + B_0 + \bar{E}_k. \tag{13}$$

It is assumed that for a given energy, $P(E)$ varies slowly with the fissioning nucleus (cf. curves given in ref.[1])). The choice through eq. (13) of a new excitation energy then gives $E_1^1 = E_0$ and therefore $P(N_1, E_1^1) \approx P(N_0, E_0)$, and finally

$$P(N_0, E_0^1)G_0 = [G_0 + G_1(1-G_0)]\frac{R(E_0^1)}{2+R(E_0^1)} - P(N_0, E_0)G_1(1-G_0). \tag{14}$$

In this way P can be estimated from the experimental values of $R(E)$ for successively higher excitation energies.

The variation of the G values in fig. 1 with energy is not known. Therefore, in accordance with the previous discussion, two extreme assumptions have been used: a) G is independent of excitation energy, and b) G is a rapidly decreasing function of energy. In the latter case Γ_f/Γ_n is assumed to follow the equation given by Fujimoto and Yamaguchi [27]) i.e.

$$\frac{\Gamma_f}{\Gamma_n} \approx T^{-1} \exp[(B-B_f)/T] \tag{15}$$

where B_f is the fission barrier and T the nuclear temperature. This formula was fitted to the G-values of fig. 1 at an excitation energy of 10 MeV. The even-odd differences were removed by using average B_f values computed by the formula [8])

$$B_f = 0.555\ (46 - Z^2/A). \tag{16}$$

The neutron separation energies, also averaged in order to remove even-odd effects, were obtained from the compilation by Foreman [28]). For the nuclear temperature the expression

$$T = \sqrt{10.5\ E/A} \tag{17}$$

was used [29]).

The method outlined above makes possible the evaluation of the function $P(E)$ for a number of different cases i.e. the compound nuclei Pa^{233}, U^{236}, U^{238}, Np^{239}, Pu^{239} and Am^{240}. For these nuclei experimental low energy mass distributions are available through the following reactions, respectively: $Th^{232}+p$ [30]), $U^{235}+n$ [31]), $Th^{232}+\alpha$ [28]), $U^{238}+\gamma$ [32]), $U^{238}+p$ [33]), $U^{235}+\alpha$ [34]) and $Pu^{239}+p$ [33]). The resulting functions are given in figs. 2 and 3 for constant and energy-dependent fission probability, respectively.

These figures indicate that the $P(E)$-functions of all the nuclei studied are quite similar. Such a behaviour of heavy nuclei has also been noted by Halpern [8]). One may deduce a logarithmic dependence of $P(E)$ on the energy up to the maximum excitation energy investigated (50 MeV). It should be pointed

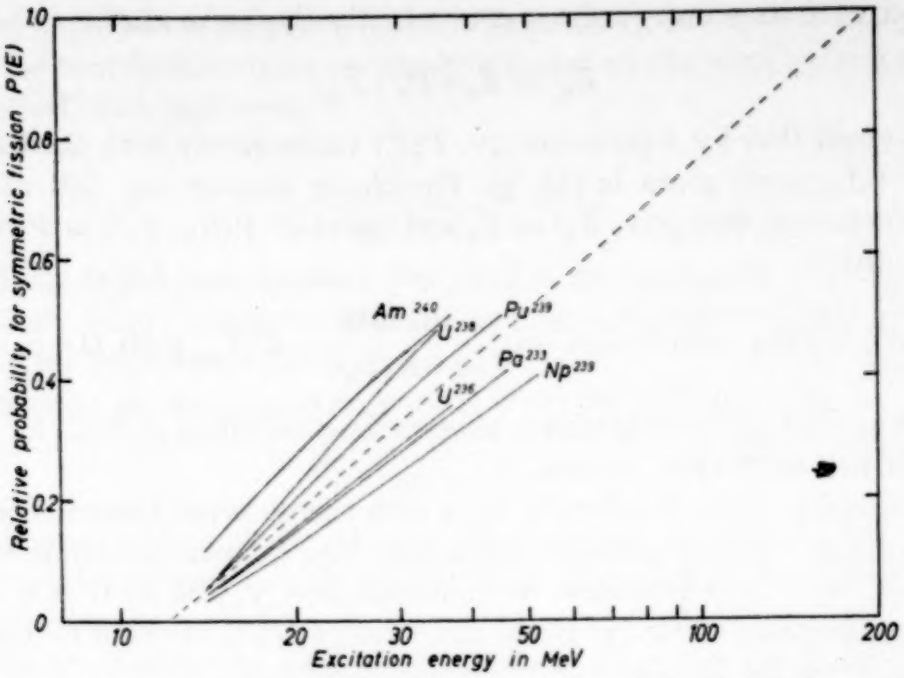

Fig. 2. Symmetric fission probability based on energy independent fission parameter G.

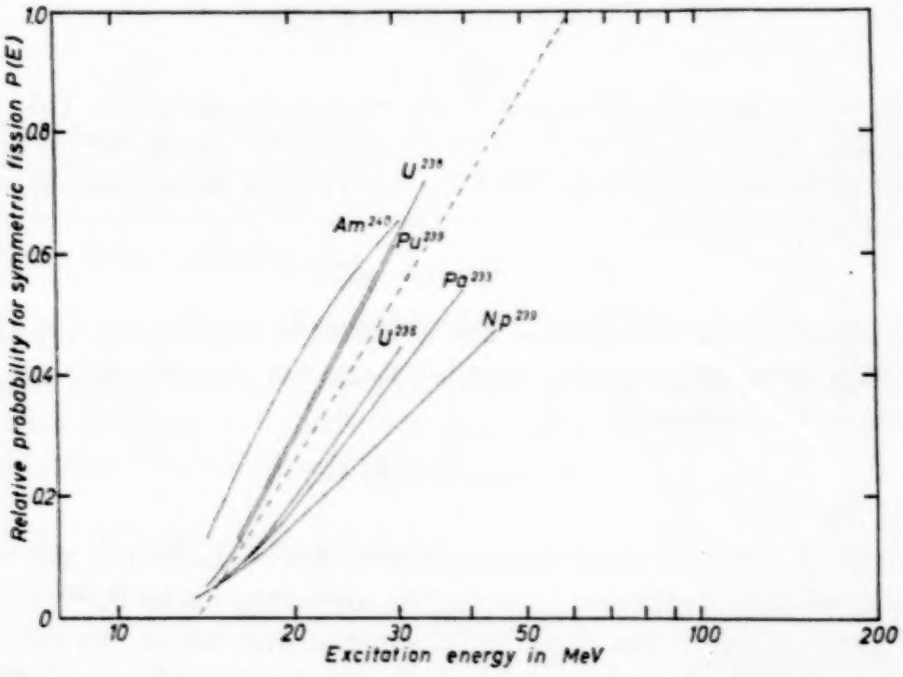

Fig. 3. Symmetric fission probability based on energy dependent fission parameter G.

out that a different $P(E)$-behaviour is to be expected for lighter elements where symmetric fission is very important even at low excitation energies [14, 15]).

2.3. THE YIELD MASS DISTRIBUTION

Nuclear reactions induced by high energy particles take place in two stages according to Serber [35]). In the first fast stage of the process a nuclear cascade

is developed inside the nucleus leaving an excited residual nucleus behind. Provided that the excitation energy distribution of the residual nuclei is known, it is possible to calculate the yield mass distribution of the products in case of fission. The cross section for formation of the residual nucleus with excitation energy between E_0 and $E_0+\Delta E_0$ is denoted by $\sigma(E_0)\Delta E_0$. The cross sections for symmetric and asymmetric fission can then be written as follows:

$$\Delta\sigma_s = \sigma(E_0)\Delta E_0\{P(N_0, E_0)G_0+\sum_{i=1}^{r} P(N_i, E_i)G_i\prod_{j=0}^{i-1}(1-G_j)\},$$
$$\Delta\sigma_a = \sigma(E_0)\Delta E_0\{[1-P(N_0, E_0)]G_0+\sum_{i=1}^{r} [1-P(N_i, E_i)]G_i\prod_{j=0}^{i-1}(1-G_j)\}, \quad (18)$$

where r is chosen so that

$$E_0-(r+1)(B+\bar{E}_k)<\text{largest of}\begin{cases}\text{the fission barrier}\\ \text{the neutron separation energy}\end{cases}\leqq E_0-r(B+\bar{E}_k). \quad (19)$$

If the neutron separation energy is larger than the barrier for fission, there exists an excitation energy range in which fission always will take place. This has to be considered in the calculation.

By means of eqs. (5) and (6) the differential yield mass curve corresponding to an excitation energy E_0 can be expressed as follows:

$$\Delta Y(A) = \sqrt{\frac{k}{\pi}}\,(2\Delta\sigma_s \exp[-k(A-A_s)^2] + \Delta\sigma_a\{\exp[-k(A-A_1)^2]+\exp[-k(A-A_h)^2]\}). \quad (20)$$

The overall mass distribution is obtained by summing or integrating over all excitation energy intervals bearing in mind that A_s, A_1 and A_h depend on the excitation energy through the number of neutrons emitted (cf. eqs. (8—10)).

2.4. THE CHARGE DISTRIBUTION

In thermal neutron fission [13, 36]) and also in fission of thorium and uranium with 13.6 MeV neutrons [37]) the maximum primary yield of isobaric fission fragments is obtained at an atomic number Z_p (usually not an integer), which can be calculated using the hypothesis of "equal charge displacement" originally advanced by Glendenin, Coryell and Edwards [36]). This states that the distances from stability of complementary most probable primary fission products are equal. As pre and post fission emitted neutrons cannot be distinguished in the present treatment, this hypothesis will here be used in the following form:

$$Z_p(E) = Z_A-\tfrac{1}{2}(Z_A+Z_{(A_c-n-\nu-A)}-Z_c), \quad (21)$$

where Z_A signifies the shell influenced β^- stability line [38]).

Assuming the charge distribution to be Gaussian, the cross section distribution can be expressed by the formula

$$\Delta\sigma(Z, A) = \Delta Y(A) \sqrt{\frac{g}{\pi}} \exp\left[-g(Z-Z_p)^2\right]. \tag{22}$$

Again, the sum of the contributions from different excitation energy intervals will give the resulting charge distribution.

The hypothesis of equal charge displacement which is shown to be valid for thermal and low energy induced fission [13]) may not be the best one for high energy induced fission. It should perhaps be replaced by the hypothesis of "unchanged charge distribution" according to which the maxima of the charge distribution curves will all have the same neutron-to-protron ratio as the "apparent" fissioning nucleus. This hypothesis was put forward by Sugarman and Turkevich [39]) and shown by Goeckermann and Perlman [40]) to explain the primary fission yields measured in the fission of bismuth induced by 190 MeV deuterons. According to this hypothesis the following expression for Z_p should be used in the present treatment:

$$Z_p(E) = \frac{Z_c}{A_c - \nu - n} A. \tag{23}$$

3. Comparison with Experimental Data

The methods outlined above have been used to calculate the mass and charge distributions to be expected in fission of uranium induced by 170 MeV protons. For this case a great number of experimental data are available [41–45]) which make a comparison between calculated and experimentally determined distributions feasible.

The maximum proton energy 170 MeV corresponds to an average proton energy of 153—154 MeV in the Uppsala synchrocyclotron where the majority of the experimental work was done. Using the Monte Carlo-technique Metropolis *et al.* [46]) have studied nucleon cascades initiated in uranium by 156 MeV protons. Their results can immediately be applied to the present case. They find that, on the average, 0.9 neutrons and 0.4 protons are emitted as cascade particles. Allowing for the fact that a small fraction of the subsequently evaporated nucleons are protons [16]), U^{237} should be a representative nucleus for the calculations of interest for the present study. The excitation energy distribution given in ref. [46]) was used in the calculation after a normalization to the total inelastic cross section of 1.9 b [47]). This distribution is found to be almost independent of the excitation energy in the range 40 MeV to 140 MeV.

The yield mass curve was computed using the two extreme assumptions mentioned earlier in this paper concerning the fission parameter G. For the

symmetric fission probability functions the broken lines in figs. 2 and 3 were used. The extrapolation of these lines to unity is quite arbitrary and open to criticism. With our present knowledge no better approach seems possible even if there is some evidence that fission may become more asymmetric again at high excitation energies [48]).

The numerical calculations were carried out using the CERN Mercury electronic computer. In order to simplify the calculations an average number of 3.5 emitted neutrons was used in estimating the average neutron separation energy, the fission barrier, and the position of the asymmetric peaks.

3.1. YIELD MASS DISTRIBUTION

The resulting yield mass distribution are shown in fig. 4. For comparison experimental cumulative cross sections taken from ref. [41–45]) for near stable

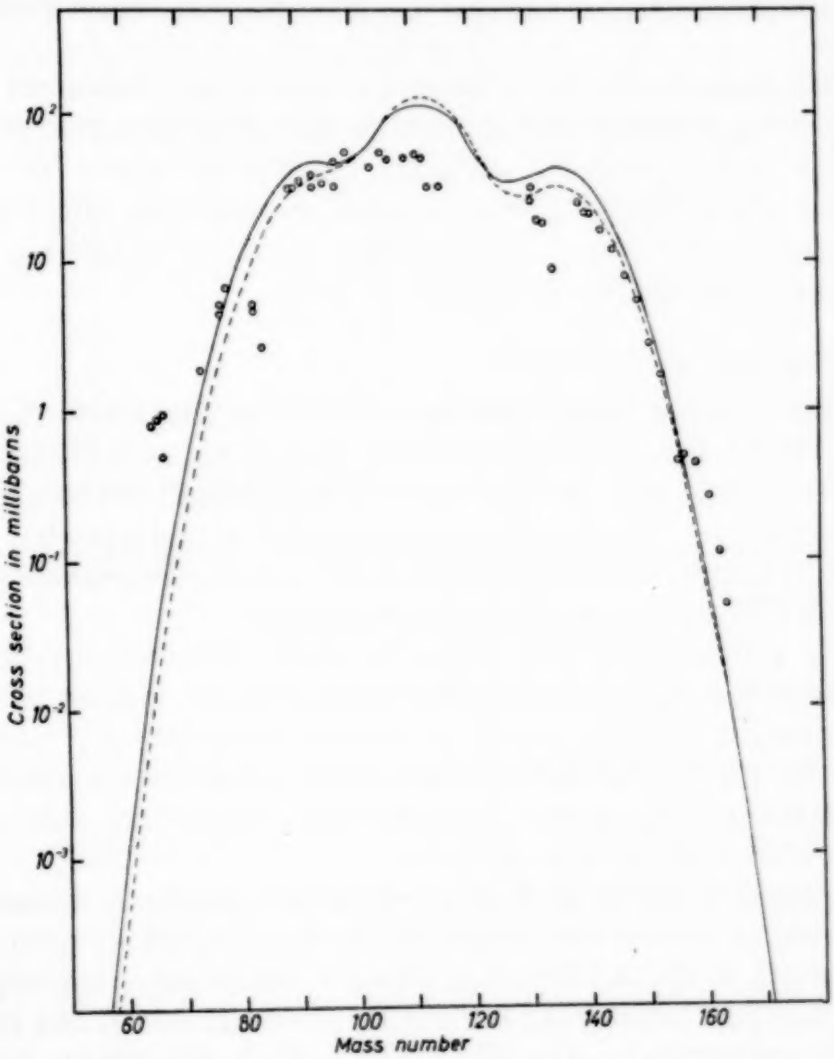

Fig. 4. Calculated yield mass curves for fission of uranium induced by 170 MeV protons. Solid line: Energy independent fission parameter. Broken line: Energy dependent fission parameter. Circles: Experimental values of cumulative yields.

fission products are plotted. These data might not always represent the total mass yields, but the eventual difference is small. In any case, the calculated curve should envelop the experimental points.

As fig. 4 discloses, the calculated distribution reproduces the experimental data quite well except for a region in the middle where the calculated cross sections are about a factor of 2 too high and far out at the wings where they are too low.

The calculated yield mass distribution is somewhat skew. The peak of the symmetric part is displaced towards the light asymmetric peak. There is also experimental evidence [9]) that the peak of the high energy yield mass distribution slowly moves to lower mass numbers with increasing energy of the bombarding protons. The reason for this is that symmetric fission is connected with the evaporation of more neutrons (before and after fission) than asymmetric fission since the former, on the average, takes place at higher excitation energies.

The yield mass distribution calculated with the energy-dependent G-function as shown in fig. 4 (broken curve) indicates that the introduction of the energy dependence of Γ_f/Γ_n does not markedly influence the results. The decreasing G-function causes fission to occur at lower energies. This effect is, however, counteracted by the steeper $P(E)$-function (see fig. 3) so that the yield mass distribution stays almost unchanged.

3.2. THE CHARGE DISTRIBUTION

The isobaric charge distribution has been calculated for several different mass numbers (70, 90, 110, 130, 150) using both the hypothesis of unchanged charge distribution (UCD) and the hypothesis of equal charge displacement (ECD). As the results obtained with the two G-functions are quite similar, the energy independent G-function was used in these calculations. The results are presented in fig. 5 (UCD: solid curve; ECD: broken curve).

Interesting parameters with respect to charge distribution studies are the neutron-to-proton ratio for the hypothetical primary nucleide corresponding to maximum yield (which should be termed "apparent" n/p ratio) and the width of the charge distribution curve. These parameters are plotted *versus* mass number in figs. 6 and 7, respectively. Apparently, there is a slight variation with mass number for both.

The charge distribution has been exprimentally studied by Aagaard *et al.* [49]) for mass number around 130. They find that the apparent n/p ratio is 1.49 and that the width of the distribution is about 4 charge units. This experimental n/p ratio falls just between the calculated values 1.47 (UCD) and 1.51 (ECD). The calculated widths are 3.2 units (UCD) and 2.9 units (ECD), both smaller than the experimental value. Pappas and Alstad [49]) draw the conclusion from their study of fission product lanthanides that the charge distribution is

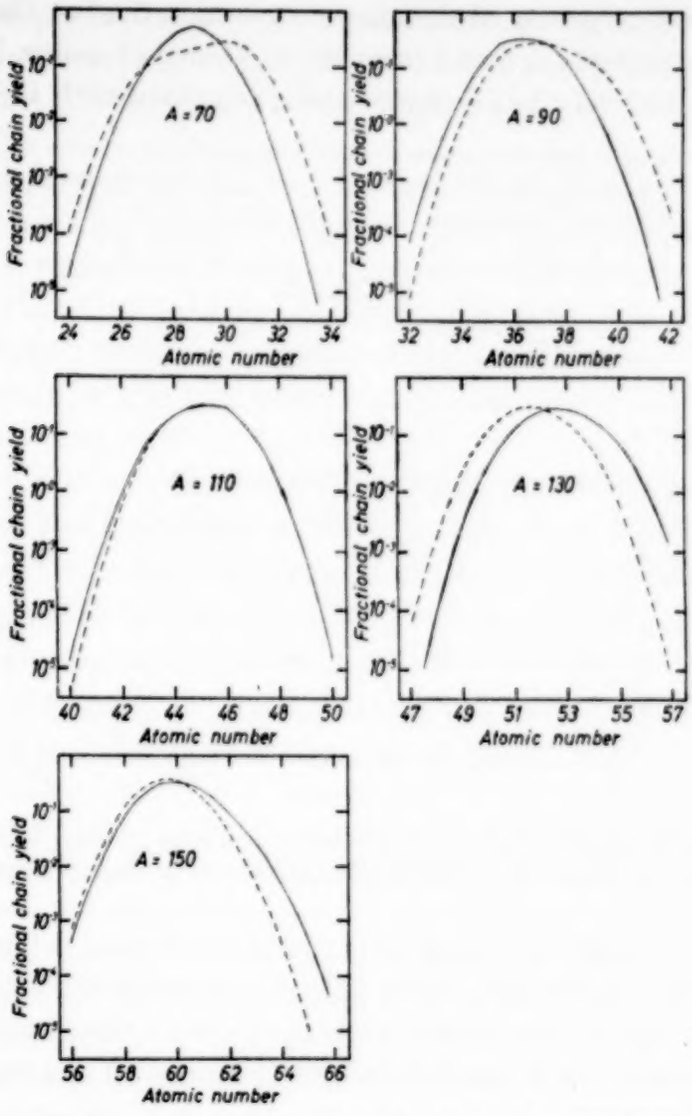

Fig. 5. Charge distribution curves for fission of uranium induced by 170 MeV protons. Solid curve: Unchanged charge distribution. Broken curve: Equal charge displacement.

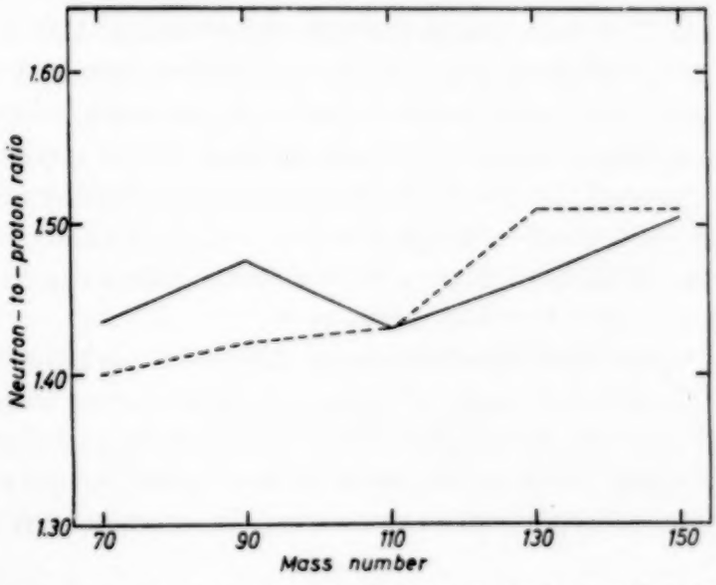

Fig. 6. Neutron-to-proton ratio of most probable primary fission product as function of mass number. Solid line: Unchanged charge distribution. Broken line: Equal charge displacement.

narrower at the heavy wing of the mass distribution than at the mass number 130. The same tendency is found from fig. 7. At mass number 150 the widths are 2.9 (UCD) and 2.7 (ECD) charge units, compared with the experimental

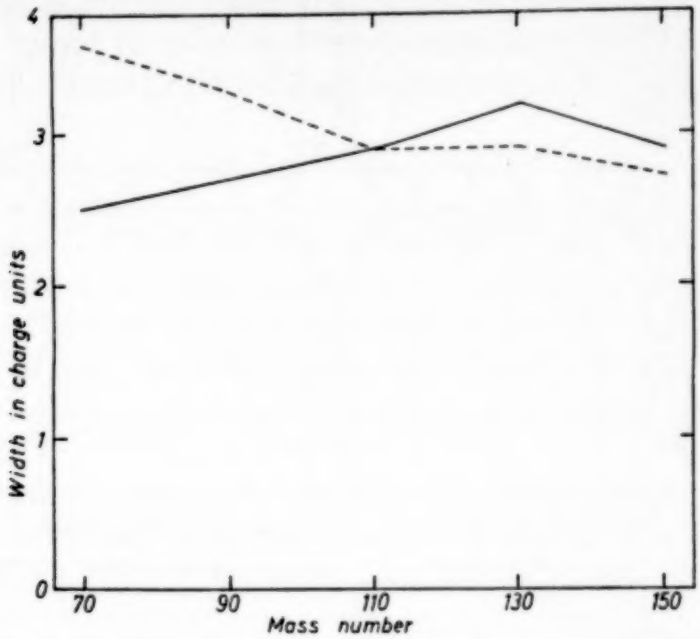

Fig. 7. Width of the charge distribution curves as function of mass number. Solid line: Unchanged charge distribution. Broken line: Equal charge displacement.

value around 2.2. At the light wing the experimental width is found by Hagebø and Pappas [45]) also to be small. In the light of the results of the presentcal culations the latter should support the unchanged charge distribution hypothesis which gives a width of 2.5 and 2.7 for mass numbers 70 and 90, respectively.

4. Discussion

The comparison between experimental and calculated cross sections reveals a fair agreement. The extrapolation of low energy fission data to higher energy therefore seems justified at least to the irradiation energy 170 MeV.

The calculated yield mass distribution seems to reach a higher maximum than does the experimental curve. Thus symmetric fission is possible too accentuated in the calculation. The reason for this can be traced back to the extrapolation of the $P(E)$-function of figs. 2 and 3 to unity. A flattening of this curve would mean an increase of asymmetric fission at the expense of symmetric fission and thus lower the symmetric peak.

At the light wing, when based on charge distribution widths, the hypothesis of unchanged distribution seems to agree somewhat better with experimental results than the hypothesis of equal charge displacement as defined by eq. (21). Hagebø and Pappas [40]), however, seem to find better support for the equal charge displacement hypothesis in evaluating the charge of the most probable

primary fission product from experimental data. At the heavy wing, however, both hypotheses seem to agree equally well — with a possible preference for the equal charge displacement hypothesis as Pappas and Alstad also conclude from their study [44]).

It should be pointed out that the calculations presented in this paper when n/p ratios and widths of charge distribution curves are concerned are limited to very few single mass numbers and can therefore only give the general trends. On the other hand, in order to obtain suitable yield data for experimental charge distribution studies one cannot study a single mass number and one must assume that for a smaller mass range the charge distribution curves have the same shape and width.

Taking these facts into consideration one should expect that a mass dependent mixture of the two hypotheses would probably give the best picture of the charge distribution in high energy induced fission. This could be ascribed to symmetric fission taking place according to the unchanged charge distribution hypothesis while asymmetric fission takes place according to the equal charge displacement hypothesis, the latter characteristic for thermal fission. This view is in accordance with the conclusions drawn by Pappas and Alstad [44]) from their experimental study, namely that the symmetric and the asymmetric fission modes are two distinct different processes; a conclusion which also can be drawn from the recent investigation by Jensen and Fairhall [50]) on fission of radium available to the authors only after the present study was carried through.

According to the results of this calculation the yield mass curve is not symmetric around the most probable mass. Thus one should not reflect measured cross section around the most probable mass as has often been done in the past. Also, the isobaric charge distributions might very well be skew as these curves are composites of different distributions.

The results obtained using an energy-dependent G-function are very similar to those obtained for a G-function independent of excitation energy. As pointed out above this is due to the counter action of two factors: a faster decrease of the G-function leads to a steeper rise of the $P(E)$-function. Thus the results cannot be used for any conclusion about the possible energy dependence of the ratio between the fission width and the neutron emission width.

It may be remarked that some approximations of the low energy results have been used, namely the representation of both the mass and the charge distributions by Gaussian distributions. The experimental distributions are not strictly Gaussian but fall off more rapidly at the wings. The use of a more appropriate kind of distribution, for instance of the form

$$\exp\left[-k_1x^2-k_2x^4\right]$$

would lead to lower yields far out at the wings but otherwise only slightly influence the results.

The calculations were also carried out for the residual nucleus Np^{238}. The results were, however, very similar to those for U^{237}. They are therefore not included in this paper.

Extension of this type of calculation to very high irradiation energies, in the GeV-region, is not possible as processes other than fission and particle evaporation will then be important [51, 52]).

Thanks are due to the staff of the CERN electronic computer for their assistance with the numerical calculations.

One of the authors (ACP) wants to express his gratitude to the late Director General of CERN, professor C. J. Bakker, for kindly inviting him to join the organization and to professors G. Bernardini and W. Gentner for the hospitality found in the SC-Division during the author's stay in Geneva in 1959.

References

1) For a review see S. Katcoff, Nucleonics **16**, no. 4 (1958) 78
2) N. Bohr and J. A. Wheeler, Phys. Rev. **56** (1939) 425
3) L. Meitner, Nature **165** (1950) 561
4) D. Hill and J. A. Wheeler, Phys. Rev. **89** (1953) 1102
5) A. Bohr and A. Mottelson, Proc. 1st Int. Conf. Peaceful Uses of Atomic Energy (United Nations, New York, 1956) Vol. **2**, 151
6) P. Fong, Phys. Rev. **102** (1956) 434
7) A. G. W. Cameron, Proc. 2nd Int. Conf. Peaceful Uses of Atomic Energy (United Nations, Geneva 1958) Vol. **15**, 425
8) J. Halpern, Ann. Rev. Nucl. Sci. **9** (1959) 245
9) J. M. Miller and J. Hudis, Ann. Rev. Nucl. Sci. **9** (1959) 159
10) A. Turkevich and J. B. Niday, Phys. Rev. **84** (1951) 52
11) R. C. Jensen and A. W. Fairhall, Phys. Rev. **109** (1958) 942
12) B. D. Pate, Can. J. Chem. **36** (1958) 1707
13) A. C. Pappas, American Report LNS-MIT-63, AECU-2806 (1953), Inaugural Dissertation University of Oslo; Proc. 1st Int. Conf. Peaceful Uses of Atomic Energy (United Nations, New York 1956) Vol. **7**, 19
14) A. W. Fairhall, Phys. Rev. **102** (1956) 1335
15) A. W. Fairhall, R. C. Jensen and E. F. Neuzil, Proc. 2nd Int. Conf. Peaceful Uses of Atomic Energy (United Nations, Geneva 1958) Vol. 15, 452
16) I. Dostrovsky, P. Rabinowitz and R. Bivins, Phys. Rev. **111** (1958) 1659
17) R. A. Glass, R. J. Carr, J. W. Cobble and G. T. Seaborg, Phys. Rev. **104** (1956) 434
18) R. E. Batzel, American Report, UCRL-4303 (1954)
19) R. Vandenbosch and J. R. Huizenga, Proc. 2nd Int. Conf. Peaceful Uses of Atomic Energy (United Nations, Geneva 1958) Vol. 15, 284
20) G. N. Harding and F. J. M. Farley, Proc. Phys. Soc. A **69** (1956) 853
21) I. Dostrovsky, Z. Fraenkel and P. Rabinowitz, Proc. 2nd Int. Conf. Peaceful Uses of Atomic Energy (United Nations, Geneva 1958) Vol. 15, 301
22) V. P. Shamov, Soviet Physics JETP **6** (1958) 268
23) R. M. Lessler, American Report, UCRL-8439 (1958)
24) I. Halpern and C. T. Coffin, Proc. 2nd Int. Conf. Peaceful Uses of Atomic Energy (United Nations, Geneva 1958) Vol. 15, 398
25) D. M. Skyrme and G. N. Harding, Nuovo Cim. **9** (1950) 1082
26) W. J. Swiatecki, Phys. Rev. **100** (1955) 936
27) Y. Fujimato and Y. Yamaguchi, Progr. Theoret. Phys. **5** (1950) 76

28) B. M. Foreman, Jr., American Report UCRL-8223 (1958)
29) J. B. M. Lang and K. J. Le Couteur, Proc. Phys. Soc. A **67** (1954) 586
30) B. J. Bowles, F. Brown and J. P. Butler, Phys. Rev. **107** (1957) 751
31) A. Turkevich, Phys. Rev. **89** (1953) 554
32) L. Katz, T. M. Kavanagh, A. G. W. Cameron, E. C. Bailey and J. W. T. Spinks, Phys. Rev. **99** (1955) 98
33) J. P. Butler, B. J. Bowles and F. Brown, Proc. 2nd Int. Conf. Peaceful Uses of Atomic Energy (United Nations, Geneva 1958) Vol. 15, 156
34) R. Vandenbosch, American Report UCRL-3858 (1957)
35) R. Serber, Phys. Rev. **72** (1947) 1114
36) L. E. Glendenin, C. D. Coryell and R. R. Edwards, in Radiochemical studies: the fission products, ed. by C. D. Coryell and N. Sugarman (McGraw Hill Co., New York 1951) Nat. Nucl. En. Ser. Div. IV, vol. **9**, paper 52
37) J. M. Alexander and C. D. Coryell, Phys. Rev. **108** (1957) 1274
38) R. A. Brightsen, C. D. Coryell and A. C. Pappas, see C. D. Coryell, Ann. Rev. Nucl. Sci. **2** (1953) 305
39) N. Sugarman and A. Turkevich, personal communication of 1946 in ref. [36]).
40) R. H. Goeckermann and I. Perlman, Phys. Rev. **84** (1951) 52
41) H. G. Hicks and R. S. Gilbert, Phys. Rev. **100** (1955) 1286
42) A. Kjelberg and A. C. Pappas, Nuclear Physics **1** (1956) 322
43) P. Aagaard and A. C. Pappas, private communication (1958)
44) A. C. Pappas and J. Alstad, J. Inorg. Nucl. Chem. (1960) in press
45) E. Hagebø and A. C. Pappas, private communication (1959)
46) N. Metropolis, R. Bivins, M. Storm, J. M. Miller and G. Friedlander, Phys. Rev. **110** (1958) 185
47) G. P. Milburn, W. Birnbaum, W. E. Crandall and L. Schecter, Phys. Rev. **95** (1954) 1268
48) V. P. Shamov and O. V. Lozhkin, JETP **2** (1956) 111
49) P. Aagaard, G. Andersson, J. O. Burgman and A. C. Pappas, J. Inorg. Nucl. Chem. **5** (1957) 105
50) R. C. Jensen and A. W. Fairhall, Phys. Rev. **118** (1960) 771
51) R. Wolfgang, E. W. Baker, A. A. Caretto, J. B. Cumming, G. Friedlander and J. Hudis, Phys. Rev. **103** (1956) 394
52) R. H. Shudde, American Report UCRL-3419 (1956)
53) G. P. Ford, Phys. Rev. **118** (1960) 1261

2.I

Nuclear Physics **22** (1961) 484—491; ©*North-Holland Publishing Co., Amsterdam*

Not to be reproduced by photoprint or microfilm without written permission from the publisher

SYSTEMATICS OF (γ, 2n) REACTIONS

I. C. NASCIMENTO, G. MOSCATI and J. GOLDEMBERG

Departamento de Fisica, Faculdade de Filosofia, Ciências e Letras, Universidade de S. Paulo, São Paulo, Brasil †

Received 26 September 1960

Abstract: The (γ, n) and (γ, 2n) cross sections in I^{127} and Au^{197} were measured from threshold up to 22 MeV. A comparison is made between the experimental result and the evaporation theory. Other data available in the literature are included.

1. Introduction

Few measurements of (γ, 2n) reactions have been made by residual activity methods due to difficulties in counting the radiations emitted by the final nucleus. Another method which has been used is to subtract the (γ, n) yield from the total neutron yield and divide the result by two; the excitation function for the (γ, 2n) reactions is thus obtained and can be solved by the usual methods.

In this paper this method is used to obtain the (γ, 2n) cross section in I^{127} and Au^{197} up to 22 MeV.

A comparison is made between the experimental results and the evaporation model [1]). In this analysis the available data for [2]) Ta^{181} [3]), Cu^{63} [4]), Nb^{93} and [5]) Pr^{141} is included in order to obtain an idea of the general trend of (γ, 2n) reactions as a function of A. Other measurements in light elements [6]) at higher energies are not included.

2. Measurements

The following cross sections were determined: $Au^{197}(\gamma, n)Au^{196}$, $Au^{197}(\gamma, 2n)Au^{195}$, $I^{127}(\gamma, n)I^{126}$, $I^{127}(\gamma, 2n)I^{125}$. Half-lives and the γ transitions of the disintegration schemes were also measured.

In the measurement of the neutron yield curves a BF_3 counter imbedded in paraffin was used; this system is similar to the one used by Nathans and Halpern [7]) with some modifications [8]).

In the residual activity measurements a one-channel analyser and a 5.1 cm by 5.1 cm NaI crystal were used; a 10-channel analyser was also used.

Figs. 1 and 2 show the yield curves obtained. The absolute values were obtained by normalization to the data of Montalbetti, Katz and Goldemberg [9]) for

† Work supported in part by the Conselho Nacional de Pesquisas.

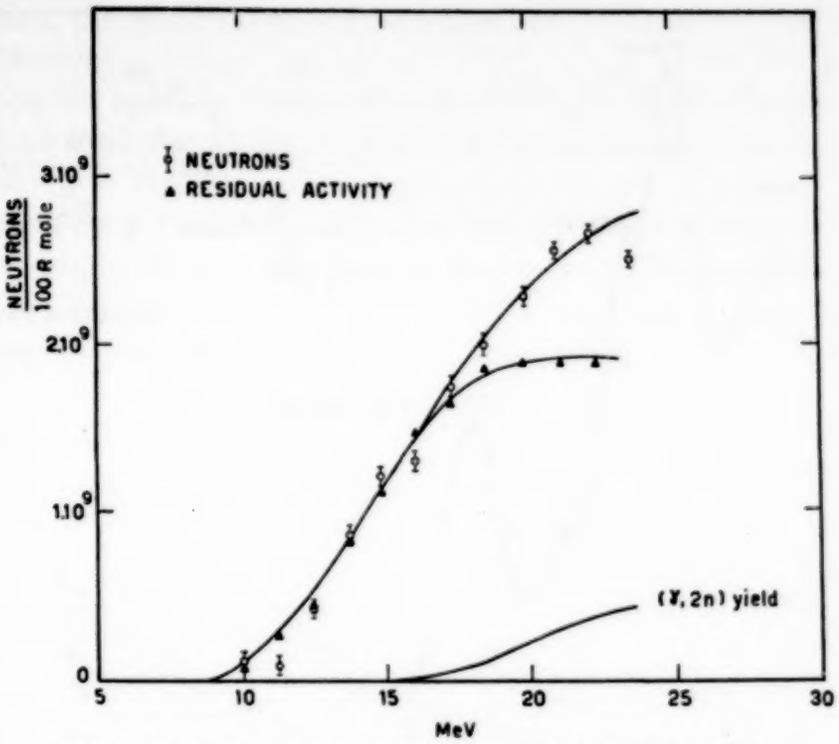

Fig. 1. Yield curves for the $Au^{197}(\gamma, n)$ and $Au^{197}(\gamma, 2n)$ reactions.

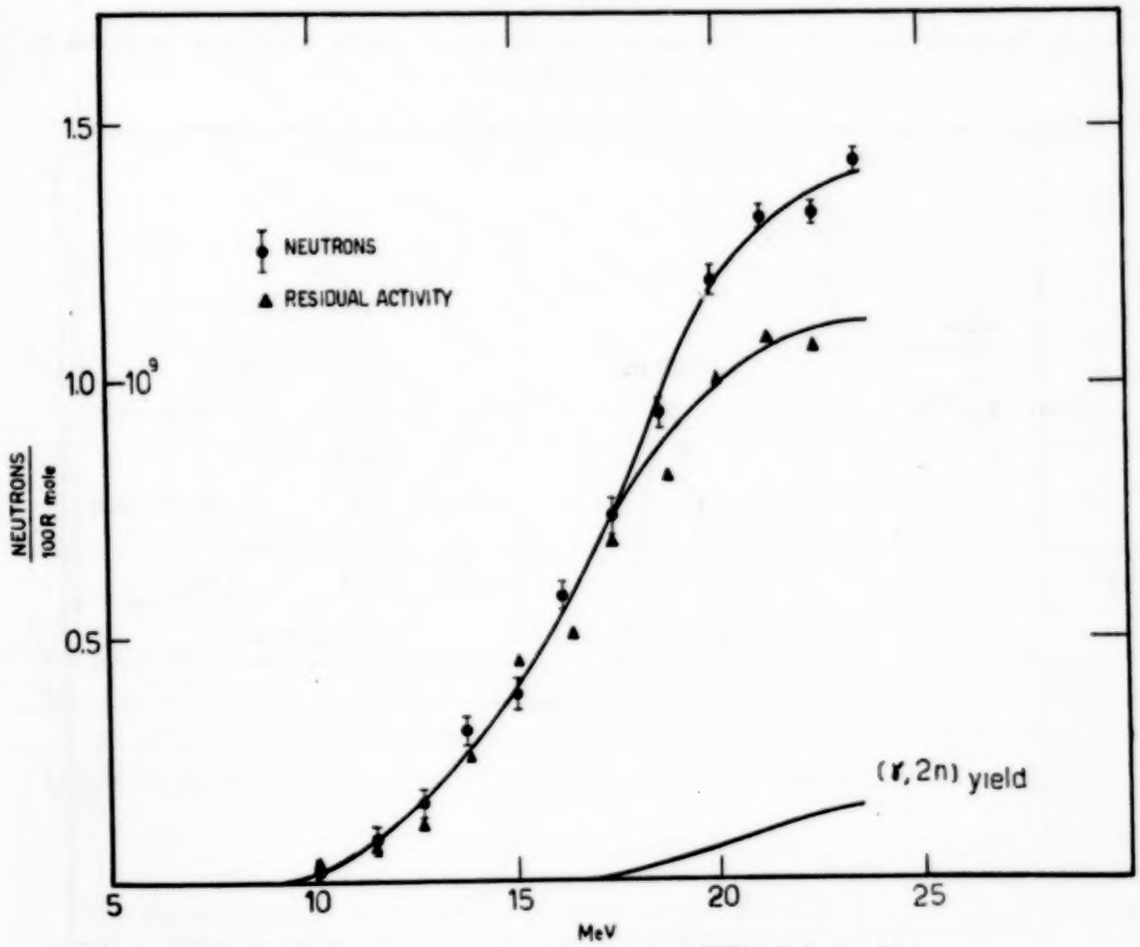

Fig. 2. Yield curves for the $I^{127}(\gamma, n)$ and $I^{127}(\gamma, 2n)$ reactions.

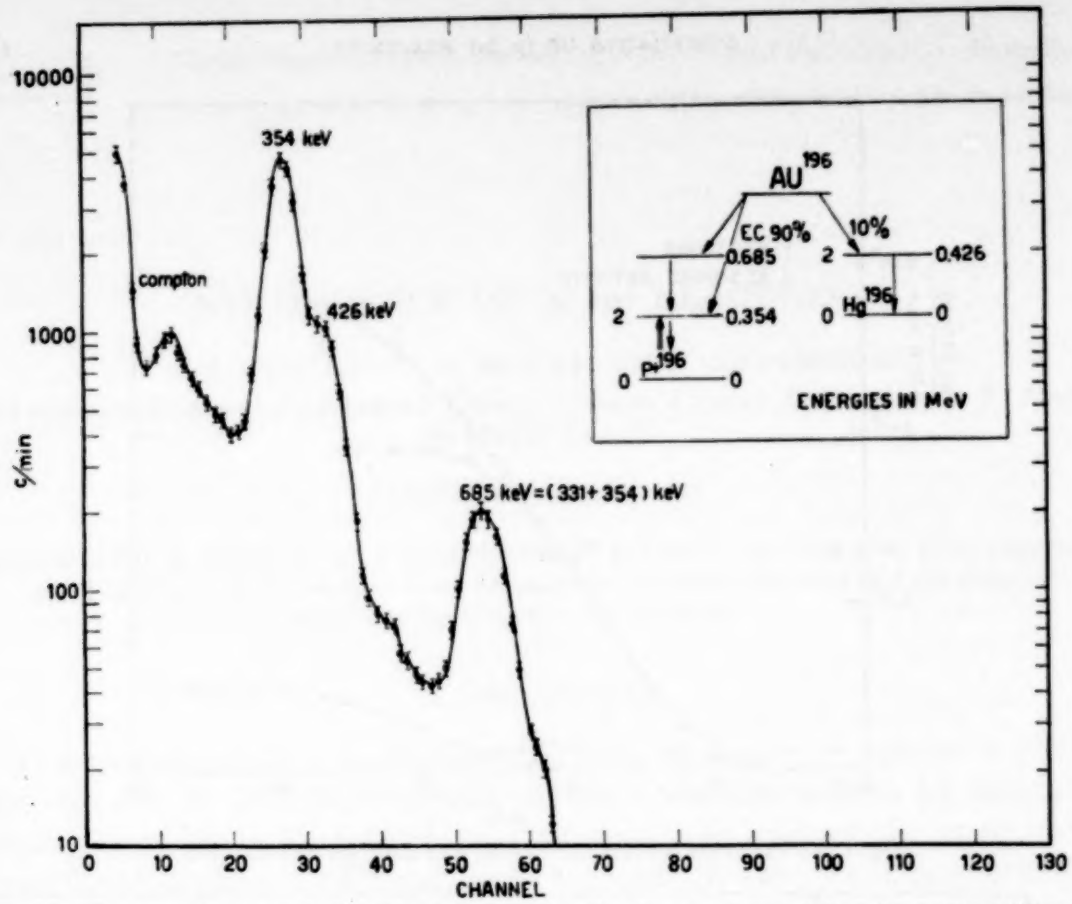

Fig. 3. The γ-spectrum of Au^{196}. The insert shows the decay scheme taken from the tables by Strominger *et al.* [10]).

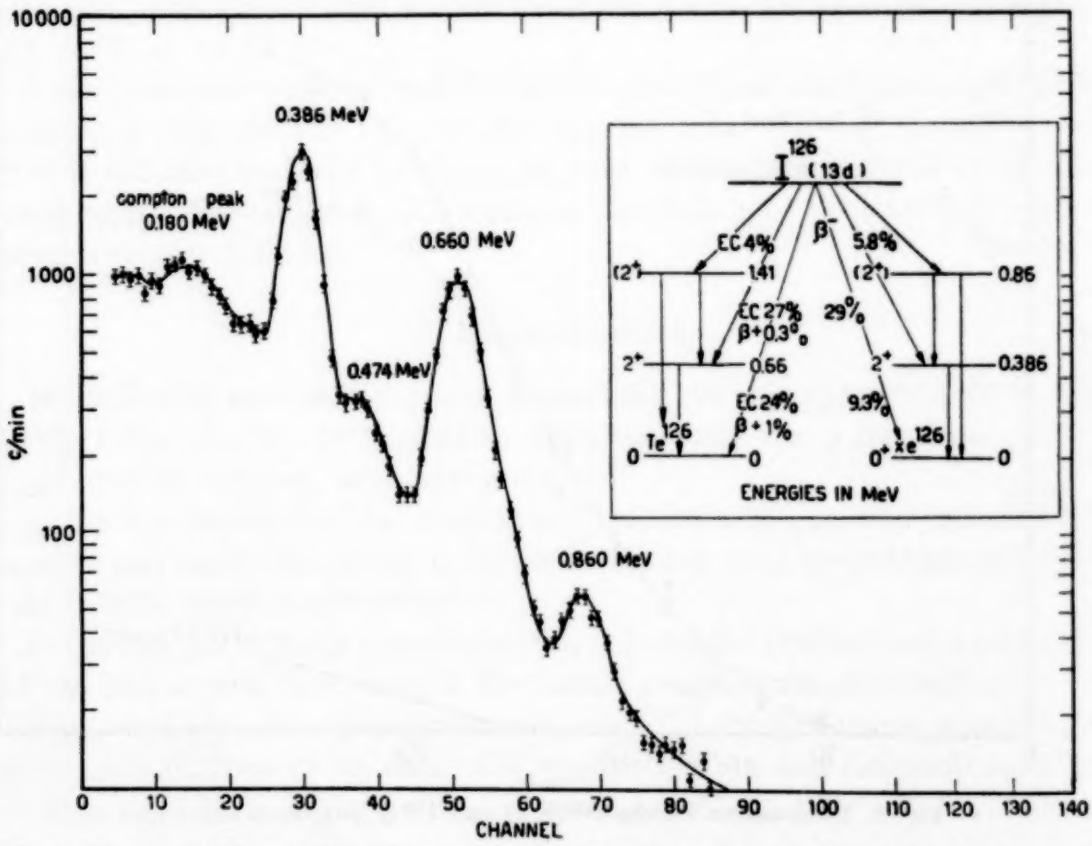

Fig. 4. The γ-spectrum of I^{126}. The insert shows the decay scheme taken from the tables by Strominger *et al.* [10]).

the neutrons; the (γ, n) curve was normalized to the neutron curve below the $(\gamma, 2n)$ threshold.

The γ-spectra were also measured with a 10-channel pulse height analyser. Figs. 3 and 4 show the results obtained and the known disintegration schemes from Strominger, Holland and Seaborg's tables [10]).

The activities of the Gold and Iodine samples were followed for 50 days; they are shown in fig. 5. A least squares fit shows that the half-life of Au^{196} is

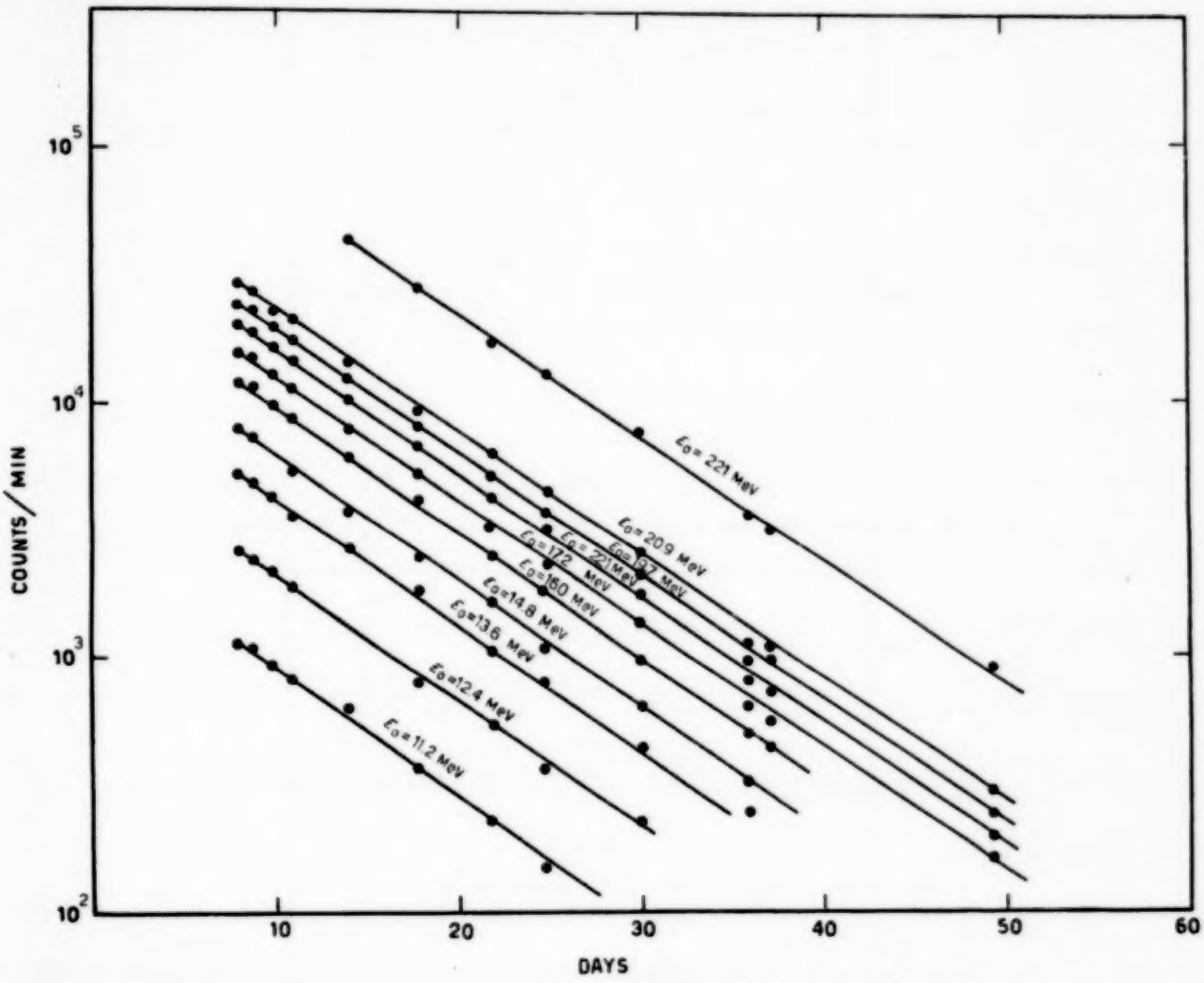

Fig. 5. The activity of Au^{196}. Errors are smaller then the size of the points. E_0 is the maximum energy of the bremsstrahlung.

6.1 ± 0.1 days and not 5.6 days as has been usually accepted. The 13 days half-life for I^{126} agrees with our data.

The cross sections were obtained with a Univac computer using the spectrum tables of Katz and Cameron [11]); they are shown in figs. 6 and 7.

3. Discussion

The data obtained were compared with the predictions of evaporation theory in the following way.

the expression for the level density. The values used for a were taken from the formule $a = 0.035\ (A-12)$ suggested by Heidmann and Bethe [12]).

Using thresholds calculated from mass spectrometer data and measurements of Y_t the ratio Y_m/Y_t was obtained; for absorption we used the cross-section curves for neutron production [9]).

The results are shown in table 1 and fig. 8. The data obtained in this work and those available in the literature are included. The solid lines of fig. 8 represent an estimate of the errors due to the poorly known parameters and thresholds.

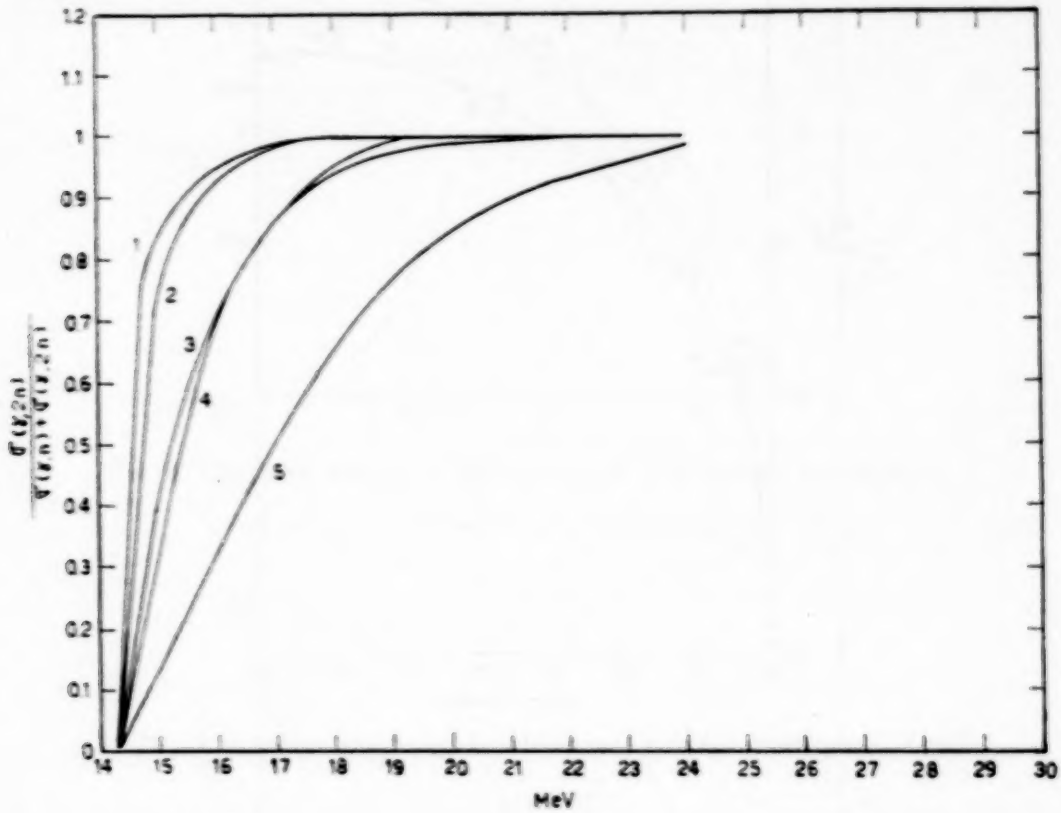

Fig. 9. Calculated ratios $\sigma(\gamma, 2n)/\sigma_{absorption}$ using the following quantities:

Curve	1	2	3	4	5
W	$Ce^{2\sqrt{aE}}$	$Ce^{2\sqrt{aE}}$	$Ce^{2\sqrt{aE}}$		$e^{0.7}$
a	$\frac{1}{5}A$	$1.6(A-40)^{\frac{1}{2}}$	10	experimental	
ref.	[1])	[1])	[1])	[14])	[13])

4. Conclusion

The ratio $\sigma(\gamma, 2n)/\sigma_{absorption}$ is not a sensitive test of the evaporation theory as can be seen in fig. 9 where calculations of this ratio were made for Ta^{181} using several level densities suggested in the literature.

Nevertheless it is possible to state that evaporation theory is satisfactory in explaining the observed $(\gamma, 2n)$ yields and that fig. 8 can be used to obtain in a semi-quantitative way Y_{2n} for most of the middle weight and heavy elements.

We wish to acknowledge Mr. H. P. Heillman for the cross-section analysis, Mr. V. Wajntal for the calculations shown in fig. 9 and to Mr. E. Lerner and Franca Tagliabue for discussions.

References

1) J. M. Blatt and V. F. Weisskopf, Theoretical Nuclear Physics (John Wiley and Sons, New York 1952)
2) E. A. Whalin and A. O. Hanson, Phys. Rev. **89** (1953) 324L
3) A. I. Berman and K. L. Brown, Phys. Rev. **96** (1954) 83
4) E. Silva, J. Goldemberg and P. B. Smith, Nuovo Cim. **9** (1958) 17
5) F. Ferrero, R. Malvano, E. Silva, G. Moscati and J. Goldemberg, Nuclear Physics, **10** (1959) 423
6) J. O'Connell, P. Dyal and J. Goldemberg, Phys. Rev. **116** (1959) 173
7) R. Nathans and J. Halpern, Phys. Rev. **93** (1954) 437
8) G. Moscati and J. Goldemberg, Anais da Academia Brasileira de Ciências (to be published)
9) R. Montalbetti, L. Katz and J. Goldemberg, Phys. Rev. **91** (1953) 659
10) D. Strominger, J. M. Hollander and G. T. Seaborg, Rev. Mod. Phys. **30** (1958) 585
11) L. Katz and A. G. W. Cameron, Can. J. Phys. **29** (1951) 518
12) J. Heidmann and H. A. Bethe, Phys. Rev. **84** (1951)274
13) E. G. Fuller, B. Petree and M. S. Weiss, NBS Report No. 5686
14) P. C. Gugelot, Phys. Rev. **81** (1950) 51
15) B. M. Spicer, Phys. Rev. **100** (1955) 791

1.E.4

Nuclear Physics **22** (1961) 492—497; ©*North-Holland Publishing Co., Amsterdam*

Not to be reproduced by photoprint of microfilm without written permission from the publisher

MATRIX ELEMENTS FOR THE ALPHA-PARTICLE

L. COHEN

Mathematics Department, University of Southampton, England

Received 26 September 1960

Abstract: The classification of alpha-particle wave functions given in an earlier paper is reformulated in terms of products of vectors and products of tensors. It is shown how, after summing over spins and isobaric spins, the matrix elements may be expressed in terms of functions of interparticle distances only.

1. Introduction

In a previous paper [1]), hereafter referred to as (I), it was shown that functions occurring in the alpha-particle ground state could be expressed in terms of products of isobaric spin functions, spin and angular momentum functions, and "internal" functions of appropriate symmetry.

In this paper the spin and angular momentum functions are further analysed in terms of scalar products of spin and space vectors (in the case of P-states) or scalar products of spin and space second rank tensors (in the case of D-states). The spin and space vectors and tensors used all have definite permutation symmetry. The processes of summing over spins and isobaric spins in the evaluation of the matrix elements is then much simplified, and it is shown that after carrying out these summations only functions of interparticle distances remain.

In addition it is shown that the kinetic energy matrix elements can be expressed concisely in terms of differential operators in the interparticle distances and of definite permutation symmetry. Euler angles are not needed at any stage of the calculation.

The meanings of the symbols not defined in the present paper are given in (I).

2. D-state Wave Functions

We consider explicitly the symmetrical traceless second rank tensors (corresponding to $L = 2$) which can be formed from the three vectors $\mathbf{r}, \boldsymbol{\varrho}_1, \boldsymbol{\varrho}_2$. A typical tensor of this form is denoted by $T^{(2)}(\mathbf{a}, \mathbf{b})$, whose components are

$$T^{(2)}_{ij}(\mathbf{a}, \mathbf{b}) = a_i b_j + a_j b_i - \tfrac{2}{3}\delta_{ij} a_k b_k. \tag{1}$$

From the six such tensors which can be formed, we can obtain the following

irreducible representations of the permutation group

$$\begin{aligned}
T^{(2)}([4]) &= T^{(2)}(\mathbf{r},\mathbf{r})+T^{(2)}(\boldsymbol{\varrho}_1,\boldsymbol{\varrho}_1)+T^{(2)}(\boldsymbol{\varrho}_2,\boldsymbol{\varrho}_2),\\
T^{(2)}([22],\mathrm{aa}) &= T^{(2)}(\boldsymbol{\varrho}_1,\boldsymbol{\varrho}_2),\\
T^{(2)}([22],\mathrm{ss}) &= \frac{1}{\sqrt{3}}\,[T^{(2)}(\mathbf{r},\mathbf{r})-\tfrac{1}{2}T^{(2)}(\boldsymbol{\varrho}_1,\boldsymbol{\varrho}_1)-\tfrac{1}{2}T^{(2)}(\boldsymbol{\varrho}_2,\boldsymbol{\varrho}_2)], \qquad (2)\\
T^{(2)}([31],\mathrm{as}) &= T^{(2)}(\mathbf{r},\boldsymbol{\varrho}_1), \quad T^{(2)}([31],\mathrm{sa}) = -T^{(2)}(\mathbf{r},\boldsymbol{\varrho}_2),\\
T^{(2)}([31],\mathrm{ss}) &= \tfrac{1}{2}T^{(2)}(\boldsymbol{\varrho}_1,\boldsymbol{\varrho}_1)-\tfrac{1}{2}T^{(2)}(\boldsymbol{\varrho}_2,\boldsymbol{\varrho}_2).
\end{aligned}$$

The corresponding spin tensor wave function, with total spin $S = 2$ is denoted by $S^{(2)}$ and has components

$$S^{(2)}_{ij} = \tfrac{1}{2}(\sigma_i^{(1)}\sigma_j^{(3)}+\sigma_j^{(1)}\sigma_i^{(3)}-\tfrac{2}{3}\delta_{ij}\sigma_k^{(1)}\sigma_k^{(3)})\phi_1, \qquad (3)$$

where the upper index refers to the particle, and the lower index to the component. The tensor $S^{(2)}$ is totally symmetric.

On taking the scalar product of the space tensors $T^{(2)}$ with the spin tensor $S^{(2)}$, to form quantities with total $J = 0$, we can readily obtain the following expressions for the $\phi_{\mathrm{D}}([\lambda],\kappa)$ which are defined in eq. (15) of (I):

$$\phi_{\mathrm{D}}([\lambda],\kappa) = T^{(2)}([\lambda],\kappa)S^{(2)} \equiv \sum_{i,j} T^{(2)}_{ij}([\lambda],\kappa)S^{(2)}_{ij}. \qquad (4)$$

The complete set of totally antisymmetric D-states is then

$$\Psi_{\mathrm{D}}([\lambda'];[\tilde{\lambda}]) = \sum_{\kappa,\kappa',\kappa''}\begin{pmatrix}[\lambda'][22][\lambda]\\ \kappa' \quad \kappa'' \quad \kappa\end{pmatrix} T^{(2)}([\lambda'],\kappa')S^{(2)}\chi([22],\kappa'')f_{\mathrm{D}}{}^{i}([\tilde{\lambda}],\kappa); \quad (5)$$

the argument of the Ψ_{D} specifies the different D-state wave functions, $[\tilde{\lambda}]$ denoting the symmetry of the "internal" part, and $[\lambda']$ that of the space tensor part; the index i can take two values when $[\tilde{\lambda}] = [\widetilde{22}]$, and indicates that an "internal" part of [22] symmetry can occur in two different wave functions.

3. P-state Wave Functions

There are three different vectors of even parity which can be formed from $\mathbf{r}, \boldsymbol{\varrho}_1, \boldsymbol{\varrho}_2$, viz. $\mathbf{r}\wedge\boldsymbol{\varrho}_1, \mathbf{r}\wedge\boldsymbol{\varrho}_2, \boldsymbol{\varrho}_1\wedge\boldsymbol{\varrho}_2$ (corresponding to $L = 1$). These span a [211] representation of the permutation group whose components, denoted by $T^{(1)}([211],\kappa)$, are

$$T^{(1)}([211],\mathrm{sa}) = \mathbf{r}\wedge\boldsymbol{\varrho}_2, \quad T^{(1)}([211],\mathrm{as}) = \boldsymbol{\varrho}_1\wedge\mathbf{r}, \quad T^{(1)}([211],\mathrm{aa}) = \boldsymbol{\varrho}_2\wedge\boldsymbol{\varrho}_1. \quad (6)$$

Similarly there are three different spin vector wave functions $\boldsymbol{\sigma}^{(1)}\phi_1, \boldsymbol{\sigma}^{(3)}\phi_1, \boldsymbol{\sigma}^{(1)}\wedge\boldsymbol{\sigma}^{(3)}\phi_1$ (corresponding to $S = 1$), spanning a [31] representation of the permutation group. The components of this representation are denoted by

$S^{(1)}([31], \kappa)$ and are

$$S^{(1)}([31], \text{as}) = \frac{1}{\sqrt{3}}\sigma^{(3)}\phi_1, \quad S^{(1)}([31], \text{sa}) = \frac{1}{\sqrt{3}}\sigma^{(1)}\phi_1,$$

$$S^{(1)}([31], \text{ss}) = \frac{i}{\sqrt{6}}\sigma^{(1)} \wedge \sigma^{(3)}\phi_1. \quad (7)$$

Taking scalar products of $T^{(1)}$ and $S^{(1)}$, the quantifies $\phi_P([\lambda], \kappa)$ defined in eq. (10) of (I) are, apart from a factor of $\sqrt{3}$, given by

$$\phi_P([\lambda], \kappa) = \sum_{\kappa', \kappa''} \begin{pmatrix} [31] & [211] & [\lambda] \\ \kappa' & \kappa'' & \kappa \end{pmatrix} T^{(1)}([211], \kappa')S^{(1)}([31], \kappa''). \quad (8)$$

The complete set of totally antisymmetric P-states is then

$$\Psi_P[\lambda']; [\tilde{\lambda}]) = \sum_{\kappa, \kappa', \kappa''} \begin{pmatrix} [\lambda'] & [22] & [\lambda] \\ \kappa' & \kappa'' & \kappa \end{pmatrix} \phi_P([\lambda'], \kappa')\chi([22], \kappa'')f_P^{\,i}([\tilde{\lambda}], \tilde{\kappa}), \quad (9)$$

where the index i can take two values when $[\tilde{\lambda}] = [31]$ or $[211]$.

4. S-state Wave Functions

For reference we write down the complete set of totally antisymmetric S-states in a similar manner,

$$\Psi_S([\tilde{\lambda}]) = \sum_{\kappa, \kappa', \kappa''} \begin{pmatrix} [22] & [22] & [\lambda] \\ \kappa' & \kappa'' & \kappa \end{pmatrix} \phi([22], \kappa')\chi([22], \kappa'')f_S([\tilde{\lambda}], \tilde{\kappa}), \quad (10)$$

the symmetry $[\tilde{\lambda}]$ of the "internal" part being sufficient to specify the different S-state wave functions.

5. Normalisation

The normalisation integrals can be readily obtained using the following results:

$$\sum_{\text{isobaric spin}} \chi^*([22], \kappa)\chi([22], \kappa') = \delta_{\kappa\kappa'},$$

$$\sum_{\text{spin}} (T^{(1)}([211]\kappa)S^{(1)}([31], \mu))^*(T^{(1)}([211], \kappa')S^{(1)}([31], \mu')) \quad (11)$$

$$= \tfrac{1}{3}T^{(1)}([211], \kappa)T^{(1)}([211], \kappa')\delta_{\mu\mu'},$$

$$\sum_{\text{spin}} (T^{(2)}([\lambda], \kappa)S^{(2)})^*(T^{(2)}([\lambda'], \kappa')S^{(2)}) = T^{(2)}([\lambda], \kappa)T^{(2)}([\lambda'], \kappa'). \quad (12)$$

After summing over spins and isobaric spins the quantities which remain contain the "internal" functions, and possibly scalar products of vectors or second rank tensors. These latter scalar products can be expressed entirely in terms of scalar products of the vectors $\mathbf{r}, \boldsymbol{\varrho}_1, \boldsymbol{\varrho}_2$, which can in turn be expressed in terms of squares of interparticle distances. The final expressions are therefore functions of interparticle distances which can be integrated in the

manner discussed in a previous paper [2]). The detailed evaluation of the integrands is straightforward, and is omitted.

6. Kinetic Energy

The methods are exemplified by considering the kinetic energy in the principal D-state †,

$$\Psi_{\mathrm{D}}([22];[4]) = \sum_{\kappa} T^{(2)}([22],\kappa)S^{(2)}\chi(\widetilde{[22]},\tilde{\kappa})f_{\mathrm{D}}([4]). \tag{13}$$

The kinetic energy operator $\mathscr{K} = \sum_{i=1}^{4}\nabla_i^2$, where the sum is over the four nucleons. Since the wave function is independent of the centre-of-gravity, we can rewrite the operator $\mathscr{K}$ in the form

$$\mathscr{K} = \nabla_r^2+\nabla_{\rho_1}^2+\nabla_{\rho_2}^2.$$

We note that $\mathscr{K}T^{(2)}([\lambda],\kappa)S^{(2)}$ vanishes for all $T^{(2)}$. Hence the effect of the kinetic energy operator on the space part of the wave function involves only

$$T^{(2)}([22],\kappa)\mathscr{K}f_{\mathrm{D}}([4])+2\sum_{r,\rho_1,\rho_2}\nabla_r T^{(2)}([22],\kappa)\nabla_r f_{\mathrm{D}}([4]). \tag{14}$$

Since $f_{\mathrm{D}}([4])$ is expressed in terms of interparticle distances, the first term can be evaluated using the expression for $\mathscr{K}$ given by eq. (5) of the paper by Cohen and Willis [2]).

The interparticle distances r_{ij} can be expressed in terms of scalar products of the vectors $\mathbf{r}$, $\boldsymbol{\varrho}_1$, $\boldsymbol{\varrho}_2$. Hence the gradients occurring in the second term of (14) can be expressed in terms of derivatives with respect to interparticle distances. A convenient set of differential operators, with permutation symmetry as indicated, is as follows

$$\begin{aligned}
\partial([4]) &= \sum_{i=1}^{6}\frac{1}{r_i}\frac{\partial}{\partial r_i},\\
\partial([22],\mathrm{aa}) &= \frac{1}{r_3}\frac{\partial}{\partial r_3}+\frac{1}{r_4}\frac{\partial}{\partial r_4}-\frac{1}{r_2}\frac{\partial}{\partial r_2}-\frac{1}{r_5}\frac{\partial}{\partial r_5},\\
\partial([22],\mathrm{ss}) &= \frac{1}{\sqrt{3}}\left(\frac{1}{r_2}\frac{\partial}{\partial r_2}+\frac{1}{r_3}\frac{\partial}{\partial r_3}+\frac{1}{r_4}\frac{\partial}{\partial r_4}+\frac{1}{r_5}\frac{\partial}{\partial r_5}-\frac{2}{r_1}\frac{\partial}{\partial r_1}-\frac{2}{r_6}\frac{\partial}{\partial r_6}\right),\\
\partial([31],\mathrm{as}) &= \frac{1}{r_2}\frac{\partial}{\partial r_2}+\frac{1}{r_3}\frac{\partial}{\partial r_3}-\frac{1}{r_4}\frac{\partial}{\partial r_4}-\frac{1}{r_5}\frac{\partial}{\partial r_5},\\
\partial([31],\mathrm{sa}) &= \frac{1}{r_2}\frac{\partial}{\partial r_2}+\frac{1}{r_4}\frac{\partial}{\partial r_4}-\frac{1}{r_3}\frac{\partial}{\partial r_3}-\frac{1}{r_5}\frac{\partial}{\partial r_5},\\
\partial([31],\mathrm{ss}) &= \sqrt{2}\left(\frac{1}{r_1}\frac{\partial}{\partial r_1}-\frac{1}{r_6}\frac{\partial}{\partial r_6}\right),
\end{aligned} \tag{15}$$

† The adjoint components $\chi(\widetilde{[22]},\tilde{\kappa})$ are given by $\chi(\widetilde{[22]},\widetilde{\mathrm{aa}}) = \chi([22],\mathrm{ss})$; $\chi(\widetilde{[22]},\widetilde{\mathrm{ss}}) = -\chi([22],\mathrm{aa})$.

where we use the notation $r_1, r_2, r_3, r_4, r_5, r_6$ for the interparticle distances $r_{12}, r_{13}, r_{14}, r_{23}, r_{24}, r_{34}$ respectively. It can then be shown that the second term of (14) can be expressed in the form

$$\sum_{r,\rho_1,\rho_2} \nabla_r T^{(2)}([22], \kappa)\nabla_r f_D([4]) = \sum_{[\lambda'],\kappa'} \sum_{[\lambda'']\kappa''} a([\lambda']; [\lambda'']) \begin{pmatrix} [\lambda'][\lambda''][22] \\ \kappa' \quad \kappa'' \quad \kappa \end{pmatrix} T^{(2)}([\lambda'], \kappa')\partial([\lambda''], \kappa'')f_D([4]), \tag{16}$$

where the coefficients a have the values

$$a([4]; [22]) = \tfrac{1}{3}, \quad a([22]; [4]) = \tfrac{4}{3}, \quad a([22]; [22]) = -\tfrac{2}{3}, \quad a([31]; [31]) = 1.$$

The final kinetic energy matrix element can then be obtained using the results of section 5. Similar expressions for the other matrix elements can be obtained, and we omit the detailed results.

7. Potential Energy

7.1. CENTRAL FORCES

Central force matrix elements can be evaluated using the results of section 5 and noticing that

$$(\sigma^{(1)} \cdot \sigma^{(2)})\psi(\overline{12}) = \psi(\overline{12}), \quad (\sigma^{(1)} \cdot \sigma^{(2)})\psi(\widetilde{12}) = -3\psi(\widetilde{12}),$$

where $\psi(\overline{12})$ is a spin wave function symmetric with respect to interchange of particles 1 and 2, and $\psi(\widetilde{12})$ is antisymmetric with respect to this interchange.

7.2. TENSOR FORCES

We require the matrix elements of the tensor operator

$$S_{12} = \frac{(\sigma^{(1)} \cdot \mathbf{r}_{12})(\sigma^{(2)} \cdot \mathbf{r}_{12})}{r_{12}^2} - \tfrac{1}{3}(\sigma^{(1)} \cdot \sigma^{(2)}). \tag{17}$$

The basic results needed to evaluate the matrix elements between S-and D-states are

$$\begin{aligned}
&\sum_{\text{spin}} \phi^*([22], \kappa)S_{12}\phi([22], \kappa') = 0, \\
&\sum_{\text{spin}} \phi^*([22], \text{aa})S_{12}S^{(2)} = 0, \\
&\sum_{\text{spin}} \phi^*([22], \text{ss})S_{12}S^{(2)}T^{(2)}([\lambda], \kappa) = \frac{1}{\sqrt{3}r_{12}^2} T^{(2)}(\mathbf{r}_{12}, \mathbf{r}_{12})T^{(2)}([\lambda], \kappa), \\
&\sum_{\text{spin}} (T^{(2)}([\lambda], \kappa)S^{(2)})^* S_{12}(T^{(2)}([\lambda'], \kappa')S^{(2)}) \\
&\qquad = -\frac{1}{r_{12}^2} \sum_{i,j,k} T_{ij}^{(2)}([\lambda], \kappa)T_{jk}^{(2)}(\mathbf{r}_{12}, \mathbf{r}_{12})T_{ki}^{(2)}([\lambda'], \kappa').
\end{aligned} \tag{18}$$

Matrix elements involving P-states can be obtained in a similar manner.

7.3. SPIN-ORBIT FORCES

We need the matrix elements of the spin-orbit operator

$$\mathbf{L}_{12} \cdot \mathbf{S}_{12} = (\boldsymbol{\sigma}^{(1)} + \boldsymbol{\sigma}^{(2)}) \cdot \boldsymbol{\varrho}_1 \wedge \operatorname{grad} \rho_1. \tag{19}$$

It is not possible to express these very concisely and we omit the full details. The essential results are

$$\begin{aligned} (\boldsymbol{\sigma}^{(1)} + \boldsymbol{\sigma}^{(2)})\phi([22], \mathrm{aa}) &= 0, \\ (\boldsymbol{\sigma}^{(1)} + \boldsymbol{\sigma}^{(2)})\phi([22], \mathrm{ss}) &= 2\sqrt{2}S^{(1)}([31], \mathrm{ss}). \end{aligned} \tag{20}$$

It follows that some of the P-states are directly coupled to some of the S-states by the spin-orbit force (but the principal P-state is not directly coupled to the principal S-state), and that no D-state is coupled in this way to an S-state.

References

1) L. Cohen, Nuclear Physics **21** (1960)
2) L. Cohen and J. B. Willis, Nuclear Physics **13** (1959) 125

2.B

Nuclear Physics **22** (1961) 498—499; ©*North-Holland Publishing Co., Amsterdam*

Not to be reproduced by photoprint or microfilm without written permission from the publisher

NEUTRON POLARIZATION BY COULOMB SCATTERING

B. MARGOLIS

Department of Physics, The Ohio State University, Columbus 10, *Ohio* †

Received 16 September 1960

Abstract: The polarization of neutrons by Coulomb scattering is examined in the low energy region ($kR \ll 1$) at energies corresponding to a Breit-Wigner s-wave resonance. It is found that one has virtually 100 % polarization at small angles.

It has been known for some time [1]) that neutrons can be polarized in small angle scattering by an atomic nucleus. This polarization is due to the interference of the strongly forward peaked spin-flip scattering of the magnetic dipole moment of the neutron by the Coulomb field of the nucleus with the nuclear scattering amplitude. One gets large polarizations at angles of the order of one degree [1, 2, 3]). Some measurements of this effect have been made [4, 5]). Schwinger [1]) shows that in the limit of low energies (as $kR \to 0$) the maximum polarization of the neutron goes to zero. The purpose of this note is to point out that this is not the case for scattering at energies corresponding to a Breit-Wigner s-wave resonance. In fact in this case one finds that for small enough angles the neutrons will be virtually 100 % transversely polarized.

Consider the interaction of the neutron with the Coulomb field of the nucleus

$$H' = \mu \frac{e\hbar}{4Mc} \sigma_{\mu\nu} F_{\mu\nu}, \tag{1}$$

where $\mu = -1.91$. Then we get in first Born approximation using Dirac spinors a scattering amplitude

$$h = -\mu Z \frac{e^2}{Mc^2} (\cos \tfrac{1}{2}\theta + \tfrac{1}{2} i \boldsymbol{\sigma} \cdot \mathbf{n} \cot \tfrac{1}{2}\theta). \tag{2}$$

For low energy s-wave resonant scattering by a spin zero nucleus, the nuclear amplitude is, neglecting neutron capture,

$$g = i/k + R. \tag{3}$$

We find then for small angle scattering with $kR \ll 1$ a scattering amplitude

$$f(\theta) = R + \frac{i}{k} - \tfrac{1}{2} i \mu Z \frac{e^2}{Mc^2} \boldsymbol{\sigma} \cdot \mathbf{n} \cot \tfrac{1}{2}\theta. \tag{4}$$

† Work supported by the U. S. Atomic Energy Commission.

This leads to a transverse polarization

$$\mathbf{P} = \frac{-\frac{1}{k}\mu Z \frac{e^2}{Mc^2}\cot\tfrac{1}{2}\theta}{\frac{1}{k^2} + \left(\tfrac{1}{2}\mu Z \frac{e^2}{Mc^2}\right)^2 \cot^2\tfrac{1}{2}\theta.}\,\mathbf{n} \tag{5}$$

This leads to 100 % polarization when

$$\tan\tfrac{1}{2}\theta = \tfrac{1}{2}|\mu|\frac{Ze^2}{\hbar c}\left(k\frac{\hbar}{Mc}\right).$$

This large polarization is due to $f(\theta)$ being almost pure imaginary at a Breit-Wigner resonance.

If we consider a resonance in a spin zero isotope of lead we get the maximum polarization at $\theta = \theta_M$, where

$$\theta_M = 0.026|\mu|\sqrt{E_{MeV}} \text{ radians.}$$

If we have an s-wave resonance say at 17 keV, $\theta_M \approx 0.37°$. The polarization as a function of θ for this case is tabulated in table 1. The corresponding calculation for other cases including the modification for non-zero target spin is easily performed.

TABLE 1

The polarization as a function of θ

θ (degrees)	0	0.1	0.2	0.37	0.6	1	2	3	4	5	7	9	12	15	30
100 P (θ)	0	25	83	100	89	66	36	25	19	15	11	8	6	5	2.4

Finally the angular distribution of the scattered neutrons is readily calculated using (4). The magnetic dipole scattering has to be corrected at very small angles [1]) due to atomic screening.

References

1) J. Schwinger, Phys. Rev. **73** (1948) 407
2) J. T. Sample, Canad. J. Phys. **34** (1956) 36
3) A. I. Baz, JETP **31** (1956) 159
4) R. G. P. Voss and R. Wilson, Phil. Mag. (Ser. 8) **1** (1956) 175
5) Hillman, Stafford and Whitehead, Nuovo Cim. **4** (1956) 67

2.B:2.G

Nuclear Physics **22** (1961) 500—504; ©*North-Holland Publishing Co., Amsterdam*

Not to be reproduced by photoprint or microfilm without written permission from the publisher

NEUTRON ANGULAR DISTRIBUTIONS FOR THE REACTION $^{16}O(^3He, n)^{18}Ne$

N. H. GALE, J. B. GARG and K. RAMAVATARAM

The Physical Laboratories, The University, Manchester, England

Received 7 October 1960

Abstract: The angular distributions of neutrons leading to the ground state of ^{18}Ne in the reaction $^{16}O(^3He, n)^{18}Ne$ have been measured at bombarding energies of 5.6 and 6.09 MeV; using a pulsed beam time-of-flight neutron spectrometer. The angular distributions were found to be strongly peaked in the forward direction. The results have been compared with a double-stripping theory, and good agreement has been obtained with the theoretical prediction for $l = 0$ stripping. It is, however, impossible from the angular distributions alone to exclude the possibility that the reaction proceeds by a knock-out mechanism. If the mechanism is that of double-stripping, the results lead to the assignment of spin zero and even parity to the ground state of ^{18}Ne, in accordance with expectation.

1. Introduction

The great interest attaching to the study of $X(^3He, n)Y$ reactions was mentioned in a previous article [1]) on the $^{12}C(^3He, n)^{14}O$ reaction. The study of the $^{16}O(^3He, n)^{18}Ne$ reaction was undertaken in order to provide further information on the mechanism involved in reactions initiated by mass three particles.

Until recently very little information was available on the nucleus ^{18}Ne [2]). A comprehensive study of the $^{16}O(^3He, n)^{18}Ne$ reaction by the neutron threshold method has now been made by Towle and Macefield [3]), who established the ground state Q-value as -3.199 ± 0.006 MeV and located the first three excited states in ^{18}Ne. The ground state threshold had previously been measured to a lower degree of accuracy by Dunning and Butler [4]). However, no measurements have previously been published of the angular distributions of the emitted neutrons. It was therefore thought of interest to study the angular distribution of the neutron group leading to the ground state of ^{18}Ne. It was possible to study only the ground state neutron group because the maximum available energy of the ^3He particles was limited to about 6 MeV.

2. Experimental Procedure

Singly charged ^3He ions were accelerated by the University of Manchester 6 MV Van de Graaff accelerator, and after analysis by a 90° deflecting magnet were used to bombard a target of zinc oxide about 200 μg per cm^2 thick. The

target was prepared by placing a drop of a suspension of finely powdered zinc oxide in alcohol on a piece of gold foil 127 μm thick, and allowing it to evaporate. This method of target preparation resulted in a zinc oxide layer which was of fairly uniform thickness over the central region bombarded by the ^{3}He beam, but of marked non-uniformity towards the edges of the deposit. For this reason it was not possible to determine accurately the target thickness by weighing.

A pulsed beam time-of-flight neutron spectrometer was used to obtain the neutron spectra. The analyzed beam was re-focussed by a magnetic quadrupole lens onto a 1 mm slit placed at a distance of three metres from the beam deflecting electrodes. A radio-frequency voltage of frequency 4 MHz, resulting in a peak field strength of 7.5 kV per cm across the deflecting electrodes, was used to sweep the beam across the slit, producing beam pulses of duration of $\approx$ 1 ns. The pulsed beam was allowed to strike the target which was placed in a target chamber situated about 2 m beyond the slit.

The arrangement of the electronic apparatus, a description of the neutron detector, and a discussion of the variation of neutron detection efficiency with energy have been given in a previous paper [1]). Both angular distributions were corrected for the dependence of efficiency on neutron energy.

A flight path of only 30 cm was used throughout this experiment. The loss of energy resolution which this entailed was acceptable because only a single neutron group was to be studied, whilst it also resulted in a useful improvement of the ratio of true coincidences to random coincidences.

3. Results and Discussion

The time-of-flight spectra obtained for the ^{16}O(^{3}He, n)^{18}Ne reaction were quite similar to those found in the ^{12}C(^{3}He, n)^{14}O reaction previously studied [1]); a typical spectrum characteristic of those observed in both studies was presented in the previous paper [1]).

Angular distributions for incident ^{3}He energies of 5.6 MeV and 6.09 MeV are presented in figs. 1 and 2. Both distributions show very pronounced forward peaking. Because of uncertainties in the target thickness our measurements do not yield reliable values for the absolute cross-section directly. The cross-sections indicated in the figures were obtained by normalizing our angular distributions at 0°, using the 0° excitation function measured by Towle and Macefield [3]). The relative cross-sections are accurate to ± 5 %, the absolute cross-sections have in addition the error associated with the determination of the 0° yield curve.

The angular distributions presented in figs. 1 and 2 were fitted by the formula for the differential cross-section given by Newns [5]),

$$\frac{\mathrm{d}\sigma}{\mathrm{d}\omega} \propto \exp\left(-\frac{K^2}{4\gamma^2}\right) j_0^2(Qr),$$

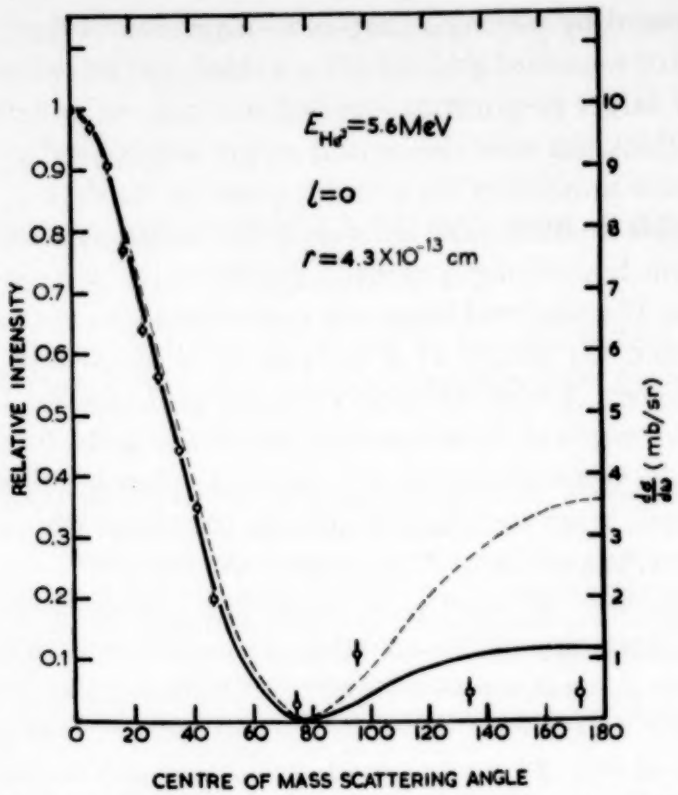

Fig. 1. Angular distribution of neutrons leading to the ground state in the reaction $^{16}O(^3He, n)^{18}Ne$ at a bombarding energy of 5.6 MeV. The solid line is the $l = 0$ double-stripping fit including the effect of the form factor; the broken line is the fit without inclusion of the form factor.

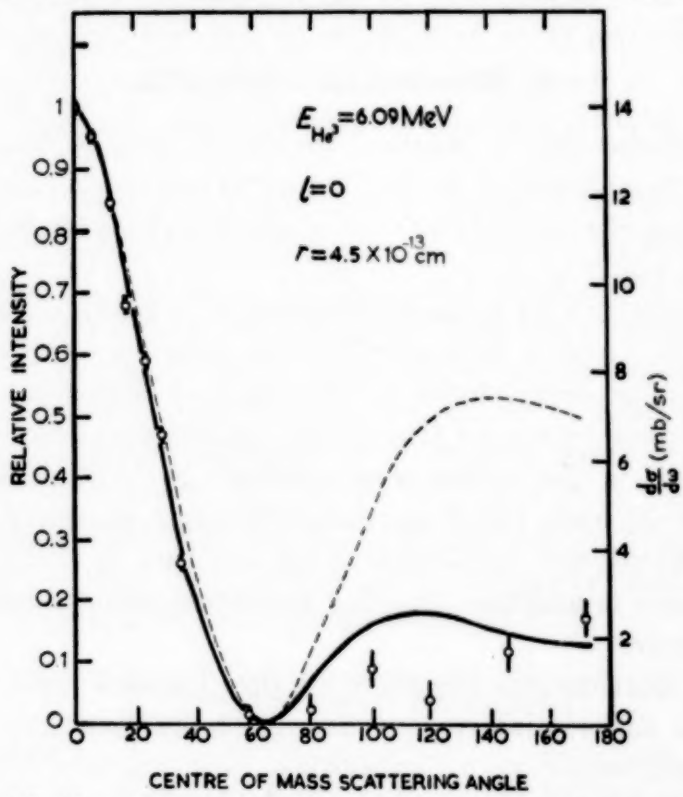

Fig. 2. Angular distribution of the ground state neutrons at a bombarding energy of 6.09 MeV. The solid line is the fit with inclusion of the form factor; the broken line is the fit without the form factor.

where the exponential term is the ^{3}He form factor and the other symbols were defined in our previous paper on the ^{12}C(^{3}He, n)^{14}O reaction [1]). In the expression for the form factor, K is given by the relation

$$\mathbf{K} = \tfrac{1}{3}\mathbf{k}_{^3\mathrm{He}} - \mathbf{k}_n,$$

and γ is defined by taking for the ^{3}He internal wave function the gaussian function

$$\chi_{^3\mathrm{He}} = \left(\frac{2\gamma^2}{\pi}\right) \exp\left[-\gamma^2(|\mathbf{r}_1-\mathbf{r}_2|^2+|\mathbf{r}_2-\mathbf{r}_p|^2+|\mathbf{r}_p-\mathbf{r}_1|^2)\right].$$

We have taken $\gamma = 2.5\times 10^{12}\,\mathrm{cm}^{-1}$ in calculating the form factor. For reactions with a large negative Q-value the form factor has quite a large effect in suppressing the theoretical cross-section at backward angles. In reactions with large positive Q-values the quantity K in general changes little with angle, leading to the result that, as found for instance by Jaffe *et al.* [6]) in their study of some (t, p) reactions, the form factor has little effect on the predicted angular distribution.

Since Newns' double-stripping theory is necessarily somewhat crude in its present form, in view of the fact that no account has been taken of coulomb and nuclear distortions which may be quite important at low energies and which may outweigh the importance of the form factor, it is probable that inclusion of the form factor is strictly an unjustifiable procedure. However, inclusion of the effect of the form factor in the present case gave a considerably better fit to the experimental angular distributions at backward angles, as can be seen from figs. 1 and 2, where fits with and without the inclusion of the form factor are given.

It is to be noted that it has been found necessary to use a cut-off radius of about 4.5×10^{-13} cm to fit our results in both the ^{16}O(^{3}He, n)^{18}Ne and the ^{12}C(^{3}He, n)^{14}O reactions. In the analogous (t, p) reactions studied by Jaffe and his colleagues [6]), a cut-off radius of about 6×10^{-13} cm was found necessary, but similar sharply peaked angular distributions were observed.

As in the case of the ^{12}C(^{3}He, n)^{14}O reaction, a knock-out mechanism cannot be excluded on the basis of the angular distributions alone. However, arguments similar to those presented in ref. [1]) appear to favour the double-stripping interpretation. If the reaction mechanism is that of double-stripping, the good fit of the angular distributions by zero order spherical Bessel functions leads to the assignment of spin zero and even parity to the ground state of ^{18}Ne, in accordance with expectation.

We are indebted to Dr. J. H. Towle and Dr. B. E. F. Macefield for kindly communicating their work to us prior to publication.

References

1) N. H. Gale, J. B. Garg, J. M. Calvert and K. Ramavataram, Nuclear Physics **20** (1960) 313
2) F. Ajzenberg-Selove and T. Lauritsen, Nuclear Physics **11** (1959) 1
3) J. H. Towle and B. E. F. Macefield, Proc. Phys. Soc. (1960) (in press)
4) K. L. Dunning and J. W. Butler, Bull. Amer. Phys. Soc. **4** (1959) 444
5) H. C. Newns, Proc. Phys. Soc. **76** (1960) 489
6) A. A. Jaffe, F. de S. Barros, P. D. Forsyth, J. Muto, I. J. Taylor and S. Ramavataram, Proc. Phys. Soc. (1960) (in press)

3.A

Nuclear Physics **22** (1961) 505—512; © *North-Holland Publishing Co., Amsterdam*

Not to be reproduced by photoprint or microfilm without written permission from the publisher

LIFETIMES OF THE 668-keV AND 961-keV EXCITED STATES IN Cu^{63}

T. ROTHEM †, F. R. METZGER and C. P. SWANN

Bartol Research Foundation of the Franklin Institute, Swarthmore, Pennsylvania ††

Received 4 July 1960

Abstract: The 668-keV and 961-keV levels of Cu^{63} have been studied by the resonance scattering method. The levels were excited by the gamma radiations from gaseous and from liquid sources of Zn^{63}, and both the resonance effect and the angular distribution of the scattered radiations have been measured. Fitting the data to a distribution of the form $W(\theta) = 1+A_2P_2(\cos\theta)$ yielded the values -0.03 ± 0.07 and 0.8 ± 0.2 for A_2 in the case of the 668-keV and 961-keV lines, respectively. Assuming spin $\frac{1}{2}$ for the 668-keV level, its mean life was measured to be $(3.1\pm0.3)10^{-13}$ s. The mean life of the 961-keV level was found to be $(9\pm1.5)10^{-13}$ s, assuming a spin of $\frac{3}{2}$.

1. Introduction

The 668-keV and 961-keV excited states in Cu^{63} have been previously studied using Coulomb excitation [1]) and resonance fluorescence techniques [2, 3]). The Coulomb excitation study led to partial E2 mean lives of 2.6×10^{-11} s and 4.5×10^{-12} s for the 668-keV and the 961-keV levels, respectively. The resonance scattering studies of Ilakovac [2]) resulted in an estimate of the mean life of the 961-keV level based on a simple picture for the slowing down process in solid and liquid sources. The self absorption measurements of Sunyar *et al.* [3]) who again used liquid and solid sources, led to a lifetime of $(3\pm1.3)10^{-13}$ s for the 668-keV level and an upper limit of 2.7×10^{-12} s for the mean life of the 961-keV state. Thus the only available estimate for the lifetime of the 961-keV was based on experiments involving considerable uncertainties connected with the appreciable slowing down of the recoil nuclei. Since these difficulties can be avoided through the use of a gaseous source, it was decided to reinvestigate the resonance scattering from the two first excited states in Cu^{63} using Zn^{63} vapor sources. The low boiling point of Zn (907° C), and the fact that Zn vapor is essentially monatomic, make Zn^{63} an ideal source material.

The decay scheme of Zn^{63} has been studied recently by Ricci *et al.* [4]). In the assignment of total angular momenta to the excited states of Cu^{63} these authors were guided by the "centre of gravity" theorem proposed by Lawson and

† Present address: SEC Centre d'Études Nucléaires, Saclay, Gif s. Yvette, S. et O., France.

†† Work assisted by the Joint Program of the United States Office of Naval Research and the United States Atomic Energy Commission. Reproduction in whole or in part is permitted for any purpose of the United States Government.

Uretsky [5]). On this basis, the 668-keV level was assigned a spin $\frac{1}{2}$ and the 961-keV level spin $\frac{5}{2}$. To check these assignments it was decided to study also the angular distribution of the resonantly scattered radiation. However, as it so often happens in odd-mass nuclei, this additional information, while narrowing down the possible choices, was not sufficient to determine uniquely the spins of the excited states. A comparison of the resonance scattering effect with liquid and gaseous sources was then carried out in the hope of obtaining supplementary information concerning the spins. Again these studies eliminated certain spin combinations but did not allow an unambiguous assignment.

2. Preparation of the Sources

Copper discs 0.015 cm thick were bombarded for one hour with 5.1 MeV protons at a current of 10μA in the Bartol-ONR electrostatic generator. The Zn^{63} so formed was liberated from the copper by heating, under vacuum, the bombarded portion of the copper and approximately 400 μg of Zn carrier beyond the melting point of the copper. The zinc was then distilled into a quartz ampoule of 1.5 ml volume which was subsequently sealed off. In general, 80—90 % of the Zn^{63} activity was distilled by this method into the ampoule, and the source strengths obtained were about 4—6 mc.

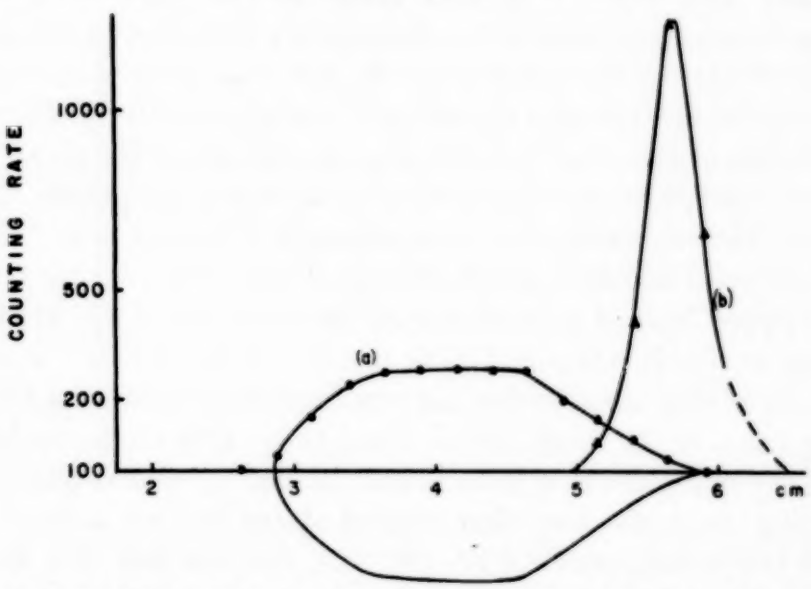

Fig. 1. Distribution of Zn activity in a quartz ampoule. Curve (a) shows the distribution at a temperature of 950° C, while curve (b) is that for the same ampoule after cooling to room temperature.

During the scattering experiments the zinc in the ampoule was maintained in the gaseous phase by keeping the ampoule at a temperature of 950° C. By measuring the distribution of the zinc activity in the ampoule it was ascertained that the radioactive zinc was indeed in the gaseous phase. This

distribution was measured by moving the oven containing the ampoule in front of a narrow lead slit, behind which a scintillation detector was used to detect the zinc radiation. A typical distribution is given in fig. 1 for a source heated to 950° C and for the same source after cooling. The end of the ampoule connected to the supporting rod was the first to cool, and practically all the activity which was previously in the gas condensed there.

Liquid sources were prepared by dissolving the upper layers of the bombarded copper discs in concentrated nitric acid. No attempt was made to separate the zinc salt from the copper one and the acid solution, diluted by the water used for rinsing the surface of the copper, was used in the scattering experiments; practically all the activity was thus transferred into 1.5 ml of solution.

3. Experimental Arrangement

The experimental arrangement used for the measurement of the level lifetimes and the angular distribution of the resonantly scattered radiations is shown in fig. 2. The quartz oven containing the source ampoule was surrounded by an

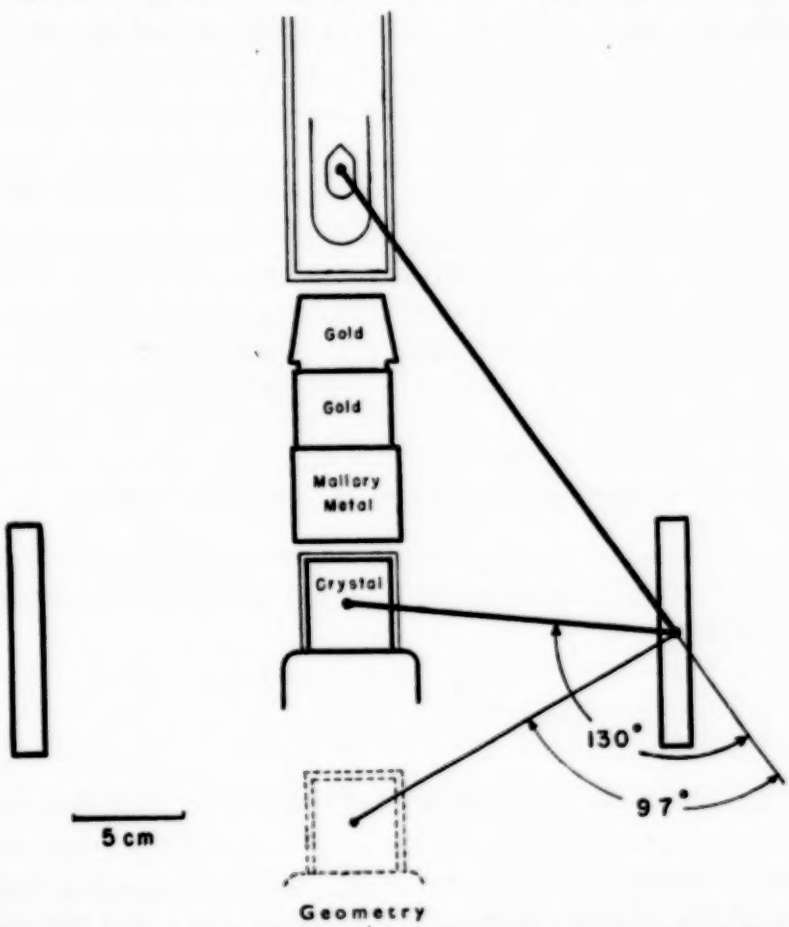

Fig. 2. Experimental arrangement for the Cu^{63} scattering experiment. The relative position of the detector for a mean scattering angle of 97° is shown by the dashed drawing of the detector, while the full lined drawing is that for the 130° scattering.

aluminium cylinder to prevent the passage of positrons to the scatterer; this reduced the intensity of the annihilation radiation seen by the detector by about one order of magnitude. The detector was a 3.8 cm by 3.8 cm NaI(Tl) scintillation crystal mounted on an RCA 6342 photomultiplier. The output of the detector was fed to an Atomic-Instrument-Company, Model-520, 20-channel pulse-height analyser. An attenuator was placed between the source and the detector to prevent the direct passage of radiations to the detector. This attenuator consisted of a cylinder of W-Cu alloy (Mallory metal) and a cone of gold.

The scatterers were cylindrical rings of copper and zinc metal with an inner diameter of 28 cm, a wall thickness of 1.4 cm, and a height of 10 cm. To realize different scattering angles the detector was moved along its axis with respect to the fixed relative position of the source and scatterer, thus insuring the same geometry for the incoming exciting radiation. As indicated in the figure, the scattering angles used were 97° and 130°. Copper and zinc scatterers were alternately used so that the net resonance effect could be obtained by a subtraction of the counting rates in the two cases. It was found that the counting rate with the zinc scatterer was essentially equal to the background counting rate above an energy of 750-keV. In the region of the 668-keV line, the counting rate was a little higher than the background but by no more than about 2 % of the resonance effect.

For additional angular distribution measurements with the 668-keV resonance radiation a different geometry was used in which the scatterers were conically shaped so that the scattering angle was practically constant for all the elements of the scatterer. Different scattering angles were realized by using scatterers of different size. In fitting the angular distribution data it was assumed that the distribution had the form $W(\theta) = 1+A_2 P_2(\cos\theta)$.

4. Experimental Results and Discussion

The lifetime of a state decaying only by gamma emission to the ground state is related to the average cross section σ_{av} for resonance fluorescence by the following relation [6]):

$$\tau_{(sec)} = \frac{g_2}{g_1} \frac{2.53}{E_{res}^2 \sigma_{av}} \frac{N(E_{res})}{N},$$

where g_1 and g_2 are the statistical weights of the ground state and excited state, respectively; E_{res} is the resonance energy in eV, σ_{av} is the average cross section for scattering measured in barns, and $N(E_{res})/N$ is the fraction per eV of the line intensity at the resonance energy. The value of σ_{av} was determined from the data by using the calculated value for the solid angle source-scatterer, and the experimentally determined solid angle scatterer-detector. In the computa-

tion of σ_{av} the electronic and resonance attenuations of the resonant γ-rays by the scatterer and oven material were taken into account. The results of the angular distribution measurements were also used in the analysis. The value of $N(E_{res})/N$ was calculated by using the decay scheme of Ricci *et al.* [4]). Fig. 3

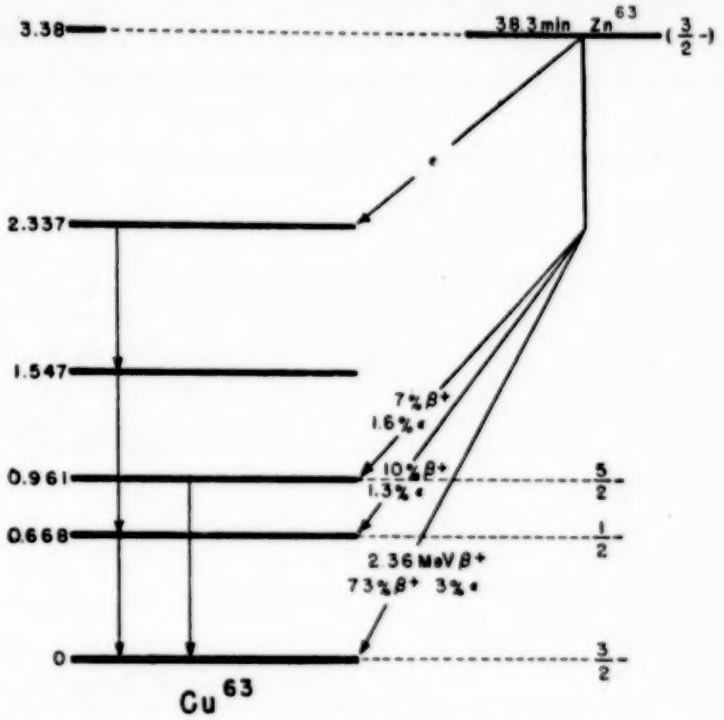

Fig. 3. Partial decay scheme of Zn^{63}. Only those features relevant to the resonance scattering experiment are reproduced.

reproduces those features of this scheme which are relevant to the resonance scattering experiments. With these intensities and branching ratios the line shapes of the 668-keV and 961-keV gamma rays were calculated and are shown in fig. 4. In this calculation no angular correlations were assumed between the

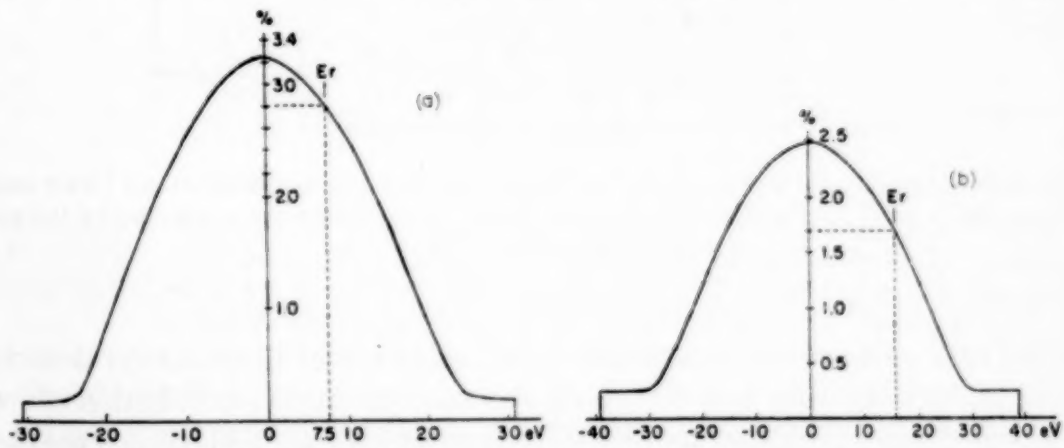

Fig. 4. Line shapes of (a) the 668-keV gamma ray and (b) 961-keV gamma ray for a gaseous source (no collisions). Both shapes were calculated on the basis of the decay scheme of fig. 3. The dashed vertical line indicates the position of the absorption line.

aluminium cylinder to prevent the passage of positrons to the scatterer; this reduced the intensity of the annihilation radiation seen by the detector by about one order of magnitude. The detector was a 3.8 cm by 3.8 cm NaI(Tl) scintillation crystal mounted on an RCA 6342 photomultiplier. The output of the detector was fed to an Atomic-Instrument-Company, Model-520, 20-channel pulse-height analyser. An attenuator was placed between the source and the detector to prevent the direct passage of radiations to the detector. This attenuator consisted of a cylinder of W-Cu alloy (Mallory metal) and a cone of gold.

The scatterers were cylindrical rings of copper and zinc metal with an inner diameter of 28 cm, a wall thickness of 1.4 cm, and a height of 10 cm. To realize different scattering angles the detector was moved along its axis with respect to the fixed relative position of the source and scatterer, thus insuring the same geometry for the incoming exciting radiation. As indicated in the figure, the scattering angles used were 97° and 130°. Copper and zinc scatterers were alternately used so that the net resonance effect could be obtained by a subtraction of the counting rates in the two cases. It was found that the counting rate with the zinc scatterer was essentially equal to the background counting rate above an energy of 750-keV. In the region of the 668-keV line, the counting rate was a little higher than the background but by no more than about 2 % of the resonance effect.

For additional angular distribution measurements with the 668-keV resonance radiation a different geometry was used in which the scatterers were conically shaped so that the scattering angle was practically constant for all the elements of the scatterer. Different scattering angles were realized by using scatterers of different size. In fitting the angular distribution data it was assumed that the distribution had the form $W(\theta) = 1+A_2 P_2(\cos\theta)$.

4. Experimental Results and Discussion

The lifetime of a state decaying only by gamma emission to the ground state is related to the average cross section σ_{av} for resonance fluorescence by the following relation [6]):

$$\tau_{(\mathrm{sec})} = \frac{g_2}{g_1}\,\frac{2.53}{E_{\mathrm{res}}^2\,\sigma_{av}}\,\frac{N(E_{\mathrm{res}})}{N},$$

where g_1 and g_2 are the statistical weights of the ground state and excited state, respectively; E_{res} is the resonance energy in eV, σ_{av} is the average cross section for scattering measured in barns, and $N(E_{\mathrm{res}})/N$ is the fraction per eV of the line intensity at the resonance energy. The value of σ_{av} was determined from the data by using the calculated value for the solid angle source-scatterer, and the experimentally determined solid angle scatterer-detector. In the computa-

tion of σ_{av} the electronic and resonance attenuations of the resonant γ-rays by the scatterer and oven material were taken into account. The results of the angular distribution measurements were also used in the analysis. The value of $N(E_{res})/N$ was calculated by using the decay scheme of Ricci *et al.* [4]). Fig. 3

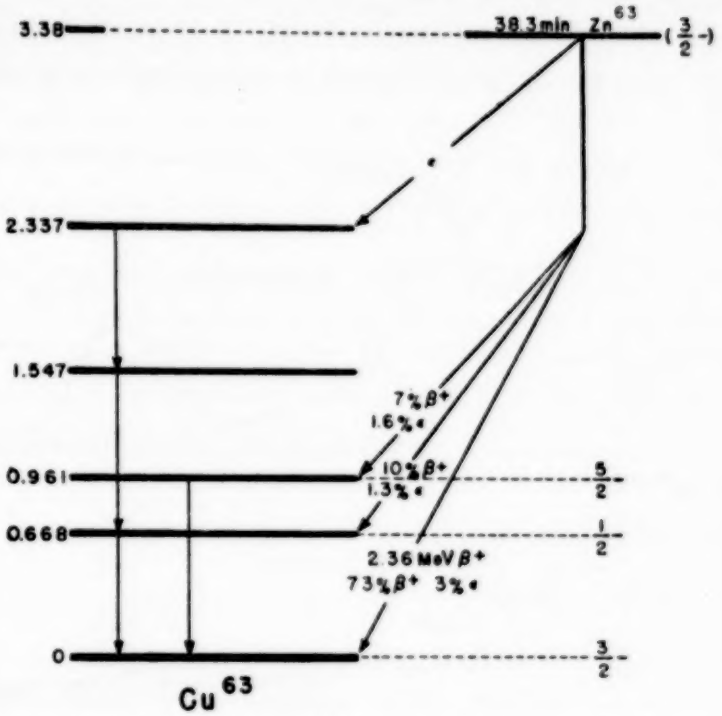

Fig. 3. Partial decay scheme of Zn^{63}. Only those features relevant to the resonance scattering experiment are reproduced.

reproduces those features of this scheme which are relevant to the resonance scattering experiments. With these intensities and branching ratios the line shapes of the 668-keV and 961-keV gamma rays were calculated and are shown in fig. 4. In this calculation no angular correlations were assumed between the

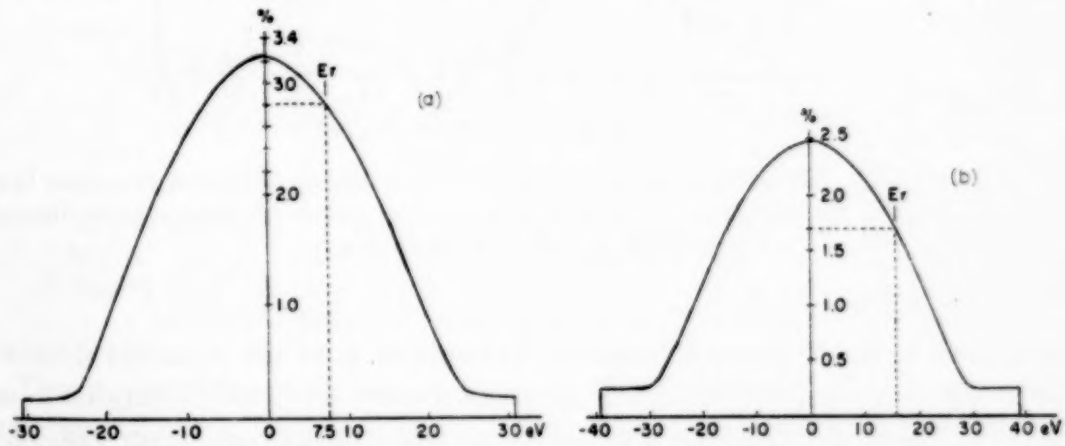

Fig. 4. Line shapes of (a) the 668-keV gamma ray and (b) 961-keV gamma ray for a gaseous source (no collisions). Both shapes were calculated on the basis of the decay scheme of fig. 3. The dashed vertical line indicates the position of the absorption line.

various radiations. The values obtained for $N(E_{res})/N$ were 2.80 and 1.68 % per eV for the 668-keV and 961-keV gamma rays, respectively. The 961-keV level is populated by only one β group; its line shape is therefore only sensitive to the ratio K capture/β^+ and very slightly so (a change of 20 % in this ratio produces a change of 1 % in $N(E_{res})/N$).

The data of a typical run are shown in fig. 5. Curve (a) is the direct beam spectrum which was taken at a distance of about 150 cm in the same plane

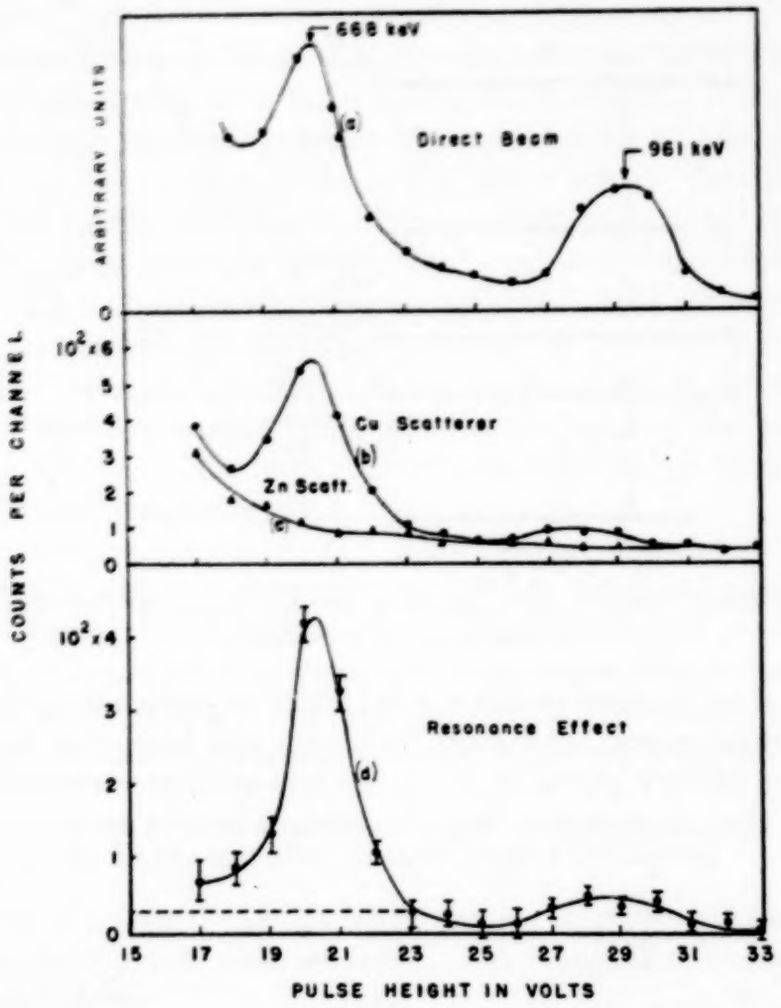

Fig. 5. Pulse height distributions of the direct beam and the scattered radiations. (a) Direct beam from a Zn^{65} source, (b) Cu scatterer, (c) Zn scatterer, (d) resonance effect obtained by the subtractions of curve (c) from (b).

which was used for the experimental determination of the scatterer-detector solid angle. Curves (b) and (c) are the spectra of the scattered radiations showing well defined peaks in the case of the copper scatterer and no such peaks in the case of the zinc comparison scatterer. Curve (d) of this figure is the net resonance effect obtained by the subtraction of curve (b) from curve (c).

A total of eight runs was taken at two scattering angles and the results are tabulated in table 1.

TABLE 1

Experimental data and the lifetimes of the 668-keV and 961-keV levels

E_{res}(eV)	g_2/g_1	A_2	σ_{av}(barns)	$\frac{N(E_{res})}{N}$	τ (sec)
6.68×10^5	$\frac{1}{2}$	-0.03 ± 0.07	$0.63\ \pm0.06$	$2.8\ \times10^{-2}$	$(3.1\pm0.3)10^{-13}$
9.61×10^5	$\frac{3}{2}$	$0.8\ \pm0.2$	0.077 ± 0.013	1.68×10^{-2}	$(9\ \pm1.5)10^{-13}$

An additional run was performed using a liquid source. This was done at one angle and a comparison was made with the gaseous source runs at the same angle. The reduction in the yield of the 668-keV resonance radiation when going from the gaseous to the liquid source was 1.5 ± 0.3, whereas the corresponding reduction for the 961-keV radiation was 5 ± 1.

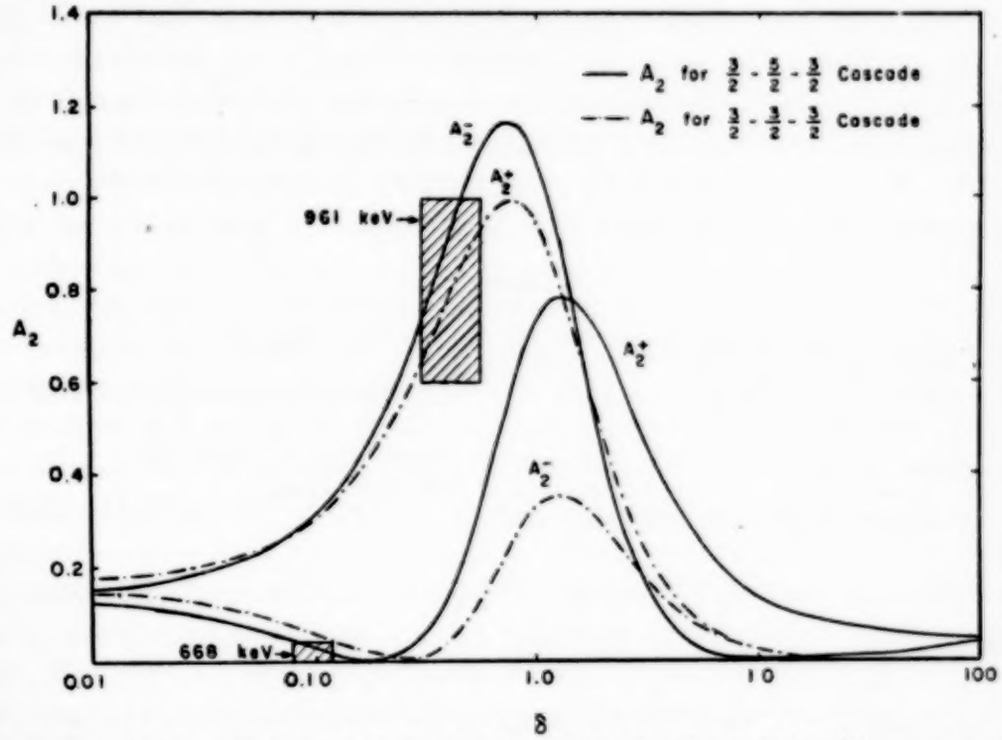

Fig. 6. Plot of the coefficient A_2 of the angular distribution $1+A_2P_2(\cos\theta)$ as a function of $\delta(\delta^2 = \text{E2/M1})$. Full curves: the A_2 coefficient for the cascade $\frac{3}{2}-\frac{5}{2}-\frac{3}{2}$ for both positive and negative δ. Dashed curve: the A_2 coefficient for the cascade $\frac{3}{2}-\frac{3}{2}-\frac{3}{2}$ for both signs of δ. The shaded rectangles indicate the range of the present experimental points.

The A_2 coefficients for the cascades $\frac{3}{2}-\frac{3}{2}-\frac{3}{2}$ and $\frac{3}{2}-\frac{5}{2}-\frac{3}{2}$, calculated as a function of the mixing amplitude δ (where $\delta^2 = \text{E2/M1}$), are given in fig. 6. The experimental results, with errors, are shown in this figure by the shaded rectangles, and it is seen that, experimentally, the possibility of $\frac{3}{2}$ spin assign-

ment to the 961-keV level cannot be definitely ruled out, nor can such a possibility be precluded for the 668-keV level, in spite of the isotropic distribution observed for the radiation scattered from this level. The value of δ for each of these lines was calculated by using our results for the level lifetimes together with the partial E2 lifetimes obtained from Coulomb excitation [1]). The angular distribution results limit the spin values of the 961-keV level to $\frac{3}{2}$ or $\frac{5}{2}$ and those of the 668-keV level to $\frac{1}{2}-\frac{3}{2}$ or $\frac{5}{2}$.

The reduction of the resonance effect in the liquid source, as mentioned above, was 1.5 ± 0.3 for the 668 resonance radiation and 5 ± 1 for the 961-keV one. Using the argument of Ilakovac [2]) that the yield reduction is $1-e^{-t/\tau}$, where t is a characteristic time for the liquid (connected with the frequency of collisions in the liquid) and τ the mean lifetime of the level, one would get for the ratio of the yield reductions (assuming the same t for both lines) a value of $[1-\exp(-t/\tau_{961})]/[1-\exp(-t/\tau_{668})] \approx \tau_{668}/\tau_{961} = \frac{1}{3}$ (if $t \ll \tau$). The experimental ratio is just about equal to this value (1.5/5). One should, however, bear in mind the fact that the position of the 961-keV absorption line is such as to make $N(E_{res})/N$ more sensitive to the slowing down process. This would mean a smaller value of t. The results still indicate that $\tau_{961} > \tau_{668}$ and this precludes the $\frac{5}{2}$ spin assignment to the 668-keV level. It is very likely that the spin of this level is indeed $\frac{1}{2}$. This would leave the possibilities of $\frac{3}{2}$ and $\frac{5}{2}$ for the spin of the 961-keV level. At this stage the $\frac{3}{2}$ assignment is the more likely one.

References

1) G. M. Temmer and N. P. Heydenburg, Phys. Rev. **104** (1956) 967
2) K. Ilakovac, Proc. Phys. Soc. A **67** (1954) 601
3) A. Sunyar, J. B. Cumming, L. Grodzins, N. T. Porile and A. Schwarzchild, Bull. Am. Phys. Soc **4** (1959) 57
4) R. A. Ricci, R. K. Girgis and R. Van Lieshout, Nuovo Cim. **11** (1959) 156
5) R. D. Lawson and J. L. Uretsky, Phys. Rev. **108** (1957) 1300
6) F. R. Metzger, Phys. Rev. **101** (1956) 286

3.A

Nuclear Physics **22** (1961) 513—523; ©*North-Holland Publishing Co., Amsterdam*

Not to be reproduced by photoprint or microfilm without written permission from the publisher

GAMMA-RAY SPECTRA FROM CAPTURE OF FAST NEUTRONS

I. BERGQVIST and N. STARFELT

Research Institute of National Defence, Stockholm 80, *Sweden*

Received 19 September 1960

Abstract: A method to study the spectrum of the gamma rays emitted in radiative capture of fast neutrons has been developed. A sodium iodide scintillation spectrometer was employed and the use of time-of-flight techniques made it possible to reduce the background of scattered neutrons sufficiently. Nickel, silver and gold were studied with 0.1 MeV neutrons and a comparison with the gamma-ray spectra from the capture of thermal neutrons was made. The agreement was good for nickel and silver. In the case of gold the relative intensity of the high-energy gamma rays was lower for 0.1 MeV neutrons than for thermal neutrons.

1. Introduction

The spectrum of the gamma rays emitted when thermal neutrons are captured in nuclei has been studied in considerable detail for most elements [1, 2]). Recently some measurements of resonance capture gamma-ray spectra in heavy nuclei have also been reported [3, 10]) but no experiments on the gamma rays from the capture of fast neutrons have been published. The experiments with resonance neutrons show that the gamma-ray spectrum varies from resonance to resonance. It is especially conspicuous for the high-energy gamma rays. This indicates that further information could be obtained by the extension of the experiments to higher energy resonances in light nuclei and the nuclei around lead and to energies above the resonance region in other nuclei. For thermal neutrons only s-wave capture is possible but with higher neutron energies larger neutron angular momenta will contribute to the capture process.

According to Lane and Lynn, and Bockelman [11, 12]) thermal neutrons can be captured either by compound nucleus formation or by a direct capture mechanism. The spectrum of the gamma rays emitted in direct capture should deviate from that of the compound nucleus process. The direct process is expected to be able to compete quantitatively with the resonance process only in light nuclei and the nuclei just below lead. In most of these nuclei 0.1 MeV neutrons should, however, be captured exclusively through compound nucleus formation. Comparison between the gamma-ray spectra obtained with thermal neutrons and those of 0.1 MeV neutrons would thus offer a possibility of a quantitative study of the direct capture process. Because of the low cross section for capture of fast neutrons all experiments on capture gamma rays will lead to considerable difficulties. The best available gamma-ray spectometer for this experiment

is the NaI(Tl) scintillation spectrometer. Its high detection efficiency is required to make the experiment possible. However, the relatively high cross section for capture of fast neutrons in iodine imposes a great background problem. It appears to be necessary to employ a pulsed neutron source and to use time-of-flight discrimination between spectrometer pulses caused by capture gamma rays from the sample and pulses due to neutrons coming directly from the source or scattered in the sample.

To elaborate and check the experimental method three elements were studied, nickel, silver and gold. Nickel has a fairly low cross section but practically only high-energy gamma rays are emitted. With some refinements of the experimental technique it should be possible to study separate resonances in nickel. Silver has a large cross section and a continuous gamma-ray spectrum. No direct capture of thermal neutrons is expected. Gold on the other hand is a nucleus with an appreciable amount of high-energy gamma rays in the thermal neutron capture gamma-ray spectrum, an effect which may be due to direct capture.

2. Experimental Arrangement and Measurements

A plan of the experimental arrangement for the neutron capture gamma-ray experiment is shown in fig. 1. The analysed proton beam from the van de Graaff generator at the University of Lund is swept over a narrow slit (B) by means of

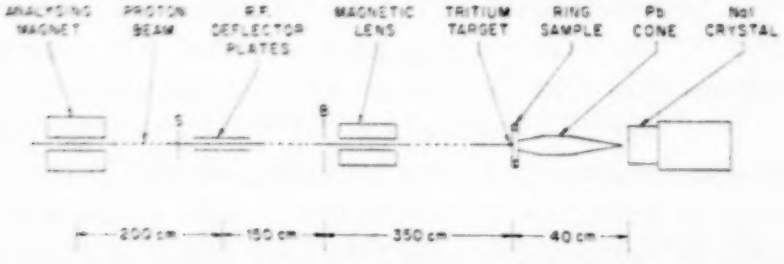

Fig. 1. Experimental arrangement for the measurement of gamma-ray spectra from radiative capture of fast neutrons.

a R.F. voltage on two 20 cm long deflector plates giving rise to proton pulses of 10 mμs duration at a frequency of 2.5 MHz. The chopped beam is focused by magnetic quadrupole lenses on an adsorbed tritium target mounted at the centre of a cubic room with five meter side. An average proton current on the target of 0.6μA is obtained. Neutrons produced in the $H^3(p, n)He^3$ reaction at 75° to the proton beam enter a ring sample of the element being studied. With a ring of an outer diameter of 14 cm and a cross sectional area of 2 by 2 cm the energy of the neutrons is 125 ± 35 keV when the proton energy is maintained at 1300 keV. The gamma-ray spectrometer consists of a NaI(Tl) crystal of diameter 12.7 cm and length 10.2 cm mounted at a distance of 40 cm from the neutron source. The direct neutrons from the tritium source are attenuated in the direction of the crystal by a lead cone.

A block diagram of the electronic equipment is shown in fig. 2. By means of a pulse shaping unit a 20 mμs pulse is obtained once every cycle from the 1.25 MHz sine-wave oscillator supplying the RF voltage to the deflector plates. This

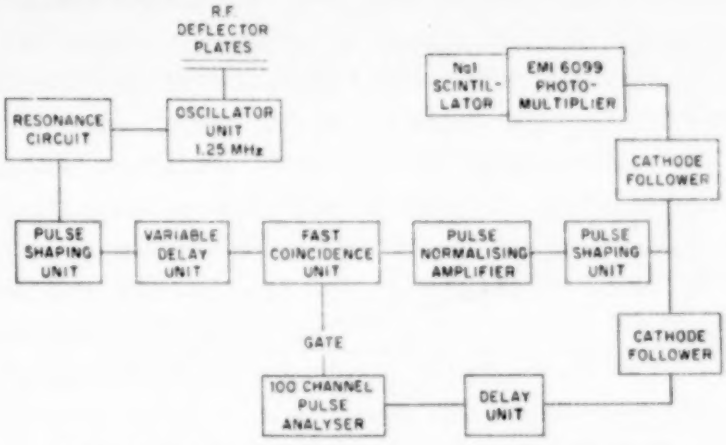

Fig. 2. Block diagram of the electronic equipment.

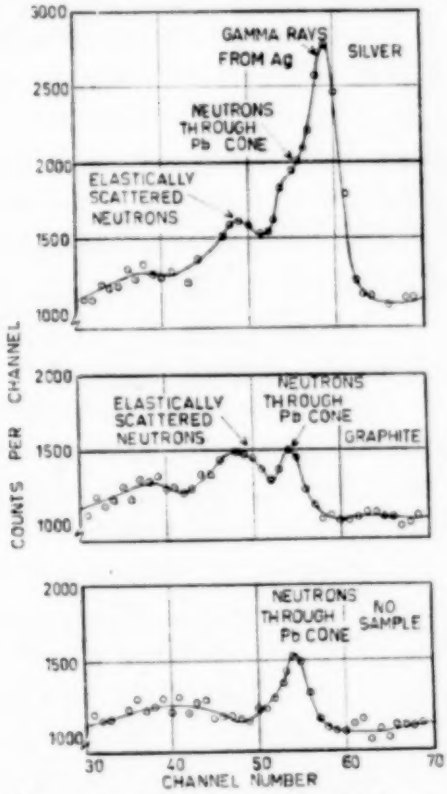

Fig. 3. Time spectra obtained from the NaI crystal using 10 mμs pulses of 100 keV neutrons with a silver sample, with a graphite sample, and without sample. Each channel represents 8 mμs. Time increases from right to left.

pulse is fed into one of the inputs of a fast coincidence circuit. To compensate for the flight times of the protons from the deflector plates to the tritium target and of the 0.1 MeV neutrons from the neutron source to the sample ring this pulse can be delayed up to 500 mμs. Before entering the other input of the coinci-

dence circuit the pulses from the NaI(Tl) crystal are amplified in a pulse normalizing amplifier [13]) yielding a standard 20 mμs output pulse which is inde-

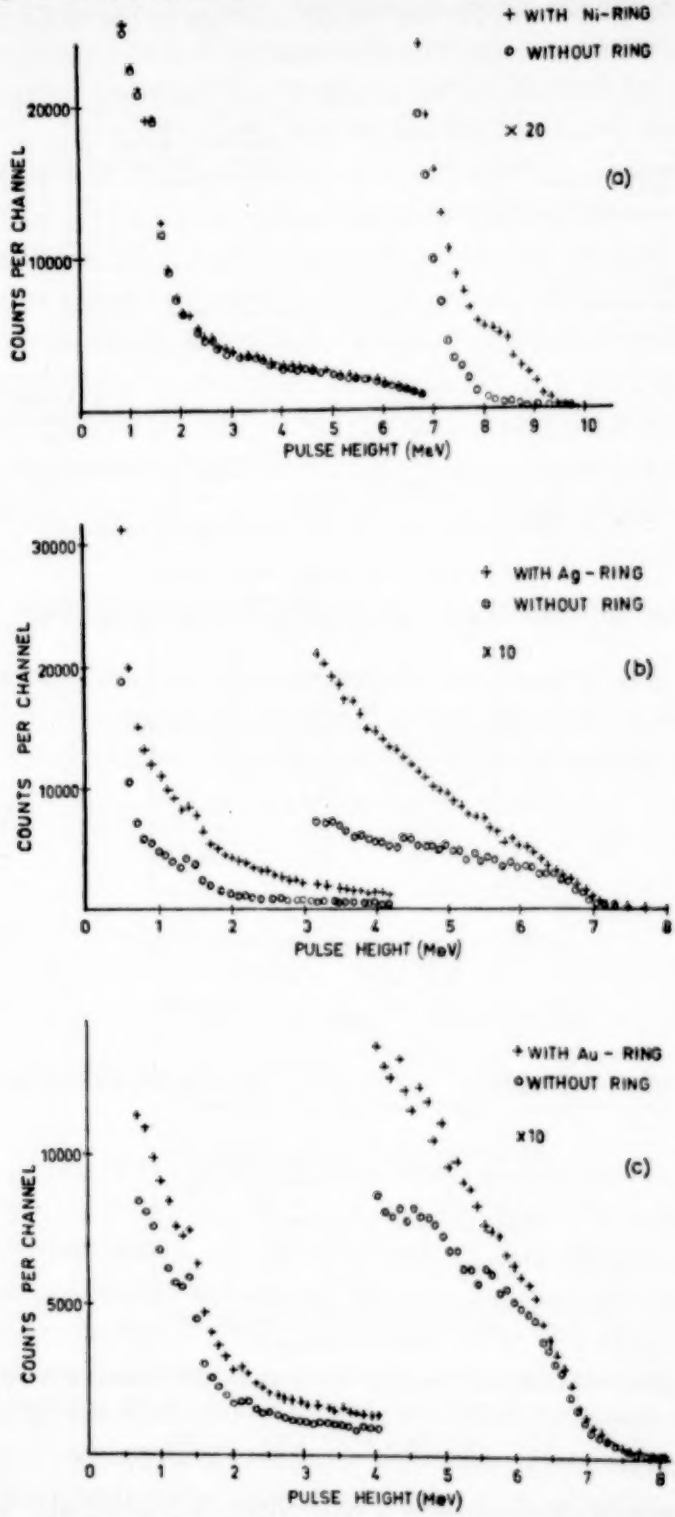

Fig. 4. Pulse spectra obtained from the NaI spectrometer with sample in (crosses) and without sample (circles).

pendent of the size of the input pulse within wide limits. The pulse from the

NaI(Tl) crystal is also brought to a 100-channel pulse-height analyser the input of which is gated by the output pulse of the fast coincidence circuit. By selecting the proper delay of the pulse originating from the RF oscillator the pulse analyser can be made to register the spectrum of capture gamma rays from the sample. With other delays the spectrum caused by neutrons scattered from the sample into the crystal, or that caused by neutrons travelling directly from the neutron source to the crystal can be obtained. The intensity of the neutrons from the source is monitored by means of a long counter.

The time spectrum of the events in the NaI(Tl) crystal can also be studied by means of a time-to-pulse-height converter used together with the 100-channel pulse analyser. Fig. 3 shows some time spectra registered in this way. In fig. 3a a silver sample was used and the spectrum is dominated by the capture gamma rays. By comparison with the run without sample the second bump in fig. 3a can be identified as due to neutrons passing directly from the source through the lead cone and by comparison with the run with a graphite sample having negligible capture cross section it is evident that the third peak is caused by neutrons elastically scattered by the sample. From this fig. it is obvious that the gamma rays emitted in the capture of 0.1 MeV neutrons in silver can be registered at a fairly favourable signal to background ratio. In fig. 3 all gamma rays with energies above about 1.5 MeV were registered. If the silver sample under these circumstances is replaced by a nickel sample no capture gamma-ray peak in the time spectrum is observed. To be able to detect the nickel gamma rays the bias has to be set very high and only photons above about 6 MeV should be registered in this case.

Fig. 4 shows the pulse spectra obtained with and without samples of nickel, silver and gold. The silver spectrum is dominating over the background at all energies while the nickel gamma rays are detectable only above 6 MeV.

To make absolute determinations of capture cross sections possible the long counter was calibrated by comparison with a methane filled proton recoil proportional counter [14, 15]) placed in the neutron beam at 0° to the proton beam. Knowing the gas pressure and the size of the sensitive volume of the counter the flux of neutrons at 0° can be obtained and from the known angular distributions [16]) of the $H^3(p, n)He^3$ neutrons the flux at the sample position corresponding to a certain long counter reading is obtained.

3. Corrections

The number of pulses $P(\varepsilon)$ per unit pulse height interval at pulse height ε obtained from the NaI(Tl) spectrometer when one neutron per unit solid angle is emitted from the neutron source in the direction of the sample is given by

$$P(\varepsilon) = \sigma_c G \int_0^{k_{max}} N(k)H(k)K(k, \varepsilon)dk. \quad (1)$$

Here, σ_c is the neutron capture cross section of the sample, k the gamma-ray energy and $N(k)$ the number of photons emitted per unit energy interval at the energy k per neutron captured. G is a factor containing the geometry of the arrangement and the attenuation and scattering of the neutrons in the sample. $H(k)$ takes into account the attenuation of the gamma rays in the sample and in the leadcone. $K(k, \varepsilon)$ is the response function of the NaI spectrometer. With $P(\varepsilon)$ and $K(k, \varepsilon)$ experimentally determined eq. (1) can be solved for $\sigma_c GH(k)N(k)$ using the matrix method described earlier [17]). G was determined through a Monte Carlo calculation on an automatic computer. The attenuation of the gamma rays in the lead cone was determined experimentally at several gamma-ray energies. Knowing $GH(k)$ the value of $\sigma_c N(k)$ can be obtained. Using the relation

$$\int_0^{k_{max}} kN(k)\mathrm{d}k = B + E_n, \tag{2}$$

the magnitude of σ_c can also be determined from this experiment. Here B is the binding energy and E_n the kinetic energy of the captured neutron.

The response function $K(k, \varepsilon)$ was determined experimentally in the actual geometry using the 1.28 and 2.62 MeV gamma-ray lines of Na^{22} and RdTh and the 4.45 MeV gamma rays from the reaction $B^{11}(p, \gamma)C^{12}$ and the 6.1 MeV gamma rays from $F^{19}(p, \alpha\gamma)O^{16}$. To obtain $K(k, \varepsilon)$ at other photon energies interpolation between the measured $K(k, \varepsilon)$ was performed.

The statistical errors ΔP in the measured pulse distributions $P(\varepsilon)$ give rise to corresponding errors ΔN in the resulting pulse spectra $N(k)$. The magnitude of ΔN can be calculated when the inverse matrix is known. It is obvious that ΔN depends strongly on the interval width used in the matrix. Narrow intervals result in a large magnification of the errors ΔP. To obtain spectra $N(k)$ of sufficient accuracy it is therefore necessary to use fairly large energy intervals. 0.4 MeV and 0.8 MeV intervals have been tried. With the present experimental accuracy it was found necessary to use the 0.8 MeV intervals.

4. Results and Discussion

The corrected gamma-ray spectra obtained when 0.1 MeV neutrons are captured in nickel, silver and gold are given in fig. 5. For comparison the spectra of thermal neutron capture gamma rays as given by Groshev *et al.* [2]) are also shown in fig. 5. These spectra were obtained with a magnetic Compton spectrometer giving much better energy resolution than the NaI spectrometer of the present investigation. To make a comparison possible the peaks in the Compton spectrometer spectra were smeared out to the resolution of the scintillation spectrometer.

In some cases, e.g. the nickel spectrum, the multiplication with the inverted response function matrix leads to fairly inaccurate results. Instead the spectrum

for capture of thermal neutrons is multiplied with the response function matrix and the result thus obtained compared with the measured pulse distribution (fig. 6).

One reason why the shape of the gamma-ray spectrum from capture of 0.1 MeV neutrons could differ from that of thermal neutrons is that for 0.1 MeV

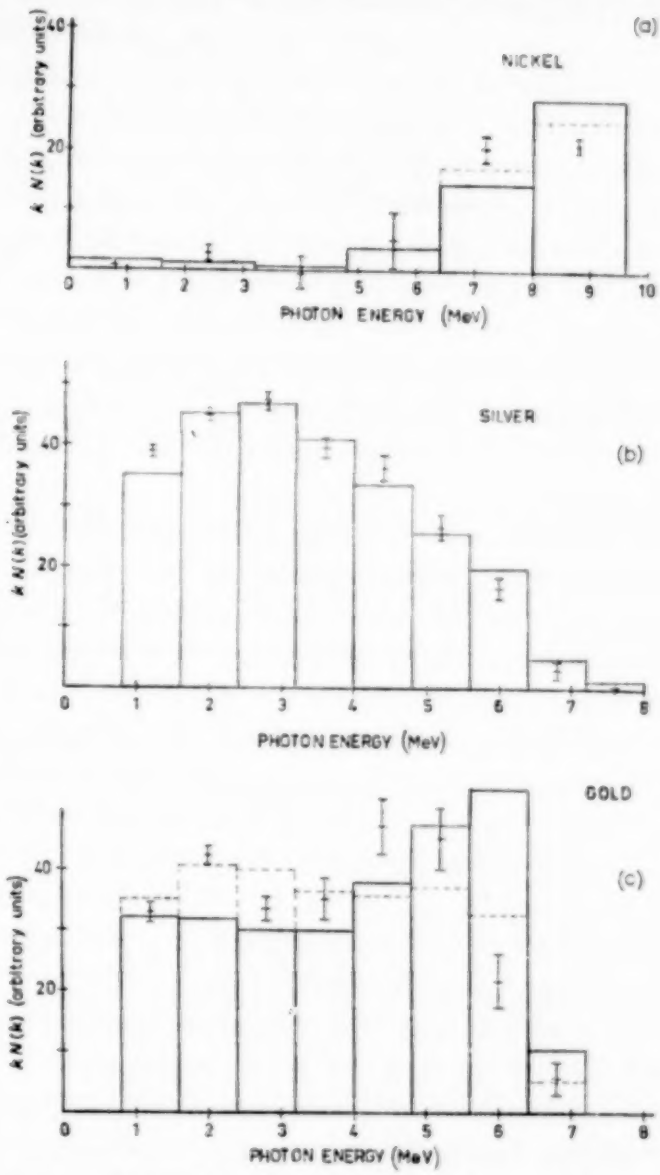

Fig. 5. Fully corrected experimental gamma-ray spectra (crosses). The histograms show the gamma-ray spectra from capture of thermal neutrons as given in ref. [2]). The dashed histogram in fig. 5a is corrected for the difference in cross section between Ni^{58} and Ni^{60} (see text) and that in fig. 5c represents a thermal capture gamma ray spectrum made up of 50 % silver and 50 % gold. The areas under the curves are normalized. The ordinate gives the gamma-ray spectrum $N(k)$ multiplied with the gamma-ray energy k. The statistical errors are shown.

neutrons p-wave capture is possible and thus states of different parity and spin in the compound nucleus are reached. This may of course change the spectrum

greatly especially in light nuclei where transitions to the ground state and a few other low-lying levels dominate. Another possibility is that the partial

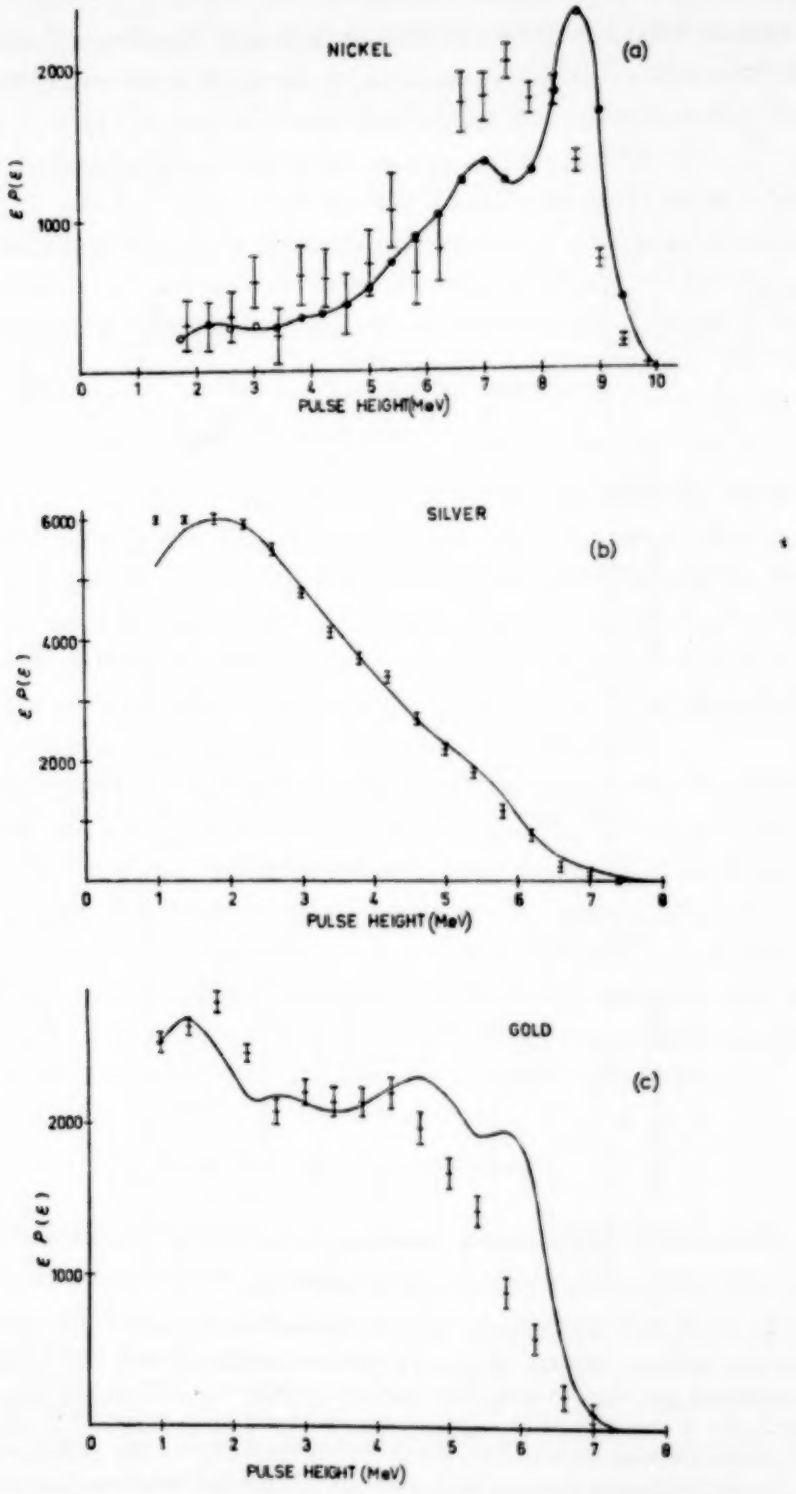

Fig. 6. Uncorrected experimental pulse spectra (crosses) and the gamma-ray spectra (solid line) from capture of thermal neutrons [2]) multiplied with the response function matrix of the NaI spectrometer. The curves are normalized. The ordinate gives the pulse spectrum $P(\varepsilon)$ multiplied with the pulse height ε. The experimental statistical errors are shown.

gamma-ray widths vary between resonances of equal spin and parity as indicated by other measurements [9]). For thermal neutrons only one or two resonances contribute appreciably to the capture cross section but for 0.1 MeV neutrons the gamma-ray spectra represent an average over many resonances. Furthermore, as mentioned above, strong high-energy gamma rays in the thermal neutron capture spectra may be due to direct interaction, a process that should be negligible for 0.1 MeV neutrons in most nuclei.

In the case of nickel the agreement between the gamma-ray spectra obtained with thermal and 0.1 MeV neutrons, respectively, is not very good. One possible explanation is that the relative contributions of the nickel isotopes may be different in the two cases. For thermal neutrons the cross section of Ni^{58} is considerably larger than that of Ni^{60}. There is no reason to believe that this difference should persist at neutron energies around 0.1 MeV. Then it is more reasonable to compare the present experimental result with a spectrum of thermal neutron capture gamma rays where the different nickel isotopes contribute in proportion to their isotopic abundances. Such a spectrum is shown as a dashed histogram in fig. 6a. This spectrum is in better agreement with the measurements.

The errors in the 0.1 MeV spectrum shown in the figs. are due only to counting statistics. The uncertainty in the energy scale is about 2 %. Because of the large background (fig. 4) a small drift in the energy calibration between the measurements with nickel sample and those without sample may result in errors in the points below about 7 MeV which are larger than those shown in fig. 6. It is then of interest to observe that the total capture cross section obtained in the present investigation is somewhat larger than that obtained by Diven [18]) at 175 keV. This confirms that the real number of low-energy gamma rays cannot be much larger than that obtained in this experiment.

All the resonances in both Ni^{59} and Ni^{61} which have been observed erarlier in the energy region covered by this experiment are s-wave resonances [19]). Thus if there are no special selection rules in thermal neutron capture the two gamma-ray spectra should be similar as obtained in this experiment. On the other hand, if the high-energy gamma rays observed in the capture of thermal neutrons are due to direct capture and the compound nucleus process dominates at 0.1 MeV the two spectra should differ in shape; the high-energy gamma rays should not dominate the spectrum obtained with 0.1 MeV neutrons. However in nickel the direct process may be of importance even at 0.1 MeV.

For silver there is good agreement between the two spectra. This is expected as there are no strong high-energy gamma rays and the direct capture should not be important in this part of the periodic system.

In gold there is an obvious decrease in the intensity of the high-energy gamma rays when going from thermal to 0.1 MeV neutrons. This is in qualitative agreement with the direct capture theory. However, in this case p-wave capture

gives a considerable contribution to the capture cross section at 0.1 MeV. It would therefore be of interest to compare the present experiment with a spectrum consisting of equal parts of the capture gamma ray spectra for thermal neutrons in silver and gold, respectively. Here the gold spectrum is taken to represent s-wave capture and the silver spectrum p-wave capture where the strong gamma-ray lines obtained from gold with thermal neutrons cannot be emitted as electric dipole radiation. The agreement between this composite spectrum and the experimental spectrum is fair (fig. 5c), indicating that the softening of the gamma-ray spectrum observed when going from thermal to 0.1 MeV neutrons may be due to the p-wave contribution at the higher energy. Thus the experimental result does not require that the gamma-ray spectrum obtained from s-wave capture of 0.1 MeV neutrons is different from that obtained with thermal neutrons if about 50 % of the capture cross section at 0.1 MeV is due to s-wave capture and p-wave neutrons are responsible for the rest of the cross section.

The absolute magnitude of the capture cross section for 125 ± 35 keV neutrons as obtained from this experiment is 0.014 barns for nickel, 0.41 barns for silver and 0.31 barns for gold. The results for silver and gold are in agreement with published data [18, 19]) within the experimental accuracy of ± 15 %.

The results obtained so far have shown the possibility of measuring gamma-ray spectra from capture of fast neutrons using the techniques described here. The background due to neutrons from the target will decrease by using lower sweep frequency. In this way it will very likely be possible to study separate resonances in some light nuclei and also to go to higher neutron energies for nuclei having large capture cross sections, e.g. silver.

The authors wish to express their sincere gratitude to Mr. E. Möller and the Van de Graaff crew at the University of Lund for valuable help in the experiment, to Mr. J. Hansén for constructing the electronic equipment, and to Mr. H. O. Zetterström for many fruitful discussions.

References

1) G. A. Bartholomew and L. A. Higgs, CRGP-784, Chalk River (1958)
2) Groshev, Demidov, Lutsenko and Pelekhov, Atlas of γ-ray spectra from radiative capture of thermal neutrons (Pergamon Press, London 1959)
3) H. H. Landon and E. R. Rae, Phys. Rev. **107** (1957) 1333
4) Fenstermacher, Bennett, Walters, Bockelman and Schultz, Phys. Rev. **107** (1957) 1650
5) Draper, Fenstermacher and Schultz, Phys. Rev. **111** (1958) 906
6) Fenstermacher, Draper and Bockelman, Nuclear Physics **10** (1959) 386
7) Kennett, Bollinger and Carpenter, Phys. Rev. Letters **1** (1958) 76
8) Coté, Kennett and Bollinger, Bull. Am. Phys. Soc. **4** (1959) 472
9) Bird, Moxon and Kirk, Nuclear Physics **13** (1959) 525
10) M. K. Brussel and L. Zimmerman, Bull. Am. Phys. Soc. **4** (1959) 472
11) A. M. Lane and J. E. Lynn, Proc. Sec. U.N. Intern. Conf. Peaceful Uses Atom. En. **15** (1958) 38; Nuclear Physics **17** (1960) 563, 586

12) C. K. Bockelman, Nuclear Physics **13** (1959) 205
13) B. Johansson, Nuclear Instruments **6** (1960) 201
14) Skyrme, Tunnicliffe and Ward, Rev. Sci. Instr. **23** (1952) 204
15) W. D. Allen and A. T. G. Ferguson, Proc. Phys. Soc. A **70** (1957) 639
16) J. E. Brolley and J. L. Fowler, in Fast Neutron Physics, edited by J. B. Marion and J. L. Fowler (Interscience Publishers, New York 1960) Part I, p. 73
17) N. Starfelt and H. W. Koch, Phys. Rev. **102** (1956) 1598
18) B. C. Diven, Proc. Sec. U. N. Intern. Conf. Peacful Uses Atom. En. **15** (1958) 60
19) D. J. Hughes and R. B. Schwartz, BNL-325 (1958)

7.A

Nuclear Physics **22** (1961) 524—528; © *North-Holland Publishing Co., Amsterdam*

Not to be reproduced by photoprint or microfilm without written permission from the publisher

CONNECTION OF SPINOR FIELDS

HIROSHI NAKAMURA

Department of Physics, Tokyo Institute of Technology

and

TOSHIYUKI TOYODA

Department of Physics, Rikkyo University, Tokyo

Received 13 October 1960

Abstract: It is proved that the field introduced by the connection of γ_i-matrices can be eliminated by a suitable gauge transformation except in the case of the gravitational and electromagnetic fields. Discussions are given on related papers.

There have been several attempts [1-4]) to introduce some freedom into the Dirac particle and necessarily some associated fields into the Dirac equation. One of them may be a generalization of the Dirac equation in the general relativistic frame [2,4]), namely, extending the Dirac γ_i-matrices in the Riemannian space,

$$\{\gamma_i, \gamma_j\} \equiv \gamma_i\gamma_j+\gamma_j\gamma_i = 2g_{ij}, \quad (i, j = 1, 2, 3, 4), \tag{1}$$

$$g^{ik}g_{kj} = \delta_j^i, \tag{2}$$

$$\gamma^i = g^{ij}\gamma_j, \tag{3}$$

we postulate the covariant form of the Dirac equation as

$$\gamma^j(\partial_j-\Gamma_j)\psi = 0, \tag{4}$$

where Γ_j may be interpreted as associated fields interacting with ψ.

In the present paper we shall discuss the possibility of introducing the physically significant fields under certain postulates. First, we should like to point out that there are many choices with respect to the form of Γ_j, although Γ_j can be expanded in general in the sedenion. For example, Green [2]) has adopted an affine connection of γ_j as Γ_j, that is,

$$\partial_j\gamma_i = \Gamma_{ij}^k\gamma_k+[\Gamma_j, \gamma_i], \tag{5}$$

where Γ_{ij}^k is Christoffel's symbol made up of g_{ij} and

$$[\Gamma_j, \gamma_i] \equiv \Gamma_j\gamma_i-\gamma_i\Gamma_j. \tag{6}$$

Then Γ_j apparently involves some physically significant fields even if they have to be subjected to the necessary integrability condition for the differential eq. (5) of γ_i,

$$[\gamma_i, R_{jk}] = R_{ijk}^l\gamma_l, \tag{7}$$

where

$$R_{jk} \equiv \partial_k \Gamma_j - \partial_j \Gamma_k + [\Gamma_j, \Gamma_k], \tag{8}$$

$$R^l_{ijk} \equiv \partial_k \Gamma^l_{ij} - \partial_j \Gamma^l_{ik} + \Gamma^h_{ij} \Gamma^l_{hk} - \Gamma^h_{ik} \Gamma^l_{hj}. \tag{9}$$

In fact, Green and Kimura [4]) have tried to interpret the fields involved in Γ_j, assuming the generalized Dirac equation. Due to the necessary condition (7) the mutual relation of these fields seems to be very intricate, so that their interpretation is not so acceptable.

The aim of the present paper is to show that there is no possibility of introducing a significant field except for the gravitational and electromagnetic fields as long as we adopt the Γ_j defined by (5). Although this seems quite obvious, it may be worthwhile to present the straightforward proof, since a generalization of the Dirac equation has been in the limelight introducing as a way some internal freedom into elementary particles.

Let us expand coordinate dependent $'\gamma_i$'s in a linear combination of the constant Dirac matrices $\mathring{\gamma}_j$:

$$'\gamma_i = h_i^{\,p} \mathring{\gamma}_p \quad (p = 1, 2, 3, 4). \tag{10}$$

Then an ordinary derivative of eq. (10) is expressed as

$$\partial'_j \gamma_i = (\partial_j h_i^{\,p}) \mathring{\gamma}_p = (\partial_j h_i^{\,p}) \bar{h}_p^{\,k}\, '\gamma_k \equiv \Lambda^k_{ij}\, '\gamma_k, \tag{11}$$

where $(\bar{h}_p^{\,k})$ is an inverse matrix of $(h_i^{\,p})$, i.e.,

$$h_i^{\,p} \bar{h}_p^{\,k} = \delta_i^{\,k}. \tag{12}$$

The general form of γ_i can be written as

$$\gamma_i = U' \gamma_i U^{-1}, \tag{13}$$

where U is a non-singular matrix [5]). Thus we obtain

$$\partial_j \gamma_i = \Lambda^k_{ij} \gamma_k + [P_j, \gamma_i], \tag{14}$$

where

$$P_j \equiv (\partial_j U) U^{-1}. \tag{15}$$

Rewriting eq. (14) as

$$\partial_j \gamma_i = \Gamma^k_{ij} \gamma_k + (\Lambda^k_{ij} - \Gamma^k_{ij}) \gamma_k + [P_j, \gamma_i], \tag{16}$$

we shall show that the second term is expressed as

$$(\Lambda^k_{ij} - \Gamma^k_{ij}) \gamma_k = [\pi_j, \gamma_i], \tag{17}$$

where

$$\pi_j = D^{rt}_j [\gamma_r, \gamma_t]. \tag{18}$$

It may be sufficient to point out that $\Lambda^k_{ij} - \Gamma^k_{ij}$ is a tensor in our Riemannian

space, though each part is not a tensor separately; and Γ^k_{ij} can be made to vanish by taking a special coordinate system at each point. Thus the generating operator of rotation π_j or D^{rt}_j is uniquely determined.

Then, comparing eqs. (5) and (16), we obtain

$$[\Gamma_j - P_j - \pi_j, \gamma_i] = 0. \tag{19}$$

An explicit form of Γ_j is now readily written down,

$$\Gamma_j = P_j + \pi_j + c_j I, \tag{20}$$

where I is a unit matrix, and c_j is an arbitrary function of x^k.

It is quite obvious that the generalized gauge transformation $\psi = U\psi'$ absorbs P_j. Concerning a physical interpretation of π_j one may consider it in a flat space. In such a case, (h_i^p) is a rotation matrix, taking a rectangular coordinate. Therefore, there must exist a transformation matrix S such that

$$\gamma_i = h_i^p \mathring{\gamma}_p = S \mathring{\gamma}_i S^{-1} \tag{21}$$

and so

$$\pi_j = (\partial_j S) S^{-1}. \tag{22}$$

Since π_j can be absorbed in the transformation when our world is flat, it may be plausible to identify π_j with the gravitational field. †

Hence we have now only $c_j(x)I$ in Γ_j except the gravitational field π_j. As usual in quantum mechanics we postulate the unitary condition, so that Γ_j may be antihermitic as ∂_j. Thus we may rewrite $c_j(x)I$ as

$$c_j(x)I = ieA_j(x)I, \tag{23}$$

where e and $A_j(x)$ are real.

We are informed by Laurent's paper [6]) that a long time ago Bargmann made a similar discussion [7]) to ours (we have not yet seen Bargmann's paper). However, our treatment is based on the equivalence theorem (unitary transformation) which is meaningful only in quantum field theory.

It should be mentioned that when the wave geometry was proposed by Mimura [8]) and developed by his collaborators, detailed mathematical discussions on the spinor-space connection were made, particularly by Morinaga [9]). Although the "complete integrability" seemed to be one of the most important guiding principles, they have tried to introduce different connections from the γ_i-connection or to replace the complete integrability condition by, for example,

† The above discussion would become more lucid in the formal view of γ-matrices if we adopt the 6-dimensional notation of the γ-ring. The most general transformation of γ can be expressed by

$$U = \exp(f^{\lambda\mu} \mathring{\gamma}_\lambda \mathring{\gamma}_\mu + f^\lambda \mathring{\gamma}_\lambda + f) \quad (\lambda, \mu = 1, 2, 3, 4, 5),$$

which corresponds to the separation of Γ_j, $\Gamma_j = P_j + \pi_j + c_j I$. The authors are indebted to Professor K. Morinaga for pointing out this.

the invariance under the transformation

$$\psi' = \gamma_5 \psi, \tag{24}$$

in order to get rid of the gauge-vanishing fields mentioned above.

Nakamura [3]) generalized the Yang-Mills' field [10]) by making use of a physical connection in a mixing space of the Minkowski space and the isospace, that is, the usual 4×4 γ_i-matrices are replaced by 8×8 matrices. His connection has been constructed with group generators which are suitable for the physical interpretation of elementary particles. Evidently his connection is not integrable if one tries to assign it to γ_i-connection.

In advance of Nakamura's paper Ikeda and Miyachi [1]) tried to interpret the Yang-Mills' theory connecting the 3-dimensional Euclidian manifold (Pais' ω-space) [11]) attached at each world point in the Minkowski space. It may be of some interest to see why the b-field introduced in the Minkowski field has some similarity with the gravitational field as described in Ikeda-Miyachi's paper. The reason is quite simple: They abandon the integrability condition for the connection, so that the connection becomes necessarily curved. Therefore, it is likely that one can expect a field similar to the gravitational field.

Very recently Kimura [4]) has developed Green's idea and been led to Heisenberg's non-linear interaction [12]). He adopted essentially the same connection as Green's, i.e., Γ_j defined by (5). Therefore, he is strongly affected with the necessary condition "integrability of (5)". We shall summarize briefly the relevant points in his paper.

Let us define the adjoint spinor

$$\bar{\psi} \equiv \psi^\dagger \eta, \tag{25}$$

where $A^\dagger$ is an hermitian matrix of A and η satisfies the following equations:

$$\eta^+ = \eta, \tag{26}$$

$$\eta\gamma_j + \gamma_j^\dagger \eta = 0, \tag{27}$$

$$\partial_j \eta = [\Gamma_j, \eta]. \tag{28}$$

Then one can construct the Lagrangian

$$\mathscr{L} = \mathscr{L}_0 + \mathscr{L}_1, \tag{29}$$

$$\mathscr{L}_1 = \tfrac{1}{2} i\bar{\psi}\gamma^j(\overrightarrow{\partial_j} - \Gamma_j)\psi - \tfrac{1}{2} i\bar{\psi}(\overleftarrow{\partial_j} + \Gamma_j)\gamma^j\psi, \tag{30}$$

where $\mathscr{L}_0$ is the same as R, and $\mathscr{L}_1$ the same as $L_0 + L_{\text{int}}$ in Kimura's paper, though 6-legs formalism was used there. Concerning 6-legs formalism, Morinaga and Senba [13]) had shown that there is no essential difference between it and the ordinary γ-formalism as far as the connection is concerned.

Making a variation in Γ_j, we obtain the following equation:

$$\frac{\delta \mathscr{L}_0}{\delta \Gamma_j} - i\bar{\psi}\gamma^j\psi = 0. \tag{31}$$

However, eq. (31) is not compatible with eq. (5). $\mathscr{L}$ must be constructed so that the equation derived from its variation with respect to L_j will be compatible with eq. (5).

In this sense the appearance of the second term in eq. (31), which may represent a source of Γ_j-field, seems undesirable. In order to avoid such a dilemma, Kimura tried to add a ψ-dependent $\bar{\Gamma}_j(\bar{\psi}, \psi)$ to Γ_j so as to satisfy the integrability condition.

As is proved in the present paper, $\Gamma_j+\bar{\Gamma}_j$ can be eliminated from the equation of motion with respect to ψ by making use of a suitable gauge transformation except in the case of the gravitational and electromagnetic fields, because $\Gamma_j+\bar{\Gamma}_j$ satisfies the integrability condition. However, in the equation an additional term appears due to the fact that $\bar{\Gamma}_j$ involves $\bar{\psi}$ explicitly. Kimura interpreted this term as Heisenberg's non-linear term. It should be noticed that in Kimura's treatment there also appear only the electromagnetic and gravitational fields, and as the matter source function Heisenberg's non-linear term is automatically introduced. Very recently Laurent has made, independently, discussions based on eq. (31). Although his argument resembles Kimura's in many respects and both give a similar non-linear term, the former seems more natural in our view of the connection described in the present paper.

Further discussions will be seen in our coming paper on an attempt to connect the inner space of elementary particles with the outer space.

References

1) M. Ikeda and Y. Miyachi, Prog. Theor. Phys. **16** (1956) 537
2) H. S. Green, Nuclear Physics **7** (1958) 373
3) H. Nakamura, Prog. Theor. Phys. **21** (1959) 827
4) T. Kimura, Prog. Theor. Phys. **24** (1960) 386
5) W. Pauli, Ins. H. Poincare Ann. **6** (1936) 109
6) B. E. Laurent, Arkiv för Fysik **16** (1959) 263
7) V. Bergmann, Berl. Ber. (1932) 346
8) Y. Mimura, Journal of Science of Hiroshima University **5** (1935) 99 (series of papers on the wave geometry can be found in the same journal)
9) K. Morinaga, Journal of Science of Hiroshima University **5** (1935) 151
10) C. N. Yang and R. L. Mills, Phys. Rev. **96** (1954) 191
11) A. Pais, Physica **19** (1953) 869
12) H. P. Dürr, W. Heisenberg, H. Mitter, S. Schlieder and K. Yamazaki, Z. Naturforsch. **14** (1959) 441
13) K. Morinaga and K. Senba, private communication

NORTH-HOLLAND BOOKS

PROCEEDINGS OF THE FIRST INTERNATIONAL

SPACE SCIENCE SYMPOSIUM

SPACE RESEARCH

NICE, 11-16 JANUARY, 1960

edited by

H. KALLMANN - BIJL

★

CONTENTS

Part I: The Earth's Atmosphere

Part II: The Ionosphere

Part III: Tracking and Telemetering

Part IV: Solar Radiation

Part V: Cosmic Radiation

Part VI: Interplanetary Dust

Part VII: The Moon and the Planets

Sponsored by COSPAR

$6^1/_2 \times 9^1/_2$" 1216 pages 650 ill. 61 plates Gld. 90.- 170s.

NORTH-HOLLAND PUBLISHING COMPANY - P.O. BOX 103 - AMSTERDAM

DISTRIBUTOR FOR U.S.A.: INTERSCIENCE PUBLISHERS, INC. - NEW YORK

We introduced a

PERSONAL SUBSCRIPTION SCHEME

for

NUCLEAR PHYSICS

8 volumes (1961, vols. 21—28) at the total price of $ 20.00 (£ 7.10.0)

Write for details:

NORTH-HOLLAND PUBLISHING COMPANY

P.O. BOX 103 — AMSTERDAM, HOLLAND